J. Bangladesh Acad. Sci. Volume 50, Issue 1, March 2026

**ISSN 2224-7270 (Online), 0378-8121 (Print)**

***Journal of Bangladesh Academy of Sciences*** is published four times a year (March, June, September and December comprising one volume) in English. Original research articles, review articles, and short communications of all branches of Science and Technology are considered for publication in this journal. Review articles are generally by invitation.

**Disclaimer**

The opinions, analysis and conclusions expressed or implied in this journal are those of the authors and do not represent the views of Bangladesh Academy of Sciences.

**Submission**

All correspondence regarding contributions for publication in the journal should be addressed to the *Editor, Journal of Bangladesh Academy of Sciences* <jbas.editor@yahoo.com>. Authors should consult the contributor's guideline at the back of the journal before submitting their manuscripts.

**Published by**

Bangladesh Academy of Sciences, National Science and Technology Complex, Agargaon, Dhaka-1207.

**Design and Printed by**

Sucharu Desktop Publishing, 1/E/1, Paribagh, Dhaka-1000, Bangladesh

**Annual Subscription:** Tk. 500.00 (Bangladesh); US $ 60.00; £ 21.50 plus postage.

**Single Copy:** Tk. 250.00 (Bangladesh); US $ 30.00; £ 11.25 plus postage.

J. Bangladesh Acad. Sci. 48(2); 141-145: December 2024 DOI:https://doi.org/10.3329/jbas.v48i2.78555

Journal of Bangladesh Academy of Sciences

Journal homepage: http://www.bas.org.bd/publications/jbas.html

**Mini Review Article**

# Ethical challenges in health and biomedical research: lessons from the COVID-19 pandemic

Liaquat Ali

*Pothikrit Institute of Health Studies, Dhaka, Bangladesh*

**ARTICLE INFO**

**Article History**

Received: 17 December 2024
Revised: 25 December 2024
Accepted: 26 December 2024

**Keywords:** Healthcare ethics, Ethics in biomedical research, Right-based ethics, Duty-based ethics, Post-Covid challenges.

**ABSTRACT**

The COVID-19 pandemic has created unprecedented health and economic challenges in mankind's history. At the same time, human civilization is facing a great ethical crisis. The duty- vs. right-based moral values led to justified dilemmas in the ethical decision-making process of health care providers, especially physicians. On the one hand, the duty towards the patients affected by the highly contagious virus (often in the face of PPE shortages) and the right (as individuals) to preserve themselves and family members, on the other hand, is difficult to solve only by a legal framework. The rationing of life-saving measures (like HFNC, ICU beds, or Ventilators) in the context of acute shortages is another example of physicians and managers needing to make very difficult ethical choices. Revelation of the self-centered nature of individual human beings, families, social groups, and even countries has been widely noticed during the pandemic, and it may not be a surprising phenomenon. However, the crisis has brought to the forefront the traditional debates on the relative merits of utility-, duty- and right-based ethics from a wider social perspective. The illusory blessings of the globalized market economy and associated neoliberal ethical principles have faced critical questions throughout these years. The rise of ultranationalism has been exposed with its vulgar faces worldwide. It is now obvious that the worst sufferers of the pandemic are poorer and marginalized people (forming the major bulk of the world population) who are now increasingly subject to rapidly increasing health and socioeconomic inequality and injustice due to the existing world order. Managing the pandemic through authoritarian approaches (lockdown, tracking, etc.) has also raised certain fundamental ethical issues related to human dignity, freedom, and autonomy, and, in many cases, the pandemic has been used to justify specific ideological platforms. Ethics of biomedical and health-related research (and their dissemination) also face some basic questions regarding the sacrifice of some age-old scientific and moral practices in the face of humanity's urgent need. Critical discussion and working consensus on those ethical issues have become urgent for biomedical research's future advancement.

## Introduction

The COVID-19 pandemic created unprecedented health and economic challenges in the history of humanity. The well-being of the global population has been profoundly affected by the pandemic in all dimensions, including morbidity, mortality, poverty, and education. In a post-pandemic analysis, Decerf et al. (2024) have recently estimated these losses (using a common metric) for 122 countries. The Authors have covered around 95% of the global population using country-specific WHO data. With an

*Corresponding author:<liaquat@pihs.ac.bd>

assumption of equal distribution among the worldwide population, every person would have spent about two weeks in poverty in 2020–2021 (the *CPY* estimate), lost eight days of life (*YLL*, discounted to the present), and would expect to spend an additional month in poverty (*FPY*, again discounted to the present) after 2021 due to the pandemic. In practice, however, the distribution of these losses was inequitable; people of lower- and middle-income countries suffered from a disproportionate burden.

Apart from being a technical challenge, the COVID-19 Pandemic has compelled the global human community to address some difficult ethical issues (Ezekiel et al., 2022). Distribution of scarce resources, mandatory imposition of certain restrictions, including long-term lockdowns and travel (with the consequent fear of violating human rights), skipping some well-established steps during clinical trials of vaccines or drugs, and inequitable distribution of vaccines among various countries are among the instances where the mere technical judgment was not sufficient to take the 'right' decision. Instead, well-thought value judgments (and thus ethics) became essential to address the issues. In addition to traditional ethical ideas, the unique nature of the COVID-19 pandemic compelled the global community with some newer ethical dilemmas (Smith et al., 2021).

In recent centuries, right-based ethics (from utilitarian and liberal systems of philosophy, leading to democratic political systems) has mostly replaced duty-based ethics (traditionally followed by various ideologies, leading to ideology-based states). The health systems and biomedical research are now mainly designed to revolve around that concept. As per this design, every citizen of the state, individually, has some constitutionally guaranteed basic rights. Many rights, such as medical care, nutrition, autonomy, and privacy, are directly related to health and biomedical research. The state's major institutions are designed to protect *individual rights* with authorities and obligations divided and balanced among legislative, executive, and judiciary wings. Under this system, like other citizens, healthcare providers and researchers operate under a 'rule of law' that prevails in a particular context.

In contrast to this system, duty-based ethics highlights collective rights where individuals may have to compromise some of their rights for the community's interest. While right-based ethics prioritizes individual rights and freedoms, emphasizing what individuals are entitled to, duty-based ethics centers on moral obligations and responsibilities, highlighting what individuals must do, often regardless of the consequences. Rights focus on 'what you can do' while duties focus on 'what you must do.'There has been an ongoing debate between these two ethical systems for centuries, and no empirical or logical instrument has been available to resolve the controversy (Moyn, 2016). The COVID-19 pandemic has raised awkward questions that perplex both systems. It has emphasized the need for rethinking and reconciling these two systems of ethics. The dichotomous issues, such as self-preservation versus duty towards patients and prioritization of patients in the case of critical shortages, may illustrate the problems.

## Self-preservation vs. Duty Toward Patients

It is well-known that SARS-COV-2 (the causative agent of COVID-19) was a highly contagious virus with lethal consequences in a considerable proportion of affected patients. The healthcare providers or HCPs (especially those in close contact with patients, such as managing physicians, nurses, and certain groups of technologists) also became potential patients, and the risk extended to their family members. As per strict right-based ethics, self-preservation is an individual's fundamental right, and an HCP is no exception. Accordingly, self-preservation supersedes the duty-related obligation of

patient care. Even if an HCP remains morally committed to caring services (following duty-based ethics), s/he violates the self-preservation right of the jointly living family members or other associates in the living space (frequently congested in a developing country setting like Bangladesh). The problem was further complicated by the substantial shortage (by quantity or quality) of Personal Protective Equipment or PPEs, and this became a common phenomenon in countries like Bangladesh (Joarder et al., 2021; Parveen et al., 2024). Even with the arrangement of isolated residential facilities in hotels (which was financially and socially demanding), the risk of contamination among the family members or other associates could not be reduced optimally, and a situation of 'burning-out' phenomenon was observed among the HCPs, both physically and psychologically (Parveen et al., 2021). A simplistic legal framework is insufficient to solve the dilemma related to the self-preservation rights of the HCPs.

**Rationing of Life-saving Measures**

It is well-known that there was a shortage of life-saving equipment and other commodities [like high flow nasal cannula (HFNC), Intensive Care Unit Beds (ICU Beds), or Ventilators] in most healthcare facilities, and the shortage was acute in resource-constrained countries like Bangladesh (Sakib, 2021). In such a situation, even in the absence of any irregularity or undue pressure, difficulty arises in rationally choosing the correct recipient of the life-saving resource in the face of limited availability. We can imagine a situation where only one Ventilator is available, and it is simultaneously needed by an elderly above 80 years of age and a young adult below 40 years of age. From one argument, older people should get priority as their risk for morbidity is greater than the younger ones, and they may also be considered to belong to a disadvantaged group. On the other hand, compared to older adults, younger adults have a much better chance of survival, which is desired from the outcome point of view (a preferred option as per utility-based ethics, which has close links with liberalism). It creates a substantial dilemma for physicians and managers to set priorities in the distribution decision. No law under the presently prevailing neoliberal political system can solve this dilemma, and an ethical judgment is mandatory in such a situation.

**Instances of Other Ethical Challenges during the Pandemic**

Revelation of the self-centered nature of individual human beings, families, social groups, and even countries has been widely noticed during the pandemic, and it may not be a surprising phenomenon. In Bangladesh, there were several reports where children abandoned parents, wives abandoned husbands (or vice-versa). At times, even the burial of dead bodies became a problem, and a charitable organization came forward with support. Such crisis has brought to the forefront the traditional debates on the relative merits of utility-, duty- and right-based ethics in a wider social perspective. The illusory blessings of the globalized market economy and associated neoliberal ethical principles have faced critical questions throughout the year.

During the period, the rise of ultranationalism was exposed with its vulgar faces worldwide. Almost every nation became conservative to protect its resources, and the so-called spirit of a 'global village' just vanished from the solidarity and unity points of view. We may remember the example when India deferred the delivery of COVID-19 vaccines to create a stock of its own vaccines. Some countries even increased the stock of essential commodities by 2-3 times the estimated actual need. These situations contrast the need for more cooperation as COVID-19 spread quickly due to a globalized world (Heilinger et al., 2020), and interconnectedness among nationalities was much more required in such situations (The Lancet, 2007).

It is now obvious that the worst sufferers of the pandemic are poorer and marginalized people (forming the major bulk of the world population) who are increasingly subject to rapidly increasing

health and socioeconomic inequality and injustice due to the existing world order. The pandemic exposed inequality in a much more straightforward way and increased inequality and injustice.

Managing the pandemic through authoritarian approaches (lockdown, tracking, etc.) has also raised certain fundamental ethical issues related to human dignity, freedom, and autonomy. All authoritarian/ dictatorial regimes in the world tried to suppress real information and promoted disinformation in indirect and direct ways. In many cases, the pandemic was used to justify certain ideological platforms.

## Revitalization of Public Health Ethics

Bioethics, in general, is discussed and emphasized more in terms of medical care and clinical research. This fact is particularly true in developing and underdeveloped countries like Bangladesh. In practice, the subdiscipline of public health ethics occupies a marginal position in the overall sphere of bioethics. The issues, as mentioned above, necessitate the revitalization of the discipline in the interest of national and global health justice (Working Group Ethics, 2020; Jamrozik and Heriot, 2020; Jamrozik, 2022). As per this ethical subsystem, a public health intervention cannot be ethically justified merely by expecting to produce a (net) improvement in public health (over and above the harms of the intervention). A public health policy is ethically justified only when two sets of key values are considered in addition to health: fairness, e.g., regarding the distribution of benefits and harms of an intervention in a population, and freedom, e.g., to move and interact with others without unjustified externally-imposed restrictions (Selgelid, 2009).

From the public health point of view, the pandemic has raised fundamental and practical issues regarding the violation of general principles of public health ethics (Jamrozik, 2022). During the pandemic, mental health and other harms increased, which, in many cases, is related to the narrow alignment of the moral value of health to the avoidance of one particular virus. The socioeconomic inequalities were exacerbated, and civil liberties were subject to sometimes undue limitations. Sometimes, without any strong justification, the interests of children were ignored in multiple ways in the name of reducing harm from a virus that poses extremely low risks to healthy children. There was a rapid rise in inequality; the public health interventions and their economic effects often disproportionately benefitted the rich sections of the population. The poor sections benefited little, were usually harmed, and were sometimes placed at higher risk of infection. There was a lack of scientific evidence that the benefits of many non-pharmacological interventions (NPIs) outweighed their harms, and there was also a failure to collect unbiased data. Transparency and legal checks on power were often limited.

## Revisiting the Ethics of Biomedical and Health-System Research

Ethics of biomedical and health-related research (and their dissemination) also faced some basic questions regarding the sacrifice of some age-old scientific and moral practices in the face of the urgent need of humanity (Dawson et al, 2020; Parker et al, 2020). For example, the approval of the human trial of the mRNA-based vaccines against COVID-19 was done by skipping the preclinical trial on higher animals, which is a prerequisite in usual times. Also, scientific evidence was considered for policy and planning, even from the non-peer-reviewed publications in pre-print journals, which is not the case in normal times. Publication norms were becoming relaxed at this time. Lack of deeper understanding (apart from other irregularities) of these ethical issues among the relevant professionals in the Bangladesh Medical Research Council (BMRC) contributed to the delay (and missed opportunity) in developing the COVID-19 vaccine by the Bangladeshi company 'Globe Pharmaceuticals Ltd.'

## Conclusions and Future Directions

The COVID-19 pandemic has shaken the confidence in the ethical basis of liberalism. The limitations of the solely right-based ethical systems have now been questioned, especially concerning individuals' autonomy and duty toward society and nature. The debate on the overdependence on 'utilitarian' and 'legalistic' systems (ignoring the 'moralistic' aspects

and normative values) is now live again, even in societies with functional democracies. It has emphasized the need for rethinking and reconciling these two major systems of ethics. The importance of a cultural revolution, at an equal pace with a political, technological, and economic revolution, is more realized now in this post-pandemic period. The need to strengthen the oversight of the ethical review or institutional review systems in biomedical research is now felt more than ever. These issues are vital to address, particularly in transitional societies like Bangladesh, where they are given only marginal importance. Critical discussion and working consensus on those ethical issues have become urgent for future healthcare and biomedical research advancement.

## References


Dawson A, Emanuel EJ, Emanuel MP, Smith MJ, Voo TC and Lin YL: Key ethical concepts and their application to COVID-19 research. *Public Health Ethics* 2020; 13(2): 127-132.

Decerf B, Friedman J, Mendes A, Pennings S and Yonzan N. Lives, Livelihoods, and Learning: A global perspective on the well-being impacts of the COVID-19 pandemic. *Policy Research Working Paper* 10728. World Bank Group, March 2024.

Ezekiel JE, Ross EGU and Maxwell JS. What covid has taught the world about ethics. *N. Engl. J. Med.* 2022; 387(17): 1542.

Jamrozik E and Heriot GS. Pandemic public health policy: with great power comes great responsibility. *Int. Med. J.* 2020; 50(10): 1169-1173.

Jamrozik E: Public health ethics: critiques of the new normal. *Monash Bioeth Rev.* 2022; 40(1): 1-16.

Joarder T, Khaled MNB and Joarder MAI. Urban educated group's perceptions of the COVID-19 pandemic management in Bangladesh: a qualitative exploration. *F1000Res.* 2021; 10: 170.

Moyn S. Rights vs Duties. *Boston Reviews* 2016. https://www.bostonreview.net/articles/samuel-moyn-rights-duties/. Downloaded on 05 November 2024.

Parker M.J., Fraser C., Abeler-Dörner L. and Bonsall D. Ethics of instantaneous contact tracing using mobile phone apps in the control of the COVID-19 pandemic. J Med Ethics 2020; 46:427–431.

Parveen S, Mahbub MS, Nahar N, Morshed KAM, Rahman N, Evana ET, Islam N and Miah ANSMJ. The impact of COVID-19 on healthcare services in Bangladesh: A qualitative study on Healthcare Providers' perspectives. *J. Prev. Med. Public Health* 2024; 57(4): 356-369.

Sakib SMN: ICU beds eluding critical patients, Situation deteriorating fast amid poor facilities in dist hospitals. *The Financial Express* 08 July 2021. Downloaded from https://today.thefinancialexpress.com.bd/first-page/icu-beds-eluding-critical-patients-1625680880.

Selgelid MJ: A moderate pluralist approach to public health policy and ethics. *Public Health Ethics*, 2009; 2(2): 195-205.

Smith MJ, Ahmad A, Arawi T, Dawson A, Emanuel EJ, Garani-Papadatos T, Ghimire P, Iliyasu Z, Lei R, Mastroleo I, Mathur R, Okeibunor J, Parker M, Saenz C, Thomé B, Upshur REG and Voo TC. Top five ethical lessons of COVID-19 that the world must learn (Open Letter). *Wellcome Open Res.* 2021, 6: 17.

The Lancet. Global solidarity needed in preparing for pandemic influenza. *The Lancet* 2007; 369: 532.

Heilinger J-C, Thompson A, Wild V, Ballantyne A, Berlinger N, Chung R, Eckenwiler L, Ehni H-J, Mitra AG, Hurst S, Maeckelberghe ELM, Marckmann G, Munthe C, Rid A, Schröder-Bäck P, Strech D and Venkatapuram S. Public Health Ethics and Covid-19 The ethical dimensions of public health decision-making during a pandemic. Health Psychology Research (HPR), University of Groningen/UMCG Research data base. *Datum der Veröffentlichung*: (22. April 2020) Version: (01) – aktuellste Version verfügbar unter.

J. Bangladesh Acad. Sci. 48(2); 147-160: December 2024 DOI:https://doi.org/10.3329/jbas.v48i2.69400

Journal of Bangladesh Academy of Sciences

Journal homepage: http://www.bas.org.bd/publications/jbas.html

**Research Article**

# Modified Cramer's rule for solving a fully fuzzy system of linear equations with a non-square coefficient matrix

Fatema Khatun*, Md. Sahadat Hossain[1] and Mst. Monjuara Akter[1]

*Department of Computer Science and Engineering, Northern University Bangladesh, Dhaka, Bangladesh*

**ARTICLE INFO**

**Article History**

Received: 17 October 2023
Revised: 04 June 2024
Accepted: 07 July 2024

**Keywords:** Triangular LR fuzzy number, Trapezoidal LR fuzzy number, Determinant of square and non-square matrix, The fuzzy system of equations.

**ABSTRACT**

In this modern technological world, several problems arise daily, whose maximum problems have been unsolved in a classical way because of their ambiguity. To solve those problems, the applications of fuzzy mathematics are increasing rapidly, whereas traditional classical methods have failed. Here, we have modified Cramer's rules method for solving the non-square coefficient matrix of the fully fuzzy system of linear equations (FFSLE) using triangular and trapezoidal LR fuzzy numbers. This modified method is compared with another method that can only solve the square coefficient matrix using fuzzy triangular and trapezoidal numbers. At last, we observe that our modified method is more general than others. This process is illustrated with numerical examples.

## Introduction

A fuzzy system of linear equations [FSLE} plays a vital role in designing the model in vast real-world problems that ensue in an extensive range of disciplines such as optimization, economics, statistics business (Khatun and Hossain, 2022), and engineering (Buckley and Qu, 1990, 1991; Islam and Hossain, 2022). That's why various researchers are paying attention to the solution methods for the FSLE.

In the previous decades, many researchers have studied and investigated fuzzy system of linear equations first proposed by Friedman et al. (1998) and Ma et al. (2000). For finding a result in the embedding method (Allahviranloo and Hashemi, 2014) they decorated the main SFLE into a crisp system of linear equations (SLE) (Friedman et al., 1998), after then studied dual fuzzy system of linear equations (DFSL) by Allahviranloo and Ghanbari (2012a, 2012b), Allahviranloo and Salahshour (2011), Allahviranloo (2004, 2005), and Abbasi and Jalali (2019); fully fuzzy system of linear equations (FFSLE) by Abbasbandy et al. (2008), Abbasbandy and Alavi (2005), Abbasbandy et al. (2005, 2006) and Asady et al. (2005), and general dual fuzzy linear system (GDFLS) by Zheng and Wang (2006). Later, the FFSLE of the form AX=b was introduced by Dehghan and Hashemi (2006), who analyzed some direct methods in fuzzy to solve FSLE and FFSLE based on classical methods such as matrix inverse method, Cramer's rule and LU-decomposition (Dehghan et al., 2007). FFLS with triangular fuzzy numbers is discussed by Muruganandam et al. (2019), and a method is proposed using Gauss-Jordan Elimination by Abidin et al. (2019). A modified associated linear system is proposed by Malkawi et al. (2018) for solving FFLS where the fuzzy numbers are hexagonal and positive. After that, Ziqan et al. (2022) extended it by using trapezoidal

*Corresponding author:<fatema.rumath@gmail.com>

[1]*Department of Mathematics, University of Rajshahi, Rajshahi, Bangladesh*

fuzzy numbers. However, all literature methods can solve only this system's square coefficient matrix. The problem of solving a system of fuzzy linear equations faces serious difficulties when the coefficient matrix of the system is rectangular (non-square coefficient matrix).

In this paper, first, we define the determinate of a non-square matrix (Arunkumar et al., 2011; Radić, 2005; Joshi, 1980)with some basic idea of fuzzy numbers. Furthermore, we modify Cramer's rule method for solving FFSLE of the form AX=b with a square and non-square coefficient matrix of the system, in which all parameters are LR fuzzy numbers (Soylu and Aslan, 2022). For this reason, it is called a fully fuzzy system of linear equations. Here, we discuss this modified method using two fuzzy number systems: a triangular LR fuzzy number and a trapezoidal LR fuzzy number. Here, we emphasize solving the non-square coefficient matrix of the FFSLE, which was not done in the previous literature. The fuzzy number was first defined by Chang and Zadeh (1972). After that, Dubois and Prade (1978) became acquainted with the LR fuzzy number. To extend this method, we use the determinant of the non-square coefficient matrix (Arunkumar et al., 2011; Radić, 2005; Joshi, 1980) of the system and define the rules separately for square and non-square matrix in triangular and trapezoidal LR fuzzy numbers. Finally, we add some numerical examples to illustrate this process.

This paper is decorated by:

Section 2 reviews the basic operations and concept of LR fuzzy numbers with a fully fuzzy system of linear equations and determinants of a non-square matrix. In section 3, the methodology of the solution system of the fully fuzzy system of linear equations for both square and non-square coefficient matrix is modified by Cramer's rule in both number systems. In section 4, we illustrate our methods with some examples. Section 5 presents results, and a discussion with future opinions is provided.

## Preliminaries

**2.1 Fuzzy number** (Muruganandam and Razak, 2013)**:** A fuzzy set U is termed as a fuzzy number on the universe R if

i. U is a normal fuzzy set,

ii. U is a convex fuzzy set and

iii. U is piecewise continuous.

The set of all fuzzy numbers is denoted by $F(E^1)$. A parametric form of this definition is given by Kaleva (Abbasbandy et al., 2005).

**2.2 Triangular LR fuzzy number** (Soylu and Aslan, 2022; Nikuie and Ahmad, 2014; Guo and Shang, 2013)**:** A triangular fuzzy number $M\ (\mathfrak{m}, \alpha, \beta)$ is said to be a triangular $LR$ fuzzy number if

$$\mu_M(y) = \begin{cases} L\left(\frac{\mathfrak{m}-y}{\alpha}\right) for y \le \mathfrak{m}, & \alpha > 0 \\ R\left(\frac{y-\mathfrak{m}}{\beta}\right) for y \ge \mathfrak{m}, & \beta > 0 \end{cases}$$

where '$\mathfrak{m}$' mean value, '$\alpha$' left spread and '$\beta$' right spread of M, and the strictly decreasing functions L and R defined on [0 1] satisfy the conditions:

$$L(0) = R(0) = 1, \quad L(1) = R(1) = 0$$

$$0 < L(y) < 1, \quad 0 < R(y) < 1, \ y \neq 0,1$$

**2.3 Trapezoidal $LR$ fuzzy number** (Karthik and Chandrasekaran, 2014)**:** A trapezoidal fuzzy number $M\ (\mathfrak{m}, \mathfrak{n}, \alpha, \beta)$ is said to be a Trapezoidal LR fuzzy number if

$$\mu_M(y) = \begin{cases} L\left(\frac{\mathfrak{m}-y}{\alpha}\right) for y \le \mathfrak{m}, & \alpha > 0 \\ R\left(\frac{y-\mathfrak{n}}{\beta}\right) for y \ge \mathfrak{n}, & \beta > 0 \end{cases}$$

where '$\mathfrak{m}$' and '$\mathfrak{n}$' are the left and right points of mean value, '$\alpha$' left spread and '$\beta$' right spread of M, and the strictly decreasing functions L and R defined on [0 1] satisfy the conditions:

$$L(0) = R(0) = 1, \ L(1) = R(1) = 0$$

$$0 < L(y) < 1, \quad 0 < R(y) < 1, \ y \neq 0,1$$

**2.4 Equal fuzzy numbers** (Elsayed et al., 2020; Guo and Shang, 2013)**:**

i. Two triangular LR fuzzy numbers, $M\ (p,q,r)\ and\ N\ (u,v,w)$, are said to be equal (Guo and Shang, 2013) if $p=u, q=v, r=w$.

ii. Two trapezoidal LR fuzzy numbers, $M(p,q,r,s)$, and $N(u,v,w,x)$, are said to be equal (Elsayed et al., 2020) if $p=u, q=v, r=w, s=x$.

**2.5 Fuzzy Arithmetic Operations:** In this sector, we discussed the actions of two fuzzy numbers, such as addition, subtraction, multiplication, and scalar multiplication.

**a) Triangular LR fuzzy number operations** (Guo and Shang, 2013)**:** let $P(p,q,r)\ and\ Q(\ u,v,w)$ be two triangular LR fuzzy numbers then their arithmetic operations are:

i. Addition: $P+Q\ =\ (p+u, q+v,\ r+w)$

ii. Opposite: $-P=-(p,q,r)=(-p,r,q)$ since A is a LR fuzzy number and 'p' is a mean value of P.

iii. Subtraction: $P-Q\ =\ (p-u, q+w, r+v)$

iv. Scalar Multiplication: Let $\lambda$ be any scalar, then

$$\lambda \otimes P = \lambda \bigotimes (p,q,r) = \begin{cases} (\lambda p, \lambda q, \lambda r), & \lambda \geq 0 \\ (\lambda p, -\lambda r, -\lambda q), & \lambda < 0 \end{cases}$$

v. Multiplication:

- $If\ P>0\ and\ Q>0, then$

$$P \otimes Q\ =\ (p,q,r) \otimes (u,v,w) = (pu, pv+qu, pw+ru)$$

- $If\ P<0\ and\ Q>0, then$

$$P \otimes Q\ =\ (p,q,r) \otimes (u,v,w) = (pu, qu-pw, ru-pv)$$

- $If\ P<0\ and\ Q<0, then$

$$P \otimes Q\ =\ (p,q,r) \otimes (u,v,w) = (pu, -pw-ru, -pv-qu)$$

vi. The cross product of two triangular LR fuzzy numbers is:

$$P \otimes Q\ =\ (p,q,r) \otimes (u,v,w) = (pu, pv+qu-pu, pw+ru-pu)$$

**a) Trapezoidal LR fuzzy number operations:** (Karthik and Chandrasekaran, 2014): The Trapezoidal LR fuzzy number operations are the same as Triangular LR fuzzy number operations. Let $P(p,q,r,s)\ and\ Q(\ u,v,w,x)$ be two trapezoidal LR fuzzy numbers, then their arithmetic operations are:

i. Addition: $P+Q\ =\ (p+u, q+v, r+w, s+x)$

ii. Opposite: $-P\ =\ -(p,q,r,s) = (-q,-p,s,r)$, since P is a LR fuzzy number and 'p' 'q' are mean values end point of P.

iii. Subtraction: $P-Q\ =\ (p-u, q-v, r+x, s+w)$

iv. Scalar Multiplication: Let $\lambda$ be any scalar, then

$$\lambda \otimes p = \lambda \otimes (p,q,r,s) = \begin{cases} (\lambda p, \lambda q, \lambda r, \lambda s), & \lambda \geq 0 \\ (\lambda q, \lambda p, -\lambda s, -\lambda r), & \lambda < 0 \end{cases}$$

v. Multiplication:

- $If\ P>0\ and\ Q>0, then$

$$P \otimes Q\ =\ (p,q,r,s) \otimes (\ u,v,w,x) = (pu, qv, pw+ru, qx+sv)$$

- $If\ P<0\ and\ Q>0, then$

$$P \otimes Q\ =\ (p,q,r,s) \otimes (\ u,v,w,x) = (qu, pv, ru-qx, sv-pw)$$

$$If\ P<0\ and\ Q<0, then$$

$$P \otimes Q\ =\ (p,q,r,s) \otimes (\ u,v,w,x) = (\ qv, pu, -qx-sv, -pw-ru)$$

vi. The cross product of two trapezoidal LR fuzzy numbers is:

$$P \otimes Q = (p,q,r,s) \otimes (\ u,v,w,x) = (pu, qv, pw+ru-pu, qx+sv-qv)$$

**2.6 The determinate of a non-square matrix** (Arunkumar et al., 2011; Radić, 2005; Joshi, 1980)**:** Let A be a non-square matrix, then the determinant of A is

$$\begin{aligned}\det(A) = \det(A_1, A_2, \dots, A_k) \\ = det(A_1, A_2, \dots, A_{k-1}) \\ +(-1)^k \det(A_1 - A_2 \\ + \cdots +(-1)^k A_{k-1}, A_k),\end{aligned}$$

Where k is the number of rows or columns of the non-square matrix.

**2.1 Fully fuzzy system of linear equations** (Dehghan et al., 2007)**:** Consider The n× $n$ fully fuzzy linear equations:

$$\begin{cases} (\check{a}_{11}\otimes\hat{y}_1) \oplus (\check{a}_{12}\otimes\bar{\hat{y}}_2) \oplus \dots\dots\dots \oplus (\check{a}_{1n}\otimes\hat{y}_n) = \underline{b}_1 \\ (\check{a}_{21}\otimes\bar{x}_1) \oplus (\check{a}_{22}\otimes\hat{y}_2) \oplus \dots\dots\dots \oplus (\check{a}_{2n}\otimes\hat{y}_n) = \underline{b}_2 \\ \vdots \\ (\check{a}_{n1}\otimes\hat{y}_1) \oplus (\check{a}_{n2}\otimes\hat{y}_2) \oplus \dots\dots\dots \oplus (\check{a}_{nn}\otimes\hat{y}_n) = \underline{b}_n \end{cases} \quad (2.1)$$

The matrix arrangement of the upstairs equations is:

$$\check{A}\otimes\hat{Y} = \underline{b} \quad (2.2)$$

Or simply $\check{A}\otimes\hat{Y} = \underline{b}$, where the coefficient matrix $\check{A} = (\check{a}_{ij}), 1 \le i,j \le n$ is a $n \times n$ fuzzy matrix and $\hat{y}_i, \underline{b}_i \in F(E^1)$, $1 \le i \le n$. This arrangement is a fully fuzzy linear Equations (FFSLE) system.

## 2. Methodology

Analytical methods are sometimes called direct methods. Here, we will discuss the fully fuzzy system of linear equations in Cramer's rule using two types of fuzzy numbers: triangular LR fuzzy numbers and Trapezoidal LR fuzzy numbers. In this method, we will use the cross product of fuzzy numbers and the determinant of the square and non-square matrix.

### 3.1 Modified Cramer's rule for triangular LR fuzzy numbers

Using Cramer's rule, we can easily solve a fully fuzzy system of linear equations that states that each entry wi in the solution is a quotient of two determinants. From Equation (2.2) where $\check{A} = (\check{a}_{ij})$that $\check{a}_{ij} = (a_{ij}, b_{ij}, c_{ij})$triangular LR fuzzy numbers with the new notation (Ă)= (A, L, M)>0, whose A, L and M are three crisp matrices with the same size of Ă such that $A = (a_{ij}), L = (b_{ij})$ and M $= (c_{ij})$ are called the center matrix and the left and right spread matrices, respectively. $\underline{b} = (b,g,h) > 0 \; and \; \hat{Y} = (w,x,y) > 0$. Then we have

$$\check{A}\otimes\hat{Y} = \underline{b}$$

$$(A,L,M)\otimes(w,x,y) = (b,g,h) \quad (3.1)$$

Using the Cross product of two triangular LR fuzzy numbers. It can be written as $(Aw, Ax + Lw - Aw, Ay + Mw - Aw)$ $(b,g,h)$

Now, using section (2.4), the equality of two fuzzy numbers, we get

$$\begin{aligned} Aw &= b \\ Ax + Lw - Aw &= g \quad (3.2) \\ Ay + Mw - Aw &= h \end{aligned}$$

i.e.,

$$\begin{aligned} Aw &= b \\ Ax &= g - Lw + Aw \quad (3.3) \\ Ay &= h - Mw + Aw \end{aligned}$$

By the Cramer's rule, we may write,

i.If A is a square matrix, then

$$w_i = \frac{\det(A^{(i)})}{\det(A)}, \quad i = 1,2,\dots,n$$

ii.If A is a non-square matrix, then

$$\begin{aligned}\det(A) = \det(A_1, A_2, \dots, A_k) \\ = det(A_1, A_2, \dots, A_{k-1}) \\ +(-1)^k \det(A_1 - A_2 \\ + \cdots +(-1)^k A_{k-1}, A_k)\end{aligned}$$

where k is the number of rows or columns of the non-square matrix.

$$w_i = \frac{\det(A^{(i)})}{\det(A)}, \quad i = 1,2,\dots,n.$$

Where$A^{(i)}$denotes the matrix, we get it by replacing the$i^{th}$ column with b of matrix A. Then, using a solution of w, we will get

$$x_i = \frac{\det(A'^{(i)})}{\det(A)}, \quad i = 1,2,\dots,n. \qquad y_i = \frac{\det(A''^{(i)})}{\det(A)}, \quad i = 1,2,\dots,n.$$

where $A'^{(i)}$ and $A''^{(i)}$ denote the matrix obtained from A by replacing its $i^{th}$ column with $g - Lw + Aw$ and $h - Mw + Aw$, respectively.

### 3.2 Modified Cramer's rule for trapezoidal LR fuzzy numbers

In this sector, we will use the analytical method to obtain the solution of the fully fuzzy linear system of equations of trapezoidal LR fuzzy numbers (2.2) where $\breve{A} = (\breve{a}_{ij})$ that $\breve{a}_{ij} = (a_{ij}, b_{ij}, c_{ij}, d_{ij})$ LR fuzzy number with the new notation $\breve{A} = (A, L, M, N) > 0$, whose A, L, M, and N are four crisp matrices with the same size of $\breve{A}$ such that $A = (a_{ij}), L = (b_{ij}), M = (c_{ij})$ and $N = (d_{ij})$ are called the center-left and center-right matrices and the left and right spread matrices, respectively. $\breve{b} = (b, g, h, p) > 0$ and $\hat{Y} = (w, x, y, z) > 0$. Then we have $\breve{A} \otimes \hat{Y} = \breve{b}$

$(A, L, M, N) \otimes (w, x, y, z) = (b, g, h, p)$ …….(4.1)

the Cross product of two trapezoidal LR fuzzy numbers. It can be written as

$$(Aw, Lx, Ay + Mw - Aw, Lz + Nx - Lx) = (b, g, h, p)$$

Now, using section (2.4), the equality of two fuzzy numbers, we get

$$Aw = b$$
$$Lx = g$$
$$Ay + Mw - Aw = h \quad \text{…..(4.2)}$$
$$Lz + Nx - Lx = p$$

i.e.,

$$Aw = b$$
$$Lx = g$$
$$Ay = h - Mw + Aw \quad \text{…..(4.3)}$$
$$Lz = p - Nx + Lx$$

By the Cramer's rule, we may write,

i.If A and L are square matrices, then

$$w_i = \frac{\det(A^{(i)})}{\det(A)}, \quad i = 1,2,\dots,n.$$
$$x_i = \frac{\det(L^{(i)})}{\det(L)}, \quad i = 1,2,\dots,n.$$

ii.If A and L are non-square matrices, then

$$\det(A) = \det(A_1, A_2, \dots, A_k) = det(A_1, A_2, \dots, A_{k-1}) + (-1)^k \det(A_1 - A_2 + \dots + (-1)^k A_{k-1}, A_k)$$

$$\det(L) = \det(L_1, L_2, \dots, L_k) = det(L_1, L_2, \dots, L_{k-1}) + (-1)^k \det(L_1 - L_2 + \dots + (-1)^k L_{k-1}, L_k)$$

where k is the number of rows or columns of the non-square matrix.

$$w_i = \frac{\det(A^{(i)})}{\det(A)}, \quad i = 1,2,\dots,n$$
$$x_i = \frac{\det(L^{(i)})}{\det(L)}, \quad i = 1,2,\dots,n$$

Where $A^{(i)}$ and $L^{(i)}$ denote the matrices we get by replacing the $i^{th}$ column with b and g of matrices A and L, respectively. Then, using the solution of w and x, we will get

$$y_i = \frac{\det(A'^{(i)})}{\det(A)}, \quad i = 1,2,\dots,n$$
$$z_i = \frac{\det(L'^{(i)})}{\det(L)}, \quad i = 1,2,\dots,n$$

where $A'^{(i)}$ and $L'^{(i)}$ denote matrices that are obtained from A and L by replacing their $i^{th}$ column with $h - Mw + Aw$ and $p - Nx + Lx$, respectively.

## 4. Numerical illustrations

### 4.1 Examples of triangular LR fuzzy numbers

**Example 1:** Suppose the fully fuzzy linear system of equations:

$$(6,1,4)\otimes(w_1, x_1, y_1) \oplus (5,2,2)\otimes(w_2, x_2, y_2) \oplus (3,2,1)\otimes(w_3, x_3, y_3) = (58, 30, 60)$$
$$(12,8,20)\otimes(w_1, x_1, y_1) \oplus (14,12,15) \otimes(w_2, x_2, y_2) \oplus (8,8,10)\otimes(w_3, x_3, y_3) = (142,139,257)$$
$$(24,10,34)\otimes(w_1, x_1, y_1) \oplus (32,30,30) \otimes(w_2, x_2, y_2) \oplus (20,19,24)\otimes(w_3, x_3, y_3) = (316,297,514)$$

where $A = \begin{bmatrix} 6 & 5 & 3 \\ 12 & 14 & 8 \\ 24 & 32 & 20 \end{bmatrix}$,

$L = \begin{bmatrix} 1 & 2 & 2 \\ 8 & 12 & 8 \\ 10 & 30 & 19 \end{bmatrix}$,

$M = \begin{bmatrix} 4 & 2 & 1 \\ 20 & 15 & 10 \\ 34 & 30 & 24 \end{bmatrix}$

$b = \begin{bmatrix} 58 \\ 142 \\ 316 \end{bmatrix}$, $g = \begin{bmatrix} 30 \\ 139 \\ 297 \end{bmatrix}$, $h = \begin{bmatrix} 60 \\ 257 \\ 514 \end{bmatrix}$,

$w = \begin{bmatrix} w_1 \\ w_2 \\ w_3 \end{bmatrix}$, $x = \begin{bmatrix} x_1 \\ x_2 \\ x_3 \end{bmatrix}$, $y = \begin{bmatrix} y_1 \\ y_2 \\ y_3 \end{bmatrix}$

Here, we see that matrix A is square, so we follow the rule (i) in this method. Then we have det(A)= 48 Now we calculate $A^1$, $A^2$, and $A^3$, which are obtained from A by replacing its $i^{th}$ column with b.

$A^1 = \begin{bmatrix} 58 & 5 & 3 \\ 142 & 14 & 8 \\ 316 & 32 & 20 \end{bmatrix} \Longrightarrow det(A^1) = 192$

$A^2 = \begin{bmatrix} 6 & 58 & 3 \\ 12 & 142 & 8 \\ 24 & 316 & 20 \end{bmatrix} \Longrightarrow det(A^2) = 240$

$A^3 = \begin{bmatrix} 6 & 5 & 58 \\ 12 & 14 & 142 \\ 24 & 32 & 316 \end{bmatrix} \Longrightarrow det(A^3) = 144$

Therefore, we get

$w_1 = \frac{192}{48} = 4, \quad w_2 = \frac{240}{48} = 5, w_3 = \frac{144}{48} = 3$

i.e., $w = \begin{bmatrix} w_1 \\ w_2 \\ w_3 \end{bmatrix} = \begin{bmatrix} 4 \\ 5 \\ 3 \end{bmatrix}$

Now we calculate x and y, so first, we calculate$A'^{(i)}$ and $A''^{(i)}$, which denote matrices obtained from A by replacing its $i^{th}$ column with $g - Lw + Aw$ and $h - Mw + Aw$, respectively.

$$g - Lw + Aw = \begin{bmatrix} 30 \\ 139 \\ 297 \end{bmatrix} - \begin{bmatrix} 1 & 2 & 2 \\ 8 & 12 & 8 \\ 10 & 30 & 19 \end{bmatrix}\begin{bmatrix} 4 \\ 5 \\ 3 \end{bmatrix} + \begin{bmatrix} 6 & 5 & 3 \\ 12 & 14 & 8 \\ 24 & 32 & 20 \end{bmatrix}\begin{bmatrix} 4 \\ 5 \\ 3 \end{bmatrix} = \begin{bmatrix} 68 \\ 165 \\ 366 \end{bmatrix}$$

$$h - Mw + Aw = \begin{bmatrix} 60 \\ 257 \\ 514 \end{bmatrix}\begin{bmatrix} 4 & 2 & 1 \\ 20 & 15 & 10 \\ 34 & 30 & 24 \end{bmatrix}\begin{bmatrix} 4 \\ 5 \\ 3 \end{bmatrix} + \begin{bmatrix} 6 & 5 & 3 \\ 12 & 14 & 8 \\ 24 & 32 & 20 \end{bmatrix}\begin{bmatrix} 4 \\ 5 \\ 3 \end{bmatrix} = \begin{bmatrix} 89 \\ 214 \\ 472 \end{bmatrix}$$

Now, $A'^1 = \begin{bmatrix} 68 & 5 & 3 \\ 165 & 14 & 8 \\ 366 & 32 & 20 \end{bmatrix} \Longrightarrow det(A'^1) = 240$

$A'^2 = \begin{bmatrix} 6 & 68 & 3 \\ 12 & 165 & 8 \\ 24 & 366 & 20 \end{bmatrix} \Longrightarrow det(A'^2) = 264$

$A'^3 = \begin{bmatrix} 6 & 5 & 68 \\ 12 & 14165 & \\ 24 & 32366 & \end{bmatrix} \Longrightarrow det(A'^3) = 168$

Therefore, we get

$x_1 = \frac{240}{48} = 5, \quad x_2 = \frac{264}{48} = 5.5, \; x_3 = \frac{168}{48} = 3.5$

i.e., $x = \begin{bmatrix} x_1 \\ x_2 \\ x_3 \end{bmatrix} = \begin{bmatrix} 5 \\ 5.5 \\ 3.5 \end{bmatrix}$

Now, $A''^1 = \begin{bmatrix} 89 & 5 & 3 \\ 21414 & 8 & \\ 4723220 & & \end{bmatrix} \Longrightarrow det(A''^1) = 336$

$A''^2 = \begin{bmatrix} 6 & 68 & 3 \\ 12 & 165 & 8 \\ 24 & 366 & 20 \end{bmatrix} \Longrightarrow det(A''^2) = 336$

$A''^3 = \begin{bmatrix} 6 & 5 & 89 \\ 12 & 14 & 214 \\ 24 & 32 & 472 \end{bmatrix} \Longrightarrow det(A''^3) = 192$

Therefore, we get

$y_1 = \frac{336}{48} = 7, \quad y_2 = \frac{336}{48} = 7, \quad y_3 = \frac{192}{48} = 4$

i.e., $y = \begin{bmatrix} y_1 \\ y_2 \\ y_3 \end{bmatrix} = \begin{bmatrix} 7 \\ 7 \\ 4 \end{bmatrix}$

Hence the solution set is

$$\begin{bmatrix} (w_1, x_1, y_1) \\ (w_2, x_2, y_2) \\ (w_3, x_3, y_3) \end{bmatrix} = \begin{bmatrix} (4, 5, 7) \\ (5, 5.5, 7) \\ (3, 3.5, 4) \end{bmatrix}$$

This solution set's figure (Fig. 1) is given below:

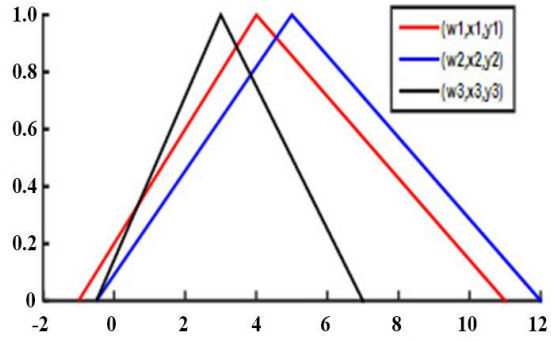


**Fig. 1. Solution set of the FFSLE of triangular LR fuzzy numbers in Cramer's rule (i) for square coefficient matrix.**

**Example 2:** Suppose the fully fuzzy system of linear equations:

$$(4,1,1)\otimes(w_1,x_1,y_1)\oplus(6,1,2)\otimes(w_2,x_2,y_2)\oplus(7,2,3)\otimes(w_3,x_3,y_3)=(45,50,5)$$
$$(7,1,2)\otimes(w_1,x_1,y_1)\oplus(5,2,1)\otimes(w_2,x_2,y_2)\oplus(8,0,2)\otimes(w_3,x_3,y_3)=(48,52,5)$$

where $A=\begin{bmatrix}467\\758\end{bmatrix}$, $L=\begin{bmatrix}1 & 12\\1 & 20\end{bmatrix}$, $M=\begin{bmatrix}1 & 23\\2 & 12\end{bmatrix}$

$b=\begin{bmatrix}45\\48\end{bmatrix}$, $g=\begin{bmatrix}50\\52\end{bmatrix}$, $h=\begin{bmatrix}5\\5\end{bmatrix}$,

$w=\begin{bmatrix}w_1\\w_2\\w_3\end{bmatrix}$, $x=\begin{bmatrix}x_1\\x_2\\x_3\end{bmatrix}$, $y=\begin{bmatrix}y_1\\y_2\\y_3\end{bmatrix}$

Here, we see that matrix A is a non-square matrix, so we follow the rule (ii) in this method. Then we have

$\det(A)=\begin{vmatrix}467\\758\end{vmatrix}=\begin{vmatrix}46\\75\end{vmatrix}+(-1)^3\begin{vmatrix}4-67\\7-58\end{vmatrix}=\begin{vmatrix}46\\75\end{vmatrix}-\begin{vmatrix}-27\\2\ 8\end{vmatrix}=-22+30=8$

Now we calculate $A^1$, $A^2$, and $A^3$, which are obtained from A by replacing its $i^{th}$ column with b.

$A^1=\begin{bmatrix}4567\\4858\end{bmatrix}$,

$\Rightarrow det(A^1)=\begin{vmatrix}4567\\4858\end{vmatrix}=\begin{vmatrix}456\\485\end{vmatrix}+(-1)^3\begin{vmatrix}45-67\\48-58\end{vmatrix}=\begin{vmatrix}456\\485\end{vmatrix}-\begin{vmatrix}397\\438\end{vmatrix}=-63-11=-74$

$A^2=\begin{bmatrix}4457\\7488\end{bmatrix}$,

$\Rightarrow det(A^2)=\begin{vmatrix}4457\\7488\end{vmatrix}=\begin{vmatrix}445\\748\end{vmatrix}+(-1)^3\begin{vmatrix}4-457\\7-488\end{vmatrix}=\begin{vmatrix}445\\748\end{vmatrix}-\begin{vmatrix}-417\\-418\end{vmatrix}=-123+41=-82$

$A^3=\begin{bmatrix}4645\\7548\end{bmatrix}$,

$\Rightarrow det(A^3)=\begin{vmatrix}4645\\7548\end{vmatrix}=\begin{vmatrix}46\\75\end{vmatrix}+(-1)^3\begin{vmatrix}4-645\\7-548\end{vmatrix}=\begin{vmatrix}46\\75\end{vmatrix}-\begin{vmatrix}-245\\2\ 48\end{vmatrix}=-22+186=164$

Therefore, we get

$w_1=\frac{-74}{8}=-9.25$, $w_2=\frac{-82}{8}=-10.25$, $w_3=\frac{164}{8}=20.5$

i.e., $w=\begin{bmatrix}w_1\\w_2\\w_3\end{bmatrix}=\begin{bmatrix}-9.25\\-10.25\\20.5\end{bmatrix}$

Now we calculate x and y, so first we calculate $A'^{(i)}$ and $A''^{(i)}$ denote matrices obtained from A by replacing its $i^{th}$ column with $g-Lw+Aw$ and $h-Mw+Aw$, respectively.

$$g-Lw+A=\begin{bmatrix}50\\52\end{bmatrix}-\begin{bmatrix}1 & 12\\1 & 20\end{bmatrix}\begin{bmatrix}-9.25\\-10.25\\20.5\end{bmatrix}+\begin{bmatrix}467\\758\end{bmatrix}\begin{bmatrix}-9.25\\-10.25\\20.5\end{bmatrix}=\begin{bmatrix}73.50\\129.75\end{bmatrix}$$

$$h-Mw+Aw=\begin{bmatrix}5\\5\end{bmatrix}-\begin{bmatrix}1 & 23\\2 & 12\end{bmatrix}\begin{bmatrix}-9.25\\-10.25\\20.5\end{bmatrix}+\begin{bmatrix}467\\758\end{bmatrix}\begin{bmatrix}-9.25\\-10.25\\20.5\end{bmatrix}=\begin{bmatrix}18.25\\40.75\end{bmatrix}$$

Now,

$A'^1=\begin{bmatrix}73.50\ 67\\129.7558\end{bmatrix}$,

$\Rightarrow det(A'^1)=\begin{vmatrix}73.50\ 67\\129.7558\end{vmatrix}=\begin{vmatrix}73.50\ 6\\129.755\end{vmatrix}+(-1)^3\begin{vmatrix}73.50-6\ 7\\129.75-58\end{vmatrix}=\begin{vmatrix}73.50\ 6\\129.755\end{vmatrix}-\begin{vmatrix}67.5\ \ 7\\124.758\end{vmatrix}=-411+333.25=-77.75$

$A'^2=\begin{bmatrix}4\ 73.50\ 7\\7129.758\end{bmatrix}$,

$\Rightarrow det(A'^2)=\begin{vmatrix}4\ 73.50\ 7\\7129.758\end{vmatrix}=\begin{vmatrix}4\ 73.50\\7129.75\end{vmatrix}+(-1)^3\begin{vmatrix}4-73.50\ 7\\7-129.758\end{vmatrix}$

$$= \begin{vmatrix} 4 & 73.50 \\ 7 & 129.75 \end{vmatrix} - \begin{vmatrix} -69.5 & 7 \\ -122.758 & \end{vmatrix} = 4.5 - 303.25$$
$$= -298.75$$

$A'^3 = \begin{bmatrix} 46 & 73.50 \\ 75 & 129.75 \end{bmatrix}$,

$\Rightarrow det(A'^3) = \begin{vmatrix} 46 & 73.50 \\ 75 & 129.75 \end{vmatrix} = \begin{vmatrix} 46 \\ 75 \end{vmatrix} +$

$(-1)^3 \begin{vmatrix} 4-6 & 73.50 \\ 7-5 & 129.75 \end{vmatrix} = \begin{vmatrix} 46 \\ 75 \end{vmatrix} - \begin{vmatrix} -2 & 73.50 \\ 2 & 129.75 \end{vmatrix} =$

$-22 + 406.5 = 384.5$

Therefore, we get

$$x_1 = \frac{-77.75}{8} = -9.72,$$

$x_2 = \frac{-298.75}{8} = -37.34,\ x_3 = \frac{384.5}{8} = 48.06$

i.e., $$x = \begin{bmatrix} x_1 \\ x_2 \\ x_3 \end{bmatrix} = \begin{bmatrix} -9.72 \\ -37.34 \\ 48.06 \end{bmatrix}$$

In a similar way, we get

$A''^1 = \begin{bmatrix} 18.2567 \\ 40.7558 \end{bmatrix}$,

$\Rightarrow det(A''^1) = \begin{vmatrix} 18.2567 \\ 40.7558 \end{vmatrix}$

$$= \begin{vmatrix} 18.256 \\ 40.755 \end{vmatrix} + (-1)^3 \begin{vmatrix} 18.25 - 67 \\ 40.75 - 58 \end{vmatrix}$$

$= \begin{vmatrix} 18.256 \\ 40.755 \end{vmatrix} - \begin{vmatrix} 12.257 \\ 35.758 \end{vmatrix} = -153.25 + 152.25 = -1$

$A''^2 = \begin{bmatrix} 418.257 \\ 740.758 \end{bmatrix}$,

$\Rightarrow det(A''^2) = \begin{vmatrix} 418.257 \\ 740.758 \end{vmatrix}$

$$= \begin{vmatrix} 418.25 \\ 740.75 \end{vmatrix} + (-1)^3 \begin{vmatrix} 4 - 18.257 \\ 7 - 40.758 \end{vmatrix}$$

$= \begin{vmatrix} 418.25 \\ 740.75 \end{vmatrix} - \begin{vmatrix} -14.257 \\ -33.758 \end{vmatrix} = 35.25 - 122.25 = -87$

$A''^3 = \begin{bmatrix} 4618.25 \\ 7540.75 \end{bmatrix}$,

$\Rightarrow det(A''^3) = \begin{vmatrix} 4618.25 \\ 7540.75 \end{vmatrix} = \begin{vmatrix} 46 \\ 75 \end{vmatrix} +$

$(-1)^3 \begin{vmatrix} 4 - 618.25 \\ 7 - 540.75 \end{vmatrix}$

$$= \begin{vmatrix} 46 \\ 75 \end{vmatrix} - \begin{vmatrix} -218.25 \\ 2 \quad 40.75 \end{vmatrix} = -22 + 118 = 96$$

Therefore, we get

$y_1 = \frac{-1}{8} = -0.125,\qquad y_2 = \frac{-87}{8} = -10.875,$

$y_3 = \frac{96}{8} = 12$

i.e., $$y = \begin{bmatrix} y_1 \\ y_2 \\ y_3 \end{bmatrix} = \begin{bmatrix} -0.125 \\ -10.875 \\ 12 \end{bmatrix}$$

Hence the solution set is

$$\begin{bmatrix} (w_1, x_1, y_1) \\ (w_2, x_2, y_2) \\ (w_3, x_3, y_3) \end{bmatrix} = \begin{bmatrix} (-9.25, & -9.72, & -0.125) \\ (-10.25, & -37.34, & -10.875) \\ (20.5, & 48.06, & 12) \end{bmatrix}$$

By observing examples 1 and 2, we see that there is no need always to be the matrix square to solve the fully fuzzy system of linear equations in the above process. Square and rectangular, both types of fully fuzzy systems of linear equations, can be solved by this method using rule (i) and rule (ii), respectively. It is more generalized than the initial Cramer's rule method.

This solution set's figure (Fig. 2) is given below:

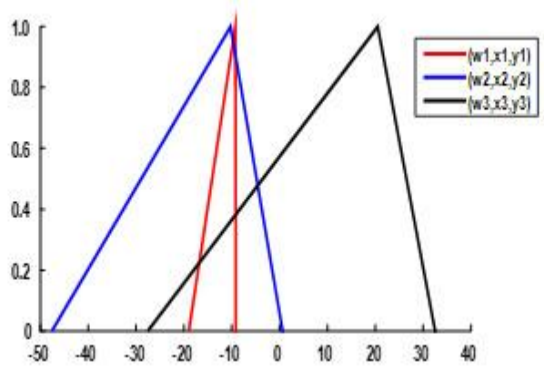


**Fig. 2. Solution set of the FFSLE of triangular LR fuzzy numbers in Cramer's rule (ii) for non-square coefficient matrix.**

### 4.2 Examples of fuzzy trapezoidal LR fuzzy numbers

**Example 3:** Consider the fully fuzzy linear system of equations of trapezoidal LR fuzzy numbers as follows:

$(4,5,1,2)(w_1, x_1, y_1, z_1)$
$\oplus\ (3,4,1,1)(w_2, x_2, y_2, z_2) = (25, 70, 26, 58)$

$(2,3,1,1)(w_1, x_1, y_1, z_1)$
$\oplus\ (5,8,1,2)(w_2, x_2, y_2, z_2) = (35, 90, 25, 55)$

where $A = \begin{bmatrix}4 & 3\\ 2 & 5\end{bmatrix}$, $L = \begin{bmatrix}5 & 4\\ 3 & 8\end{bmatrix}$,

$M = \begin{bmatrix}1 & 1\\ 1 & 1\end{bmatrix}$, $N = \begin{bmatrix}2 & 1\\ 1 & 2\end{bmatrix}$

$b = \begin{bmatrix}25\\ 35\end{bmatrix}, g = \begin{bmatrix}70\\ 90\end{bmatrix}$, $h = \begin{bmatrix}26\\ 25\end{bmatrix}$, $p = \begin{bmatrix}58\\ 55\end{bmatrix}$,

$w = \begin{bmatrix}w_1\\ w_2\end{bmatrix}$, $x = \begin{bmatrix}x_1\\ x_2\end{bmatrix}$, $y = \begin{bmatrix}y_1\\ y_2\end{bmatrix}$, $z = \begin{bmatrix}z_1\\ z_2\end{bmatrix}$

Here, the matrices A and L are square, so we follow this method's rule (i). Then we have

det(A)= 14

det(L)= 28

Now we calculate ($A^1$, $A^2$) and ($L^1$, $L^2$), which are obtained from A and L by replacing their $i^{th}$ column with b and g, respectively. Then

$A^1 = \begin{bmatrix}25 & 3\\ 35 & 5\end{bmatrix} \Longrightarrow det(A^1) = 20$

$A^2 = \begin{bmatrix}4 & 25\\ 2 & 35\end{bmatrix} \Longrightarrow det(A^2) = 90$

$L^1 = \begin{bmatrix}70 & 4\\ 90 & 8\end{bmatrix} \Longrightarrow det(L^1) = 200$

$L^2 = \begin{bmatrix}5 & 70\\ 3 & 90\end{bmatrix} \Longrightarrow det(L^1) = 240$

Therefore, we get

$w_1 = \frac{20}{14} = 1.43$, $w_2 = \frac{90}{14} = 6.43$, $x_1 = \frac{200}{28} = 7.14$, $x_2 = \frac{240}{28} = 8.57$

i.e., $w = \begin{bmatrix}w_1\\ w_2\end{bmatrix} = \begin{bmatrix}1.43\\ 6.43\end{bmatrix}$, $x = \begin{bmatrix}x_1\\ x_2\end{bmatrix} = \begin{bmatrix}7.14\\ 6.07\end{bmatrix}$

Now we calculate y and z, so first, we calculate$A'^{(i)}$ and $L'^{(i)}$, which denote matrices obtained from A and L by replacing their $i^{th}$ column by $h - Mw +$ Aw and $p - Nx + Lx$, respectively.

$$h - Mw + Aw = \begin{bmatrix}26\\ 25\end{bmatrix} - \begin{bmatrix}1 & 1\\ 1 & 1\end{bmatrix}\begin{bmatrix}1.43\\ 6.43\end{bmatrix} + \begin{bmatrix}4 & 3\\ 2 & 5\end{bmatrix}\begin{bmatrix}1.43\\ 6.43\end{bmatrix} = \begin{bmatrix}43.14\\ 52.14\end{bmatrix}$$

$$p - Nx + Lx = \begin{bmatrix}58\\ 55\end{bmatrix} - \begin{bmatrix}2 & 1\\ 1 & 2\end{bmatrix}\begin{bmatrix}7.14\\ 6.07\end{bmatrix} + \begin{bmatrix}5 & 4\\ 3 & 8\end{bmatrix}\begin{bmatrix}7.14\\ 6.07\end{bmatrix} = \begin{bmatrix}97.64\\ 105.71\end{bmatrix}$$

Now, $A'^1 = \begin{bmatrix}43.14 & 3\\ 52.14 & 5\end{bmatrix}$

$\Longrightarrow det(A'^1) = 59.28$

$A'^2 = \begin{bmatrix}4 & 43.14\\ 2 & 52.14\end{bmatrix}$

$\Longrightarrow det(A'^2) = 122.28$

Therefore, we get

$y_1 = \frac{59.28}{14} = 4.23$, $y_2 = \frac{122.28}{14} = 8.73$,

i.e., $y = \begin{bmatrix}y_1\\ y_2\end{bmatrix} = \begin{bmatrix}4.23\\ 8.73\end{bmatrix}$

Now, $L'^1 = \begin{bmatrix}97.64 & 4\\ 105.71 & 8\end{bmatrix}$

$\Longrightarrow det(A''^1) = 358.28$

$L'^2 = \begin{bmatrix}5 & 97.64\\ 3 & 105.71\end{bmatrix}$

$\Longrightarrow det(A''^2) = 235.63$

Therefore, we get

$z_1 = \frac{358.28}{28} = 12.80$, $z_2 = \frac{235.63}{28} = 8.41$,

i.e., $z = \begin{bmatrix}z_1\\ z_2\end{bmatrix} = \begin{bmatrix}12.80\\ 8.41\end{bmatrix}$

Hence, the solution set is

$$\begin{bmatrix}(w_1, x_1, y_1, z_1)\\ (w_2, x_2, y_2, z_2)\end{bmatrix} = \begin{bmatrix}(1.43, 7.14, 4.23, 12.80)\\ (6.43, 8.57, 8.73, 8.41)\end{bmatrix}$$

This solution set's figure (Fig. 3) is given below:

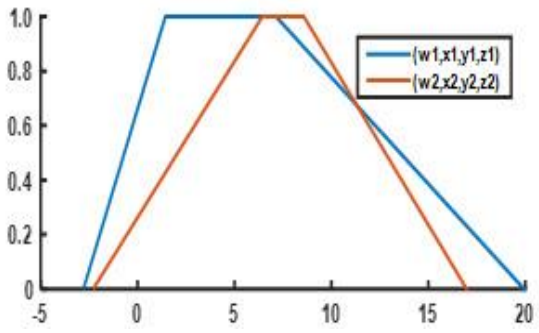


**Fig. 3. Solution set of the FFSLE of trapezoidal LR fuzzy numbers in Cramer's rule (i) for square coefficient matrix.**

**Example 4:** Consider the fully fuzzy linear system of equations of trapezoidal LR fuzzy numbers as follows:

$$(1,4,4,4)\otimes(w_1, x_1, y_1, z_1) \oplus (3,6,1,2) \otimes(w_2, x_2, y_2, z_2) \oplus (2,4,3,6)\otimes(w_3, x_3, y_3, z_3) = (10,36,172, 160)$$

$$(2,6,6,6)\otimes(w_1,x_1,y_1,z_1)\oplus(8,12,4,3)$$
$$\otimes(w_2,x_2,y_2,z_2)\oplus(6,9,4,6)\otimes(w_3,x_3,y_3,z_3)$$
$$=(20,42,216,186)$$

where $A=\begin{bmatrix}132\\286\end{bmatrix}$, $L=\begin{bmatrix}4&6&4\\6&12&9\end{bmatrix}$ $M=\begin{bmatrix}4&13\\6&44\end{bmatrix}$,

$$N=\begin{bmatrix}4&26\\6&36\end{bmatrix}$$

$b=\begin{bmatrix}10\\20\end{bmatrix}$, $g=\begin{bmatrix}36\\42\end{bmatrix}$, $h=\begin{bmatrix}172\\216\end{bmatrix}$, $p=\begin{bmatrix}160\\186\end{bmatrix}$

$w=\begin{bmatrix}w_1\\w_2\\w_3\end{bmatrix}$, $x=\begin{bmatrix}x_1\\x_2\\x_3\end{bmatrix}$, $y=\begin{bmatrix}y_1\\y_2\\y_3\end{bmatrix}$, $z=\begin{bmatrix}z_1\\z_2\\z_3\end{bmatrix}$

Here, we see that the matrices A and L are non-square matrices, so we follow rule (ii) (Joshi, 1980) in this method. Then we have

det(A)= $\begin{vmatrix}132\\286\end{vmatrix}=\begin{vmatrix}13\\28\end{vmatrix}+(-1)^3\begin{vmatrix}1-32\\2-86\end{vmatrix}=\begin{vmatrix}13\\28\end{vmatrix}-\begin{vmatrix}-22\\-66\end{vmatrix}=2-0=2$

det(L)= $\begin{vmatrix}4&6&4\\6&12&9\end{vmatrix}=\begin{vmatrix}4&6\\6&12\end{vmatrix}+(-1)^3\begin{vmatrix}4-6&4\\6-12&9\end{vmatrix}=\begin{vmatrix}4&6\\6&12\end{vmatrix}-\begin{vmatrix}-24\\-69\end{vmatrix}=4$

Now we calculate ($A^1$, $A^2$, $A^3$) and ($L^1$, $L^2$, $L^3$), which are obtained from A and L by replacing their $i^{th}$ column with b and g, respectively. Then

$A^1=\begin{bmatrix}1032\\2086\end{bmatrix}$,

$\Longrightarrow det(A^1)=\begin{vmatrix}1032\\2086\end{vmatrix}=\begin{vmatrix}103\\208\end{vmatrix}+(-1)^3\begin{vmatrix}10-32\\20-86\end{vmatrix}=\begin{vmatrix}103\\208\end{vmatrix}-\begin{vmatrix}7&2\\126\end{vmatrix}=20-18=2$

$A^2=\begin{bmatrix}1102\\2206\end{bmatrix}$,

$\Longrightarrow det(A^2)=\begin{vmatrix}1102\\2206\end{vmatrix}=\begin{vmatrix}110\\220\end{vmatrix}+(-1)^3\begin{vmatrix}1-102\\2-206\end{vmatrix}=\begin{vmatrix}110\\220\end{vmatrix}-\begin{vmatrix}-9&2\\-186\end{vmatrix}=0+18=18$

$A^3=\begin{bmatrix}1&3&10\\2&8&20\end{bmatrix}$,

$\Longrightarrow det(A^3)=\begin{vmatrix}1310\\2820\end{vmatrix}=\begin{vmatrix}13\\28\end{vmatrix}+(-1)^3\begin{vmatrix}1-310\\2-820\end{vmatrix}=\begin{vmatrix}13\\28\end{vmatrix}-\begin{vmatrix}-210\\-620\end{vmatrix}=2-20=-18$

$L^1=\begin{bmatrix}36&6&4\\42&12&9\end{bmatrix}$,

$\Longrightarrow det(L^1)=\begin{vmatrix}36&6&4\\42&12&9\end{vmatrix}=\begin{vmatrix}36&6\\42&12\end{vmatrix}+(-1)^3\begin{vmatrix}36-6&4\\42-12&9\end{vmatrix}=\begin{vmatrix}36&6\\42&12\end{vmatrix}-\begin{vmatrix}304\\309\end{vmatrix}=180-150=30$

$L^2=\begin{bmatrix}4364\\6429\end{bmatrix}$,

$\Longrightarrow det(L^2)=\begin{vmatrix}4364\\6429\end{vmatrix}=\begin{vmatrix}436\\642\end{vmatrix}+(-1)^3\begin{vmatrix}4-364\\6-429\end{vmatrix}=\begin{vmatrix}436\\642\end{vmatrix}-\begin{vmatrix}-324\\-369\end{vmatrix}=-48+144=96$

$L^3=\begin{bmatrix}4&6&36\\61&242\end{bmatrix}$,

$\Longrightarrow det(L^3)=\begin{vmatrix}4&6&36\\61&242\end{vmatrix}=\begin{vmatrix}4&6\\612\end{vmatrix}+(-1)^3\begin{vmatrix}4-6&36\\6-1242\end{vmatrix}=\begin{vmatrix}4&6\\612\end{vmatrix}-\begin{vmatrix}-236\\-642\end{vmatrix}=12-132=-120$

Therefore, we get

$w_1=\frac{2}{2}=1, w_2=\frac{18}{2}=9, w_3=\frac{-18}{2}=-9$

$x_1=\frac{30}{4}=7.5,\quad x_2=\frac{96}{4}=24,$

$$x_3=\frac{-120}{4}=-30$$

i.e., $w=\begin{bmatrix}w_1\\w_2\\w_3\end{bmatrix}=\begin{bmatrix}1\\9\\-9\end{bmatrix}$, $x=\begin{bmatrix}x_1\\x_2\\x_3\end{bmatrix}=\begin{bmatrix}7.5\\24\\-30\end{bmatrix}$

Now we calculate y and z, so first, we calculate$A'^{(i)}$ and $L'^{(i)}$, which denote matrices obtained from A and L by replacing their $i^{th}$ column by $h-Mw+$ Aw and $p-Nx+Lx$, respectively.

$$h-Mw+Aw=\begin{bmatrix}172\\216\end{bmatrix}-\begin{bmatrix}4&13\\6&44\end{bmatrix}\begin{bmatrix}1\\9\\-9\end{bmatrix}+\begin{bmatrix}132\\286\end{bmatrix}\begin{bmatrix}1\\9\\-9\end{bmatrix}=\begin{bmatrix}196\\230\end{bmatrix}$$

$$p - Nx + Lx = \begin{bmatrix}160\\186\end{bmatrix} - \begin{bmatrix}4 & 26\\6 & 36\end{bmatrix}\begin{bmatrix}7.5\\24\\-30\end{bmatrix} + \begin{bmatrix}4\ 6\ 4\\6129\end{bmatrix}\begin{bmatrix}7.5\\24\\-30\end{bmatrix} = \begin{bmatrix}316\\312\end{bmatrix}$$

Now, $A'^1 = \begin{bmatrix}19632\\23086\end{bmatrix}$

$\Rightarrow det(A'^1) = \begin{vmatrix}19632\\23086\end{vmatrix} = \begin{vmatrix}1963\\2308\end{vmatrix} +$
$(-1)^3 \begin{vmatrix}196-32\\230-86\end{vmatrix} = \begin{vmatrix}1963\\2308\end{vmatrix} - \begin{vmatrix}1932\\2226\end{vmatrix} = 878 - 714 = 164$

$A'^2 = \begin{bmatrix}11962\\22306\end{bmatrix}$,

$\Rightarrow det(A'^2) = \begin{vmatrix}11962\\22306\end{vmatrix}$

$= \begin{vmatrix}1196\\2230\end{vmatrix} + (-1)^3 \begin{vmatrix}1-1962\\2-2306\end{vmatrix}$

$= \begin{vmatrix}1196\\2230\end{vmatrix} - \begin{vmatrix}-1952\\-2286\end{vmatrix} = -162 + 714 = 552$

$A'^3 = \begin{bmatrix}13196\\28230\end{bmatrix}$,

$\Rightarrow det(A'^3) = \begin{vmatrix}13196\\28230\end{vmatrix} = \begin{vmatrix}13\\28\end{vmatrix} +$
$(-1)^3 \begin{vmatrix}1-3196\\2-8230\end{vmatrix} = \begin{vmatrix}13\\28\end{vmatrix} - \begin{vmatrix}-2196\\-6230\end{vmatrix} = 2 - 716 = -714$

Therefore, we get

$y_1 = \frac{164}{2} = 82,\ y_2 = \frac{552}{2} = 276,\quad y_3 = \frac{-714}{2} = -357$

i.e., $y = \begin{bmatrix}y_1\\y_2\\y_3\end{bmatrix} = \begin{bmatrix}82\\276\\-357\end{bmatrix}$

Now, $L'^1 = \begin{bmatrix}316\ 6\ 4\\312129\end{bmatrix}$,

$\Rightarrow det(L'^1) = \begin{vmatrix}316\ 6\ 4\\312129\end{vmatrix} = \begin{vmatrix}316\ 6\\31212\end{vmatrix} +$
$(-1)^3 \begin{vmatrix}316-6\ 4\\312-129\end{vmatrix} = \begin{vmatrix}316\ 6\\31212\end{vmatrix} - \begin{vmatrix}3104\\3009\end{vmatrix} = 1920 - 1590 = 330$

$L'^2 = \begin{bmatrix}43164\\63129\end{bmatrix}$,

$\Rightarrow det(\mathrm{L}'^2) = \begin{vmatrix}43164\\63129\end{vmatrix} = \begin{vmatrix}4316\\6312\end{vmatrix} +$
$(-1)^3 \begin{vmatrix}4-3164\\6-3129\end{vmatrix} = \begin{vmatrix}4316\\6312\end{vmatrix} - \begin{vmatrix}-3124\\-3069\end{vmatrix} = -648 + 1584 = 936$

$L'^3 = \begin{bmatrix}4\ 6\ 316\\612312\end{bmatrix}$,

$\Rightarrow det(L'^3) = \begin{vmatrix}4\ 6\ 316\\612312\end{vmatrix} = \begin{vmatrix}4\ 6\\612\end{vmatrix} +$
$(-1)^3 \begin{vmatrix}4-6\ 316\\6-12312\end{vmatrix} = \begin{vmatrix}4\ 6\\612\end{vmatrix} - \begin{vmatrix}-2316\\-6312\end{vmatrix} = 12 - 1272 = -1260$

Therefore, we get

$z_1 = \frac{330}{4} = 82.5, z_2 = \frac{936}{4} = 234,\quad z_3 = \frac{-1260}{4} = -315$

i.e., $z = \begin{bmatrix}z_1\\z_2\\z_3\end{bmatrix} = \begin{bmatrix}82.5\\234\\-315\end{bmatrix}$

Hence the solution set is

$$\begin{bmatrix}(w_1, x_1, y_1, z_1)\\(w_2, x_2, y_2, z_2)\\(w_3, x_3, y_3, z_3)\end{bmatrix} = \begin{bmatrix}(1,\ 7.5,\ 82,\ 82.5)\\(9,\ 24,\ 276,\ 234)\\(-9,-30,-357,-315)\end{bmatrix}$$

This solution set's figure (Fig.4) is given below:

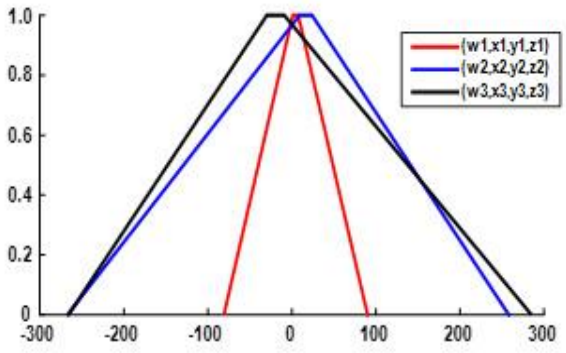


**Fig. 4. Solution set of the FFSLE of trapezoidal LR fuzzy numbers in Cramer's rule (ii) for non-square coefficient matrix.**

## Results and Discussion

In this work, we consider two cases for solving FFSLE: the triangular LR fuzzy numbers and the trapezoidal LR fuzzy numbers. We have used the determinate of square and non-square coefficient

matrix, the cross product of two fuzzy numbers, and the equality of fuzzy numbers. We have proposed a modified Cramer's rule method to solve the FFSLE. We have applied this proposed method using four numerical examples in two cases: according to the

first case (triangular LR fuzzy number), figure 1 and figure 2 are a graphical representation of the solution set of square and non-square coefficient matrices of FFSLE, respectively and figure 3 and figure 4 are graphical representation of the solution set of square and non-square coefficient matrices of FFSLE, respectively according to the second case (trapezoidal LR fuzzy number).

Compared with the previous work, we observe that the provided Modified Cramer's rules method can solve FFSLE with both square and non-square coefficient matrix, whereas the previous work could only solve the square coefficient matrix of FFSLE. So, the above-described modified methods are more generalized than the initial methods provided by the previous researchers.

We observed that all the above methods for describing trapezoidal numbers can also work for those methods in triangular numbers, but the converse is not always true.

In conclusion, the Modified Cramer's rules method for trapezoidal numbers is more generalized than those for triangular numbers.

All calculations were made using MATLAB tools.

## Future opinion

There are several avenues for further investigation:

- To investigate the formation of a fuzzy system of linear equations (FSLE)and a fully fuzzy system of linear equations (FFSLE) form for bell-shaped fuzzy numbers and Gaussian fuzzy numbers.
- To seek exact solutions to bell-shaped fuzzy numbers and Gaussian fuzzy numbers of FSLE and FFSLE through analytical methods.

## Author contribution

**Fatema Khatun:** Writing-review & editing, writing–original draft, conceptualization, lead, Methodology, Formal analysis, Software, resources, Validation, Investigation, Funding acquisition. **Md. Sahadat Hossain:** Writing-review & editing, Visualization, Supervision, conceptualization, Methodology, Formal analysis, Software, resources, Validation, Data curation. **Mst. Monjuara Akter:** Writing-review & editing, writing–original draft, conceptualization , Methodology, Formal analysis, Validation, Investigation.

## Conflict of Interest

The authors declare that they have no conflict of interest.

## Acknowledgements

The authors are grateful to the Editor-in-chief, the handling editor, and the anonymous referees for a number of helpful and perceptive comments for improving the manuscript. This work was partially supported by a grant from the National Science and Technology (NST), Government of Bangladesh, by providing NST fellowship. The first and third authors acknowledge this support, respectively.

## References

Abbasbandy S and Alavi M. A method for solving fuzzy linear systems. *Iran. J. Fuzzy Syst*. 2005; 2(2): 37-43.

Abbasbandy S, Ezzati Rand Jafarian A. LU decomposition method for solving fuzzy system of linear equations. *Appl. Math.Comput*. 2006; 172(1): 633-643.

Abbasbandy S, Jafarian Aand Ezzati R. Conjugate gradient method for fuzzy symmetric positive definite system of linear equations. *Appl. Math. Comput*. 2005; 171(2): 1184-1191.

Abbasbandy S, Otadi M and Mosleh M. Minimal solution of general dual fuzzy linear systems. *Chaos Solitons Fractals*, 2008; 37(4): 1113-1124.

Abbasi SMM and Jalali A. A novel approach for solving fully fuzzy linear systems and their duality. *J. Intell. Fuzzy Syst.* 2019; 37(2): 2609-2619.

Abidin AS, Mashadi M and Sri G. Algebraic modification of trapezoidal fuzzy numbers to complete fully fuzzy linear equations system using gauss-jacobi method. *Int. J. Manag. Fuzzy Syst.* 2019; 5(2): 40-46.

Allahviranloo T. Numerical methods for fuzzy system of linear equations. *Appl. Math.Comput.* 2004; 155(2): 493-502.

Allahviranloo, T. Successive over relaxation iterative method for fuzzy system of linear equations. *Appl. Math. Comput*. 2005; 162(1): 189-196.

Allahviranloo T and Ghanbari M. A new approach to obtain algebraic solution of interval linear systems. *Soft Comput*. 2012a; 16(1): 121-133.

Allahviranloo T and Ghanbari M. On the algebraic solution of fuzzy linear systems based on interval theory. *Appl. Math. Model*. 2012b; 36(11): 5360-5379.

Allahviranloo T and Hashemi A. The embedding method to obtain the solution of fuzzy linear systems. *Int.J.Ind.Math*. 2014; 6(3): 229-233.

Allahviranloo T and Salahshour S. Fuzzy symmetric solutions of fuzzy linear systems. *J.Comput. Appl. Math*. 2011; 235(16): 4545-4553.

Arunkumar M, Murthy S and Ganapathy G. Determinant for non-square matrices. *Int. J. Math. Sci. Eng. Appl*. 2011; 5(5): 389-401.

Asady B, Abbasbandy S and Alavi M. Fuzzy general linear systems. *Appl. Math. Comput*. 2005; 169(1): 34-40.

Buckley JJ and Qu Y. Solving linear and quadratic fuzzy equations. *Fuzzy Sets Syst*. 1990; 38(1): 43-59.

Buckley JJ and Qu Y. Solving systems of linear fuzzy equations. *Fuzzy Sets Syst*. 1991; 43(1): 33-43.

Chang S and Zadeh L. On fuzzy mapping and control. *IEEE Trans. Syst. Man Cybern*. 1972; 2(1): 30-34.

Dehghan M and Hashemi B. Iterative solution of fuzzy linear systems. *Appl. Math. Comput*. 2006; 175(1): 645-674.

Dehghan M, Hashemi B and Ghatee M. Solution of the fully fuzzy linear systems using iterative techniques. *Chaos, Solitons & Fractals*. 2007; 34(2): 316-336.

Dubois D and Prade H. Operations on fuzzy numbers. *Int. J. Syst. Sci.* 1978; 9(6): 613-626.

Elsayed AAA, Ahmad N and Malkawi G. On the solution of fully fuzzy Sylvester matrix equation with trapezoidal fuzzy numbers. *Comput. Appl. Math*. 2020; 39(4): 1-22.

Friedman M, Ming M and Kandel A. Fuzzy linear systems. *Fuzzy Sets Syst*. 1998; 96(2): 201-209.

Guo X and Shang D. Fuzzy approximate solution of positive fully fuzzy linear matrix equations. *J. Appl. Math*. 2013; 2013: 178209.

Islam MA and Hossain MS. Mathematical comparison of defuzzification of fuzzy logic controller for smart washing machine. *J. Bangladesh Acad.Sci.* 2022; 46(1): 1-8.

Joshi VN. A determinant for rectangular matrices. *Bull. Aust. Math. Soc*. 1980; 21(1): 137-146.

Karthik NJ and Chandrasekaran E. Solving fully fuzzy linear systems with trapezoidal fuzzy number matrices by partitioning the block matrices. *Ann. Pure Appl. Math.* 2014; 8(2): 261-267.

Khatun F and Hossain MS. Mathematically forecasting for generalized business by using fuzzy trapezoidal numbers. *J. Bangladesh Acad.Sci.* 2022; 45(2): 147-154.

Ma M, Friedman M and Kandel A. Duality in fuzzy linear systems. *Fuzzy Sets Syst.* 2000; 109(1): 55-58.

Malkawi G, Rida I and Ahmad N. An associated linear system approach for solving fully fuzzy linear system with hexagonal fuzzy number.

*Advances in Science and Engineering Technology International Conferences (ASET)*. IEEE 2018; 1-7.

Muruganandam S, Razak KA and Rajakumar K. Solving fully fuzzy linear systems by gauss jordan elimination method. In: *Journal of Physics: Conference Series, IOP Publishing*. 2019; 1362: 012087.

Muruganandam S and Razak KA. Matrix inversion method for solving fully fuzzy linear systems with triangular fuzzy numbers. *Int. J. Comput. Appl*. 2013; 65(4): 9-11.

Nikuie M and Ahmad MZ. Minimal solution of singular LR fuzzy linear systems. *Sci. World J*. 2014; 2014: 517218.

Radić M. About a determinant of rectangular matrix and its geometric interpretation. *Beiträge Zur Algebra Und Geometrie*. 2005; 46(2): 321-349.

Soylu G and Aslan ME. LR representation of TA fuzzy arithmetic and its application to solving fuzzy equations. *Iran. J. Fuzzy Syst*. 2022; 19(5): 63-78.

Zheng B and Wang K. General fuzzy linear systems. *App. Math.Comput.* 2006; 181(2): 1276-1286.

Ziqan A, Ibrahim S, Marabeh MAA and Qarariyah A. Fully fuzzy linear systems with trapezoidal and hexagonal fuzzy numbers. *Granul. Comput.* 2022; 7(2): 229-238.

J. Bangladesh Acad. Sci. 48(2); 161-163: December 2024 DOI:https://doi.org/10.3329/jbas.v48i2.70047

Journal of Bangladesh Academy of Sciences

Journal homepage: http://www.bas.org.bd/publications/jbas.html

**ResearchArticle**

# First confirmed record of *Schizodactylus monstrosus* (Orthoptera: Schizodactylidae) based on its nymph from Bangladesh

Azizul Islam Barkat, Ashikur Rahman Shome, Riffat Sultana[1] and Md. Fazle Rabbe[*]

*Department of Zoology, University of Dhaka, Dhaka, Bangladesh*

**ARTICLE INFO**

**Article History**

Received: 22 November 2023
Revised: 16 May 2024
Accepted: 06 July 2024

**Keywords:** Dune cricket, Nymph, Distribution, Diversity, Conservation, Sylhet hilly area.

**ABSTRACT**

The orthopteran insect group is poorly explored, and there is no confirmed record of any species under the Schizodactylidae family in Bangladesh. Here, we provided the first confirmed record of *Schizodactylus monstrous* under the family Schizodactylidae. A single individual of a species belonging to the family, a nymph of *Schizodactylus monstrous*, was sighted from a protected area of the country.

## Introduction

Schizodactylidae Blanchard (1845) is a family under the order Orthoptera characterized by unique and long tegmina or forewings that are spirally coiled at the posterior end in repose. The family consists of two genera: the winged *Schizodactylus* Brullé (1835), distributed from Turkey to China, and the wingless *Comicus* Brunner von Wattenwyl (1888), distributed in Africa (Leubner et al., 2017).

*Schizodactylus* possesses several peculiar features that distinguish it from other Ensiferans. Indeed, species of *Schizodactylus* have intimidating habits and apparent predatory adaptations, including raptorial prothoracic legs and powerful, enlarged mouthparts. Both nymphal and adult stages are solitary burrowers, and they prefer to inhabit moist, sandy areas where tunneling is easy. The genus *Schizodactylus* has been reported in China, Thailand, Myanmar, Bhutan, India, Sri Lanka, Pakistan, Afghanistan, and Turkey (He and Liu, 2021). Several new species have been described recently under the genus *Schizodactylus* (Dawwrueng et al., 2018; He and Liu, 2021). However, in India, the genus is represented by only *Schizodactylus monstrosus* Drury (1773). This species is documented in Pakistan and several parts of India, including Assam, Bihar, West Bengal, South India, Jammu and Kashmir, and Chhattisgarh (Chandra and Gupta, 2005), but there were no previous confirmed records of this insect family from Bangladesh with proper evidence. Ahmad (2008) mentioned species distribution in Bangladesh, India, and Pakistan based on a single literature (Maxwell-Lefroy, 1909). The article mentioned some areas, including Assam, Bihar, Karnataka, Sindh, and Punjab, where the species could be found, excluding Bangladesh.

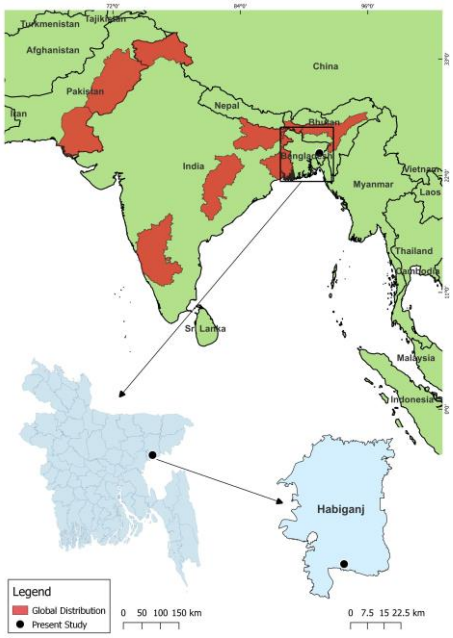


**Fig. 1. Global distribution of *Schizodactylus monstrosus* (Maxwell-Lefroy, 1909; Chandra and Gupta, 2005) and present record in Bangladesh.**

[*]Corresponding author:< fazle_zool@du.ac.bd>
[1]*Department of Zoology, University of Sindh, Jamshoro, Pakistan*

During a night survey on 11 August 2023 (at 12:45 AM), a single individual of a dune cricket was found on a sandy and dry stream bed at Satchari National Park (SNP), Habiganj, Bangladesh (24°07'34.9"N, 91°26'39.93"E) (Fig. 1). It is situated in Sylhet's hilly area and is one of the most diverse parks among the 22 bio-ecological zones of Bangladesh. The area is part of a protected National Park, and we were prohibited from collecting samples. Therefore, we only captured some photographs of the species and left the place. The nymph was approximately 2.5 cm long (Fig. 2), with robust eyes and long filiform antennae, longer than the body. Each scape of the antennae was broad with a black dot.

**Fig. 2. Lateral and dorsal view of *Schizodactylus monstrosus* observed in Satchari National Park, Habiganj, Bangladesh.**

The labrum and mandibles were significant, indicating its ferocious carnivorous nature. The cerci were white and long. The species consists of nine nymphal stages in development, and it takes more than a year to complete its life cycle. The insect walks very fast and often jumps on the sand bed. Adults cannot fly and generally do not unfold their wings. Only the ninth nymphal instar can fly. Adults can be identified based on the dichotomous key following Dawwrueng et al. (2018), while nymphal stages can be separated following Khattar (1972). According to existing knowledge (Khattar, 1972), the specimen is a sixth-instar nymph of *S. monstrosus*.

Little is known about the ecological importance of *S. monstrosus*. It is a burrowing insect commonly known as Dune cricket, Maize cricket, or Monster cricket. The species is extremely nocturnal and keeps in its long tunnel during the day. The tunnel the species makes is unbranched, running deeper until adequate humidity. They burrow the tunnel in the loose, sandy area with plenty of moisture. Excess dryness, hardness, or watery regions are not suitable for their survival. The insect is exclusively carnivorous and feeds on beetles, grasshoppers, and other insects (Khattar, 1972; Khatua et al., 2020).

The orthopteran diversity is poorly studied in Bangladesh, though this group of arthropods is considered one of the most destructive pest insects. Few studies have explored orthopteran diversity (Aktar et al., 2018; Mahdi et al., 2018). However, there were no previous confirmed records of the family from Bangladesh. Based on our understanding, this is the first confirmed record of the family with photographic evidence of the species in Bangladesh. Further studies are highly recommended to explore the status and ecology of the species in Bangladesh.

**Acknowledgment**

This study was opportunistically conducted during a field study in Satchari National Park and was funded by the Biotechnology Research Centre, University of Dhaka.

**Conflicts of Interest**

The author declares that there is no conflict of interest regarding the publication of this article.

**References**

Ahmad M. *Schizodactylus monstrosus*. In: Encyclopedia of Flora and Fauna of Bangladesh: Arthropoda: Insecta - I, *Asiatic Society of Bangladesh*. 2008; p. 157-158.

Aktar M, Islam MA and Alim MA. Orthopteran diversity at Keraniganj, Dhaka. *Bangladesh J. Zool.* 2018; 46: 21-32.

Chandra K and Gupta SK. Record of Monster Cricket, *Schizodactylus monstrosus* (Drury) (Schizodactylidae : Orthoptera) from Chhattisgarh. *Insect Env.* 2005; 11(2): 56.

Dawwrueng P, Panitvong N, Mooltham K, Meebenjamart P and Jaitrong W. First record of the family Schizodactylidae (Orthoptera: Ensifera) from Thailand, with the description of a new species. *Zootaxa*. 2018; 4472: 060-070.

He Z and Liu Y. A new species of Dune Cricket from China (Orthoptera: Ensifera: Schizodactylidae). *Zootaxa.* 2021; 4999: 356-362.

Khattar N. A description of the adult and the nymphal stages of *Schizodactylus monstrosus* (Drury) (Orthoptera). *J. Nat. Hist.* 1972; 6: 589-600.

Khatua S, Dhara S, Sahu R and Ghorai SK. Burrowing adaptations and anthropogenic threats of a dune cricket, *Schizodactylus monstrosus* (Drury) : A case study from Champa river bank, West Bengal, India. *Int. J. Exp. Res. Rev.* 2020; 23: 43-51.

Leubner F, Bradler S and Wipfler B. The thoracic morphology of the wingless dune cricket *Comicus calcaris* (Orthoptera: Schizodactylidae): Novel apomorphic characters for the group and adaptations to sand desert environments. *Arthropod Struct. Dev*. 2017; 46: 449-461.

Mahdi SHA, Ahmed M and Ahsan MK. Species diversity, seasonal abundance and morphometric analysis of grasshopper (Orthoptera: Caelifera) in Rajshahi city, Bangladesh. *Serangga*. 2018; 23: 24-34.

Maxwell-Lefroy H. Indian Insect Life. New Delhi, *Indian Agriculture Research Institute*. 1909; p.95.

J. Bangladesh Acad. Sci. 48(2); 165-170: December 2024 DOI:https://doi.org/10.3329/jbas.v48i2.70546

Journal of Bangladesh Academy of Sciences

Journal homepage: http://www.bas.org.bd/publications/jbas.html

**Research Article**

# A qualitative structure activity relationship (SAR) study of selected pyroglutamates

Halima Bagum*, Mark G. Moloney[1] and Md Rabiul Islam[2]

*The Department of Chemistry, University of Barishal, Barishal, Bangladesh*

**ARTICLE INFO**

**Article History**

Received: 24 December 2023
Revised: 16 May 2024
Accepted: 11 July 2024

**Keywords:** Antibacterial screening, Pyroglutamate, Pyrrolinone, Pyrrolidinone.

**ABSTRACT**

A library of pyroglutamate derivatives (Fig. 1-4: **8a-8f**, **9a-9d**, **10a-10e**, **11a-11f**, **12a-12c**, **13** and **14**) have been analyzed qualitatively to investigate their Structure Activity Relationships (SAR). Antibacterial screening data used for this work was against the selected multidrug-resistant pathogens, including Gram-positive and Gram-negative bacteria. Among the synthesized compounds, pyroglutamates **8e** and **11d** are more potent as antibacterial agents..

## Introduction

Pyrroglutamate is an intermediate of glutathione metabolism. It marks glutathione insufficiency. Glutathione, a potent anti-oxidant in the human body, is essential in throwing away toxins. Moreover, pyroglutamates play a vital role in drug discovery (Mollica et al., 2014; Stefanucci et al., 2015). We recently reported the preparation of highly functionalized pyroglutamates, pyrrolinones, and pyrrolidinones (Scheme 1) (Bagum et al., 2019a, 2019b, 2020). Antibacterial screening of the selected compounds was done (Table 1), which was further studied to find Structure-Activity Relationships, and we report the result of this work here.

## Test method for bioassay

Oxford Antibiotic Group, Austria, screened the novel compounds against selected multidrug-resistant pathogens. The compounds were examined in a primary 96-well plate screening assay, according to SOP 0906. The compounds were diluted in "MHB" (Mueller-Hinton broth) for a bacteria culture test to a standard solution of 1000 µg/mL, serially diluted, and overlaid with a microbe solution in a 104 CFU/mL concentration. At 35°C, the plates were incubated for 24 hours. MIC values were assessed by visual inspection of optical density, and complete bacterial growth inhibition was achieved by a clear saturation of the solution following SOP.

### *Antibacterial screening*

Representative compounds among the synthesized compounds were tested (Bagum et al., 2019a, 2019b, 2020) for antibacterial activity in the case of the following Gram-negative and Gram-positive bacteria (Table 1):

1. *E. coli* (EC 34)
2. *K. pneumoniae* (KL 18)
3. *P. aerogenosa* (PS 23)
4. Methicillin resistant *S. aureus* (MRSA 1)
5. Methicillin resistant *S. aureus* (MRSA 2)

It is to be mentioned that the antibacterial activity of selected compounds was not found against the tested Gram-negative bacteria (EC 34, KL 18, and PS 23).

## Results and Discussion

Compounds **8d** and **11d** showed antibacterial activity against Gram-positive bacteria MRSA1 and MRSA2. However, they showed no activity against Gram-negative bacteria EC 34, KL 18, and PS 23.

*Corresponding author:<halimaju35@gmail.com>

[1]*The Department of Chemistry, University of Oxford, Oxford, United Kingdom*
[2]*The Department of Chemistry, Jahangirnagar University, Savar, Dhaka, Bangladesh*

Compounds **10a**, **12c**, **13**, and **14** exhibited antibacterial activity against only MRSA2. The study on the structure of the compounds **8a-8f**, **9a-9d**, and **10a-10e** (Fig. 1) reveals that the presence of the –CHO group on the aromatic ring assists in exhibiting appreciable activity.

Similarly, pyroglutamates **11a-11f**, derived from cysteine, showed the contribution of the –CHO group to the activity (Fig. 2).

Comparing the structure and activities of **8d**, **10d**, and **11d** supports the previous observation of the antibacterial activity due to the presence of the –CHO group on the aromatic ring. The reduction of the –CHO group to the $–CH_2OH$ group lost the compound's activity, which is evident if we juxtapose the structure and activity of **8d** and **10d**. Again, compounds **8a**, **8b**, and **10a** have similar structures. They differ only in the presence or absence of methyl group at C-4, its stereochemistry, and unsaturation at C-6 (Fig. 1). The activity of **10a** showed moderate antibacterial activity against Gram-positive bacteria MRSA 2, whereas **8a** and **8b** are not active. This result implies that C-4 methyl is unnecessary for activity and provably imposes steric hindrance. Moreover, the presence of unsaturation at C-6 diminishes activity in case of 6(4-methoxyphenyl)- derivatives **8a**, **8b** and **9a**.

Of interest, **12c** showed appreciable activity. Observation of the structures of **11e** and **12c** (Fig. 2 and Fig. 3) showed that the presence of sulfoxide is essential for the antibacterial activity of 4-chlorophenyl pyroglutamate derivatives. Sulfur systems are inactive for all other systems (e.g., 4-methoxyphenyl, phenyl).

Moreover, *N*, *O*-acetaldeprotection of some inactive compounds, e.g., **9b** and **9c**, leads to weakly active compounds **13** and **14**, respectively (Fig. 4). This indicates that the hydrophilicity of compounds increases activity.

Generally, the presence of –CHO on the aromatic ring increases antibacterial activity in every series. In addition, for the 4-chlorophenyl derivative, the replacement of the S atom by sulfoxide increases antibacterial activity. The free NH and OH in pyroglutaminol help to improve activity, probably due to the increased solubility.

Among the compounds studied, pyroglutamates **8d** and **11d** are more potent antibacterial agents, while pyroglutaminols**13** and **14** are weakly active.

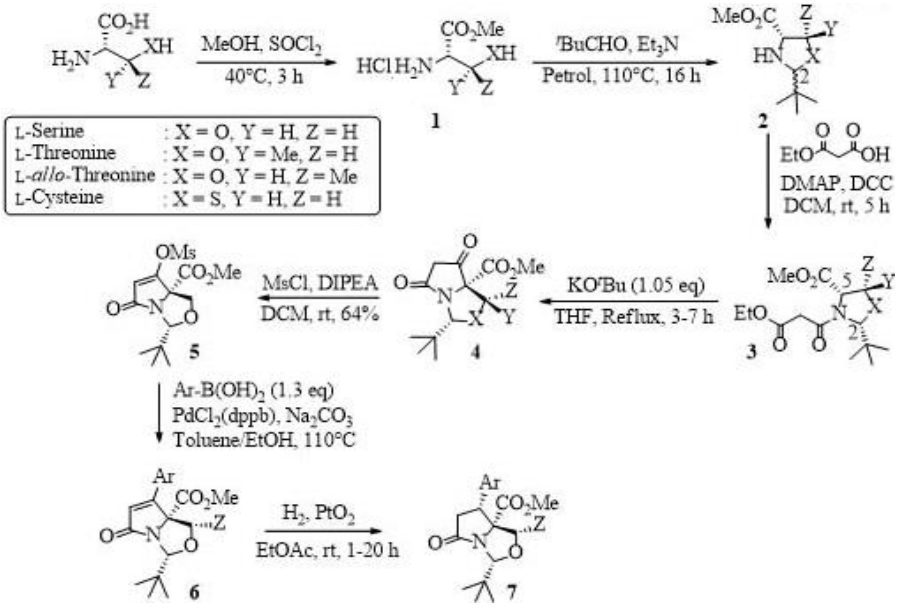


**Scheme 1. Preparation of highly functionalized pyroglutamates.**

**Table 1. MIC values for the screening of selected compounds against several pathogens.**

| Sl No | Compound | Gram-positive bacteria | |
|---|---|---|---|
| | | MRSA 1 | MRSA 2 |
| 1 | 8a | n. a. | n. a. |
| 2 | 8b | | |
| 3 | 8c | | |
| 4 | 8d | 31.25 µg/mL | 15.63 µg/mL |
| 5 | 8e | | |
| 6 | 8f | n. a. | n. a. |
| 7 | 9a | | |
| 8 | 9b | | |
| 9 | 9c | | |
| 10 | 9d | | |
| 11 | 10a | n. a. | 62.00 µg/mL |
| 12 | 10b | n. a. | n. a. |
| 13 | 10c | | |
| 14 | 10d | | |
| 15 | 10e | | |
| 16 | 11a | | |
| 17 | 11b | | |
| 18 | 11c | | |
| 19 | 11d | 15.63 µg/mL | 15.63 µg/mL |
| 20 | 11e | n. a. | n. a. |
| 21 | 11f | | - |
| 22 | 12a | | n. a. |
| 23 | 12b | | |
| 24 | 12c | n. a. | 31.25 µg/mL |
| 25 | 13 | n. a. | 125.00 µg/mL |
| 26 | 14 | n. a. | 125.00 µg/mL |

n. a. = not active

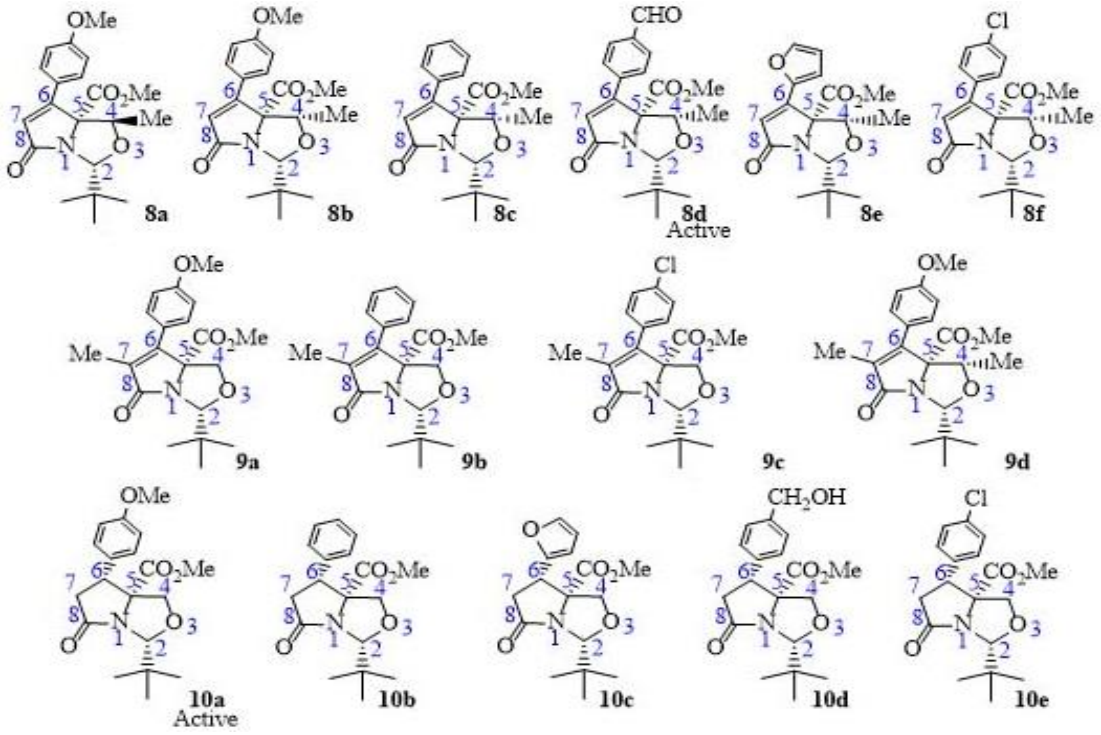


**Fig. 1. Pyroglutamates derived from L-Serine, L-Threonine and L-*allo*-Threonine**

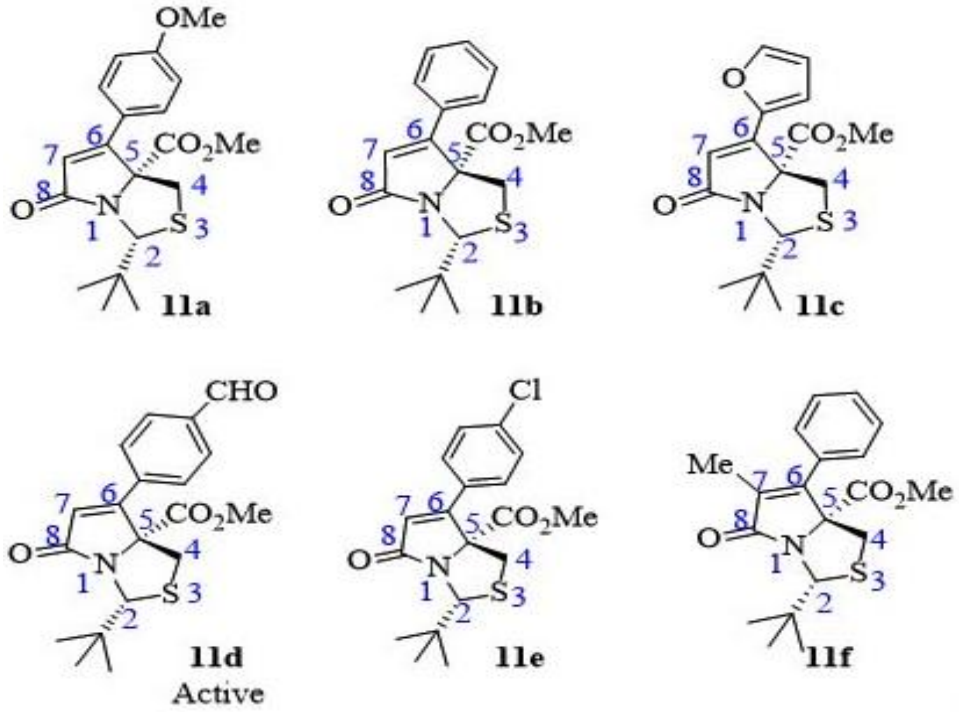


**Fig. 2. Pyroglutamates derived from L-Cysteine.**

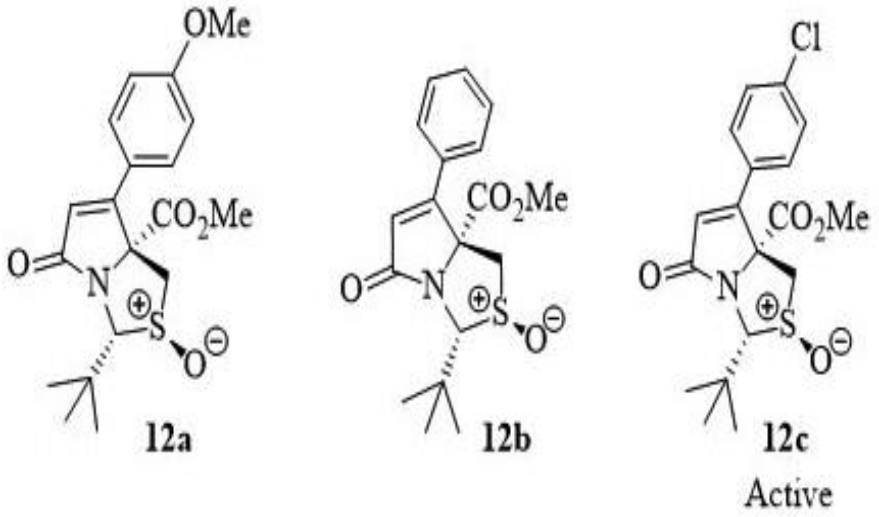


**Fig. 3. Sulfoxides.**

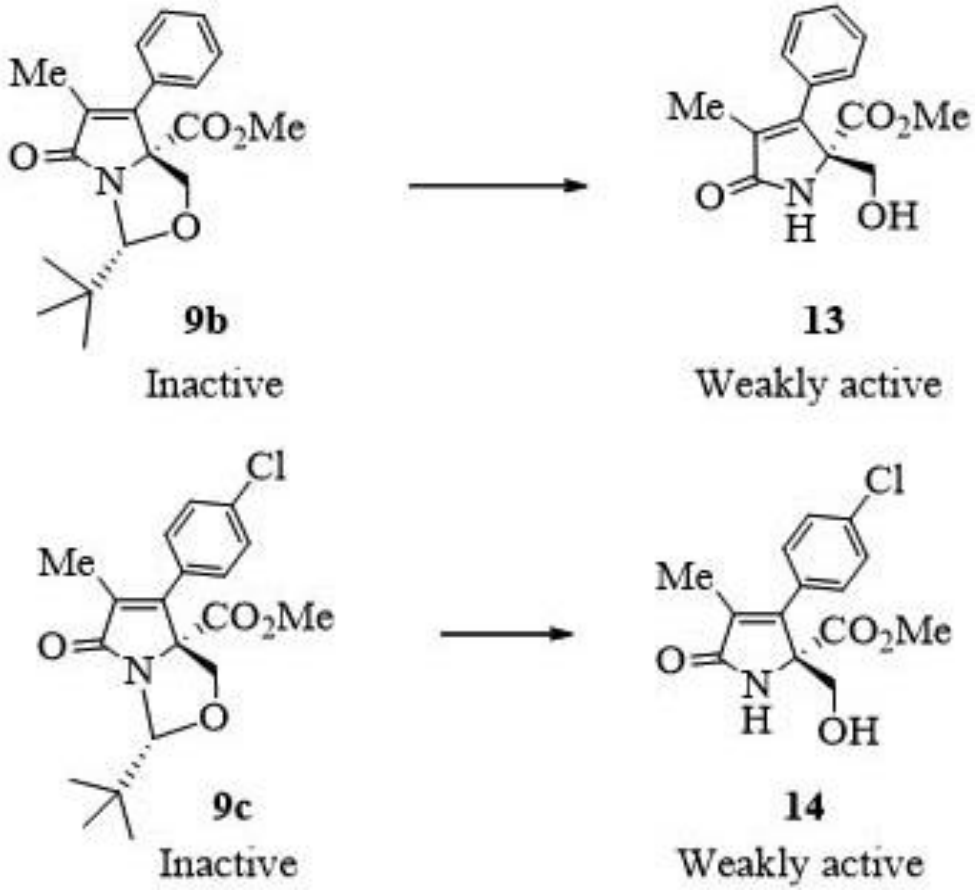


**Fig. 4.*N, O*-Acetaldeprotection of pyrrolinones to yield pyroglutaminol.**

## Conclusion

The Structure-Activity Relationships (SAR) of pyroglutamate derivatives were studied qualitatively. Compounds **8e** and **11d** showed antibacterial activity against Gram-positive bacteria MRSA1 and MRSA2. Compounds **10a**, **12c**, **13**, and **14** exhibited antibacterial activity against only MRSA2. It has been observed that the presence of the –CHO group on the aromatic ring assists in exhibiting appreciable activity. Also, the hydrophilicity of compounds increases activity.

## Acknowledgments

I want to take the opportunity to express my sincere appreciation to Professor M. G. Moloney for allowing me the chance to perform this study in his research batch. This research was furnished with the monetary reinforcement of the Commonwealth Scholarship Commission in the UK and the University of Oxford, UK.

## Conflict of Interest

The writers of this article announce that they have no conflict of interest.

## Authors Contribution

Begum, H., with the cooperation of Moloney, M. G., outlined the experiment. Bagum performed the analysis. Furthermore, Begum devised the article manuscript, and Islam, M. R., assessed it.

## References

Bagum H, Christensen KE, Genov M, Pretsch A, Pretsch D and Moloney MG. Synthetic access to 3-substituted pyroglutamic acids from tetramate derivatives of serine, threonine, *allo*-threonine, and cysteine. *J. Orga. Chem.*, 2019a; 84(16): 10257-10279.

Bagum H, Christensen KE, Genov M, Pretsch A, Pretsch D and Moloney MG. Synthetic access to 3,4-disubstituted pyroglutamates from tetramate derivatives from serine, allo-threonine and cysteine. *Tetrahedron*, 2019b; 75(40): 130561.

Bagum H, Shire BR, Christensen KE, Genov M, Pretsch A, Pretsch D and Moloney MG. Bicyclic lactams derived from serine or cysteine and 2-methylpropanal. *Synlett*, 2020; 31(4): 378-382.

Mollica A, Stefanucci A, Costante R and Novellino E. Pyroglutamic acid derivatives: building blocks for drug discovery. *Heterocycles*, 2014; 89(8): 1801.

Stefanucci A, Costante R, Carradori S, Novellino E and Mollica A. Synthetic strategies for aspartic and glutamic acid-proline chimeras: a review. *Mini-Rev. Org. Chem.* 2015; 12(3): 216-236.

J. Bangladesh Acad. Sci. 48(2); 171-184: December 2024 DOI:https://doi.org/10.3329/jbas.v48i2.72132

Journal of Bangladesh Academy of Sciences

Journal homepage: http://www.bas.org.bd/publications/jbas.html

**Research Article**

# Characterization of sewage sludge particles influencing dewaterability

M. Feroze Ahmed[*1] and Tanvir Ahmed[2]

*Department of Civil Engineering, University of Strathclyde, Glasgow, UK*

**ARTICLE INFO**

**Article History**

Received: 21 March 2024
Revised: 24 June 2024
Accepted: 14 July 2024

**Keywords:** Sewage sludge, Bound water, Surface charge, Particle size, Electrophoresis.

**ABSTRACT**

This study presents an investigation into the fundamental characteristics of sludge particles that influence the dewaterability of sewage sludge. Dewatering of sewage sludge is required for the reduction of sludge volume, sludge treatment, and safe disposal of sludges having very high pollution potentials. Particle characteristics important for dewatering, like particle size distribution, particle density, bound water content, surface charge, protein, and polysaccharide content of activated and digested sludges, were determined. Without a suitable method for analyzing the total range of particles in sewage sludge and effective density, new techniques have been developed to determine particle size distribution and particle density with reasonable accuracy. Particles larger than 45 µm were analyzed by wash sieving, while particles smaller than 45 µm were analyzed using a Coulter counter. The results from both methods were combined, maintaining their proportional contribution to the overall particle size distribution. Particle density was computed by determining the dry density and bound water content. Additionally, particle size and velocity were measured using an interference microscope, and these values were inserted into Stokes' Law equation to calculate the effective density of sludge particles.

## Introduction

Sewage sludge is an aqueous suspension of particulate solids composed of complex organic and inorganic matter with significant water within the particles. Coackley (1956) indicated that sludge is a mixture of proteins, fats, carbohydrates, polysaccharides, microorganisms, and floes composed of all or some of these materials, grit, and anything else that may get into the sewage system. Treatment and dewatering of sewage sludge have become very important to achieve sustainable sanitation development goals (SDG) (Target 6.2). Most developing countries are lagging behind the target of attaining safely managed sanitation in which on-site and off-site treatment and safe disposal of sludge are major barriers. Sludge contains 99 to around 95% water after proper sedimentation, depending on the type of sludge. Dewatering of sludge is required by drainage on the granular bed, vacuum , or pressure filtration, which tremendously reduces sludge volume for safe handling and treatment. Characteristics of sludge particles greatly influence the dewaterability of sludge.

Determining particle properties of sewage sludges is very difficult due to the complex nature of the particles. Some of the properties of activated and digested sludges have been determined with sufficient accuracy using acceptable methods. These properties include surface charge, bound water content, protein and polysaccharide content, and viscosity of sludges. Without standard procedures

[*]Corresponding author:<ferozeahmed45@gmail.com>
[1]*Stamford University Bangladesh, Dhaka, Bangladesh.*
[2]*Department of Civil Engineering, and Director, ITN-BUET Centre, Dhaka, Bangladesh.*

applicable to sewage sludges, the determination of particle size, particle size distribution, and particle density has always been complex. Still, these sludge particle characteristics are believed to influence sludge dewaterability significantly. Most of the investigators working on particle size and particle density of sewage sludges agree with the complexities of the problem of measuring these characteristics.

In this study, considering the relative importance of various characteristics of sludge particles, efforts have been made to develop new techniques for determining particle size distribution and particle density. Some other properties of activated and digested sludge particles, such as surface charge, bound water content, protein and polysaccharide content, and viscosity of sludges, are also measured with sufficient accuracy using acceptable methods used by most investigators to evaluate mutual interaction and relative influence on sludge dewaterability.

## Materials and Methods

### *Sampling*

Sewage sludge is a liquid-solid suspension resulting from the sedimentation phase of wastewater treatment. The high concentration of active microorganisms in sludge causes rapid changes in its characteristics. To reduce the effect of microbial action on sludge particles, fresh activated and digested sludge samples were collected in the morning from the Dalmernock Sewage Treatment Plant and the Philipshill Sewage Works in Scotland, respectively, on pre-scheduled dates for conducting laboratory experiments. Experiments on several batches of samples were conducted over nine months.

### *Particle Size Analysis*

The main objectives of this work were to examine the basic characteristics of the sludge particle, including particle size distribution, surface charge, bound water content, protein and polysaccharide content, and viscosity of sewage sludge. These characteristics of sludge particles greatly influence the dewaterability of sludge. Microscopic examination of sludge particles was made using Vicker's M41 Photoplan microscope. The M41 Photoplan is designed on a modular basis, allowing the use of many accessory components that cover the most widely used microscope techniques. Comprehensive camera facilities cover all the photographic requirements of a routine or research laboratory. The photographs of digested and activated sludges were taken as shown in Figs. 1 and 2, and a few drops of sludges were spread over microscope slides as instructed in the manual. The photographs of sludges show that they are composed of particles of different sizes and shapes, and many of the particles are aggregates of small particles.

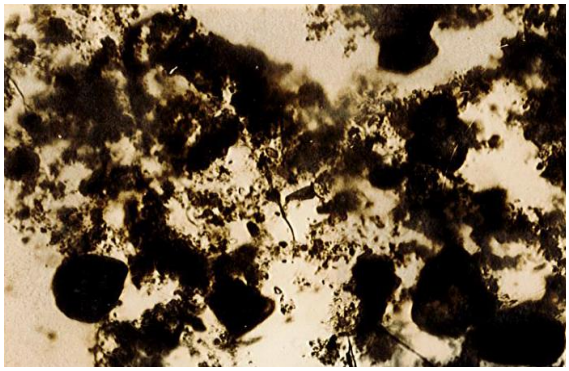

**Fig. 1. Digested sludge particles (300X).**

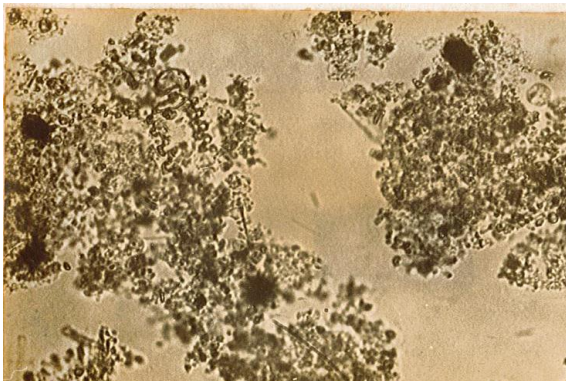

**Fig. 2. Activated sludge particles (300X).**

Digested sludge comprises larger particles and activated sludge particles are clusters of biomasses in the liquor. Small primary particles, such as microorganisms visible at higher magnification, are held together by surface polymers to form flocs.

The photograph of digested sludge particles shown in Fig. 1 indicates that digested sludge comprises particles of different sizes and shapes. Activated sludge particles are aggregates of smaller particles. The visual examination (Fig. 2) has good agreement with the observations made by Javaheri and Dick (1969) for activated sludge.

In the study of the dewaterability of sewage sludges, analysis of particle size and its distribution with reasonable accuracy is required, but a lack of proper techniques to measure such a wide range of particles of a complex nature is a barrier to investigating the influence of particle size on dewatering behavior of sewage sludges. Previous investigators have used different techniques for fractionating and particle size analysis, such as sedimentation, elutriation, centrifugation, sieve analysis, coulter counter, and microscopic analysis. In sedimentation and elutriation techniques, the particles are fractionated based on their settling velocity, primarily dependent on particle size and the effective density of the particles. Waring (1961), using a modified, improved version of Jone's (1954) elutriator, could achieve little success in fractionating sewage sludge. The failure was probably for two reasons:

(1) Many large fibrous particles entrap fines and settle rapidly, but the fines are released under favorable conditions.

(2) During the elutriation process, fragile aggregate formation is observed, probably due to the reduction of surface charges because of washing the sludge's alkalinity. The fragile aggregates settle with higher velocity than the settling velocity of individual units.

The main difficulty in particle fractionation by sedimentation and elutriation arises from the low effective density of the sludge particles. The larger particles fractionated by sedimentation, as observed under a microscope, are not free from fines. Centrifuging can successfully fractionate sludge particles of smaller size with very low settling velocity, but centrifuging is an accelerating process; the result is the same as elutriation (Coackley, 1965). Moreover, the fractionated particles obtained as a compressed cake at the bottom of the tube could not be dispersed in water to bring back the original properties of the particles. Particle size can be measured very accurately with the help of a microscope, and a particle size distribution can be obtained by counting a large number of particles. The method is tedious, especially for sludges with a wide range of particles, appearing on different levels of focus.

Moreover, difficulty arises in the identification of individual particles. Due to its gelatinous nature, sludge can only be easily sieved by wet sieving B.S. 1377 method (British Standard Institution, 1975) if it is dispersed in enough water. As particles are compressible, there exists a possibility of passing larger particles through smaller sieve sizes, and a layer of sludge deposited on the sieve prevents the passing of particles smaller than the sieve size. The Coulter counter has been used successfully for the analysis of the finer fractions of sludge particles (Abdel-Magid, 1982; Armanazi, 1977; Aziz, 1974; Elhassan, 1973; Faisst, 1980; Smyllie, 1969), but it cannot measure the larger size of particles present in sludge with reasonable accuracy. The error in the analysis of larger particles also arises from the breakup of the particles or floes due to agitation of the stirrer, which is required to keep the larger particles in suspension during analysis by the Coulter counter.

It has been found that larger sewage sludge particles can be easily fractionated by wash sieving under gentle water spray. Considering the advantages and disadvantages of the different methods, it was decided to use both sieves and the Coulter counter to analyze the total range of particles in sewage sludge. The compatibility of the two methods was checked by examining the common size fraction between $45x10^{-6}$m and $75x10^{-6}$ m, which both sieves and the Coulter counter can analyze. The result showed that particle size analysis by wash sieving matched better

than wet sieving with Coulter counter analysis (Table 1). In the analysis of the particle size distribution of the original sludge, a $100x10^{-6}m^3$ portion of representative sludge sample was diluted in $200x10^{-6}m^3$ distilled water and sieved through $599x10^{-6}$m, $300x10^{-6}$m, $150x10^{-6}$m, $75x10^{-6}$m and $45x10^{-6}$m sieves in succession by wash sieving. The Coulter counter model ZB analyzed particles passing the $45x10^{-6}$m sieve and added them to the larger sizes obtained by sieve analysis to get the total particle size distribution. Thus, particle size analysis using wash sieving and Coulter counter becomes a new technique for constructing particle size distribution curves of sewage sludge.

***Particle Electrophoresis***

Electrophoresis refers to the motion of charged particles when an electric field is applied. When the particle's velocity is measured, it is possible to calculate the electrical potential at the surface of the shear between the particle and the surrounding medium and the electrical charge contained within the surface of the shear. A particle's surface potential and charge are reproducible quantities that give information about how the particle can interact with other particles and the nature of the particle surface. The surface charge of sewage sludge particles is considered one of the fundamental properties influencing surface activity and behavior towards settling and filtration (Jorden, 1963, Maulik et al., 1967; Yukawa 1971). The electrophoretic mobility of sludge particles was determined using particle electrophoresis apparatus Mk. II of Rank Brothers.

Since electroosmosis occurs in the cell's content when the electric field is applied, the mobility of the particles was observed at the 'stationary levels' of the cell. The 'stationary levels' were computed using the Komagata formula quoted by Show (1969).

$$\frac{s}{d} = 0.500 - \left(0.0833 + \frac{32}{n5}\frac{d}{h}\right)½ \quad (1)$$

where s is the distance of stationary levels from the faces of the cell, and d and h are the width and height of the cell section, respectively. The flat cell was then filled with the suspension of sludge particles and placed in the bath containing water at $25^0$C, where the stationary levels were located. The particles were timed alternatively by reversing the polarity of electrodes to eliminate any effect of drift, and electrophoretic velocities were determined from the equation:

$$U_e = \frac{x/t}{Ve/1} \quad (2)$$

where $U_e$ is the electrophoretic velocity, t is the time required for a particle to travel a distance x under the applied voltage, Ve. l is the effective interelectrode distance.

***Bound Water***

Bound water is defined as water in the vicinity of macromolecules whose properties differ from those of bulk water. Bound water of sewage sludges has been measured by the Dilatometer technique and Differential Thermal Analysis (DTA) technique (Heukelekian and Weisberg, 1956; Katsiris, 1977; Peters, 1972). The Differential Thermal Analysis method used in this study has been proven to be reliable, fast, and very useful for studying the bound water content and consequently, the properties of the surface of the sludge particles (Katsiris, 1977). The method of bound water determination by DTA is based on the theory that the bound water does not freeze at temperatures below the freezing point of the free water. The area between the DTA curve and the baseline, i.e. $\int \Delta T dt$, within the limits of the beginning of the effect and its return to the baseline, expresses quantitatively the amount of active substance, i.e., the free water. The difference between total and free water is the bound water of the sludge (Table 2). The apparatus used for this study was a Stanton Redcroft Differential Thermal Analyzer, model 671.

***Particle Density***

Density is one of the fundamental properties of sludge particles. It has great importance in any solid-liquid separation technique, especially in the study of settleability and filterability. Unfortunately, its determination for sewage sludges is difficult, if not impossible, because of the physio-chemical nature of sludge particles. Despite the importance of particle

density, minimal effort has been made to evaluate this characteristic of sewage sludge. Hall (1962) tried density bottles to determine sludge density and achieved little success. Smyllie (1969) used a centrifuge technique to determine particle density, in fact, discovered the density of centrifuged sludge cake. Waring (1961) and Coakley and Kliger (1964) used an interference microscope to measure the particle density of sewage sludge. El Hassan (1973) applied the same interferometric method to measure the density of particles in secondary effluent. In this study, attempts have been made to determine the density of sludge particles from settling velocity and a new technique for computing the density of sludge particles from the densities of different components (fixed residue, volatile solids, and bound water) of sludge particles.

The computation of the density of sludge particles $\rho_{SP}$, or effective density , $\rho_{sp} - \rho_w$, using the following Stokes law requires the values of settling velocity, $V_{SP}$ and size of the particle, $D_{SP}$ where values of acceleration due to gravity 'g' and dynamic viscosity 'μ' are known.

$$V_{sp} = \frac{1}{18} \left(\frac{\rho_{sp}-\rho_w}{\mu}\right) g \ {D_{sp}}^2 \quad (3)$$

The experimental determination of these two parameters is not simple for sludge particles, which cannot be identified without a microscope. This work uses the particle microelectrophoresis apparatus with a flat cell to determine particles' size and settling velocity.

Sludge solids may be classified broadly into volatile and fixed solids, and water may be classified as free water in which the particles are suspended and bound with water present in and around the particles and moving with the particles. The general equation representing the density of sludge can be written as:

$$\frac{1}{p_s} = \frac{m_v}{p_v} + \frac{m_f}{p_f} + \frac{m_{bw}}{p_w} + \frac{m_{fw}}{p_w} \quad (4)$$

where $m_V$, $m_f$, $m_{bw}$, and $m_{fw}$ are the mass fractions of volatile solids, fixed solids, bound water,and free water, respectively. $\rho_V$,$\rho_f$ and $\rho_W$ are the densities of volatile solids, fixed solids, and water, respectively.

The density of sludge particles $\rho_{SP}$ is important, which can be written from Eqn. (4) considering the particle phase only, i.e., excluding free water component as:

$$\frac{1}{p_{sp}} = \frac{m_{sd}}{p_{sd}} + \frac{m_{bw}}{p_w} \quad (5)$$

Where

$$\frac{m_{sd}}{p_{sd}} = \frac{m_v}{p_v} + \frac{m_f}{p_f} \quad (6)$$

$m_{Sd}$is the mass fraction of dry sludge, and $p_{Sd}$ is its density. Therefore $m_{Sd}/\ p_{Sd}$ represents the volume fraction of dry solids in the sludge particles. The effective density of the particles, $\rho_{SP}-\rho_W$, can be written from Eqn. (5) in terms of bound water as:

$$p_{sp} - p_w = \frac{p_{sd}-p_w}{1+\frac{p_{sd}m_{bw}}{p_w\ m_{sd}}} \quad (7)$$

where $m_{bw}/m_{Sd}$ is the bound water of the sludge particles, the value of which largely determines the density of the particles. Hence, as the bound water content of the sludge particles increases, the density of the particles approaches that of water, i.e., the effective density approaches near zero. As a result, the particles at very low effective density tend to remain in suspension.

When the bound water content measured in this study by DTA represents the water associated with the particles, determining dry density,$\rho_{Sd}$ is required to compute particle density, $\rho_{SP}$ using eqn. (5 or 7). The dry density of sludge particles can be measured using a specific gravity bottle. The procedure for determining the specific gravity of solids, as described in BS 1377 (British Standard Institution, 1975), was followed with some modifications.

The dry density of the sludge solids was computed using the equation:

$$p_{sd} = \frac{m_{sd}}{V_b-(\frac{m_s-m_{sd}}{p_w})} \quad (8)$$

where $V_b$ is the volume of the sp. gr. bottle calibrated by weighing the mass of water at a known

temperature required to fill the bottle; $m_S$ is the mass of sludge needed to fill the same bottle. The sludge is deaired under a vacuum before weighing to remove any gas entrapped in the sludge particles; $m_{Sd}$is the mass of dry solids in the sludge mass $m_S$ determined by drying in an oven at $103^0$C - 105°C. To obtain a better understanding of the density of volatile and fixed components of sludge solids, the mass fraction of fixed solids and their density were determined for digested and activated sludges. The density of the volatile component of the solids, $\rho_v$ then computed using Eqn. (6) and presented in Table 3.

***Protein and Polysaccharide Content***

The protein content of sewage sludges was determined by the method used by Coackley (1950-52). The method involves the determination of organic nitrogen which is the difference between total and ammoniacal nitrogen. The protein content is then determined by using the relationship:

Protein content = 6.25 (Total nitrogen - Ammoniacal nitrogen).

Ammoniacal nitrogen was determined by Nesslerization using an optical spectrophotometer as described in standard methods (APHA, AWWA, WPCF, 1980). Total nitrogen was determined by Kjeldahl digestion.

The method followed for the extraction of polysaccharides was like that used by Zang (1966), Pavoni et al. (1972), and Brand (1982). 25 ml of properly settled sludge was diluted to 200 ml. with distilled water and boiled for 20 minutes. The boiled sample was centrifuged at 3000 rpm for 20 minutes. The supernatant liquor was decanted. The precipitates were washed with distilled water, diluted to 200 ml., boiled and centrifuged as before. Each time, the trace of polysaccharides in the decanted liquor was detected by the Anthrone test. The process continued until the diluting water could not extract some polysaccharides from the sediments. The concentration of polysaccharides in the combined supernatant liquor was determined by the Anthrone test.

***Viscosity***

The resistance to movement of one layer of fluid over an adjacent one is ascribed to the fluid's viscosity, but the presence of sewage particles increases resistance to such movement. Newton postulated that, for the straight and parallel motion of a fluid, the tangential stress, $\tau$, between two adjacent layers is proportional to the velocity gradient, $\frac{dv}{dy}$in the direction perpendicular to the layer, i.e.

$$\tau = \mu \frac{dv}{dy} \quad (9)$$

where the constant of the proportionality, μ, is termed the liquid's viscosity, which is a characteristic physical property of the liquid at a given temperature. From Eqn. (9), viscosity may be defined as the tangential shear force per unit area that will produce a unit velocity gradient. Hence, viscosity can be determined by measuring either the rate of shear caused by a known shear stress or the shear stress required to induce a known rate of shear.

The apparatus used was a Ferranti viscometer model VM. The viscometer consists of a rotating outer cylinder driven by a small two-phase synchronous motor of high torque and an inner cylinder suspended in jeweled bearings and situated co-axially within the outer cylinder. The resulting rotation of the liquid exerts a viscous drag on the inner cylinder, which is free to rotate against a calibrated spring with a pointer to show the angular deflection. The deflection is proportional to the viscosity of the liquid. To determine the behavior of non-Newtonian fluids, a wide range of shear rates may be produced by the combined effect of a quick-change 3-speed gearbox and a set of three interchangeable inner cylinders. This means the range of the instrument may be extended from low to high viscosity units. The instrument was verified for accuracy at various speeds with different combinations of cylinders, using oils of different viscosities. The viscosity of sludge was then measured at different shear rates using multiple combinations of cylinders and gears.

## Results and Discussion

The visual examination of sludge particles revealed their size, distribution, and aggregation modes. The particles present in activated sludge and digested sludge, based on visual examination, may be classified into three major classes:

- Primary particles, include microorganisms, fine cellulose, silt, clay and other fine-grained materials that find their way into the sludge. The size of these particles may vary from 0.5 to 10 µm.
- Flocs or coagulated particles are formed by bio-flocculation and conditions favorable for flocculation during treatment. The size of floes ranges from 5 to 100 µm.
- Fragile aggregates; formed by the loose grouping of flocs or primary particles under favorable conditions. They disperse on agitation or change in the liquid environment.

The particle size distribution of digested sludge from Philips Hill sewage works and activated sludge from Dalmarnock sewage treatment plant have been shown in Fig. 3. It may be observed that activated sludge has 86% particles finer than $45x10^{6}$ m whereas digested sludge has 50% particles finer than that size, although the concentration of fines smaller than $12x10^{-6}$m is nearly equal in both sludges. This difference in particle size distribution is also visible in microscopic views in Figs. 1 and 2. The higher percentage of large particles in digested sludge was probably because both primary and secondary sludges were being digested together, and the total particle size distribution was influenced by the presence of larger particles in the primary sludge. The digestion process has also promoted particle aggregation to larger sizes. A sample calculation combining the results of two different methods of particle size analysis is shown in Table 1. The availability of the total particle distribution in sludge, for the first time, will now help determine the parameters influencing filterability, such as effective size ($d_{10}$), median size ($d_{50}$), uniformity coefficient ($\frac{d_{60}}{d_{10}}$), and the slope of the particle size distribution curve.

The distribution of electrophoretic velocities of digested and activated sludge particles has been shown in Fig. 4. The mean electrophoretic velocity of activated sludge particles was found to be $1.66x10^{-8}m^2\ sec^{-1}\ volt^{-1}$ (SD 6.99%), and that of

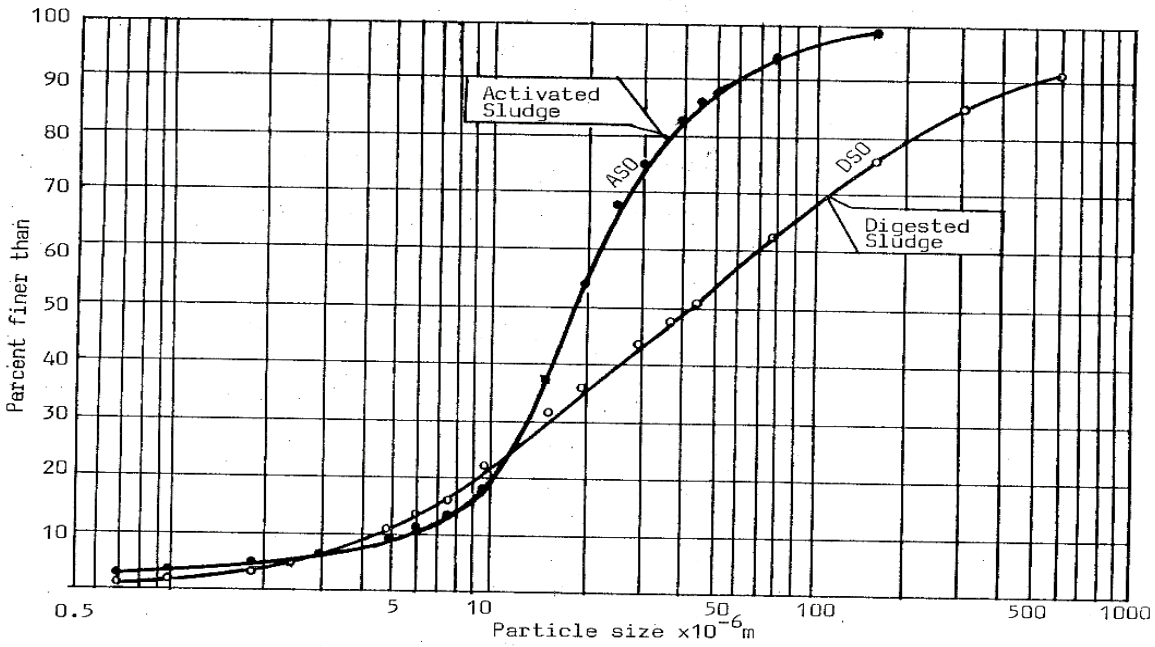


**Fig. 3. Particle size distribution of activated and digested sludges**

**Table 1. Computation of total particle size distribution combining the results of sieve and Coulter counter analysis.**

| Range of Tools for Analysis | Particle Size $x10^{-6}m$ | Materials Passing | % Materials Passing | Multiplier | Percent Finer |
|---|---|---|---|---|---|
| Range of Sieve | - | 5.460 | 100.00 | | 100.00 |
| | 599 | 4.969 | 91.01 | | 91.01 |
| | 300 | 4.619 | 84.60 | | 84.60 |
| | 150 | 4.157 | 76.14 | | 76.14 |
| | 75 | 3.458 | 63.33 | | 63.33 |
| | 45 | 2.723 | 49.87 | | 49.87 |
| Range of Coulter counter | 39.79 | | 96.06 | X 0.4987 = | 47.91 |
| | 31.79 | | 86.84 | | 43.31 |
| | 24.75 | | 79.84 | | 39.82 |
| | 19.64 | | 71.82 | | 35.82 |
| | 15.59 | | 62.51 | | 31.17 |
| | 9.89 | | 44.94 | | 22.41 |
| | 7.79 | | 32.96 | | 16.44 |
| | 6.19 | | 23.81 | | 11.87 |
| | 4.91 | | 20.26 | | 10.10 |
| | 3.09 | | 13.50 | | 6.73 |
| | 2.45 | | 10.09 | | 5.03 |
| | 1.94 | | 7.81 | | 3.85 |
| | 1.08 | | 4.19 | | 2.09 |
| | 0.68 | | 1.64 | | 0.82 |
| Range Projected | 0.43 | | 0.60 | | 0.30 |
| | 0.00 | | 0.00 | | 0.00 |

Note: The fraction of particles <45µm is within Coulter Counter's range which is distributed as 100% and then multiplied by fraction <45µm (0.4987) to obtain % finer.

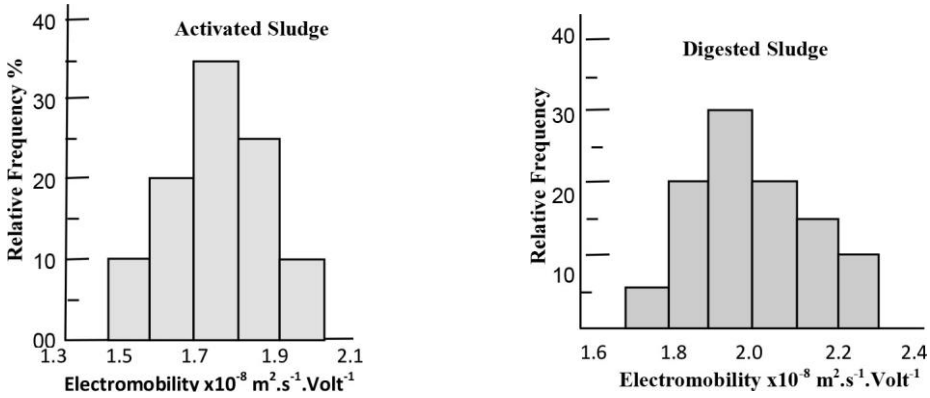


**Fig. 4. Distribution of electrophoretic velocities of activated and digested sludge**

digested sludge particle was $1.99 \times 10^{-8} m^2\ sec^{-1}\ volt^{-1}$ (SD 7.15%). The corresponding electrical potentials at the shear surface between the particles and surrounding medium are $21.33 \times 10^{-3}$ volts and $25.57 \times 10^{-3}$ volts for activated and digested sludge respectively.

The electrophoretic mobilities obtained agree with the values obtained by other investigators (Coackley, 1950-52; Elhassan, 1973; Katsiris, 1977; Langmuir, 1975). As mentioned by Coackley (1959), the reason for the higher velocities in the digested sludge is that there are many more ions in the liquid surrounding the particles; the adsorption of some of these ions may tend to give the particles a higher charge.

The computation of bound water from experimental data has been shown in Table 2. The bound water contents of activated and digested sludge, expressed as a bound water/dry solids ratio, were 9.60 and 4.21, respectively.

Katsiris (1977) used a dilatometer and DTA techniques to determine the bound water content. They found that the activated sludge he examined had a bound water content in the range of 900 to 1100 percent on dry solids, while digested sludge had a bound water content of 300 percent.

Peters (1972) and Forster and Lewin (1972) reported similar values for the bound water of activated sludge, both using a dilatometer. Heukelekian and Weisberg (1956) found a lower value of bound water content in digested sludge. The results clearly indicate that the bound water content is directly related to the sludge's organic matter content.

The distribution of settling velocities of activated and digested sludge particles of nearly the same size (around 20 µm) and shape is shown in Fig. 5. The average settling velocities of activated and digested sludges were found to be 6.860 µm/s (SD 2.152) and

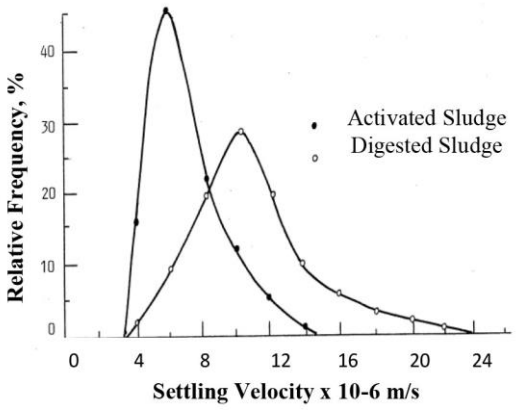


**Fig. 5. Distribution of settling velocities of activated and digested sludge particles.**

**Table 2. Differential thermal analysis of free and bound water.**

| Cooling rate: 3°C/min<br>Range of Temp: +20°C to -20°C<br>Amplifier: 250 µV | | | Recorder<br>T(x-axis) : 0.2 mV/cm<br>ΔT (y-axis): 2mV/cm | | | |
|---|---|---|---|---|---|---|
| **Sludge Type** | **Mass of Sludge (mg)** | **Dry Sludge (mg)** | **Total Water (mg)** | **Free Water (mg)** | **Bound Water/ Dry Sludge** | **Average Value of Bound Water** |
| | 56.5 | 1.1 | 55.4 | 43.8 | 10.55 | |
| **AS** | 45.9 | 0.9 | 45.0 | 36.8 | 9.11 | $\bar{x} = 9.60$ |
| | 32.2 | 0.7 | 31.5 | 24.4 | 10.14 | $SD = \pm 9.38\%$ |
| | 24.8 | 0.5 | 24.3 | 20.0 | 8.60 | |
| | 55.3 | 2.3 | 53.0 | 43.3 | 4.26 | |
| **DS** | 45.7 | 1.9 | 43.8 | 35.4 | 4.42 | $\bar{x} = 4.21$ |
| | 29.2 | 1.3 | 27.9 | 22.8 | 3.92 | SD = ±4.96% |
| | 20.3 | 0.9 | 19.4 | 15.6 | 4.22 | |

10.537 µm/s (SD 3.516) respectively. A wide distribution, particularly in the case of digested sludge, indicates that all particles are not composed of the same material of equal density.

Moreover, the digested sludge particles are more compact, as shown in Fig.1, due to the partial digestion of organic matter on sludge particles. The values of the effective density of particles, $\rho_{SP}-\rho_W$, computed from the particle size and mean settling velocities using Eqn. (3) are $0.032x10^3$ kg/m$^3$ and $0.048x10^3$ kg/m$^3$ for activated sludge and digested sludge respectively. The density of sludge particles and their different solid components are presented in Table 3. The rate of change of shear stress and apparent viscosity of activated sludge with the change in the rate of shear has been shown in Fig. 6. The rheological behavior of digested sludge at different solids concentrations has been presented in Fig. 7. The results indicate that sewage sludges are non-Newtonian fluid as the shear stress - shear rate relationship does not follow the characteristics linear flow curves of a Newtonian fluid. The study clearly

**Table 3. Density of solid components of sludge.**

| Sludge Solids | Density x10$^3$ kg/m$^3$ | |
|---|---|---|
| | Activated Sludge | Digested Sludge |
| Sludge Particles (Using Av. Settling Velocity) | 1.032 | 1.048 |
| Sludge Particles (Using Av. Component Density) | 1.031 | 1.093 |
| Fixed Residue | 2.487 (SD = ±1.47%) | 2.494 (SD = ±1.11%) |
| Dry Particles | 1.504 (SD = ±1.05%) | 1.815 (SD = ±1.91%) |
| Volatile Solids | 1.359 | 1.396 |

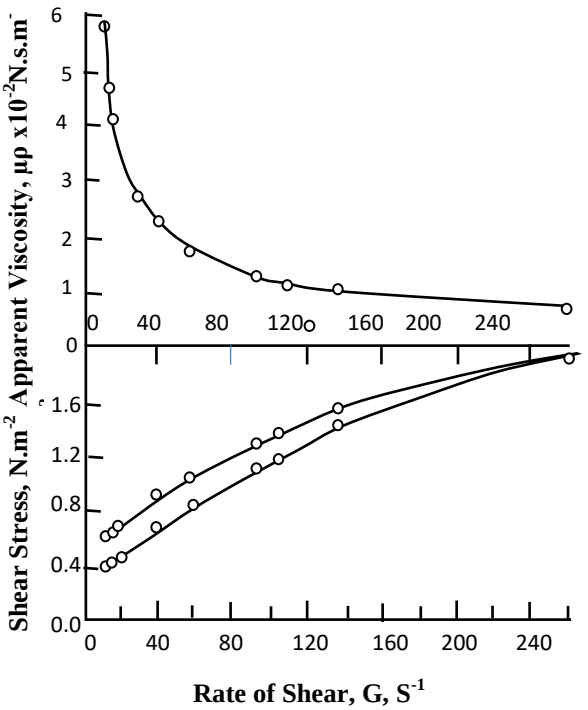


**Fig. 6. Effect of solid content on rheology of activated sludge**

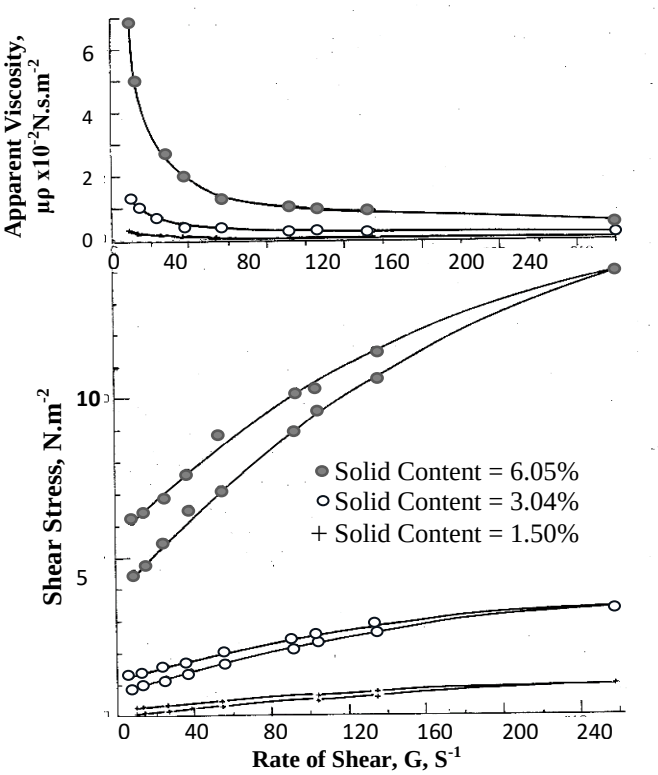


**Fig. 7. Effect of solid content on rheology of digested sludge**

demonstrates that activated and digested sludges exhibit pseudo and Bingham plastic characteristics with thixotropic behavior. For many liquids, the shear stress-shear rate relationship is not linear; such liquids are broadly classified as non-Newtonian, and this group includes sewage sludge (Buzzel and Sawyer, 1963; Hatfield, 1938; Inkster, 1945; McGeachie, 1970; Somerville, 1971). The viscosity of sewage sludges has mostly been studied regarding its flow through pipelines and transportation (Hatfield, 1938; McGeachie, 1970; Somerville, 1971).

The results in Table 3 show that the dry density of sludge particles increases with the digestion of the organic component of the sludge. The volatile solids and fixed residue of activated and digested sludges have nearly the same densities. So, the dry density depends on the percentage of volatile matter in the sludges. Baskerville et al. (1971) determined the dry density by weighing a sample of dry cake of known volume in air and water and reported a value of $1.360 \times 10^3$ kg/m$^3$.

The dry density of sludge solids has also been computed to be $1.40 \times 10^3$ kg/m$^3$, assuming the density of volatile solids is equal to $1 \times 10^3$ kg/m$^3$ (Metcalf and Eddy Inc., 1972). The density of volatile solids in sludges, as shown in Table 3, is not equal to the density of water. Tylor (1957) found that the specific gravity of combined dry solids of sludge varied from 1.62 to 1.78, where the inorganic and organic components of solids had sp. gr. 2.71 and 1.36, respectively. These values found by Tylor (1957) are in close agreement with those presented in Table 3. The dry density values of different fractions of digested sludge particles indicate that the smallest fraction has the highest dry density. The effective densities of sludge particles presented in Table 3 are a bit higher than values measured by the interferometric method (Coackley, 1964; Elhassan, 1973; Waring, 1961).

The density or effective density of particles is the most important parameter to study the settling of sludge, which depends on the dry density of sludge solids and bound water content, as shown in Eqns. (5) and (7). A graphical presentation of the Eqn. (7) has been shown in Fig. 8, which indicates that the effective density decreases at a higher rate at low bound water content. The difference between the densities of water and sludge particles at high bound water content becomes negligible.

The average protein contents of activated and digested sludge particles, expressed as a percent of total solids, were found to be 38.06% and 15.94%, respectively. The standard deviation of protein contents obtained in several determinations for each sludge type was checked. The coefficients of variation were found to be 5.55% and 4.58%, respectively, for activated and digested sludges. It appears that digestion is quite effective in the digestion or dissolution of protein from the particle phase of the sludge. The protein contents of sewage sludges were well within the range reported by Coackley (1950-52) and Katsiris (1977) but higher than the values found by Waring (1961) and lower than those found by Zang (1966) for activated sludge.

The polysaccharides extracted from activated sludge were found to be 10.65 percent of the total solids content of the sludge. The quantity of polysaccharides extracted from activated sludge agreed with the average value reported by Zang (1966) but was higher than the polysaccharides extracted by El Hassan (1973) from particles in effluent. Brand (1982) found that the number of polysaccharides extracted from activated sludge varied widely depending on the solids content; however, the value reported here is in the lower range of the values he found.

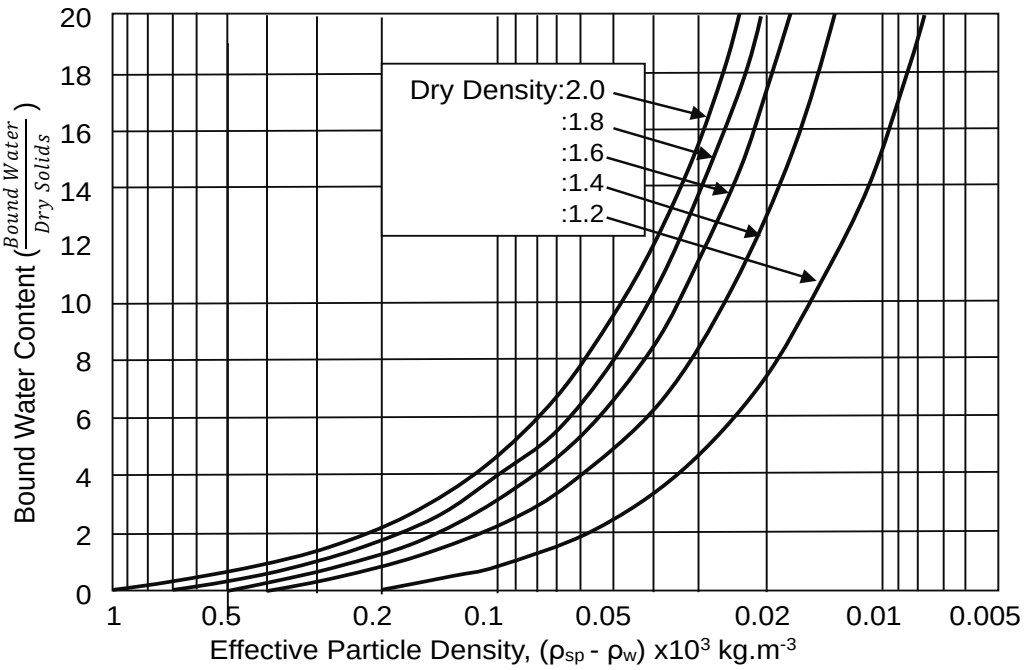


**Fig. 8: Correlation among effective density, bound water, and dry density of sludge particles.**

The apparent viscosity of digested sludge tremendously increases with the increase in solids concentration. This finding agrees with Buzzel and Sawyer, 1963; Hatfield, 1938; Abdel- Magid, 1982. It may be observed in Fig. 8 that the increase in solids concentration increases the yield stress and the degree of thixotropy. The bigger displacement between the up and down curves of the hysteresis loop has increased the degree of thixotropy. The reason for such behavior may be attributed to the fact that the increase in sludge concentration forms a connected and continuous particle structure, which requires higher initial stress to break down the particle contacts and initiate the particle layers to move relative to the adjacent layers.

The study reveals that for the same solid concentration, activated sludge has a higher viscosity than digested sludge; this is because activated sludge with high bound water content has a higher particle volume producing more flow resistance. The viscosity of sludge decreases rapidly with the decrease in solids content, as shown in Fig. 7, and approaches to a constant viscosity equal to that of water at very low solids.

## Conclusions

The particle size distribution of the total range of particles in sewage sludge, determined for the first time using sieves and a Coulter counter, has demonstrated very good reproducibility. This method can be used confidently to study filterability. Additionally, the density of sludge particles, determined for the first time using dry density and bound water measurements, can be correlated mathematically or graphically. This correlation can help obtain sludge particles' density or effective density for any given dry density value and bound water. The density of the dry matter of sludge particles depends on the percentage of organic matter

present in the particles. The dry density of the finer fraction of sludge particles is higher than that of the larger fraction. The density of particles in water decreases with water adsorption, and the density of water is approached at higher water content of the particles.

The study reveals that the stability of sludge particles is due to their high surface potential and low effective density. The presence of higher surface charge on digested sludge particles indicates that the protein and polysaccharide contents are not the only factors that determine the intensity of surface charge, the adsorption of ions from the surrounding media also increases the surface charge of the particles. The resident surface charge on particles produces resistance to flow, but it exerts a greater influence on filterability by regulating the stability and aggregation of the particles.

As evident from the experimental results, the proteins and polysaccharide contents of the particles regulate the bound water content and consequently, the density of the particles. Since specific filtration resistance is measured on a dry mass basis, particle density greatly influences the specific resistance. The probable modes through which proteins and polysaccharides influence specific resistance are through lowering particle density by water adsorption and producing a hydrated surface on the particles.

The viscosity of the sludge's liquid phase is equal to that of water. In cake filtration, as the liquid phase flows through cake's pore channels as filtrate, it seems logical to use water's viscosity in computing specific resistance to filtration.

## Declaration

The corresponding author declares that he carried out the experimental works in the article in the laboratories of the Civil Engineering Department, Strathclyde University, Glasgow, UK, and certifies that the contents of this paper have not been published before in any journal. The co-author, Tanvir Ahmed, has edited the paper and consented to the article being considered by the Editorial Board for publication in the Journal of Bangladesh Academy of Sciences.

## References

Abdel-Magid IM. The role of filter aids in sludge dewatering. *PhD. Thesis*, 1982; University of Strathclyde, Glasgow, UK.

APHA, AWWA, WPCF. *Standard methods for the examination of water and wastewater*, 15th Edn. 1980. Am. Pub. Health Assoc., Washington, D. C., USA.

Armanazi S. The influence of filter aids on dewatering of sewage sludge. *Ph.D. Thesis*, 1977; University of Strathclyde, Glasgow, UK.

Aziz MZA. The drying mechanism of sewage sludge.*Ph.D.Thesis*, 1974; University of Strathclyde, Glasgow, UK.

Baskerville RC, Komarek JA. and Gale RS. Effect of operating variables on filter press performance, *Wat. Poll. Contr*. 1971; 70(4): 400.

Brand CA. The effect of polyelectrolytes and natural polysaccharides on the settlement of activated sludge. *M.Sc. Thesis*, 1982; University of Strathclyde, Glasgow, UK.

British Standard Institution. *Methods of test far sails for Civil Engineering purposes*. 1975. British Standard 1377.

Buzzel JC and Sawyer CN. Biochemical vs. physical factors in digester failure, *J. Wat. Poll. Cantr. Fed*. 1963; 35: 205.

Coackley P and Kliger B. Some interferometric observations on the water /solids relation of activated sludge flocs using a compression technique. *Nature*, 1964; 203: 77.

Coackley P. Laboratory scale filtration experiments and their application to sewage sludge dewatering. In: *Biological Treatment of Sewage and Industrial Wastes.Vol II*, McCabe J and. Eckenfelder WW, eds., 1956. Reinhold Publishing Corp. NY, USA.

Coackley P. *Report No 1: Research work on sewage sludges*. University College, London, UK. 1950-52.

Coackley P. Principles of vacuum filtration and their application to sewage sludge drying problems. Sym. on Treat. of Waste Waters at the Univ. of Durham, Waste Treatment, edi. Isaac, P.C.G. Pergamon Press, 1959; 317.

Coackley P. The theory and practice of sludge dewatering. *J. Inst. of Pub. Health Engrs*; 1965; 64(1): 34.

Elhassan BM. A study of effluent particle properties in relation to tertiary treatment process design. *Ph.D. Thesis*, 1973; University of Strathclyde, Glasgow, UK.

Faisst, WK Characterization of particles in digested sewage sludge. In: *Particles in Water*. Kavanaugh and Leckie, eds., Sym. Am. Chem. Soc., Divn. Env. Chem.; Washington D.C.. 1980: 259.

Forster, C.F. and Lewin, D.C. "Polymer interactions at activated sludge surfaces" Effl. Wat. Treat. J., 1972; 21: 520.

Hall EJ. Sewage density variation in sedimentation tanks, *J. Inst. Sew. Pur*., 1962; 5: 469-477.

Hatfield WD. The viscosity or pseudo-plastic properties of sewage sludges, *Sew. Wks, J*. 1938; 10:1.

Heukelekian H. and Weisberg E. Bound water and activated sludge bulking. *Sew. and Ind. Wastes;* 1956; 28(4): 558574.

Inkster JE. Changes in viscosity of humus sludges during coagulation. *J. Inst. Sew. Purif*., 1945; 11: 177.

Javaheri AR and Dick RI. Aggregate size variation during thickening of activated sludge. *J. Wat. Poll. Contr. Fed.*, 1969; 41:197.

Jones BRS. *Some aspects of sewage sludge filtration. Report No 4.* Dept. of Civil and Municipal Engineering, Univ. College, London, UK. 1954.

Jorden RM. Electrophoretic studies of filtration. *J. Am. Wat. Wks. Assoc.* 1963; 55: 771.

Katsiris N. Bound water content of biological sludges in relation to settling and filterability. *Ph.D. thesis*. University of Strathclyde, Glasgow, UK. 1977.

Langmuir G. Studies on the nature of activated sludge. *Ph.D. thesis.* University of Strathclyde, Glasgow, UK. 1975.

Maulik SP, Cooper FC and Bier M. Forced flow electrophoretic filtration of clay suspensions. *J. Coll. Inter. Sci*., 1967; 24(4) : 427.

McGeachie G. The rheological properties of sewage sludge related to the hydraulic transport of such sludges through long pipelines. *MSc. Thesis*. University of Strathclyde, Glasgow, UK. 1970.

Metcalf and Eddy Inc. *Wastewater Engineering: Collection, Treatment, Disposal*. McGraw-Hill, NY, USA. 1972.

Pavoni JL, Tenney MW and Echelberger WF. Bacterial exocellular polymers and biological flocculation. *J. Wat. Poll. Contr. Fed.,* 1972; 44: 414.

Peters DJ. Bound water content and filterability of some biological sludge. *M.Sc. Thesis*. University of Strathclyde, Glasgow, UK. 1972.

Smyllie RT. Cake filtration. *Ph.D. Thesis.* University of Str2thclyde, Glasgow, UK. 1969.

Somerville JP. An investigation into the rheological properties of digested sewage sludge, *M.Sc. thesis,* University of Strathclyde, Glasgow, UK. 1971.

Tylor D. Sludge conditioning and filtration at Cincinati's Little Miami Sewage Works. *Sew. and Ind. Wastes;*1957; 29(12): 1332.

Waring GL. An investigation of some fundamental properties of sewage sludges. *M.Sc. Tech Thesis*. Manchester Univ. UK.. 1961.

Yukawa H, Chigira H, Hasino T and Iwata M. Fundamental study of electroosmotic filtration. *J. Chem. Eng.* 1971; 4(4): 370.

Zang M. Activated sludge and its polysaccharides. *M.Sc. Thesis.* University of Strathclyde, Glasgow, UK. 1966.

J. Bangladesh Acad. Sci. 48(2); 185-191: December 2024 DOI:https://doi.org/10.3329/jbas.v48i2.72703

Journal of Bangladesh Academy of Sciences

Journal homepage: http://www.bas.org.bd/publications/jbas.html

**Research Article**

# Estimation of the ablation velocity of atoms in a laser-induced plasma through the Doppler effect

Z H Khan*, Rebeka Sultana Lubna and A F M Y Haider[1]

*Department of Physics, University of Dhaka, Bangladesh*

**ARTICLE INFO**

**Article History**

Received: 17 April 2024
Revised: 19 June 2024
Accepted: 01 July 2024

**Keywords:** LIBS, Laser-Induced Plasma, Ablation velocity, Doppler Effect.

**ABSTRACT**

The dynamics of laser-induced plasma plumes were investigated using the Doppler effect and the spectroscopic analysis for the first time. Plasma is generated on silver, copper, and gold targets in ambient air at atmospheric pressure and room temperature using laser ablation with a Q-switched Nd: YAG laser. The laser setup included specific parameters: a pulse duration of 8 ns, a repetition rate of 10 Hz, laser pulse energies of 40 mJ, and a grating with 2400 grooves/mm. When the input end of the optical fiber is perpendicular to the sample surface, a Doppler shift in the emitted wavelength occurs. By analyzing this Doppler shift of the emission wavelengths at two distinct source-detector relative positions, we can accurately estimate the velocities of silver, copper, and gold atoms within the laser-induced plasma.

## Introduction

Laser-induced breakdown spectroscopy (LIBS) is a widespread technique recognized for its rapid and effective elemental analysis (Cremers and Radziemski, 2013; Singh and Thakur, 2020; Mizioleket al., 2006). This technique harnesses the intense power of a high-energy laser pulse, channeling its focused energy onto a sample to induce the formation of a transient micro-plasma at very high temperatures. The emitted light is then analyzed using a high-resolution spectrometer coupled with a gated and intensified charge-coupled device (ICCD) to determine the sample's elemental composition.

LIBS has a wide range of applications, including ion source formation (Gammino et al., 2002; Okamura et al., 2014), nanoscale synthesis (Lin et al., 2020; Xiao et al., 2020), thin film growth (Cheung and Sankur, 1988; Harris et al., 2019) and nuclear fusion (Wu et al., 2019; Xiao et al., 2013). Therefore, a thorough understanding of the composition and dynamics of the plasma plume is crucial for optimizing performance in these fields.

Plasma velocity is critical, as it affects stability, transport properties, and wave propagation within the plasma. Knowledge of plasma velocity is essential in material processing techniques like plasma etching and deposition, as the velocity of plasma species plays a critical role in these processes; it can either accelerate thin film deposition when a certain velocity threshold is used (Shul and Pearton, 2011; Chrisey and Hubler, 1994) or compromise the integrity of the deposited film when exceeding it (Chen et al., 2021). Hence, gaining a comprehensive understanding of plasma particle dynamics, particularly in laser-induced plasma, is necessary. Additionally, measuring plasma velocity can provide valuable diagnostic information for determining plasma properties such as temperature and flow patterns.

*Corresponding author:<zulfiqarshuvo@du.ac.bd>

[1]*Department of Mathematics and Natural Sciences, BRAC University, Dhaka, Bangladesh*

Previous studies have mainly focused on measuring plasma velocity using direct methods like ICCD (Anoop et al., 2014; Yuan et al., 2020). However, our study explores an alternative approach by utilizing the Doppler effect to estimate velocity. We demonstrate the capability of LIBS coupled with the Doppler effect to estimate the velocities of ablated particles within laser-induced plasma. Specifically, we estimate the velocities of copper (Cu), silver (Ag), and gold (Au) atoms within the plasma, shedding light on this crucial aspect of plasma dynamics. This is yet another novel application of LIBS.

## Experimental setup

Fig. 1 shows the experimental setup for estimating the velocity of silver atoms (Haider et al., 2014). To prepare the silver plate for the experiment, a 10 mm × 10 mm × 1 mm plate of ~99.99% pure silver was mechanically polished and cleaned multiple times in an ultrasonic bath with nano-pure water to remove impurities from its surface. Similarly, copper and gold plates of similar dimensions were also polished and cleaned for conducting the velocity estimation experiment using LIBS.

The experiment utilized a Q-switched Nd: YAG laser (Spectra-Physics LAB-170-10) as the excitation laser. This laser emitted light at a fundamental wavelength of 1064 nm, with a pulse duration of 8 ns, a repetition rate of 10 Hz, and a maximum pulse energy of 850 mJ. The laser had harmonic generators capable of producing the second, third, and fourth harmonics using KDP crystals. For this experiment, we used the fundamental wavelength of 1064 nm to generate plasma. The laser beam had a Gaussian profile in the far field and a beam divergence of less than 0.5 mrad. All experiments were conducted in the air (Abedin et al., 2011).

To generate a high-intensity transient plasma, the fundamental beam of the Nd: YAG laser was focused onto the sample using a 100 mm focal length convex lens. The spot size at the sample was approximately 200 μm measured using a beam profiler. This resulted in a peak power density of approximately 16 GW/cm² for a 40 mJ pulse. The plasma was generated at a repetition rate matching the laser's frequency, occurring 10 times per second.

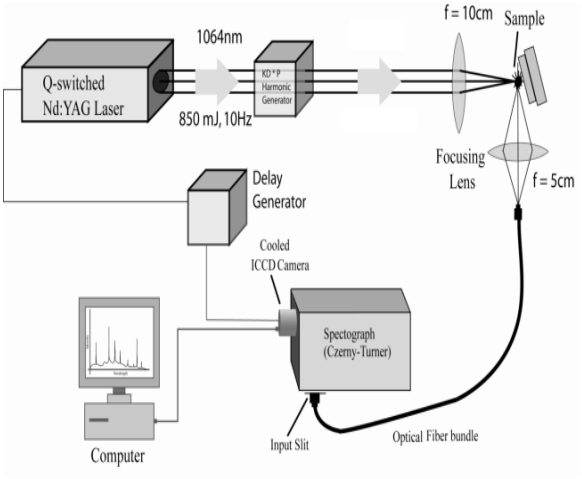


**Fig. 1. Schematic diagram of the ablation velocity measurement setup.**

The light emitted from the plasma was directed through a fused quartz lens with a focal length of 50 mm and collected by a 3 m long multimode silica optical fiber. This light was transmitted through the fiber to the entrance slit of a computerized Czerny-Turner spectrograph with a focal length of 750 mm (Acton Model SP-2758). The spectrograph had three interchangeable ruled gratings: 2400, 600, and 300 grooves/mm blazed at 240, 500, and 300 nm, respectively. These gratings, controlled by a computer, provided high and low-resolution spectra across a wavelength range of 200 nm to 960 nm.

For this experiment, we used a grating with 2400 grooves/mm to achieve the highest resolution for our detection system. The spectrograph output was connected to a gated ICCD camera (Princeton PI-MAX with Unigen II coating and programmable delay generator). This ICCD camera had 1024x1024 pixels and was cooled to -20°C using a Peltier cooler to minimize noise.

The synchronous pulse of the Nd: YAG laser electrically triggered the ICCD camera after applying a software-controlled adjustable time

delay. This setup effectively reduced the intense background initially generated by the high-temperature plasma, enabling clearer observation of the elements' atomic/ionic emission lines. For an optimal signal, we selected a delay time ($t_d$) of 1.5 µs and a gate width ($T_w$) of 50 µs (Haider and Khan, 2012).

Typically, spectra from multiple laser shots (10 in our case) were acquired and averaged to enhance the signal-to-noise ratio. The captured spectrum from the ICCD camera was transferred to a computer via a USB cable. The manufacturer-provided WinSpec/32 software allowed complete control over all functions of the ICCD camera and the Acton spectrograph.

## Results

LIBS spectra were recorded for each sample in the 200-960 nm spectral range using high-resolution gratings with 2400 grooves/mm. The wavelengths of the observed line peaks in the spectra were compared to the online database available from the US National Institute of Standards and Technology (NIST database, 2024). Since the samples primarily consisted of pure silver, gold, and copper, strong emission lines of these elements were analyzed to estimate the ablation velocity of their atoms/ions. Figs. 2(a) and 2(b) show the LIBS spectra for the Ag atom in the spectral window of 323.5 nm to 332.5 nm. In Fig. 2(a), the spectrum corresponds to a fiber input parallel to the surface of the sample, while Fig. 2(b) represents the corresponding spectra when the fiber input is perpendicular to the surface of the sample.

When the detection direction is parallel to the sample surface, the velocity component of the ablated atom/ion in that direction can be considered zero (Cremers and Radziemski, 2013). Therefore, the emitted wavelength remains unshifted (no Doppler shift). However, when the input end of the optical fiber is aligned perpendicularly to the sample surface, the emitting atom/ion moves toward the input end with a certain velocity (Kwapis et al., 2024). This results in a noticeable shortening of the wavelength due to the Doppler effect. The ablation velocities of the emitting atoms can be estimated by measuring the change in wavelengths. Table 1 illustrates the estimation of plasma plume velocity through Doppler shift analysis of emission wavelengths at different source-detector relative positions. In our work, the estimated velocity for neutral copper, silver, and gold atoms is 2.40 X $10^4$ m/s, 2.29 X $10^4$ m/s, and 2.21 X $10^4$ m/s, respectively, at atmospheric pressure in the direction perpendicular to the sample surface.

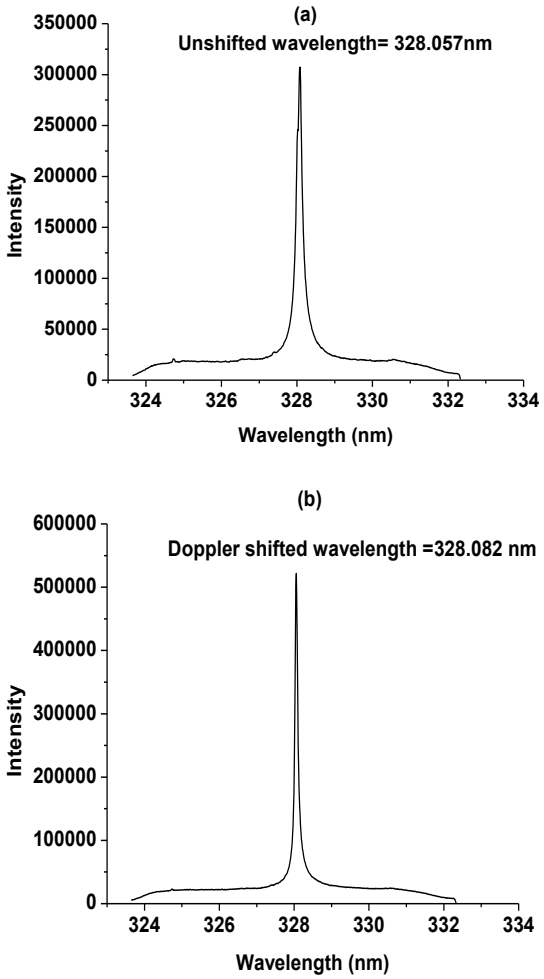


**Fig. 2. Comparative analysis of emission lines from Ag I (a) Before the Doppler Shift and (b) After the Doppler Shift.**

**Table 1. Estimation of plasma plume velocity through Doppler shift analysis of emission wave lengths at various source-detector relative positions.**

| Element | Charge state | Unshifted wavelength λ (in nm) (at θ= $0^0$) | Doppler shifted wavelength λ' (in nm) (at θ= $90^0$) | The velocity of the atom in the plasma plume (x$10^4$ m/s) |
|---|---|---|---|---|
| Cu | I | 324.752 | 324.726 | 2.40 |
| Ag | I | 328.082 | 328.057 | 2.29 |
| Au | I | 312.279 | 312.256 | 2.21 |

## Discussion

When a high-power laser pulse impacts a sample surface, a fraction of the material vaporizes or ablates, creating a micro-plasma. Initially, this plasma is extremely hot and dense, which causes a broad continuum emission of background radiation. As the plasma expands and cools, ions and electrons recombine, producing excited atoms that release photons as they decay to lower energy states. By analyzing the spectrum of these emitted radiations, we can identify the different elements in the plasma that come from the target material.

The expansion of the laser-induced plasma shows an elongation perpendicular to the sample surface, resembling a pear or cigar shape. This suggests that the expansion rates vary in different directions, with the highest expansion occurring perpendicular to the surface. At laser powers of around 16 GW/cm², the plasma elongates by approximately 1 centimeter. Figure 3 provides a schematic representation of the laser-produced spark in the air, which helps visualize this phenomenon. When the detection is parallel to the sample surface, the velocity of the ablated particles in that direction is minimized because the plume primarily expands perpendicular to the surface, resulting in minimal net velocity parallel to it (Cremers and Radziemski, 2013; Singh and Thakur, 2020).

We can determine this velocity by using the Doppler effect of light. In this case, the ablated atom/ion acts as a moving source of the light wave, while the input end of the optical fiber acts as the stationary detector. When a light source moves towards an observer, the wavelengths of the emitted light waves become compressed in the direction of motion. This compression leads to an apparent increase in frequency and a decrease in the wavelength of the light observed by the observer. We can express the Doppler-shifted frequency f ' of the light as:

$$f' = f (1+ v / c) \quad (1)$$

In this equation, f represents the unshifted frequency, v denotes the relative velocity between the source and the detector, c is the velocity of light, and f ' is the observed frequency. From the above equation, we derive the following relation:

$$v = c (\lambda' - \lambda) / \lambda \quad (2)$$

Here, λ represents the unshifted wavelength, and λ' is the observed Doppler-shifted wavelength. By using these wavelengths in equation (2) for two different relative angular positions between the sample and the detector, we can easily determine the ablation velocity of a specific atom/ion.

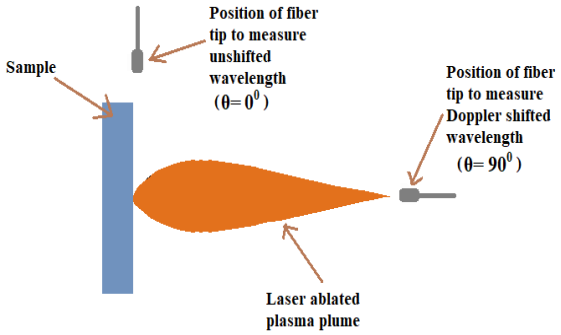


**Fig. 3. Schematic shape of Laser-produced plasma plume in air.**

Through this experiment, we have successfully demonstrated the capability of LIBS in estimating the velocities of ablated particles within laser-induced plasma obtained using an Nd: YAG laser. Specifically, for angles of 90 degrees between the sample surface and detector, we obtained a velocity of 2.40X$10^4$ m/s for neutral copper atoms in plasma at atmospheric pressure. This contrasts with the findings of Anoop et al.(2014), who investigated the ablation of a copper target in a high vacuum using a Ti: Sapphire laser and an ICCD to image the plasma plume. They found that the peak velocity of the neutral component was 9 x $10^3$ m/s. On the other hand, our study involved ablation in atmospheric conditions using a different laser and parameters, resulting in higher velocity for the neutral atom.

Additionally, our approach utilized the Doppler effect to estimate the velocity of neutral Cu atoms instead of direct measurement using ICCD.

Yuan et al. (2020) observed splitting a laser-induced plasma plume into two components at reduced pressures (50 Pa to 200 Pa). They employed a Q-switched Nd:YAG laser to ablate a copper target and imaged the plasma using ICCD. The fast component exhibited a velocity of approximately $10^4$ m/s at a 200 ns delay, while the slow component had a velocity of around $10^3$ m/s at the same delay. However, in our study, the background gas pressure was sufficiently high (atmospheric pressure) to maintain a continuous plume (Noll et al., 2004). Consequently, we did not observe any splitting of the plume.

Noll et al. (2004) examined the effects of collinear double pulses from an Nd:YAG laser on pure iron targets in the air. Using a long-distance microscope on a streak camera, they found that the material ablated by the second pulse expands faster, resulting in a noticeably larger plasma volume. Expansion velocities measured 60 ns after the second laser pulse were found to be 1.2x$10^4$ m/s. In our measurement, however, we utilized a single pulse from a Nd:YAG laser in air and obtained different expansion velocities accordingly.

According to the Maxwell-Boltzmann distribution (though rarely this is so simple in most cases), the most probable velocity depends on both mass and plasma temperature($v_{mp} = \sqrt{\frac{2kT}{m}}$).

However, the ablation velocity of different species is influenced by a complex interplay of factors, including plasma temperature, material properties (such as density and boiling point), environmental conditions (such as constituent gases and ambient temperature), and laser parameters (such as power and spot size).

In our study, we observed that $v_{Cu} > v_{Ag} > v_{Au}$ which suggests a trend where plasma velocities decrease with atomic number. It is important to note that the plasma was generated from three different target materials with varying boiling points and densities. Additionally, the environmental conditions and laser parameters were somewhat different. Since we measured the velocity with a fairly long delay of 1.5 us for eliminating the plasma radiation background, we effectively measured the tail (lower part) of the velocity components of the atoms in the plasma plume. Therefore, our results only partially reflect significant differences in atomic mass.

Finally, while we utilized a 2400 grooves/mm diffraction grating boasting a resolution of 0.002 nm, the highest available within our experimental setup, accessing an even higher resolution (for example, using 3600 grooves/mm grating) could have yielded even greater accuracy in our results.

## Conclusion

In this study, we used the Doppler Effect of light to estimate the velocities of Ag, Cu, and Au atoms within LIBS plasma for the first time. Unlike experiments conducted under reduced pressures, our study operated under atmospheric conditions to maintain a continuous plasma without splitting the plume. Using this approach, we found that the average velocities of Cu, Ag, and Au atoms were 2.40x$10^4$ m/s, 2.29x$10^4$ m/s, and 2.21x$10^4$ m/s, respectively. The highest resolution available in our experiment was 0.002 nm. Improving the resolution

and sensitivity of the spectrometer will result in more accurate measurements and better velocity estimations. This alternative method for assessing plasma species dynamics holds promising implications for optimizing performance in various fields, such as material processing, thin film deposition, and nuclear fusion. Estimating the velocity of atoms and ions in the plasma plume is another novel application of the laser-induced breakdown spectroscopic technique.

## Conflicts of Interest

Concerning the publication of this paper, the authors have no conflicts of interest.

## Acknowledgment

The experimental work was carried out in the Nonlinear Optics and Laser Spectroscopy Laboratory of the Center for Advanced Research in Sciences (CARS) of the University of Dhaka.

## References

Abedin KM, Haider AFMY, Rony MA and Khan ZH. Identification of multiple rare earths and associated elements in raw monazite sands by laser-induced breakdown spectroscopy. *Opt. Laser Technol.* 2011; 43(1): 45-49.

Anoop KK, Xiaochang Ni, Bianco M, Paparo D, Wang X, Bruzzese R and Amoruso S. Two-dimensional imaging of atomic and nanoparticle components in copper plasma plume produced by ultrafast laser ablation. *Appl. Phys.*, 2014; 117: 313-318.

Chen J, Lu X, Wen Q, Jiang F, Lu J, Lei D and Pan Y. Review on laser-induced etching processing technology for transparent hard and brittle materials. *Int. J. Adv. Manuf. Technol.* 2021; 117(9-10): 2545-2564.

Cheung JT and Sankur H. Growth of thin films by laser-induced evaporation, *Crit. Rev. Solid State Mater. Sci.* 1988; 15 (1): 63-109.

Chrisey DB and Hubler GK. *Pulsed laser deposition of thin films*. John Wiley & Sons Inc., Hoboken, 1994.

Cremers DA and Radziemski LJ. *Handbook of laser-induced breakdown spectroscop*. 2nd Ed., John Wiley & Sons Inc, 2013. p.418.

Gammino S, Torrisi L, Andò L, Ciavola G, Celona L, Laska L, Krasa J, Pfeifer M, Rohlena K and Woryna E. Production of low energy, high intensity metal ion beams by means of a laser ion source. *Rev. Sci. Instrum.* 2002; 73: 650-653.

Haider AFMY and Khan ZH. Determination of Ca content of coral skeleton by analyte additive method using the LIBS technique. *Opt. Laser Technol.* 2012; 44(6): 1654-1659.

Haider AFMY, Ullah MH, Khan ZH, Kabir F and Abedin KM. Detection of trace amount of arsenic in groundwater by laser-induced breakdown spectroscopy and adsorption. *Opt. Laser Technol.* 2014; 56: 299-303.

Harris SB, Paiste JH, Holdsworth TJ, Arslanbekov RR and Camata RP. Laser-generated plasmas in length scales relevant for thin film growth and processing: Simulation and experiment. *J. Phys. D: Appl. Phys.* 2019; 53(1): 015203.

Kwapis EH, Borrero J, Latty KS, Andrews HB and Hartig KC. Laser ablation plasmas and spectroscopy for nuclear applications. *Appl. Spectrosc.* 2024; 78(1): 9-55.

Lin Zi, Yue J, Liang L, Tang B, Liu B, Ren L, Li Y and Jiang L. Rapid synthesis of metallic and alloy micro/nanoparticles by laser ablation towards water.*Appl. Sur. Sci.* 2020; 504: 144461.

Miziolek AW, Palleschi V and SchechterI. *Laser induced breakdown spectroscopy*. Cambridge University Press, 2006. p.620.

Noll R, Sattmann R, Sturm V and Winkelmann S. Space-and time-resolved dynamics of plasmas generated by laser double pulses interacting with metallic samples. *J. Anal. At. Spectrom.* 2004; 19(4): 419-428.

NIST database. *National Institute of Standards and Technology (NIST) Atomic Spectra Database Lines Form.* Available from 2024: https://physics.nist.gov/PhysRefData/ASD/lines_form.html.

Okamura M, Sekine M, Takahashi K, Kondo K and Kanesue T. Laser ablation ion source for heavy ion inertial fusion. *Nucl. Instr. Meth. Phys. Res. Section A*, 2014; 733: 97-102.

Shul RJ and Pearton SJ. *Handbook of advanced plasma processing techniques*. Springer Science & Business Media, 2011. p.655.

Singh JP and Thakur SN. *Laser-induced breakdown spectroscopy*. 2nd Ed., Elsevier, 2020.

Wu J, Qiu Y, Li X, Yu H, Zhang Z and Qiu A. Progress of laser-induced breakdown spectroscopy in nuclear industry applications. *J. Phys. D: Appl. Phys.* 2019; 53(2): 023001.

Xiao Q, Huber A, Sergienko G, Schweer B, Mertens PH, Kubina A, Philipps V and Ding H. Application of laser-induced breakdown spectroscopy for characterization of material deposits and tritium retention in fusion devices. *Fusion Eng. Des.* 2013; 88: 1813-1817.

Xiao M, Zheng S, Shen D, Duley WW and Zhou NY. Laser-induced joining of nanoscale materials: processing, properties, and applications, *Nano Today*, 2020; 35: 100959.

Yuan H, Gojani AB, Gornushkin IB, Wang X, Liu D and Rong M. Dynamics of laser-induced plasma splitting, *Opt. Lasers Eng.* 2020; 124: 105832.

J. Bangladesh Acad. Sci. 48(2); 193-206: December 2024 DOI:https://doi.org/10.3329/jbas.v48i2.72239

Journal of Bangladesh Academy of Sciences

Journal homepage: http://www.bas.org.bd/publications/jbas.html

## Research Article

# The temperature and solvent effect on the structural, thermodynamic and electronic properties of Auxin: A computational study

Md. Alauddin*, Nasima Tabassum Barna, Md. Masud Parvez[1], Gazi Jahirul Islam[1], Mohammad Abdul Matin[2]

*Department of Theoretical and Computational Chemistry, University of Dhaka, Bangladesh*

**ARTICLE INFO**

**Article History**

Received: 24 March 2024
Revised: 08 September 2024
Accepted: 10 September 2024

**Keywords:** Auxin, DFT, TD-DFT, Solvent, Temperature.

**ABSTRACT**

Indol-3-acetic acid (IAA) is the major and naturally synthesized auxin that can regulate plant growth and many physiological processes involving the response to directional light. Computational analysis of the impacts of solvents on different polarity and temperature (100K–1000K) on the structural, thermodynamic, and electrical properties of IAA is done using the density functional theory (DFT) approach. The optimized structure of the IAA molecule shows four (4) stable conformers depending on their energies. The increasing intensities of molecular vibration were seen to generate a rise in enthalpy (H), entropy (S), and specific heat capacity (Cv) with temperature. Conversely, it was found that Gibbs's free energy (G) decreased when temperature increased. Our computations demonstrate that when solvation lowers excitation energies, the UV-light absorption maxima ($\lambda_{max}$) are red-shifted in the presence of polar protic, aprotic, and non-polar solvents. Conversely, exothermic and spontaneous behavior is seen in the interactions between IAA and solvents with varying polarity.

## Introduction

Growth is essential to all multicellular or living things, including plants and animals. In plants, growth results from an increase in the quantity and size of cells. Although there is a distinction between growth in plants and animals, in both cases, the growth is regulated by hormones (Liu et al., 2014). Several types of hormones can regulate plant growth, like auxin, gibberellins (GA), cytokinins, abscisic acid (ABA), and ethylene. Auxin is the most significant of them all for plant growth and development in a variety of areas, including the form of the plant, stimulated cell division, and cell elongation (Fendrych et al., 2018; Frim, 2003; Zivanovic et al., 2018; Sorefan et al., 2009). Furthermore, it contributes to flowering and postpones senescence (McSteen et al., 2007). It also promotes the normal growth of plant stem cells toward the light (Fuente and Leopold, 1968). It is essential for numerous physiological processes in plant life cycles that result in plant development and growth. The major and most naturally cell-synthesized auxin is indole-3-acetic acid (IAA), which is found in plants to a greater extent (Masuda and Kamisaka, 2000). Because it has a carboxylic acid group and an aromatic ring, IAA is significant (Fig. 1) (Simon and Petrasek, 2011).

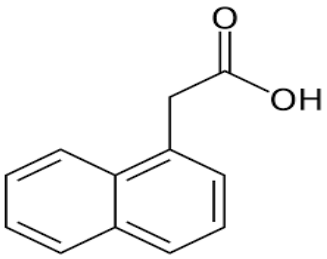


**Fig. 1. Structure of indole-3-acetic acid (IAA).**

*Corresponding author:<alauddin1982@du.ac.bd>

[1]*Department of Chemistry, University of Barishal, Bangladesh*

[2]*Centre for Advanced Research in Sciences (CARS), University of Dhaka, Bangladesh*

The structural motifs and the properties of the phytohormone IAA have been studied experimentally and theoretically to reveal its physicochemical behaviors (Ilbeigi et al., 2022; Ung et al., 2023; Bogaert et al., 2022). Nigivic et al. studied some of the alkylated derivatives of IAA and revealed that these derivatives had exhibited their growth-promoting activity in plants and they also exhibited their physicochemical properties in plants (Nigović et al., 2000; Schmit et al., 2011; Förner and Badawi, 2014). Flasinski and Hac-Wydro (2014) studied and emphasized the discrepancies in the interaction of natural IAA and synthetic 1-naphthalene acetic acid (NAA) (Fig. 2) phytohormones with phospholipids in the plasma membranes of both plants and animals.

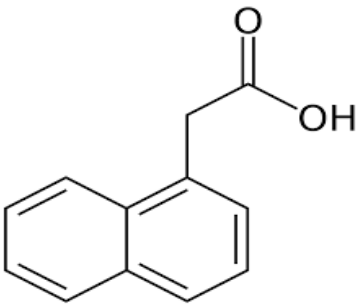


**Fig. 2. Structure of 1-naphthalinic acetic acid (NAA).**

They reported that the naturally occurring IAA interacts with biological membranes or lipids more strongly than the synthetic auxin, NAA, due to its capability of forming an H-bond by its NH donor group of indoles ring (Flasiński and Hac-Wydro, 2014).

The plant hormone auxin can rapidly degrade the AUX/IAA protein family of transcription. This auxin-induced degron (AID) system can be transplanted into non-plant cells to control the stability of proteins (Nishimura et al., 2009; Luo et al., 2018). Addressing particular protein activities within a given time frame is not viable. Having conditional and reversible control over particular proteins is ideal for better understanding how the brain works. Auxin-induced protein degradation systems can be applied in neuroscience to control the specific protein functions in the brain (Nakano et al., 2019). Nowadays, chemical herbicides have been used to accommodate crop production with the increasing global population. Such kinds of herbicides are unsafe for agricultural products and also for the environment. A higher amount of IAA can degrade the plant growth activity. So, IAA-producing microbes have been used recently to reduce the use of chemical herbicides in crop production and to save agricultural products and the environment. These microbes can evaluate and enhance the inhibitory effect of IAA.

However, an optimum process for commercial-scale IAA production will be needed, and this process can replace the toxic elements in the agricultural sectors (Bunsangiam et al., 2021).

IAA is a weak polar molecule. Therefore, organic solvents close to IAA's polarity are the most effective for extracting IAA from plant tissues (Su et al., 2017). Moreover, all auxins are always stored in the refrigerator at 5-10℃ because of the effect of light. Therefore, in this work, indole-3-acetic acid (IAA) has been investigated to examine its structural and conformational landscape and the temperature and solvent impacts on its electronic and thermodynamic properties. All of these analyses have been done with the aid of computational analysis. The thermodynamic and electronic properties have been analyzed only for the most stable conformer of IAA.

## Computational Methodology

IAA, the most abundant plant hormone among the natural and synthetic auxins, has been studied computationally. All the calculations have been performed with the *Gaussian* 16 software packages (Frisch et al., 2016). *GaussView* 6.0 has also been used for all the visual presentations. The possible

conformers of IAA have been optimized in the gas phase using density functional theory (DFT) without any imaginary frequency. The DFT computations were implemented and presented with the help of Origin Pro 2018 software (OriginPro, 2018).

Temperature effects on the most stableconformer of IAA have been analyzed by varying the temperature from 100K to 1000K. The solvent effect has been observed using the Integral Equation Formalism Variant Polarizable Continuum Model (IEF-PCM) model at the DFT/$\omega$B97XD/cc-pVTZ level of theory. Nineteen (19) solvents of different polarities have been used in this calculation and optimized without any imaginary frequency. TD-DFT calculations of these solvent-IAA interactions have been also carried out at the same level of theory.

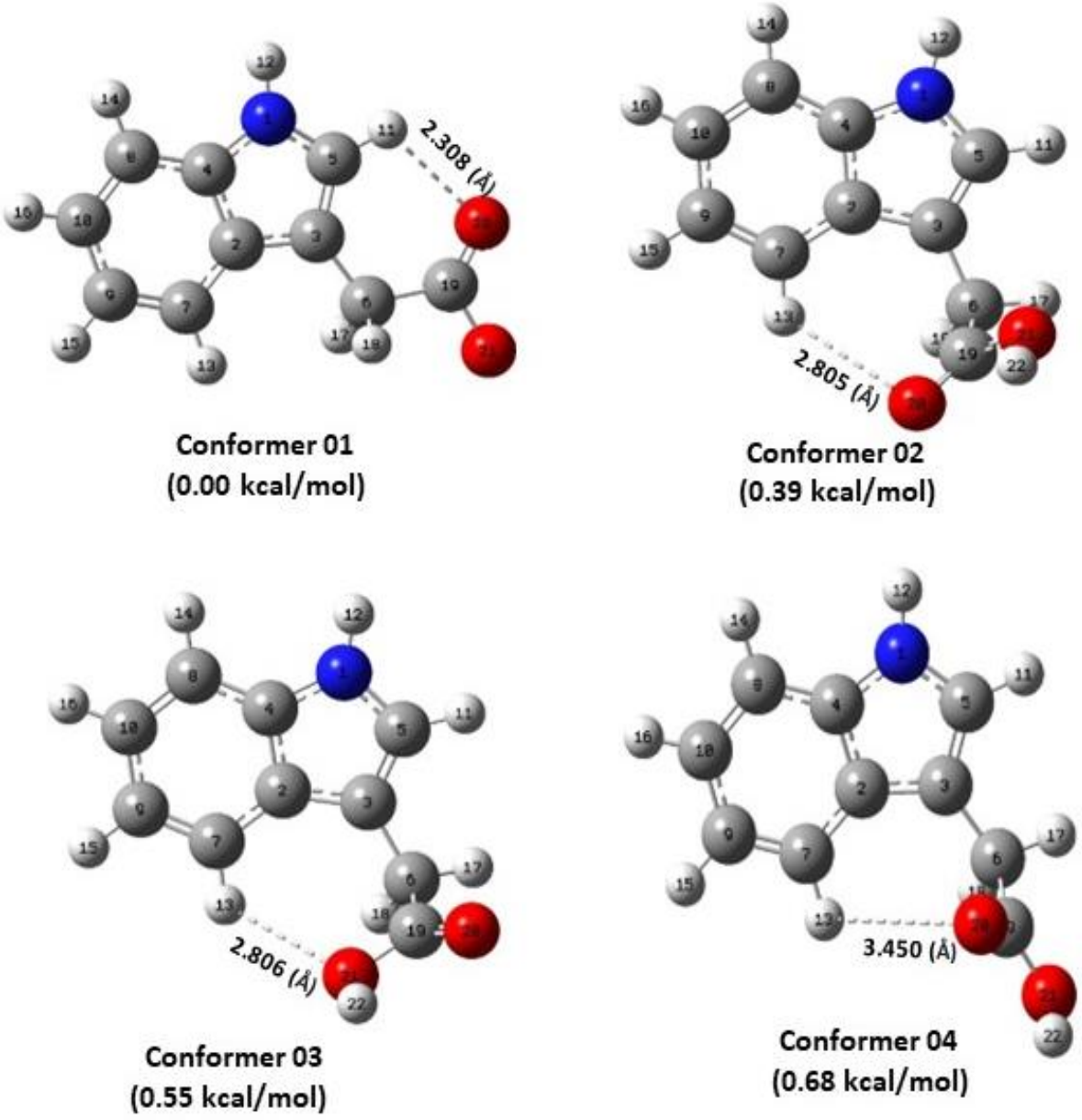


**Fig. 3. The optimized structures of the four (4) conformers of the indole-3-acetic acid (IAA)**

## Results and Discussion

### *Optimization of Molecular Geometry*

The possible structures of the IAA molecule have been optimized using DFT with hybrid functional of $\omega$B97XD and basis set of cc-pVTZ. Through the optimization of the IAA molecule without any imaginary frequency, four (4) stable conformershavebeen found. They are shown in Fig. 3, along with their atom number, stability order, and relative energies. The most stable conformer is assigned as conformer 01. The second lowest energy conformer is conformer 02, which is only 0.39 kcal/mol higher than conformer 01. Conformers 03 and 04 are 0.55 and 0.68 kcal/mol higher than conformers 01.

### *Temperature effect on the thermodynamic properties*

The most significant thermodynamic parameters, H, G, S, and $C_v$, of the most stable conformer of IAA have been computed and presented in Table 1. The calculations were done in the region of 100K to 1000K at 1 atmospheric pressure. To understand the effect oftemperature on these parameters, the graphical representation of thermodynamic properties vs temperature plots for conformer 01 are presented in Fig. 4, and data are tabulated in Table 2. Using quadratic formulae, the correlation fitting equation between changes in H, G, S, and Cv with temperatures was fitted. Origin Pro 2018 software was then used to produce the fitting equations using regression factors ($R^2$). Equations for fitting thermodynamic correlations are

$$H = 107.98146 + 0.01781T + 4.5177 \times E^{-5}T^2 \ (R^2 = 0.99944)$$

$$G = 111.12551 - 0.06641T - 6.44468 \times E^{-5}T^2 \ (R^2 = 0.99997)$$

$$S = 17.16729 + 0.04975T - 1.03511 \times E^{-5}T^2 \ (R^2 = 0.99999)$$

$$C_v = -0.34162 + 0.04899T - 2.03210 \times E^{-5}T^2 \ (R^2 = 0.99908)$$

**Table 1. Calculated thermodynamic parameters of the conformers of indole-3-acetic acid (IAA) at the DFT/*w*B97XD/cc-pVTZ level of theory in the gas phase.**

| Conformers | Enthalpy, H (kcal/mol) | Free energy, G (kcal/mol) | Entropy, S (kcal/mol) | Heat capacity, Cv (kcal/mol) | Dipole moment, μ (Debye) | Polarizability, α (a.u.) |
|---|---|---|---|---|---|---|
| 01 | 116.84 | 85.78 | 31.030 | 12.203 | 0.619 | 120.831 |
| 02 | 117.09 | 86.35 | 30.732 | 12.134 | 3.679 | 120.136 |
| 03 | 117.08 | 86.23 | 30.828 | 12.136 | 1.929 | 120.637 |
| 04 | 116.82 | 85.52 | 31.295 | 12.223 | 2.410 | 120.522 |

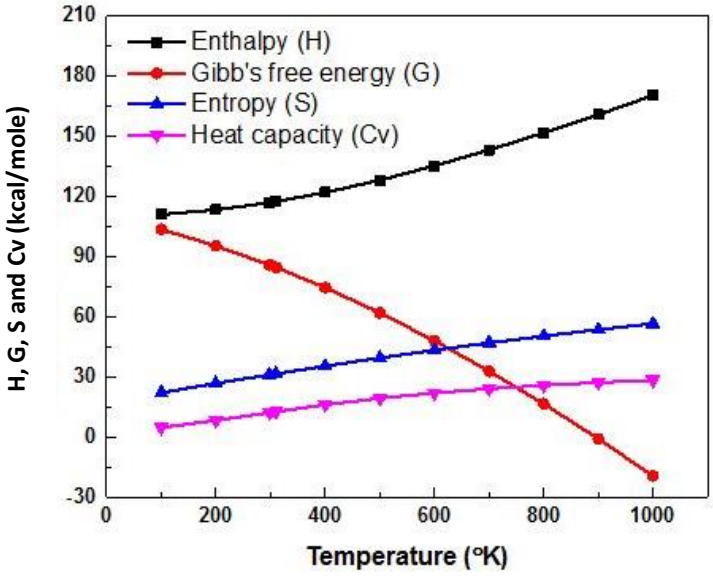


**Fig. 4. The dependency of Gibbs free energy, enthalpy, entropy, and specific heat capacity at different temperatures (100k-1000k) for the most stable confirmer (01) of indole-3-acetic acid (IAA).**

Following the related Figure and Table, the H rises slowly at lower temperatures but increases steeply at higher temperatures. This is because, at a lower temperature, the translational and rotational motion are the major contributions to the thermodynamic functions in a molecule. In contrast, the vibrational motion also contributes to the molecule at a higher temperature. Because thermal energy is distributed among translational, rotational, and vibrational motions, the S value rises as temperature rises. It also can be seen that the value of G decreases steeply as the temperature increases due to the dependency of G on the -TΔS, and the relation between them is the free energy change, ΔG = ΔH-TΔS. That means the G decreases with the increase of entropy along with the increase of temperature. Another thermodynamic parameter, $C_v$, rises slowly and gradually with increased temperatures. At very high temperatures, the molecule will be fragmented into atoms, and the molecular motion is not increased, resulting in the constant value of specific heat capacity (Alauddin, 2021).

***Solvent effect on the thermodynamic properties***

The effect of various solvent types (polar protic, aprotic, and non-polar) on the thermodynamic characteristics has been performed using the IEFPCM model at the $\omega$B97XD/cc-pVTZ method. Nineteen (19) solvents of different polarities have been applied to quantify the solvent effect on the thermodynamic parameters of the conformer 01. Among the solvents, the polar protic solvents are ($H_2O$), methanol ($CH_3OH$), ethanol ($C_2H_5OH$), and aniline ($C_6H_5$-$NH_2$).

The polar aprotic solvents are dimethyl sulfoxide (DMSO), nitromethane ($CH_3NO_2$), acetonitrile ($CH_3CN$), acetone ($C_2H_6CO$), dichloro-ethane($C_2H_4Cl_2$), dichloromethane ($CH_2Cl_2$), tetrahydrofuran (THF), chlorobenzene ($C_6H_5$-Cl). And the chosen non-polar solvents are diethyl ether (($C_2H_5)_2O$), toluene ($C_6H_5$-$CH_3$), benzene ($C_6H_6$), carbon tetra chloride ($CCl_4$), cyclohexane ($C_6H_{12}$), heptane ($C_7H_{16}$).

The thermodynamic parameters H, G, S, and Cv and ΔH, ΔG, and ΔS values have been calculated at

room temperature (298.15 K) and 1 atmospheric pressure and presented in Tables 3 and 4, respectively.

According to the calculated data, the values of H, G, and Cv of the conformer 01 in the solvent phase are less than in the gas phase.

The values also increase with the decrease of polarity. This means the molecules are stabilized in the presence of solvents (Srivastava and Khan, 2020).

On the other hand, the value of S in the solvent phase is larger than in the gas phase and decreases with the decrease of the polarity. Strong hydrogen bonding forms between the carboxylic (-COOH) group of IAA and polar solvents, releasing energy to the system.

Due to these hydrogen bonding interactions, entropy increases with the increase in polarity of the solvents (Crane-Robinson and Privalov, 2022). The results obtained from our calculation show that the studied molecule is highly stabilized in polar solvents compared to the non-polar solvents.

On the other hand, in all types of solvents, the values of ΔH are negative, which means the reactions are exothermic. Consequently, ΔH becomes more negative as the polarity of the solvent increases. The values of ΔG are also negative in all the solvent cases, which indicates that the reactions are spontaneous. The ΔG becomes more negative with the increase of the polarity of the solvent. Calculations also show that the values of ΔS become more positive as the polarity increases. That means the solvents' polarity increases the system's randomness or disorder.

**Table 2. Temperature affects the thermodynamic parameters of the most stable conformer (01) indole-3-acetic acid (IAA) calculated by the DFT/*w*B97XD/cc-pVTZ method.**

| Temperature (Kelvin) | Energy E (kcal/mol) | Enthalpy H (kcal/mol) | Gibbs free energy G (kcal/mol) | Entropy S (kcal/mol) | Heat capacity Cv (kcal/mol) |
|---|---|---|---|---|---|
| 100 | 110.73 | 110.92 | 103.53 | 22.04 | 4.78 |
| 200 | 112.89 | 113.29 | 95.31 | 26.78 | 8.25 |
| 298.15 | 116.25 | 116.84 | 85.79 | 31.04 | 12.20 |
| 310 | 116.75 | 117.36 | 84.54 | 31.55 | 12.68 |
| 400 | 121.10 | 121.89 | 74.43 | 35.36 | 16.10 |
| 500 | 127.07 | 128.06 | 61.88 | 39.45 | 19.33 |
| 600 | 134.01 | 135.20 | 47.98 | 43.32 | 21.94 |
| 700 | 141.74 | 143.13 | 32.83 | 46.96 | 24.04 |
| 800 | 150.10 | 151.69 | 16.49 | 50.36 | 25.75 |
| 900 | 158.99 | 160.78 | -0.94 | 53.55 | 27.17 |
| 1000 | 168.31 | 170.29 | -19.42 | 56.54 | 28.35 |

**Table 3. Solvent effect on thermodynamic properties for the most stable conformer (01) of indole-3-acetic acid (IAA) calculated by DFT/*w*B97XD/cc-pVTZ method.**

| Types of solvent | Name of Solvent | H (kcal/mol) | G (kcal/mol) | S (kcal/mol) | C v(kcal/mol) | μ (Debye) | α (a.u) |
|---|---|---|---|---|---|---|---|
| | Gas phase | 116.840 | | 31.040 | 12.203 | 0.619 | 120.831 |
| | Water | 116.805 | 84.737 | 32.052 | 12.173 | 0.752 | 163.935 |
| Polar protic | Methanol | 116.809 | 85.051 | 31.742 | 12.174 | 0.748 | 162.368 |
| | Ethanol | 116.812 | 85.132 | 31.664 | 12.174 | 0.746 | 161.557 |
| | Aniline | 116.828 | 85.422 | 31.391 | 12.178 | 0.727 | 153.699 |
| | DMSO | 116.807 | 84.934 | 31.857 | 12.174 | 0.750 | 163.174 |
| | Nitromethane | 116.808 | 85.015 | 31.777 | 12.174 | 0.749 | 162.653 |
| | Acetonitrile | 116.808 | 85.059 | 31.733 | 12.174 | 0.749 | 162.598 |
| | Acetone | 116.813 | 85.185 | 31.613 | 12.174 | 0.745 | 160.847 |
| Polar aprotic | Dichloroethane | 116.823 | 85.351 | 31.455 | 12.176 | 0.735 | 156.961 |
| | Dichloromethane | 116.825 | 85.376 | 31.432 | 12.177 | 0.733 | 156.001 |
| | THF | 116.827 | 85.409 | 31.402 | 12.178 | 0.729 | 154.411 |
| | Chlorobenzene | 116.832 | 85.451 | 31.365 | 12.180 | 0.721 | 151.719 |
| | Chloroform | 116.834 | 85.477 | 31.342 | 12.181 | 0.715 | 149.467 |
| | Diethylether | 116.834 | 85.489 | 31.331 | 12.183 | 0.711 | 148.095 |
| | Toluene | 116.837 | 85.550 | 31.271 | 12.191 | 0.683 | 138.932 |
| | Benzene | 116.837 | 85.556 | 31.265 | 12.191 | 0.680 | 138.117 |
| Non-polar | Carbon tetrachloride | 116.836 | 85.558 | 31.262 | 12.192 | 0.679 | 137.765 |
| | Cyclohexane | 116.837 | 85.570 | 31.251 | 12.193 | 0.672 | 135.872 |
| | Heptane | 116.837 | 85.578 | 31.242 | 12.194 | 0.669 | 134.825 |

## Electronic properties

### *Frontier molecular orbital (FMO) analysis*

The highest occupied molecular orbital (HOMO) and lowest unoccupied molecular orbital (LUMO) are known as frontier molecular orbitals (FMO). Whereas LUMO is an electron acceptor, HOMO is an electron donor. These molecular orbitals play a significant role in determining how molecular interactions with other species occur. TD-DFT has calculated the energies of HOMO and LUMO with $\omega$B97XD/cc-pVTZ in the ground state. The energy of HOMO denotes the ability of electron-donating, and the energy of LUMO denotes the ability of electron-accepting. The data obtained show that the HOMO-LUMO gap of conformer 01 is 8.96 eV.

### *Solvent effect on the electronic excitation*

The type of solvent has a great impact on the FMOs and the electronic excitation of any molecule. Another important property for exploring the solvent effect is the dipole moment of a molecule. To observe the solvent effect on the absorption spectra, the TD-DFT calculations have been carried out on the optimized structure of the most stable conformer in the nineteen (19) solvents of different polarity using the IEFPCM model at $\omega$B97XD/cc-pVTZ method.

**Table 4. Solvent effect on the ΔH, ΔG, and ΔS of conformer 01 calculated at the DFT/*w*B97XD/cc-pVTZ level of method.**

| Types of solvent | Name of Solvent | ΔH (kcal/mol) | ΔG (kcal/mol) | ΔS (kcal/mol) |
|---|---|---|---|---|
| Polar protic | Water | -0.035 | -1.048 | 1.008 |
| | Methanol | -0.030 | -0.733 | 0.698 |
| | Ethanol | -0.028 | -0.653 | 0.620 |
| | Aniline | -0.011 | -0.362 | 0.347 |
| Polar aprotic | DMSO | -0.032 | -0.851 | 0.813 |
| | Nitromethane | -0.031 | -0.769 | 0.733 |
| | Acetonitrile | -0.032 | -0.726 | 0.689 |
| | Acetone | -0.026 | -0.599 | 0.569 |
| | Dichloro ethane | -0.017 | -0.433 | 0.412 |
| | Dichloro methane | -0.015 | -0.408 | 0.389 |
| | THF | -0.013 | -0.375 | 0.358 |
| | Chloro benzene | -0.008 | -0.334 | 0.321 |
| | Chloroform | -0.006 | -0.308 | 0.298 |
| Non-polar | Diethylether | -0.006 | -0.296 | 0.287 |
| | Toluene | -0.003 | -0.234 | 0.227 |
| | Benzene | -0.003 | -0.229 | 0.221 |
| | Carbon tetrachloride | -0.004 | -0.226 | 0.218 |
| | Cyclohexane | -0.003 | -0.215 | 0.207 |
| | Heptane | -0.003 | -0.206 | 0.198 |

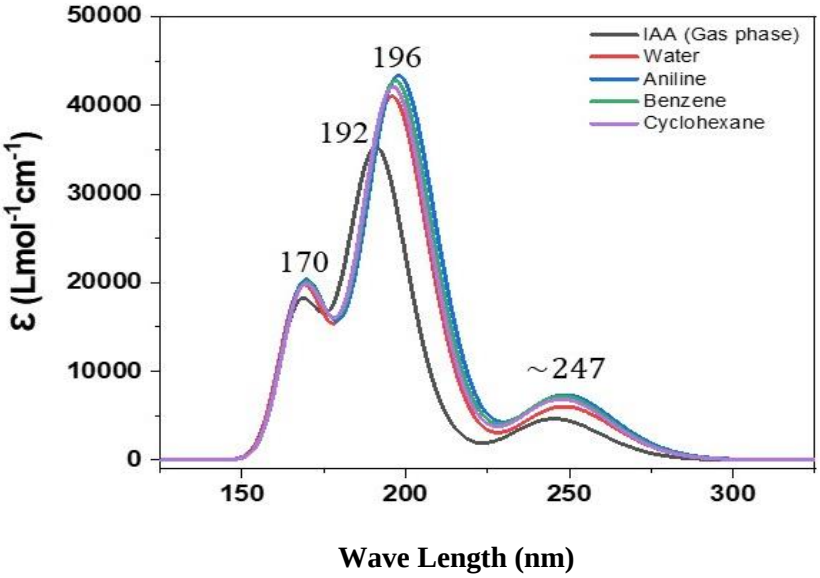


**Fig. 5. Solvent effects on the UV/Visible spectrum of the most stable conformer (01) of indole-3-acetic acid (IAA)**

The solvent effect on the absorption maxima of UV/Vis spectra has been presented in Table 5, and the absorption spectra for conformer 01 in the gas and solvent phases are presented in Figure 5. To avoid complexity, two polar solvents (water and aniline) and two non-polar solvents (benzene and cyclohexane) along with the gas phase are chosen to present UV/Vis spectral data of solvents. Following Table 5 and Figure 5, the UV/Visible absorption maxima ($\lambda_{max}$) in solvents of various polarity shift towardsthe longer wavelength, which is known as redshift or bathochromic shift, compared to the gas phase. This is because the dipole moment is expected to be larger in the solvent than in the gas phase.

It has been found that the dipole moment of the conformer 01 is less in the gas phase than in polar or non-polar solvents. That means the presence of solvation reduces the gas phase's excitation energies and induces the electronic absorption spectrum's redshift (Alauddin, 2021).

**Table 5. Solvent effect on the UV/Visible spectrum of the most stable conformer (01) of indole-3-acetic acid (IAA) calculated by TD-DFT/*w*B97XD/cc-pVTZ method.**

| Types of solvent | Name of solvents | $\lambda_{max1}$/ nm | $\lambda_{max2}$/nm | $\lambda_{max3}$/nm |
|---|---|---|---|---|
| Polar protic | Gas phase | 192.49 | 169.84 | 247.23 |
| | Water | 195.89 | 169.88 | 251.02 |
| | Methanol | 195.87 | 169.89 | 250.94 |
| | Ethanol | 196.09 | 169.97 | 251.02 |
| | Aniline | 197.33 | 170.5 | 251.38 |
| Polar aprotic | DMSO | 196.42 | 170.07 | 251.29 |
| | Nitro methane | 196.21 | 170.17 | 251.14 |
| | Acetonitrile | 195.97 | 169.92 | 251.01 |
| | Acetone | 196.08 | 169.98 | 250.98 |
| | Dichloro methane | 196.49 | 170.18 | 250.98 |
| | Dichloro ethane | 196.61 | 170.21 | 251.1 |
| | THF | 196.38 | 170.16 | 250.84 |
| | Chloro benzene | 197.04 | 171.33 | 251.09 |
| | Chloroform | 196.63 | 170.32 | 250.73 |
| Non-polar | Diethyle ether | 196.04 | 170.15 | 250.34 |
| | Toluene | 196.86 | 170.57 | 250.32 |
| | Benzene | 196.89 | 170.59 | 250.29 |
| | Carbon tetrachloride | 196.65 | 170.53 | 250.14 |
| | Cyclohexane | 196.43 | 170.5 | 249.91 |
| | Heptane | 196.18 | 170.44 | 249.72 |

*Experimental value obtained in ethanol solutions (Kamnev et at., 2001)

### *Solvent effect on the global reactivity descriptors*

Since the solvent has an important effect on the frontier molecular orbitals (FMO), it also affects the global chemical reactivity descriptors (GCRD) parameters. Ionization potential (I), electron affinity (A), chemical potential (μ), absolute electronegativity (χ), hardness (η), softness (S), and electrophilicity index (ω) are the key GCRD metrics. For closed-shell molecules, all of these values are calculated using the HOMO and LUMO energies, formulating Koopman's theorem (Koopmans, 1934).

$\chi = \left(\frac{I+A}{2}\right)$, $\eta = \left(\frac{I-A}{2}\right)$, $\mu = -\left(\frac{I+A}{2}\right)$,

$$S = \frac{1}{2\eta}, \omega = \frac{\mu^2}{2\eta}$$

where the energy of LUMO is represented by A (electron affinity) and the energy of HOMO by I (ionization potential). The calculated GCRD parameters are presented in Table 6.

The chemical potential energy becomes lower with the increase of polarity. No significant effect of the polarity of solvents on the global hardness and softness has been observed. Compared to the gas phase, the electrophilicity increases with solvent polarity, confirming that conformer 01 would be energetically preferred for electrophilic attack. The effect of solvent on the FMO and global chemical reactivity descriptors (GCRD) of the conformer 01 are listed and tabulated in Table 7.

**Table 6. Global chemical reactivity descriptors (GCRD) of the most stable conformer of IAA at DFT/*w*B97XD/cc-pVTZ method.**

| Molecular properties | Mathematical descriptors | Energy (eV) |
|---|---|---|
| $E_{HOMO}$ | Energy of HOMO | -7.57 |
| $E_{LUMO}$ | Energy of LUMO | 1.39 |
| Energy gap | $\Delta E_g = E_{LUMO} - E_{HOMO}$ | 8.96 |
| Ionization Potential (IP) | $IP = - E_{HOMO}$ | 7.57 |
| Electron Affinity (EA) | $EA = - E_{LUMO}$ | -1.39 |
| Electronegativity (χ) | $\chi = - ½ (E_{LUMO} + E_{HOMO})$ | 3.09 |
| Chemical Potential (μ) | $\mu = ½ (E_{LUMO} + E_{HOMO})$ | -3.09 |
| Global hardness (η) | $\eta = ½ (E_{LUMO} - E_{HOMO})$ | 4.48 |
| Global softness (S) | $S = \frac{1}{2\eta}$ | 0.11 |
| Electrophilicity index (ω) | $\omega = \frac{\mu^2}{2\eta}$ | 1.07 |

**Table 7. Solvent effect on the FMO and Global chemical reactivity descriptors (GCRD) of the indole-3-acetic acid (IAA).**

| Types of solvent | Name of solvents | $E_{HOMO}$ (eV) | $E_{LUMO}$ (eV) | (H-L) gap | μ | η | S | ω |
|---|---|---|---|---|---|---|---|---|
| Polar protic | Gas phase | -7.57 | 1.39 | 8.96 | -3.09 | 4.48 | 0.1116 | 1.065 |
| | Water | -7.70 | 1.23 | 8.93 | -3.24 | 4.47 | 0.1119 | 1.172 |
| | Methanol | -7.69 | 1.23 | 8.92 | -3.23 | 4.46 | 0.1121 | 1.169 |
| | Ethanol | -7.69 | 1.24 | 8.93 | -3.23 | 4.47 | 0.1119 | 1.165 |
| | Aniline | -7.66 | 1.27 | 8.93 | -3.20 | 4.47 | 0.1119 | 1.143 |
| Polar aprotic | DMSO | -7.69 | 1.23 | 8.92 | -3.23 | 4.46 | 0.1121 | 1.169 |
| | Nitromethane | -7.69 | 1.23 | 8.92 | -3.23 | 4.46 | 0.1121 | 1.169 |
| | Acetonitrile | -7.69 | 1.23 | 8.92 | -3.23 | 4.46 | 0.1121 | 1.169 |
| | Acetone | -7.69 | 1.24 | 8.93 | -3.23 | 4.47 | 0.1119 | 1.165 |
| | Dichloro methane | -7.67 | 1.26 | 8.93 | -3.21 | 4.47 | 0.1119 | 1.150 |
| | Dichloro ethane | -7.67 | 1.26 | 8.93 | -3.21 | 4.47 | 0.1119 | 1.150 |
| | THF | -7.66 | 1.27 | 8.93 | -3.20 | 4.47 | 0.1119 | 1.143 |
| | Chlorobenzene | -7.65 | 1.28 | 8.93 | -3.19 | 4.47 | 0.1119 | 1.136 |
| | Chloroform | -7.64 | 1.29 | 8.93 | -3.18 | 4.47 | 0.1119 | 1.129 |
| Non-polar | Diethyl ether | -7.64 | 1.29 | 8.93 | -3.18 | 4.47 | 0.1119 | 1.129 |
| | Toluene | -7.61 | 1.33 | 8.94 | -3.14 | 4.47 | 0.1118 | 1.103 |
| | Benzene | -7.61 | 1.33 | 8.94 | -3.14 | 4.47 | 0.1118 | 1.103 |
| | Carbon tetrachloride | -7.61 | 1.33 | 8.94 | -3.14 | 4.47 | 0.1118 | 1.103 |
| | Cyclohexane | -7.60 | 1.34 | 8.94 | -3.13 | 4.47 | 0.1118 | 1.096 |
| | Heptane | -7.60 | 1.34 | 8.94 | -3.13 | 4.47 | 0.1118 | 1.096 |

## Conclusion

The present study examines the effects of temperature (100K–1000K) and solvents (polar protic, aprotic, and non-polar) on the electronic, thermodynamic, and structural characteristics of the indole-3-acetic acid (IAA) molecule using the DFT/ωB97XD/cc-pVTZ computational technique. The four (4) lowest energy conformers have been obtained and assigned as conformers 01, 02, 03, and 04 depending on their relative energies. To simplify, the most stable conformer (01) is considered for studying the effect of solvent and temperature. The temperature effect on the thermodynamic properties has been observed, and it is seen that the calculated values of H and S increase. At the same time, G decreases steeply with the increase in temperature. The Cv rises slowly and gradually as the temperature increases. According to the calculations, the solvent-IAA interactions are found to be spontaneous and exothermic. The UV/Visible absorption spectra have been calculated and occurred $\pi \rightarrow \pi^*$ transition at the maximum absorption wavelength ($\lambda_{max}$) ~192 nm with two weak absorption bands at 167 & 247 nm. The polarity of solvents has no significant effect on the GCRD parameters. The solvent effect on the UV/Visible spectra of the most stable conformer has been analyzed, and significant bathochromic or redshifts, as well as hyperchromic effects, have been observed due to the decrease of HOMO-LUMO gap for the presence of the solvent of different (polar protic, aprotic and non-polar) polarities.

## Declaration of interests

The authors declare that they have no known competing financial interests or personal relationships that could have appeared to influence the work reported in this paper.

## Authors contribution

Manuscript prepared by Md. Alauddin, all the computational tasks have been completed by Nasima Tabassum Barna and Md. Masud Parvez, Gazi Jahirul Islam, and Mohammad Abdul Matin played a role in the final version of the manuscript.

## References

Alauddin M. Effect of solvents and temperature on capped phenylalanine's structural, thermodynamic and electronic properties: A computational study. *J. Bangladesh Acad. Sci.* 2021; 45: 205-215.

Bogaert KA, Blomme J, Beeckman T and Clerck OD. Auxin's origin: do PILS hold the key? *Trends Plant Sci.* 2022; 27: 227-236.

Bunsangiam S, Thongpae N, Limtong S and Srisuk N. Large scale production of indole-3-acetic acid and evaluation of the inhibitory effect of indole-3-acetic acid on weed growth. *Sci. Rep.* 2021; 11: 1-13.

Crane-Robinson C and Privalov P. Energetic basis of hydrogen bond formation in aqueous solution. *Eur. Biophys. J.* 2022; 51: 515–517.

Fendrych M, Akhmonova M, Merrin J, Glanc M, Hagihara S, Takahashi K, Uchida N, Torii KU and Firml J. Rapid and reversible root growth inhibition by TIR1 auxin signalling. *Nat. Plant,* 2018; 4(7): 453-459.

Flasiński M and Hąc-Wydro K. Natural vs synthetic auxin: Studies on the interactions between plant hormones and biological membrane lipids. *Environ. Res.* 2014; 133: 123-134.

Förner W and Badawi HM. A study of the conformational profile and the vibrational spectra of the plant hormone indole-3-acetic acid. *J. Theor. Comput. Chem.* 2014; 13(1): 1350073.

Frim J. Auxin transport-shaping the plant.*Curr. Opin. Plant Biol.* 2003; 6: 7-12.

Frisch MJ, Trucks GW, Schlegel HB, Scuseria GE, Robb MA, Cheeseman JR, Scalmani G, Barone V, PeterssonGA,Nakatsuji H, Li X, Caricato M, Marenich AV, Bloino J, Janesko BG, Gomperts R, Mennucci B, Hratchian HP, Ortiz JV,

Izmaylov AF, Sonnenberg JL, Williams-Young D, Ding F, Lipparini F, Egidi F, Goings J, Peng B, Petrone A, Henderson T, Ranasinghe D, Zakrzewski VG, Gao J, Rega N, Zheng G, Liang W, Hada M, Ehara M, Toyota K, FukudaR, Hasegawa J, Ishida M, Nakajima T, Honda Y, Kitao O, Nakai H, Vreven T, ThrossellK,Montgomery JA, Peralta JE, Ogliaro F, Bearpark MJ, Heyd JJ, Brothers EN, KudinKN,Staroverov VN, Keith TA, Kobayashi R, Normand J, Raghavachari K, Rendell AP, Burant JC, Iyengar SS, Tomasi J, Cossi M, Millam JM, Klene M, Adamo C, Cammi R, Ochterski JW, Martin RL, Morokuma K, Farkas O, Foresman JB and Fox DJ. *Gaussian 16, Revision B.01. Gaussian, Inc., Wallingford.* 2016

Fuente RKD and Leopold AC. Lateral movement of auxin in phototropism. *Plant Physiol.*1968; 43: 1031-1036**.**

Ilbeigi V, Valadbeigi Y, Moravsky L and Matejčík Š. Effect of ion source polarity and dopants on the detection of auxin plant hormones by ion mobility-mass spectrometry. *Anal. Bioanal. Chem.* 2022; 414: 6259-6269.

Kamnev AA, Shchelochkov AG, Tarantilis PA, Polissiou MG and Perfiliev YD. Complexation of Indole-3-acetic Acid with Iron(III): Influence of coordination on the pi-Electronic system of the ligand. *Monatsheftefür Chemie* 2001; 132: 675-681.

Koopmans TA. Uber Die Zuordnung Von Wellenfunktionen and EigenwertenZu Den. Einzelnen ElektronenEines. *Atoms Physica* 1934; 1: 104-113.

Liu L, Guo G, Wang Z, Ji H, Mu F and Li X. Tran Auxin in plant growth and stress responses. In: *Phytohormones: A window to metabolism, signaling and biotechnological applications*. LS and Pal S (eds), Springer, New York, 2014. pp. 1-35.

Luo J, Zhou JJ and Zhang JZ. Aux/IAA Gene Family in Plants: Molecular Structure, Regulation, and Function. *Int. J. Mol. Sci.* 2018; 19(1): 259.

Masuda Y and Kamisaka S. Discoveries inplant biology: Volume III, World Scientific 2000; pp. 43-57.

Mc Steen P, Malcomber S, Skirpan A, Lunde C, Wu X, Kellogg E and Hake S. Barren inforescence 2 encodes a co-ortholog of the PINOID serine/threonine kinase and is required for organogenesis during inforescence and vegetative development in maize. *Plant Physiol.* 2007; 144: 1000-11.

Nakano R, Ihara N, Morikawa S, Nakashima A, Kanemaki MT, Ikegaya Y and Takeuchi H. Auxin-mediated rapid degradation of target proteins in hippocampal neurons, *Neuroreport*, 2019; 30: 908-913.

Nigović B, Antolić S, Kojić-Prodić B, Kiralj R, Magnus V and Salopek-Sondi B. Correlation of structural and physico-chemical parameters with the bioactivity of alkylated derivatives of indole-3-acetic acid, a phytohormone (auxin). *Acta Crystallogr. Sect. B Struct. Sci.* 2000; 56: 94-111.

Nishimura K, Fukagawa T, Takisawa H, Kakimoto T and Kanemaki M. An auxin-based degron system for the rapid depletion of proteins in non-plant cells. *Nat. Methods*, 2009; 6: 917-922.

O'boyle NM, Tenderholt AL and Langner KM. Cclib: a library for package-independent computational chemistry algorithms. *J. Comput. Chem.* 2008; 29: 839-845.

OriginPro (Version 2018), OriginLab Corporation, Northampton, MA, USA.

Schmit MCP, Jubert AH, Vitale A and Lobayan RM. Electronic structure and conformational properties of 1H-indole-3-acetic acid. *J. Mol. Model.* 2011; 17: 1227-1239.

Simon S and Petrasek J. Why plants need more than one type of auxin. *Plant Sci.* 2011; 180: 454-60.

Sorefan K, Girin T, Liljegren SJ, Ljung K, Robles P, Galvan-Ampudia CS, Offringa R, Friml J, Yanofsky MF and Ostergaard L. A regulated auxin minimum is required for seed dispersal in Arabidopsis. *Nature*, 2009; 459: 583-586.

Srivastava AA and Khan MS. Density functional theory calculations for electronic, optoelectronic and thermodynamic properties of dibenzothiophene metal complexes. *Mater. Res. Express*, 2020; 7: 016311.

Su. Y, Luo W, Chen X, Liu H, Hu Y, Lin W and Xiao L. Auxin extraction and purification based on recombinant Aux/IAA proteins. *Biol. Proced. Online.* 2017; 19: 1-9.

Ung KL, Schulz L, Kleine-Vehn J, Pedersen BP and Hammes UZ. Auxin transport at the endoplasmic reticulum: roles and structural similarity of PIN-FORMED and PIN-LIKES. *J. Exp. Bot.* 2023; 74(22): 6893-6903.

Zivanovic BD, Ullrich KK, Stefens B, Spasic SZ and Galland P. The effect of auxin (indole-3-acetic acid) on the growth rate and tropism of the sporangiophore of phycomyces blakesleeanus and identification of auxin-related genes. *Protoplasma*, 2018; 255: 1331-1347.

J. Bangladesh Acad. Sci. 48(2); 207-215: December 2024 DOI:https://doi.org/10.3329/jbas.v48i2.72587

Journal of Bangladesh Academy of Sciences

Journal homepage: http://www.bas.org.bd/publications/jbas.html

**Research Article**

# Triangle group associated with generalized modular equation

Md. Shafiul Alam* and Bijan Krishna Saha

*Department of Mathematics, University of Barishal, Bangladesh*

**ARTICLE INFO**

**Article History**

Received: 17 April 2024
Revised: 18 August 2024
Accepted: 10 September 2024

**Keywords:** Triangle group, Generalized modular equation, Hecke group, Hypergeometric function.

**ABSTRACT**

In this study, we investigate the triangle group $G = \left(\frac{1}{1-2s}, \infty, \infty\right)$ associated with the generalized modular equation $\frac{{}_2F_1(s,1-s;1;1-\beta)}{{}_2F_1(s,1-s;1;\beta)} = p\,\frac{{}_2F_1(s,1-s;1;1-\alpha)}{{}_2F_1(s,1-s;1;\alpha)}$, where $p \in \mathbb{N} \setminus \{1\}$ and $s \in \left(0, \frac{1}{2}\right]$. We determine the generators of group $G$ and prove that the group $G$ is a subgroup of the Hecke group $H_k$. Also, we show that $G$ is an even-type subgroup of $H_k$. We provide examples in the cases of Ramanujan's theories of signatures 2, 3, and 4.

**2020 Mathematics Subject Classification:** 11F06; 33C05.

## Introduction

The great mathematician Srinivasa Ramanujan investigated the generalized modular equation

$$\frac{{}_2F_1(s,1-s;1;1-\beta)}{{}_2F_1(s,1-s;1;\beta)} = p\,\frac{{}_2F_1(s,1-s;1;1-\alpha)}{{}_2F_1(s,1-s;1;\alpha)}, \qquad (1.1)$$

where

$$\alpha, \beta \in (0,1), s \in \left(0, \frac{1}{2}\right], p \in \mathbb{N} \setminus \{1\},$$

and provided many remarkable formulas and identities (Berndt, 1991; 1998). Here, ${}_2F_1$ is the Gaussian hypergeometric function defined as

$${}_2F_1(a, b;\ c; \alpha) = \sum_{j=0}^{\infty} \frac{(a,j)(b,j)}{(c,j)\,j!}\alpha^j,$$

where $a, b, c \in \mathbb{C}$ with $c \neq 0, -1, -2, \ldots$, $|\alpha| < 1$, and $(a, j)$ denotes the Pochhammer symbol given by

$$(\alpha, j) = \begin{cases} 1 & \text{if } j = 0, \\ \alpha(\alpha+1)\cdots(\alpha+j-1) & \text{if } j \geq 1. \end{cases}$$

The integer $p$ is called the degree or order, and $\frac{1}{s}$ is called the signature of the equation (1.1).

The function ${}_2F_1$ can be extended to the slit plane $\mathbb{C}\setminus[1,+\infty)$ by Euler's integral representation formula (Bateman, 1953; Whittaker and Watson, 1927). The identities given by Ramanujan were published in his unpublished notebooks without original proofs (Ramanujan, 1957; 1988).

Ramanujan mainly investigated the generalized modular equation in the theories of signatures 2, 3, 4, and 6. Before the 1980s, there were no organized and developed theories associated with the generalized modular equation in the theories of signatures 2, 3, 4, and 6. Later, many mathematicians studied Ramanujan's theories and tried to prove the results provided by Ramanujan. For example, Borwein and Borwein (1987), Berndt (1985; 1989; 1991; 2006), and Berndt et al. (1995) proved many results given by Ramanujan and organized the theories related to Ramanujan's modular equation for $\frac{1}{s} = 2, 3, 4$, and 6. In their proofs, they used hypergeometric functions and the nontrivial identities for Jacobi's theta functions in addition to several new ideas. Also, Anderson et al. (1997) and Anderson et al. (2000) have studied Ramanujan's theories of modular equations from other perspectives. Alam and Sugawa (2022) provided a geometric method to prove Ramanujan's modular equations arising from the

*Corresponding author:<msalam@bu.ac.bd, shafiulmt@gmail.com>

generalized modular equation. Alam (2024) studied the Hecke groups associated with the generalized modular equation in the theories of signatures $\frac{1}{s} = 2$, 3, and 4.

This paper studies the triangle groups associated with the generalized modular equation. We show that the triangle group $G = \left(\frac{1}{1-2s}, \infty, \infty\right)$, where $s \in \left(0, \frac{1}{2}\right]$, is generated by

$$A_1 = \begin{pmatrix} 1 & 2\sin\pi s \\ 0 & 1 \end{pmatrix}$$

and

$$A_2 = \begin{pmatrix} 1 & 0 \\ 2\sin\pi s & 1 \end{pmatrix},$$

and is related to the generalized modular equation. The generators of the triangle group $G$ can also be expressed by

$$A_1 = \begin{pmatrix} 1 & 2\sin\pi s \\ 0 & 1 \end{pmatrix}$$

and

$$A'_2 = \begin{pmatrix} 4\sin^2\pi s - 1 & -2\sin\pi s \\ 2\sin\pi s & -1 \end{pmatrix}$$

where $s \in \left(0, \frac{1}{2}\right]$. For $k \geq 3$, the Hecke group $H_k$ is generated by

$$U = \begin{pmatrix} 1 & 2\cos\frac{\pi}{k} \\ 0 & 1 \end{pmatrix}$$

and

$$V = \begin{pmatrix} 0 & -1 \\ 1 & 0 \end{pmatrix}.$$

We prove that the triangle group $G$ is a subgroup of $H_k$ and show that $G$ is an even-type subgroup of $H_k$. Finally, we give examples in the cases of Ramanujan's theories of signatures $\frac{1}{s} = 2$, 3, and 4.

**Preliminaries**

Let us consider the following hypergeometric differential equation

$$\alpha(1-\alpha)\frac{d^2w}{d\alpha^2} + \{c - (a+b+1)\alpha\}\frac{dw}{d\alpha} - abw = 0. \tag{2.1}$$

The equation (2.1) has two linearly independent solutions

$$w_1 = {}_2F_1(a, b;\ \mathrm{c};\ \alpha)$$

and

$$w_2 = {}_2F_1(a, b;\ \mathrm{a} + \mathrm{b} + 1 - \mathrm{c};\ 1 - \alpha).$$

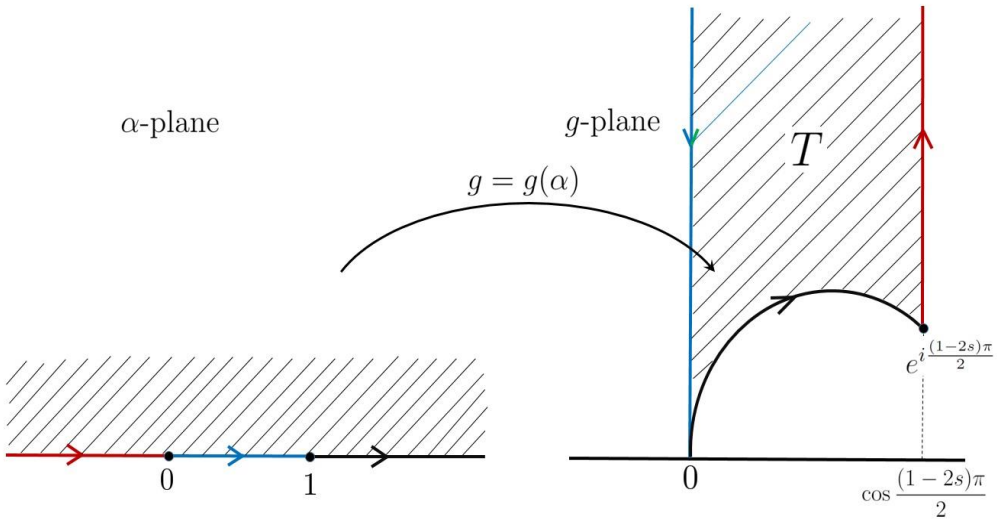


**Fig. 1. The map $g$ transforms the upper half of the $\alpha$-plane to $T$ on the $g$-plane.**

We denote the upper half-plane $\{\alpha \in \mathbb{C} : \text{Im } \alpha > 0\}$ by $\mathcal{H}$. If

$$g(\alpha) = i\frac{{}_2F_1(a,b;\ \text{a} + \text{b} + 1 - \text{c}; 1-\alpha)}{{}_2F_1(a,b;\ \text{c};\alpha)},$$

then $g$ maps $\mathcal{H}$ conformally onto a hyperbolic triangle $T$ (Fig. 1). At the vertices $g(0)$, $g(1)$, and $g(\infty)$, the interior angles of $T$ are $(1-c)\pi, (c-a-b)\pi$ and $(b-a)\pi$, respectively (Nehari, 1952).

For $s \in \left(0, \frac{1}{2}\right]$, let

$$a = s,\ b = 1 - s \text{ and } c = 1.$$

Then

$$g(\alpha) = i\frac{{}_2F_1(s, 1-s;\ 1; 1-\alpha)}{{}_2F_1(s, 1-\text{s};\ 1;\alpha)}. \quad (2.2)$$

The following lemma describes the above facts.

***Lemma 2.1*** *(Lemma 4.1 of (Anderson et al., 2010)). Consider the map*

$$g(\alpha) = i\frac{{}_2F_1(s, 1-s;\ 1; 1-\alpha)}{{}_2F_1(s, 1-s;\ 1;\alpha)},$$

*where* $s \in \left(0, \frac{1}{2}\right]$, *then* $g$ *maps*

$$\mathcal{H} = \{\alpha \in \mathbb{C} : Im\ \alpha > 0\}$$

*onto the following hyperbolic triangle*

$$T = \left\{ g \in \mathcal{H}: 0 < Re\ g < cos\frac{(1-2s)\pi}{2},\ \left|2g\ cos\frac{(1-2s)\pi}{2} - 1\right| > 1 \right\}$$

*in the* $g$*-plane. At the vertices* $g(\infty) = e^{i\frac{(1-2s)}{2}}$, $g(0) = \infty$ *and* $g(1) = 0$, *the interior angles of* $T$ *are* $(1-2s)\pi$, 0, *and* 0, *respectively.*

The following set of matrices

$$\left\{\begin{pmatrix} a & b \\ c & d \end{pmatrix} : a, b, c, d \in \mathbb{R},\ ad - bc = 1\right\}$$

constructs a group known as the unimodular group and is denoted by $\text{SL}_2(\mathbb{R})$. The group $\text{PSL}_2(\mathbb{R})$ is defined as

$$\text{PSL}_2(\mathbb{R}) = \text{SL}_2(\mathbb{R})/\{\pm I_2\},$$

where $I_2$ is the $2 \times 2$ identity matrix (Serre, 1973; Katok, 1992). The action of the group $\text{P L}_2(\mathbb{R})$ on $\mathcal{H}$ is as follows:

$$\alpha \mapsto \begin{pmatrix} a & b \\ c & d \end{pmatrix}\alpha = \frac{a\alpha + b}{c\alpha + d},$$

where $\begin{pmatrix} a & b \\ c & d \end{pmatrix} \in \text{PSL}_2(\mathbb{R})$ and $\alpha \in \mathcal{H}$.

Consider the boundary $\partial\mathcal{H} = \mathbb{R} \cup \{\infty\}$ of $\mathcal{H}$. Vertical lines and semicircles orthogonal to the real axis, known as geodesics (Katok, 1992). The group $\text{PSL}_2(\mathbb{R})$, together ith the transformation

$$\gamma(\alpha) = -\overline{\alpha}$$

construct the group $\text{Isom}(\mathcal{H})$ of isometries of $\mathcal{H}$ (Gannon, 2007), i.e.,

$$\text{Isom}(\mathcal{H}) \cong \text{PSL}_2(\mathbb{R}) \cup \gamma\text{PSL}_2(\mathbb{R})$$

and the group of analytic automorphisms of $\mathcal{H}$, denoted by $\text{Aut}(\mathcal{H})$, is the group $\text{PSL}_2(\mathbb{R})$.

Let the internal angles of a triangle be $\frac{\pi}{m_1}$, $\frac{\pi}{m_2}$, $\frac{\pi}{m_3}$, then the triangle is

(i) Euclidean if $\frac{1}{m_1} + \frac{1}{m_2} + \frac{1}{m_3} = 1$,

(ii) spherical if $\frac{1}{m_1} + \frac{1}{m_2} + \frac{1}{m_3} > 1$,

(iii) hyperbolic if $\frac{1}{m_1} + \frac{1}{m_2} + \frac{1}{m_3} < 1$.

In our study, we are interested in the hyperbolic triangle. We will denote the hyperbolic triangle by $T$. If the angles of two hyperbolic triangles are the same, then they are congruent. The area of $T$ depends on the angles $\frac{\pi}{m_1}$, $\frac{\pi}{m_2}$, $\frac{\pi}{m_3}$ and is given by the following theorem known as Gauss-Bonnet theorem (Katok, 1992)).

***Theorem 2.2*** *(Gauss-Bonnet). Let* $T$ *be a hyperbolic triangle with angles* $\frac{\pi}{m_1}, \frac{\pi}{m_2}$, *and* $\frac{\pi}{m_3}$, *then*

$$Area(T) = \pi\left(1 - \frac{1}{m_1} - \frac{1}{m_2} - \frac{1}{m_3}\right).$$

The upper half-plane $\mathcal{H}$ can be tessellated by the successive reflections of the hyperbolic triangle $T$ about its sides. Let $K$ be the group generated by the three reflections of $T$ about its sides; then, it is the

discrete subgroup of Isom($\mathcal{H}$). Let $G$ be the subgroup of $K$ such that $G$ has only orientation-preserving isometries. Then,

$$G = K \cap \mathrm{PSL}_2(\mathbb{R}).$$

Group $G$ is the triangle group with signature $(m_1, m_2, m_3)$. One can also represent the triangle group $G$ as

$$\langle A, B \mid A^{m_1} = B^{m_2} = (AB)^{m_3} = 1 \rangle,$$

where $A$, $B$ and $AB$ represent the rotations, respectively, by $\frac{2\pi}{m_1}$, $\frac{2\pi}{m_2}$ and $\frac{2\pi}{m_3}$ about the vertices of $T$.

Let $D$ be a subset of $\mathcal{H}$, and let $G$ be a subgroup of $\mathrm{PSL}_2(\mathbb{R})$. If the following conditions are satisfied, then $D$ is called a fundamental domain for $G$ (Shimura, 1971):

(i) all points of $D$ are $G$-inequivalent,

(ii) the subset $D$ is open and connected,

(iii) if $x \in \mathcal{H}$ and $y$ is a point of the closure of $D$, then $x$ is $G$-equivalent to $y$.

When the subgroup $G$ is a triangle group, the fundamental domain for $G$ is given by the hyperbolic triangle $T$ and its reflection about one of its sides. Note that one can construct a fundamental domain for a subgroup of $\mathrm{PSL}_2(\mathbb{R})$ in different ways.

For $k \geq 3$, the Hecke group $H_k$ is generated by

$$U = \begin{pmatrix} 1 & \delta_k \\ 0 & 1 \end{pmatrix}$$

and

$$V = \begin{pmatrix} 0 & -1 \\ 1 & 0 \end{pmatrix},$$

where $\delta_k = 2\cos\frac{\pi}{k}$. The element $V$ has a fixed point at $\alpha = i$ of order 2. The Hecke group $H_k$ is a discrete subgroup of $\mathrm{PSL}_2(\mathbb{R})$. For $l \geq 2$, let $k = 2l$. Then $H_l$ is isomorphic to $\mathbb{Z} * \mathbb{Z}/l\mathbb{Z}$ and $G = \langle U_{2l}, V_{2l} \rangle$ is a normal subgroup of $H_{2l}$ of index 2, where

$$U_{2l} = \begin{pmatrix} 1 & \delta_{2l} \\ 0 & 1 \end{pmatrix}$$

and

$$V_{2l} = V^{-1} U_{2l}^{-1} V = \begin{pmatrix} 1 & 0 \\ \delta_{2l} & 1 \end{pmatrix}.$$

If $l = 2$ and $l = 3$, then the Hecke subgroups $H_4$ and $H_6$ are important and interesting as the elements of $H_4$ and $H_6$ are completely known (Parson, 1977). Note that the Hecke subgroup $H_3$ is the classical modular group $\mathrm{PSL}_2(\mathbb{Z})$ generated by

$$\begin{pmatrix} 1 & 1 \\ 0 & 1 \end{pmatrix} \text{ and } \begin{pmatrix} 0 & -1 \\ 1 & 0 \end{pmatrix}.$$

The elements of Hecke group $H_k$ are of the following two types:

(1) $\begin{pmatrix} a\delta_k & b \\ c & d\delta_k \end{pmatrix}$, where $a, b, c, d \in \mathbb{Z}$ and $ad\delta_k^2 - bc = 1$,

(2) $\begin{pmatrix} a & b\delta_k \\ c\delta_k & d \end{pmatrix}$, where $a, b, c, d \in \mathbb{Z}$ and $ad - bc\delta_k^2 = 1$.

Type (1) is known as the odd type Hecke subgroup, and type (2) is known as the even type Hecke subgroup (Cangul, 1997; Cangul and Singerman, 1998).

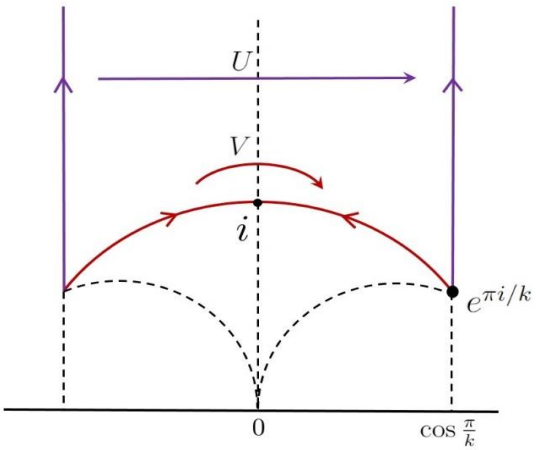


**Fig. 2. Fundamental domain for $H_k$.**

Let $W_k = UV = \begin{pmatrix} \delta_k & -1 \\ 1 & 0 \end{pmatrix}$. Then, $W_k$ has a fixed point at $e^{i\pi/k}$ of order $k$. The following set of points

$$D_k = \left\{ \alpha \in \mathcal{H} : |\alpha| \geq 1, |Re\ \alpha| \leq \cos\frac{\pi}{k} \right\}$$

is a fundamental domain for the Hecke group $H_k$ (Fig. 2). One can easily see that the group $H_k$ is a triangle group with signature $(2, k, \infty)$.

**Main Results**

***Theorem 3.1.*** *The triangle group associated with the generalized modular equation*

$$\frac{{}_2F_1(s,1-s;1;1-\beta)}{{}_2F_1(s,1-s;1;\beta)} = p\,\frac{{}_2F_1(s,1-s;1;1-\alpha)}{{}_2F_1(s,1-s;1;\alpha)}$$

*is* $G = \left(\frac{1}{1-2s}, \infty, \infty\right)$ *generated by*

$$A_1 = \begin{pmatrix} 1 & 2\sin\pi s \\ 0 & 1 \end{pmatrix}$$

*and*

$$A_2 = \begin{pmatrix} 1 & 0 \\ 2\sin\pi s & 1 \end{pmatrix},$$

*where* $s \in \left(0, \frac{1}{2}\right]$.

***Proof.*** From Lemma 2.1, we have the function

$$g(\alpha) = i\,\frac{{}_2F_1(s,1-s;\ 1;1-\alpha)}{{}_2F_1(s,1-\mathrm{s};\ 1;\alpha)}$$

maps the upper half $\alpha$-plane to the hyperbolic triangle $T$ with angles $(1-2s)\pi$, 0 and 0 at $g(\infty) = e^{i\frac{(1-2s)\pi}{2}}$, $g(0) = \infty$ and $g(1) = 0$, respectively, in the upper half $g$-plane.

Let

$$\theta_1 = \frac{\pi}{m_1},\ \ \theta_2 = \frac{\pi}{m_2} \text{ and } \ \theta_3 = \frac{\pi}{m_3}$$

be the internal angles of a hyperbolic triangle $T$, then $T$ can be continued across its sides as a single-valued function if and only if $m_j > 1$ and $m_j \in \mathbb{N} \cup \{\infty\}$ for $j = 1, 2, 3$ (Sansone and Gerretsen, 1969). Therefore,

$$\frac{1}{m_1} + \frac{1}{m_2} + \frac{1}{m_3} < 1$$

and

$$m_1 = \frac{1}{1-2s},\ \ m_2 = \infty \text{ and } m_3 = \infty.$$

It follows that we can tessellate $\mathcal{H}$ by the triangle $T$. Since a triangle group preserves a tessellation by a triangle, the triangle group associated with the generalized modular equation is

$$G = (m_1, m_2, m_3) = \left(\frac{1}{1-2s}, \infty, \infty\right).$$

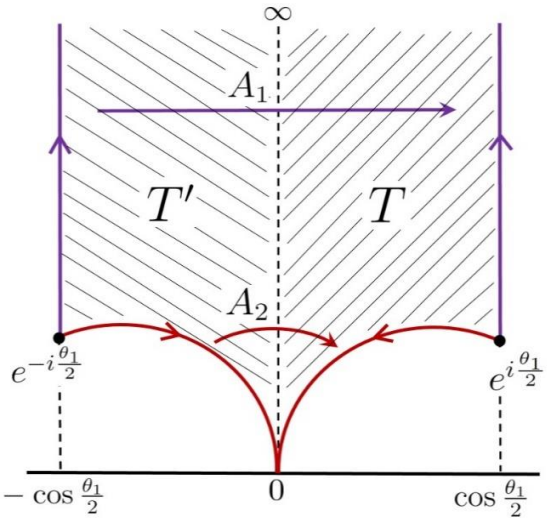


**Fig. 3. Fundamental domain for the triangle group $G = \left(\frac{1}{1-2s}, \infty, \infty\right)$.**

If we reflect the hyperbolic triangle $T$ about the geodesic side joining 0 and ∞, then we obtain the hyperbolic triangle $T'$ with vertices at ∞, 0 and $e^{-i\frac{\theta_1}{2}}$ (see Fig. 3). The triangle $T$ represents $\mathcal{H}$, and the triangle $T'$ represents the lower half-plane. Note that one can reflect $T$ about any side of $T$. If the geodesic side between $e^{-i\frac{\theta_1}{2}}$ and ∞ is identified with the geodesic side between $e^{i\frac{\theta_1}{2}}$ and ∞, then the side-pairing transformation is

$$\begin{aligned} A_1 &= \begin{pmatrix} 1 & 2\cos\frac{\theta_1}{2} \\ 0 & 1 \end{pmatrix} \\ &= \begin{pmatrix} 1 & 2\cos\frac{(1-2s)\pi}{2} \\ 0 & 1 \end{pmatrix} \\ &= \begin{pmatrix} 1 & 2\sin\pi s \\ 0 & 1 \end{pmatrix}. \end{aligned}$$

The transformation $A_1$ divides the upper half of the $\alpha$-plane into infinite strips parallel to the $y$-axis and width $2\cos\frac{\theta_1}{2}$. If the geodesic side between 0 and $e^{-i\frac{\theta_1}{2}}$ is identified with the geodesic side between 0 and $e^{i\frac{\theta_1}{2}}$, then the side-pairing transformation is

$$A_2 = \begin{pmatrix} 1 & 0 \\ 2\cos\frac{\theta_1}{2} & 1 \end{pmatrix} = \begin{pmatrix} 1 & 0 \\ 2\sin\pi s & 1 \end{pmatrix}.$$

Therefore, the triangle group $G = \left(\frac{1}{1-2s}, \infty, \infty\right)$ is generated by

$$A_1 = \begin{pmatrix} 1 & 2\sin\pi s \\ 0 & 1 \end{pmatrix}$$

and

$$A_2 = \begin{pmatrix} 1 & 0 \\ 2\sin\pi s & 1 \end{pmatrix}.$$

***Remark 1.*** The triangle group $G$ acts properly discontinuously on $\mathcal{H}$, and we obtain the quotient surface $G\backslash\mathcal{H}$, which is the thrice punctured Riemann sphere $\hat{\mathbb{C}} \setminus \{0, 1, \infty\}$.

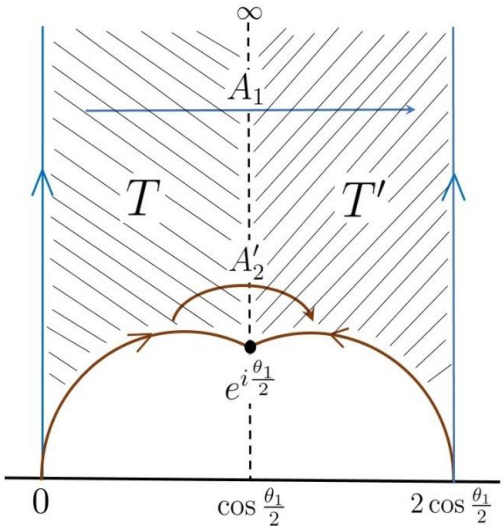


**Fig. 4. The modified fundamental domain for $G = \left(\frac{1}{1-2s}, \infty, \infty\right)$.**

***Lemma 3.2.*** The generators of the triangle group $G = \left(\frac{1}{1-2s}, \infty, \infty\right)$ can be expressed by

$$A_1 = \begin{pmatrix} 1 & 2\sin\pi s \\ 0 & 1 \end{pmatrix}$$

*and*

$$A'_2 = \begin{pmatrix} 4\sin^2\pi s - 1 & -2\sin\pi s \\ 2\sin\pi s & -1 \end{pmatrix},$$

where $s \in \left(0, \frac{1}{2}\right]$.

***Proof.*** By Theorem 3.1, the generators of the triangle group $G = \left(\frac{1}{1-2s}, \infty, \infty\right)$ are

$$A_1 = \begin{pmatrix} 1 & 2\sin\pi s \\ 0 & 1 \end{pmatrix}$$

and

$$A_2 = \begin{pmatrix} 1 & 0 \\ 2\sin\pi s & 1 \end{pmatrix},$$

where $s \in \left(0, \frac{1}{2}\right]$. The fundamental domain for the triangle group $G$ is modified as follows. If we reflect the hyperbolic triangle $T$ about the geodesic side joining $e^{i\frac{\theta_1}{2}}$ and $\infty$, then we obtain the hyperbolic triangle $T'$ whose vertices are at $2\cos\frac{\theta_1}{2} = 2\sin\pi s$, $e^{i\frac{\theta_1}{2}} = e^{i\frac{(1-2s)\pi}{2}}$, and $\infty$ (Fig. 4).

The triangle $T$ represents $\mathcal{H}$, and the triangle $T'$ represents the lower half-plane. If the geodesic side between 0 and $\infty$ is identified with the geodesic side between $2\sin\pi s$ and $\infty$, then the side-pairing transformation is

$$A_1 = \begin{pmatrix} 1 & 2\sin\pi s \\ 0 & 1 \end{pmatrix}$$

and if the geodesic side between 0 and $e^{i\frac{(1-2s)\pi}{2}}$ is identified with the geodesic side between $2\sin\pi s$ and $e^{i\frac{(1-2s)\pi}{2}}$, then the side-pairing transformation is

$$\begin{aligned} A'_2 &= -A_1 A_2^{-1} \\ &= -\begin{pmatrix} 1 & 2\sin\pi s \\ 0 & 1 \end{pmatrix}\begin{pmatrix} 1 & 0 \\ -2\sin\pi s & 1 \end{pmatrix} \\ &= \begin{pmatrix} 4\sin^2\pi s - 1 & -2\sin\pi s \\ 2\sin\pi s & -1 \end{pmatrix}. \end{aligned}$$

Therefore, $A_1$ and $A'_2$ are the generators of $G$.

***Remark 2.*** The generator $A'_2$ is an elliptic element of order $m_1 = \frac{1}{1-2s}$.

***Theorem 3.3.*** The group associated with the generalized modular equation

$$\frac{{}_2F_1(s,1-s;1;1-\beta)}{{}_2F_1(s,1-s;1;\beta)} = p\frac{{}_2F_1(s,1-s;1;1-\alpha)}{{}_2F_1(s,1-s;1;\alpha)}$$

is a subgroup of the Hecke group $\mathrm{H_k}$.

***Proof.*** According to Theorem 3.1, the triangle group $G = \left(\frac{1}{1-2s}, \infty, \infty\right)$ is associated with the generalized modular equation. The generators of the group $G$ are

$$\begin{aligned} A_1 &= \begin{pmatrix} 1 & 2\sin \pi s \\ 0 & 1 \end{pmatrix} \\ &= \begin{pmatrix} 1 & 2\cos\frac{(1-2s)\pi}{2} \\ 0 & 1 \end{pmatrix} \\ &= \begin{pmatrix} 1 & 2\cos\frac{\pi}{2m_1} \\ 0 & 1 \end{pmatrix} \end{aligned}$$

and

$$\begin{aligned} A_2 &= \begin{pmatrix} 1 & 0 \\ 2\sin \pi s & 1 \end{pmatrix} \\ &= \begin{pmatrix} 1 & 0 \\ 2\cos\frac{\pi}{2m_1} & 1 \end{pmatrix}. \end{aligned}$$

For $k \geq 3$, the Hecke group $H_k$ is generated by

$$U = \begin{pmatrix} 1 & 2\cos\frac{\pi}{k} \\ 0 & 1 \end{pmatrix}$$

and

$$V = \begin{pmatrix} 0 & -1 \\ 1 & 0 \end{pmatrix}.$$

Let $k = 2m_1$, then

$$A_1 = U$$

and

$$A_2 = V^{-1}U^{-1}V.$$

Since the generators of the group $G$ can be expressed in terms of the generators of the Hecke group $H_k$, we conclude that $G$ is a subgroup of $H_k$.

***Lemma 3.4.*** The triangle group $G = \left(\frac{1}{1-2}, \infty, \infty\right)$ is an even type subgroup of $H_k$.

***Proof.*** It is known that an even type subgroup of $H_k$ is of the following form:

$$\begin{pmatrix} a & b\delta_k \\ c\delta_k & d \end{pmatrix},$$

where $a, b, c, d \in \mathbb{Z}, \delta_k = 2\cos\frac{\pi}{k}$ and $ad - bc\delta_k^2 = 1$. In the proof of Theorem 3.3, we have seen that the generators of the triangle group $G = \left(\frac{1}{1-2s}, \infty, \infty\right)$ are

$$A_1 = \begin{pmatrix} 1 & 2\cos\frac{\pi}{2m_1} \\ 0 & 1 \end{pmatrix}$$

and

$$A_2 = \begin{pmatrix} 1 & 0 \\ 2\cos\frac{\pi}{2m_1} & 1 \end{pmatrix}.$$

Let $k = 2m_1$ and $a = 1, b = 2, c = 0, d = 1$ or $a = 1, b = 0, c = 2, d = 1$. Then, we conclude that $G$ is an even-type subgroup of $H_k$.

***Remark 3.*** The triangle group G can be represented by

$$G = \left\{\begin{pmatrix} a & b\delta_k \\ c\delta_k & d \end{pmatrix} : a, b, c, d \in \mathbb{Z} \text{ and } ad - bc\delta_k^2 = 1\right\}.$$

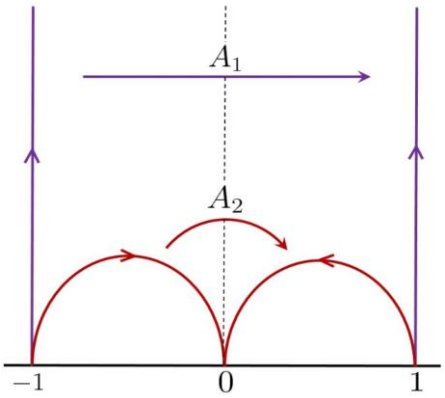


**Fig. 5. Fundamental domain for the triangle group $G = (\infty, \infty, \infty)$.**

**Example 3.1.** For the signature $\frac{1}{s} = 2$, the generalized modular equation is

$$\frac{{}_2F_1\left(\frac{1}{2},\frac{1}{2};1;1-\beta\right)}{{}_2F_1\left(\frac{1}{2},\frac{1}{2};1;\beta\right)} = p\frac{{}_2F_1\left(\frac{1}{2},\frac{1}{2};1;1-\alpha\right)}{{}_2F_1\left(\frac{1}{2},\frac{1}{2};1;\alpha\right)}.$$

In this case, the corresponding triangle group is $G = (\infty, \infty, \infty)$ and the generators of $G$ are

$$A_1 = \begin{pmatrix} 1 & 2 \\ 0 & 1 \end{pmatrix} \text{ and } A_2 = \begin{pmatrix} 1 & 0 \\ 2 & 1 \end{pmatrix}.$$

The fundamental domain for $G = (\infty, \infty, \infty)$ is shown in Fig. 5. The vertices of the triangle $T$ are at 0, 1, and ∞; the angles of $T$ are 0, 0, and 0.

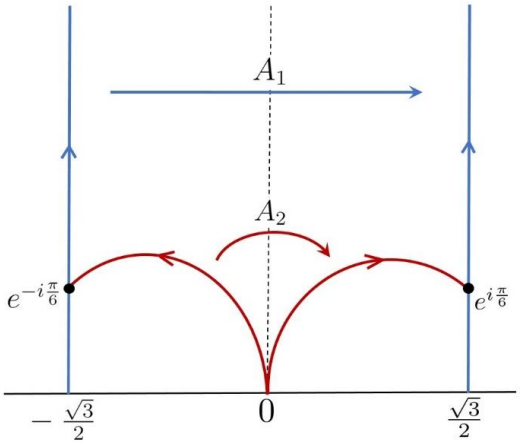


**Fig. 6. Fundamental domain for the triangle group $G = (3, \infty, \infty)$.**

**Example 3.2.** If the signature $s = \frac{1}{3}$, then the generalized modular equation is

$$\frac{{}_2F_1\left(\frac{1}{3},\frac{2}{3};1;1-\beta\right)}{{}_2F_1\left(\frac{1}{3},\frac{2}{3};1;\beta\right)} = p\frac{{}_2F_1\left(\frac{1}{3},\frac{2}{3};1;1-\alpha\right)}{{}_2F_1\left(\frac{1}{3},\frac{2}{3};1;\alpha\right)}$$

and the corresponding triangle group is $G = (3, \infty, \infty)$ and the generators of $G$ are

$$A_1 = \begin{pmatrix} 1 & \sqrt{3} \\ 0 & 1 \end{pmatrix} \text{ and } A_2 = \begin{pmatrix} 1 & 0 \\ \sqrt{3} & 1 \end{pmatrix}.$$

The fundamental domain for $G = (3, \infty, \infty)$ is shown in Fig. 6. In this case, the triangle $T$ has internal angles 0, 0, and $\frac{\pi}{3}$ at the vertices ∞, 0, and $e^{i\frac{\pi}{6}}$, respectively.

**Example 3.3.** If the signature $\frac{1}{s} = 4$, then the generalized modular equation is

$$\frac{{}_2F_1\left(\frac{1}{4},\frac{3}{4};1;1-\beta\right)}{{}_2F_1\left(\frac{1}{4},\frac{3}{4};1;\beta\right)} = p\frac{{}_2F_1\left(\frac{1}{4},\frac{3}{4};1;1-\alpha\right)}{{}_2F_1\left(\frac{1}{4},\frac{3}{4};1;\alpha\right)}.$$

In this case, the corresponding triangle group is $G = (2, \infty, \infty)$ generated by

$$A_1 = \begin{pmatrix} 1 & \sqrt{2} \\ 0 & 1 \end{pmatrix} \text{ and } A_2 = \begin{pmatrix} 1 & 0 \\ \sqrt{2} & 1 \end{pmatrix}.$$

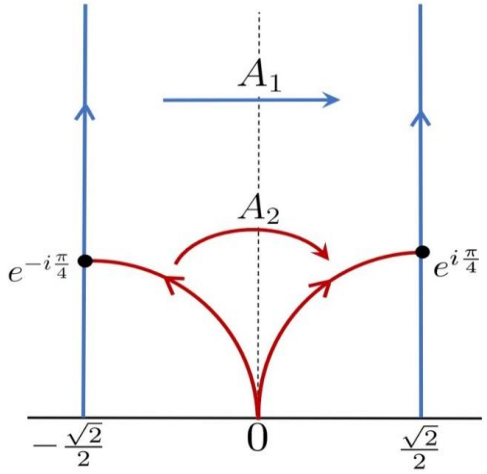


**Fig. 7. Fundamental domain for the triangle group $G = (2, \infty, \infty)$.**

The fundamental domain for $G = (2, \infty, \infty)$ is shown in Fig. 7. The internal angles of the triangle $T$ are 0, 0, and $\frac{\pi}{2}$ at the vertices ∞, 0, and $e^{i\frac{\pi}{4}}$, respectively.

## Conclusion

We have studied the triangle group $G = \left(\frac{1}{1-2s}, \infty, \infty\right)$ associated with the generalized modular equation

$$\frac{{}_2F_1(s, 1-s; 1; 1-\beta)}{{}_2F_1(s, 1-s; 1; \beta)} = p\frac{{}_2F_1(s, 1-s; 1; 1-\alpha)}{{}_2F_1(s, 1-s; 1; \alpha)}$$

where $s \in \left(0, \frac{1}{2}\right]$ and $p \in \mathbb{N} \setminus \{1\}$. It has been proved that the triangle group $G$ is generated by

$$A_1 = \begin{pmatrix} 1 & 2\sin\pi s \\ 0 & 1 \end{pmatrix}$$

and

$$A_2 = \begin{pmatrix} 1 & 0 \\ 2\sin\pi s & 1 \end{pmatrix}.$$

Also, we have proved that the group $G$ is a subgroup of the Hecke group $H_k$. In fact, the group $G$ is an even-type subgroup of $H_k$. Finally, three examples have been given in the cases of signatures $\frac{1}{s} = 2$, 3, and 4.

**Acknowledgments**

The University Grants Commission of Bangladesh supported this research under research funds allocated to the University of Barishal.

**Conflict of Interest**

The authors declare that they have no conflict of interest regarding the publication of this article.

**Author's Contributions**

Md. Shafiul Alam contributed to conceptualization, formal analysis, supervision, and manuscript drafting. Bijan Krishna Saha contributed to validation, analysis, and manuscript editing.

## References

Alam MS and Sugawa T. Geometric deduction of the solutions to modular equations. *Ramanujan J.* 2022; 59(2): 459-477.

Alam MS. On Ramanujan's modular equations and Hecke groups. *Ann. Fenn. Math.* 2024; 49(2): 61-47.

Anderson GD, Qiu SL, Vamanamurthy MK and Vuorinen M. Generalized elliptic integrals and modular equations. *Pacific J. Math.* 2000; 19: 1-37.

Anderson GD, Sugawa T, Vamanamurthy MK and Vuorinen M. Twice-punctured hyperbolic sphere with a conical singularity and generalized elliptic integral. *Math. Z.* 2010; 266: 181-191.

Anderson GD, Vamanamurthy MK and Vuorinen M. *Conformal Invariants, Inequalities, and Quasiconformal Maps*. Wiley-Interscience; 1997.

Bateman H. *Higher Transcendental Functions*. Vol. I. McGraw-Hill. New York; 1953.

Berndt BC, Bhargava S and Garvan FG. Ramanujan's theories of elliptic functions to alternative bases. *Trans. Amer. Math. Soc*. 1995; 347: 4163-4244.

Berndt BC. *Ramanujan's Notebooks*. Part II. Springer-Verlag. New York; 1989.

Berndt BC. *Number Theory in the Spirit of Ramanujan*. Amer. Math. Soc. Providence, RI; 2006.

Berndt BC. *Ramanujan's Notebooks*. Part V. Springer-Verlag. New York; 1998.

Berndt BC. *Ramanujan's Notebooks*. Part I. Springer-Verlag. New York; 1985.

Berndt BC. *Ramanujan's Notebooks*. Part III. Springer-Verlag. New York; 1991.

Borwein J and Borwein PB. *Pi and the AGM*. Wiley. New York; 1987.

Cangul IN and Singerman D. Normal subgroups of Hecke groups and regular maps. *Math. Proc. Camb. Phil. S*oc. 1998; 123: 59-74.

Cangul IN. About some normal subgroups of Hecke groups. *Turk. J. Math*. 1997; 21(2): 143-151.

Gannon T. *Moonshine beyond the Monster: The bridge connecting algebra, modular forms and physics*. Cambridge University Press; 2007.

Katok S. *Fuchsian Groups*. The University of Chicago Press. Chicago and London; 1992.

Nehari Z. *Conformal Mapping*. McGraw-Hill. New York; 1952.

Parson LA. Normal congruence subgroups of the Hecke groups $G(2^{(1/2)})$ and $G\left(3^{\left(\frac{1}{2}\right)}\right)$. *Pacific J. Math*. 1977; 70(2): 481-487.

Ramanujan S. *Notebooks (2 Volumes)*. Tata Institute of Fundamental Research. Bombay; 1957.

Ramanujan S. *The lost notebook and other unpublished papers*. Narosa. New Delhi; 1988.

Sansone G and Gerretsen *J. Lectures on the Theory of Functions of a Complex Variable: II. Geometric Theory*. Wolters-Noordhoff; 1969.

Serre JP. *A Course in Arithmetic*. Graduate Texts in Mathematics 7. Springer-Verlag. New York; 1973.

Shimura G. *Introduction to the Arithmetic Theory of Automorphic Functions*. Princeton University Press. Princeton, New Jersey; 1971.

Whittaker ET and Watson GN. *A Course of Modern Analysis*. Cambridge University Press. Cambridge; 1927.

J. Bangladesh Acad. Sci. 48(2); 217-230: December 2024 DOI:https://doi.org/10.3329/jbas.v48i2.73000

Journal of Bangladesh Academy of Sciences

Journal homepage: http://www.bas.org.bd/publications/jbas.html

**Research Article**

# Toxic effects of cadmium chloride on behavior and histopathology of butter catfish *Ompok pabda* (Hamilton, 1822)

Atakiya Galiba, Md. Mostavi Enan Eshik and Mohammad Shamsur Rahman*

*Aquatic Animal Health Group, Department of Fisheries, Faculty of Biological Sciences, University of Dhaka, Bangladesh*

**ARTICLE INFO**

**Article History**

Received: 05 May 2024
Revised: 02 September 2024
Accepted: 04 September 2024

**Keywords:** Heavy metal, Cadmium chloride, *Ompok pabda*, Behavior, Histopathology.

**ABSTRACT**

Cadmium is very harmful to aquatic organisms and the environment as a toxicant. The present study investigated cadmium's morphological, behavioral, and histopathological effects on *Ompokpabda*. Initially, the fish were divided into 6 groups and exposed to different concentrations (20 mg/L, 40 mg/L, 80 mg/L, 160 mg/l, 320 mg/L, 400 mg/L) of $CdCl_2$. After 96 hours of exposure, the $LC_{50}$ value of $CdCl_2$ for *O. pabda*was calculated as 190.9 mg/L. Finally, based on $LC_{50}$, three concentrations of $CdCl_2$ viz., 100 mg/L, 190.9 mg/L, and 300 mg/L, respectively, with three replica and control groups were used to observe morphological, behavioral, and histopathological changes in fish. There were no abnormalities in behavior or deaths in the control group at any point in the experiment. At the same time, the behavioral abnormalities of the $CdCl_2$-treated fish were increased as the dose increased. The behavioral abnormalities observed were loss of balance, breathing difficulty, hyperactivity, frequent surfacing, excessive mucus secretion, and gasping. After 96 hours of exposure to the final treatment, tissue samples (gill and intestine) were collected. Histopathological results revealed clear and significant alterations in the gill and intestine tissues. The alteration in the gill was characterized by hyperplasia of primary and secondary lamellae, epithelial edema, lamellar aneurism, and necrosis. In contrast, the intestine was characterized by intact serosa, less organized mucosa, a consequent fusion of mucosa, and edema between the intestinal submucosa and lamina propria. Compared with the control group, *Ompokpabda* of treatment groups showed severe intestinal and gill tissue injury. The result revealed that acute cadmium toxicity has a detrimental effect on the exposed fish's normal behavior and essential organs.

## Introduction

Pollutants in aquatic systems, particularly heavy metals, are a severe global issue (Soltan et al., 2018). Aquatic systems are a major source of water pollution, as they are subjected to a variety of pollutants produced mainly through wastewater discharged from industries, wastewater treatment facilities, and drainage systems from urban and agricultural regions that contain suspended particles, fertilizers, organic and inorganic compounds, and other hazardous metal compounds (Silva and Martinez, 2014). Uncontrolled agricultural chemical discharge into water bodies has caused damage to aquatic ecosystems, affecting all kinds of aquatic organisms. Heavy metals, which are not degraded by biological breakdown, are the most common contaminants in aquatic bodies worldwide. Heavy

*Corresponding author:<shamsur@du.ac.bd>

metals cause environmental problems by interfering with various physiological, biochemical, and cellular processes (Ferro et al., 2019). Fish growth rates, physiological functions, mortality, and reproduction may be hampered by the harmful effects of different heavy metals (Ebrahimi and Taherianfard, 2011). Several studies have found that fish exposed to metals have a weak immune system and a higher mortality risk. Heavy metals can increase genotoxicity by causing toxicity in other chemical agents, either directly or indirectly (Pretto et al., 2011). Heavy metals can also increase genotoxicity by generating toxicity in other chemical agents (Pretto et al., 2011). Heavy metals seriously threaten many aquatic organisms by degrading water quality (Garcia et al., 2006).

Cadmium is a heavy metal linked to a detrimental effect on aquatic species (Nordberg et al., 2007). It enters the aquatic environment as a result of both natural and manmade activities (Heath, 1987). With the increase in pollution in aquatic bodies and pisciculture, studies on heavy metal toxicity in fish are receiving more and more attention worldwide. Cadmium chloride, a heavy metal that poses a serious threat to organisms due to its high toxicity and tissue accumulation, contaminates aquatic environments from air and land (Kumar et al., 2006). Cadmium pollution is caused by organic and inorganic materials in household and industrial effluents (McCarty et al., 1978). In Bangladesh's economy, the aquatic ecosystem is extremely important. In the aquatic ecology, fish serve as bioindicators. Pollutants from the water and food chain accumulate directly and indirectly in aquatic species. As a result, discharging contaminants in water has a negative impact on the health of fish and other aquatic species. As a result, fish production is often hampered, and fishermen suffer significant financial losses. It is vital to monitor and understand the pathophysiology of pollutants to reduce negative effects and protect public health (Pandey et al., 2008).

*Ompok pabda* (Hamilton Bouchanan, 1822) is a valuable commercial species in Bangladesh and other Southeast Asian countries (Talwar and Jhingran, 1991). *O. pabda* is a small freshwater catfish native to Bangladesh, colloquially known as pabda. This species is also a well-established model for toxicological study because of its ease of handling, culture, and maintenance in the laboratory and its rapid response to environmental changes. The objectives of the experiment were to determine the $LC_{50}$ value of Cadmium Chloride ($CdCl_2$) for *O. pabda* along with observing morphological and behavioral changes of fish due to cadmium chloride exposure and to identify histological changes of gill and intestine of *O. pabda* due to cadmium chloride exposure.

## Materials and Methods

### Collection of samples

The fingerlings of *O. pabda* were collected from Babul Motsho Hatchery and Nursery at Ishwargonj, Mymensingh. Almost identical-sized fish were used for the experiment. The fish were carried to the laboratory of the Department of Fisheries, University of Dhaka. The average weight of the sample was 12.05±0.12 gm, and the average length was 10.27±0.23 cm.

### Acute toxicity

Short-term acute toxicity tests were conducted using the renewal bioassay method (Reish and Oshida 1975; USEPA, 2002) for 96 h and different concentrations of toxicants. To perform this experiment, 98% of Cadmium chloride hemi (pentahydrate) was used as a toxicant, and this chemical was collected from Shanghai Titan Scientific Co. Ltd. in its original package form.

### Pre-exposure acclimation of the test animals

After arrival in the laboratory, the fishes were immediately released into three big aquariums containing filter water and maintained there for about 7 days. Fish were fed on artificial feed once daily. Any debris or unwanted particles were removed from

the tank after feeding. The water was changed at 24-hour intervals to remove the metabolic waste products. Aerators were used for the continuous oxygenation of water. The water quality parameters of the acclimation tank were studied daily. However, only healthy fishes were transferred to the experimental system after acclimation.

### Experimental system and dose preparation

The static bioassay $LC_{50}$ was conducted using the recommendation by Committee on Methods for Toxicity Tests with Aquatic Organisms (1975). For the $LC_{50}$ assay, seven independent glass aquaria were used. Each aquarium was 30 cm x 20 cm x 25 cm, containing 10 liters of water. The water was aerated for one day before starting the experiment. Stone aerators connected to a compressed air supply were used to maintain an adequate dissolved oxygen level in each aquarium. Cadmium chloride was measured, and serial dilutions were made with deionized water. Six concentrations (0, 20, 40, 80, 160, 320 and 400 mg/L of $CdCl_2$) were used as stock solution. Fresh solutions were prepared and used for each test on the same day. The solution was directly mixed with test water.

### Samples are in Treatment

An organism loading of approximately 1.0 g/L of water was maintained in all the tests as recommended by APHA (1985). Eight randomly selected fish were transferred to each aquarium. In all cases, control groups of fish were maintained. Each experimental trial was carried out for 96 hours, as Sprague (1969, 1970) and APHA (1985) recommended. According to Sprague (1969), 96 hours of $LC_{50}$ is the most reproducible. The mortality of the fish was recorded at logarithmic time intervals (Sprague, 1970), that is, after 6, 12, 24, 48, 72, and 96 hours of exposure.

**Table 1. Concentration of $CdCl_2$ for final treatment.**

| Serial No. | Treatment | Concentrations of $CdCl_2$ (mg/L) |
|---|---|---|
| 1 | Control | 0.00 |
| 2 | T1 | 100.00 |
| 3 | T2 | 190.90 |
| 4 | T3 | 300.00 |

Each treatment: 3 replication.

### Measurement and analysis of water quality

The physicochemical characteristics of the water, such as temperature, pH, salinity, and oxygen concentration, were frequently conducted following the standard procedures described in APHA (1985). Temperature, Salinity, DO, and $P^H$ were measured with a thermometer, Salinometer, DO meter, and $P^H$ meter, respectively.

### Evaluation of Median Lethal Concentration ($LC_{50}$)

The concentration of $CdCl_2$ at which 50 percent of the test organisms die during a particular period, or the concentration lethal to 50 percent of the test population, is called the median lethal concentration ($LC_{50}$). The $LC_{50}$ values of $CdCl_2$ were estimated using Finney's probit method and ExcellProbit analysis.

### Final Experiment

### Pre-exposure acclimation of the test fish

The fish were immediately released into twelve tanks containing filter water and maintained there in a static condition for about one day. They were fed artificial feed once daily, and aerators were used to oxygenate the water.

### Dose Preparation

The next day, Cadmium chloride was measured, and serial dilutions were made with deionized water. Three different concentrations were used as stock solutions. Different test doses were prepared by diluting the stock concentration (Table 1). Fresh solutions were prepared and used for each test on the same day.

### Samples are in the final treatment

The final treatment was conducted using the recommended method (Ahmed et al., 2014). An

organism loading of approximately 1.0 g/L of water was maintained in all the tests as recommended by APHA (1985). Eight randomly selected fish were transferred to each aquarium. In all cases, control groups of fish were maintained. Each experiment was carried out for 96 hours, as Sprague (1969, 1970) and APHA (1985) recommended. Initial length and weight were recorded on the 1st day of the exposed chemical. The physicochemical characteristics test of the water, such as temperature, pH, salinity, and oxygen concentration, were conducted frequently following the standard procedures described in APHA (1985). Temperature, Salinity, DO, and PH were measured with a thermometer, Salinometer, DO meter, and PH meter. Aerators were used to oxygenate the water. Fish were fed on artificial feed once daily. The mortality of the fish was recorded at logarithmic time intervals (Sprague, 1970), that is, after 24, 48, 72, and 96 hours of exposure. External behavior was observed according to (Test Guideline No. 203, Fish, Acute Toxicity Testing) after 24, 48, 72 and 96 hours of exposure.

**Behavioral changes**

Behavioral changes were observed every 24 hours. Loss of schooling, abnormal vertical orientation, hyperactivity, etc., were observed every day. Those behavioral activities were observed because they showed differences between the control and different treatments.

**Histopathology**

After 4 days, tissue samples of the gill and intestine were isolated from the treated fish of all treatments. The gill and intestine were aseptically removed by sacrificing from the study fish and transferred to vials with 10% formalin, which was immediately processed for further analysis.

## Results

**Acute Toxicity Estimation for $LC_{50}$**

The water quality parameters were measured during the experimental period (Table 2). Here, the range of temperature, dissolved oxygen, $^{pH,}$ and salinity did not fluctuate much. All values are in the optimal range for treatment. However, there was a linear relationship between increased $CdCl_2$ and $P^H$. With the increased $CdCl_2$ concentration, the $P^H$ also increased. However, this is also in the optimal range for every treatment.

In the initial experiment, no behavioral changes were observed in the control group, but various abnormalities gradually increased with increasing $CdCl_2$ concentration and number of days of exposure (Table 3). No behavioral changes or deaths occurred in the control group during the trial. All control fish were active and swimming normally. Behavioral abnormalities include loss of schooling, vertical orientation, hyperactivity, spiral swimming, gulping, gasping, surface activity, and increased mucus secretion. These toxic effects increase as the dose is increased.

The first visible behaviors were observed at the highest concentrations of 400 mg/L and 320 mg/L on day one. On the first day, at 400 mg/L and 320 mg/L, loss of schooling, abnormal vertical orientation, hyperactivity, gulping, gasping, surface escape, secretion of mucus, and dark skin color were observed. On the second day at 160 mg/L and 80 mg/L, loss of schooling, abnormal vertical orientation, hyperactivity, gulping, gasping, surface escape, mucus secretion and darkening of skin color were observed. On day four of 40 mg/L, loss of schooling, hyperactivity, abnormal vertical orientation, gulping, gasping, and mucous secretions were observed. However, at a concentration of 20 mg/L, no significant behavior change was observed during the four days of treatment. No behavioral changes were observed in the control treatment.

**Table 2. Water quality parameters during $LC_{50}$ determination of different experimental aquariums.**

| Concentration of $CdCl_2$ (mg/L) | Physical-chemical properties | | | |
|---|---|---|---|---|
| | Temperature (°C) (January) | Dissolved oxygen (mg/L) | pH | Salinity |
| 0.0 (Control) | 20.3± 0.17 | 8.21 ± 0.07 | 7.35±0.05 | 0 |
| 20 | 20.2± 0.12 | 6.79 ± 0.50 | 7.42± 0.08 | 0 |
| 40 | 20.1± 0.19 | 8.75±0.11 | 7.49± 0.10 | 0 |
| 80 | 20.3± 0.90 | 8.66± 0.09 | 7.50± 0.11 | 0.1 |
| 160 | 20.3±0.18 | 8.99± 0.16 | 7.68±0.16 | 0.1 |
| 320 | 20.0±0.21 | 8.02± 0.13 | 7.77± 0.15 | 0.2 |

**Table 3. Fish behaviors observation on $LC_{50}$ treatments.**

| Clinical Sign | Doses for $LC_{50}$ (mg/L) | | | | | | |
|---|---|---|---|---|---|---|---|
| | 0.0 (Control) | 20 | 40 | 80 | 160 | 320 | 400 |
| **Loss of Schooling** | × | × | × | × | √ | √ | √ |
| **Vertical orientation** | × | × | × | × | √ | √ | √ |
| **Hyper activity** | × | × | × | × | √ | √ | √ |
| **Spiral swimming** | × | × | × | × | √ | √ | √ |
| **Gulping** | × | × | × | × | √ | √ | √ |
| **Gasping** | × | × | × | × | √ | √ | √ |
| **Cannabalism** | × | × | × | × | √ | √ | √ |
| **Skin color darkness** | × | × | × | √ | √ | √ | √ |
| **Mucous Secretion** | × | × | × | √ | √ | √ | √ |

x- no response, √- showed response

**Table 4. Cumulative mortality (%) of 96 hours exposure time for $LC_{50}$.**

| Treatment | Concentration of $CdCl_2$(mg/L) | Exposure time (hours) | | | | | | |
|---|---|---|---|---|---|---|---|---|
| | | Cumulative mortality (%) of 8 fishes | | | | | | |
| | | 6 | 12 | 18 | 24 | 48 | 72 | 96 |
| Control | 0.0 | 0 | 0 | 0 | 0 | 0 | 0 | 0 |
| 1 | 20 | 0 | 0 | 0 | 0 | 0 | 0 | 0 |
| 2 | 40 | 0 | 0 | 0 | 0 | 0 | 0 | 0 |
| 3 | 80 | 0 | 0 | 0 | 0 | 0 | 0 | 0 |
| 4 | 160 | 0 | 0 | 0 | 0 | 12.5 | 25 | 37.5 |
| 5 | 320 | 0 | 25 | 100 | 100 | 100 | 100 | 100 |
| 6 | 400 | 12.5 | 100 | 100 | 100 | 100 | 100 | 100 |

**Observation of fish mortality for $LC_{50}$ treatment**

Table 4 show the cumulative mortality rate (percentage) for $CdCl_2$ treatment in the preliminary trials for $LC_{50}$ determination. No mortality occurred at control, 20 mg/L, 40 mg/L, and 80 mg/L of $CdCl_2$ after 96-h exposure. Mortality increased steadily as the concentration of $CdCl_2$ increased. The cumulative mortality (%) of the initial treatment for $CdCl_2$ is presented in Table 4. After 96 hours of exposure to 20 mg/L, 40 mg/L, and 80 mg/L of $CdCl_2$, no mortality was recorded. At 160 mg/L of $CdCl_2$, 12.5%, 25%, and 37.5% mortalities were recorded after 48 hours, 72 hours, and 96 hours of exposure, respectively. At 400 mg/L $CdCl_2$, however, complete death (100%) occurred within 12 hours.

**Table 5. Relation between the concentration of $CdCl_2$ and the percentage mortality of the fish.**

| Concentration (mg/L) | Log10 transfer | Mortality (%) | Probit |
|---|---|---|---|
| 20 | 1.301029996 | 0 | 0 |
| 40 | 1.602059991 | 0 | 0 |
| 80 | 1.903089987 | 0 | 0 |
| 160 | 2.204119983 | 37.5 | 4.82 |
| 320 | 2.505149978 | 100 | 7.37 |
| 400 | 2.602059991 | 100 | 7.37 |

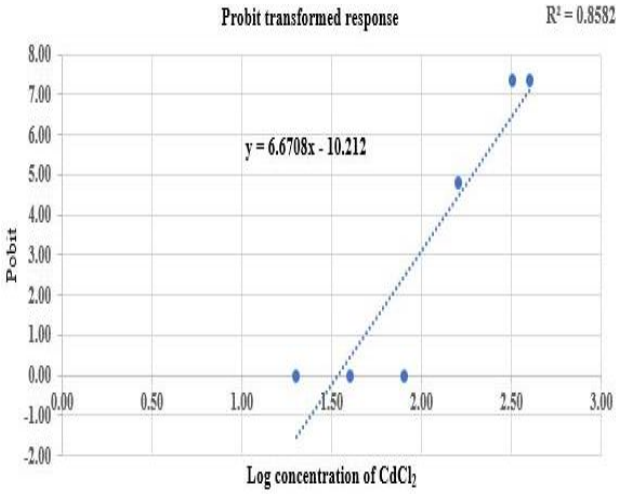


**Fig. 1. Regression line between the probit of *O. pabda* and log concentration of $CdCl_2$.**

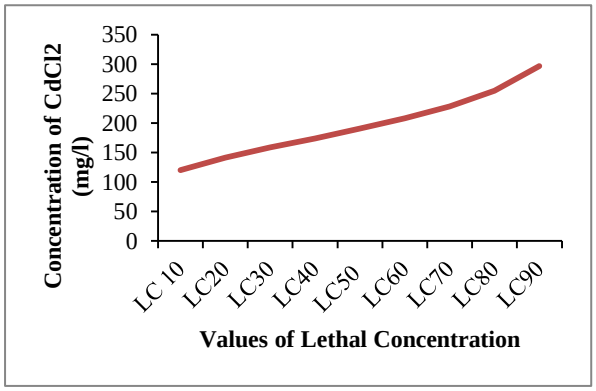


**Fig. 2. Different values of lethal concentration of $CdCl_2$ on *O. pabda.***

### Prediction of lethal concentration

After the treatment of $CdCl_2$, fish mortalities data were analyzed using ExcellProbit Analysis software. $LC_{50,}$ $LC_{60}$, $LC_{70,}$ $LC_{80,}$ and $LC_{90}$ values were calculated after analyzing the mortalities data.

According to probit analysis the $LC_{50,}$ $LC_{60}$, $LC_{70}$, $LC_{80}$, $LC_{90}$ values were 190.90 mg/L, 207.89 mg/L, 228.20 mg/L, 254.86 mg/L, 296.66 mg/L, respectively (Table 5; Fig. 1 & 2).

### Acute toxicity estimation for final treatment

Potential hazardous consequences can be seen through behavioral changes, the most sensitive signs. Behavioral abnormalities were observed in *O. pabda* when treated with various doses of $CdCl_2$ while conducting the initial treatment for $LC_{50}$ determination. Behavioral alterations became more pronounced and lasted longer as the concentration increased. The following is a list of the behavioral changes seen in *O. pabda* (Table 6).

**Control group:** During the experiment, no behavioral changes or deaths were observed in the control group. All fish were active and swimming normally.

**Table 6. Fish behaviors observation on final treatments.**

| Clinical Sign | Different concentrations for final treatment (mg/L) | | | | | | | | | | | |
|---|---|---|---|---|---|---|---|---|---|---|---|---|
| | $C_1$ | $T_1R_1$ | $T_1R_2$ | $T_1R_3$ | $C_2$ | $T_2R_1$ | $T_2R_2$ | $T_2R_3$ | $C_3$ | $T_3R_1$ | $T_3R_2$ | $T_3R_3$ |
| | 0.0 | 100 | 100 | 100 | 0.0 | 190.9 | 190.9 | 190.9 | 0.0 | 300 | 300 | 300 |
| Loss of schooling | × | √ | √ | √ | × | √ | √ | √ | × | √ | √ | √ |
| Vertical orientation | × | √ | √ | √ | × | √ | √ | √ | × | √ | √ | √ |
| Hyper activity | × | × | × | × | × | √ | √ | √ | × | √ | √ | √ |
| Spiral swimming | × | √ | √ | √ | × | √ | √ | √ | × | √ | √ | √ |
| Gulping | × | √ | √ | √ | × | √ | √ | √ | × | √ | √ | √ |
| Gasping | × | × | × | × | × | √ | √ | √ | × | √ | √ | √ |
| Surface escape | × | × | × | × | × | √ | √ | √ | × | √ | √ | √ |
| Cannibalism | × | × | × | × | × | × | × | × | × | × | × | × |
| Skin color darkness | × | × | × | × | × | √ | √ | √ | × | √ | √ | √ |
| Mucus secretion | × | × | × | × | × | √ | √ | √ | × | √ | √ | √ |

**C = Control, T = Treatment, R = Replica**

**Treatment 1 group (100 mg/L):** After 72 hours, behavioral abnormalities, such as a spiral swimming pattern, floating motionless on the water's surface, and gulping, were observed, and fish tended to gather on the surface.

**Treatment 2 group (190.9 mg/L):** After 12 hours, the fish's movement became very slow, and they developed behavioral abnormalities such as overturn in the water, breathing problems, loss of coordination, swimming disorders, gulping, and gasping. Increased mucus was also seen on the body's surface.

**Treatment 3 (300 mg/L**): The fish lost coordination immediately after the CdCl2 was added. Swimming difficulties were seen, and fish had trouble breathing and congregating. The fish initially sank to the bottom of the aquarium and remained immobile. The first fish died after 6 hours, while the rest died within 48 hours.

**Observation on fish mortality for final treatment**

The cumulative mortality (%) data for the final treatment is shown in Table 7. No mortality was observed in the control, which $CdCl_2$ did not treat. No mortalities were observed in three replicas of treatment 1, which were treated with 100 mg/L of $CdCl_2$. 53.5% average mortality wasobserved at a concentration of 190.9 mg/L of $CdCl_2$ of treatment 2 with three replica, but 100% mortality was noticed in concentration of 300 mg/L (Table 7; Fig. 3).

**Histopathology in gill and intestine of *O. pabda***

Histopathological changes in the gill and intestine of *O. pabda* were observed after 96 hours of treatment.

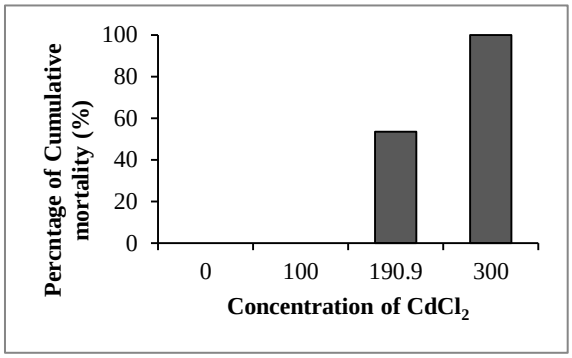


**Fig. 3. Cumulative mortality (%) at different concentrations of $CdCl_2$ after 96 hours of exposure time for $LC_{50}$ determination.**

**Table 7. Cumulative mortality (%) of 96 hours exposure time for final treatment.**

| Treatment | Concentration of $CdCl_2$ (mg/L) | Exposure time (hours) | | | |
|---|---|---|---|---|---|
| | | Cumulative mortality (%) of 8 fishes | | | |
| | | 24 | 48 | 72 | 96 |
| Control 1 | 0.0 | 0 | 0 | 0 | 0 |
| $T_1 R_1$ | 100 | 0 | 0 | 0 | 0 |
| $T_1 R_2$ | 100 | 0 | 0 | 0 | 0 |
| $T_1 R_3$ | 100 | 0 | 0 | 0 | 0 |
| Control 2 | 0.0 | 0 | 0 | 0 | 0 |
| $T_2R_1$` | 190.9 | 0 | 25 | 37.5 | 60.5 |
| $T_2R_2$ | 190.9 | 0 | 12.5 | 25 | 50 |
| $T_2R_3$ | 190.9 | 0 | 12.5 | 25 | 50 |
| Control 3 | 0.0 | 0 | 0 | 0 | 0 |
| $T_3R_1$ | 300 | 37.5 | 75 | 100 | 100 |
| $T_3R_2$ | 300 | 37.5 | 87.5 | 100 | 100 |
| $T_3R_3$ | 300 | 37.5 | 87.5 | 100 | 100 |

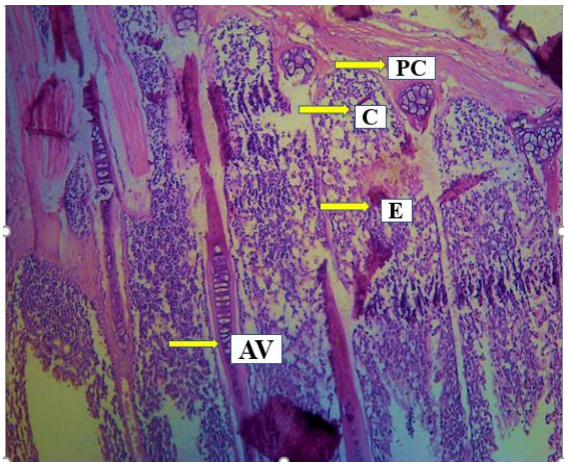


**a. Gill tissue of control fish which was not treated by $CdCl_2$.**

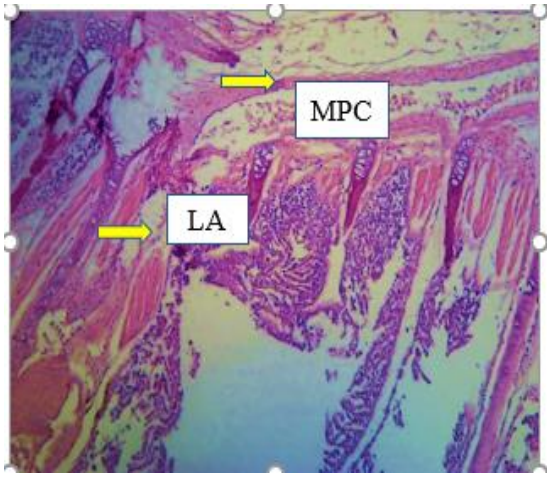


**b. Gill tissue of treatment 1 (treated by 100 mg/L of $CdCl_2$).**

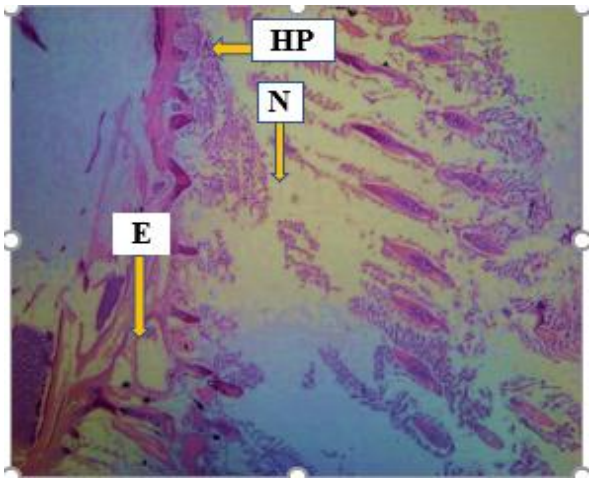


**c. Gill tissue of treatment 2 (treated by 190.9 mg/L of $CdCl_2$).**

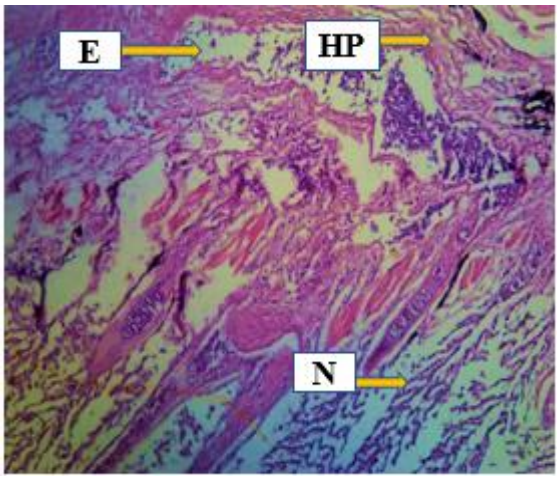


**d.Gill tissue of treatment 3 (treated by 300 mg/L of $CdCl_2$).**

**Fig. 4 (a-d): Pathological changes in gill tissues. AV: afferent vessel; C: chloride cell; E: erythrocyte; N: neutrophil; LA: lamenar aneurism; E: edema; MPC: moderately disorganized primary cell; HP: hyperplasia; PC: pillar cell;**

**Observation of gill tissue**

There were no histological alterations in the gill tissue of the fish in the control group. A consistent arrangement of gill lamellae and filaments with inter lamellar space (ILS) was seen throughout the experiment, and no modifications were noticed. At the same time, pillar cells, epithelial cells, primary gill lamellae, and secondary gill lamellae were observed well structured, as shown in Fig. 4a.

Chloride cells and mucous cells were present and well structured. Histopathological examination of the gill section after 96 hours of 100 mg/L $CdCl_2$ of treatment 1 exposure showed moderate fusion of secondary lamellae and lamellar aneurism that led to eluding of the tips of the secondary lamellae (Fig. 4b). Pillar cell systems were found to be moderately disorganized (Fig. 4b).

After 96 hours of exposure, the gill of treatment 2, treated by $LC_{50}$ doses, 190.9 mg/L of $CdCl_2$, showed severe histopathological changes. Primary lamellae and secondary lamellae were severely damaged. Gill hyperplasia and interlamellar spacing between secondary lamellae were observed in fish gills. Edema was detected in the resulting interlamellar gaps. Secondary lamellae were found to be shorter in length, and the length of secondary lamellae was shown to besignificantly shorter (about 50 percent or less than normal as shown as Fig. 4c. The gill of fish after 96 hours of exposure at 300 mg/L of $CdCl_2$ showed severe hyperplasia of primary lamellar and secondary lamellar epithelium, and edema was observed in the resulting interlamellar spaces (Fig. 4d). The number of chloride cells in the primary lamellar epithelium increased significantly (Fig. 4d). Histopathological results indicated that the gill was the primary target tissue affected by $CdCl_2$. The most common changes at all doses of $CdCl_2$ were hyperplasia of secondary lamellae (Table 8).

**Table 8. Summary of histopathological effects in the gills of *O. pabda* treated with different concentrations of $CdCl_2$ and control fish.**

| Treatment | Concentration of $CdCl_2$ (mg/L) | Edema | Hyperplasia of Primary lamellae | Hyperplasia of secondary lamellae |
|---|---|---|---|---|
| Control | 0.0 | - | - | |
| 1 | 100 | - | - | + |
| 2 | 190.9 | ++ | ++ | + |
| 3 | 300 | +++ | +++ | +++ |

None (−), mild (+), moderate (++), and severe (+++)

## Observation of intestinal tissue

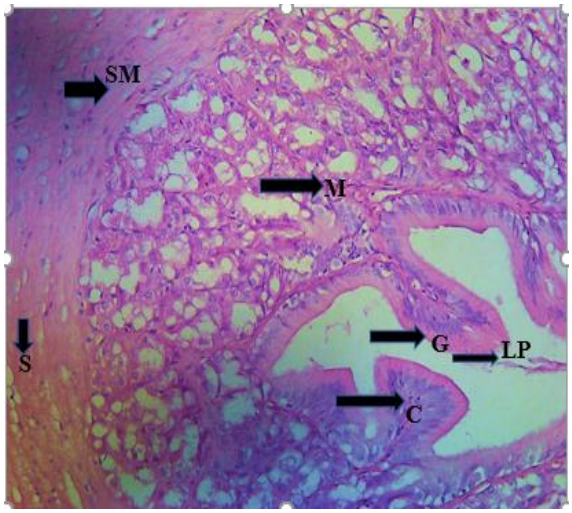


**a. Intestine of control fish, which was not treated by $CdCl_2$.**

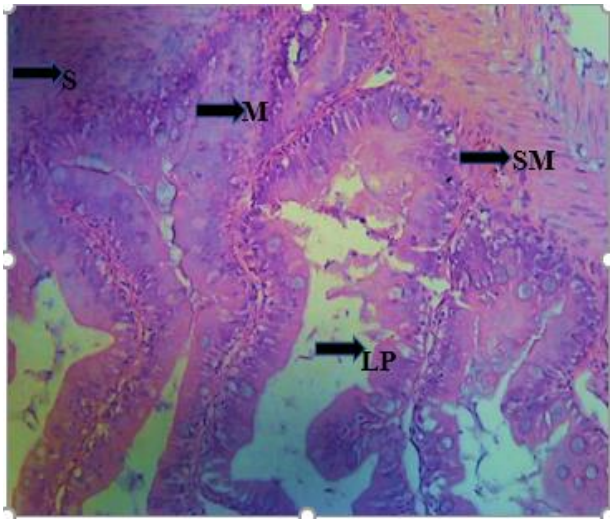


**b. Intestine of treatment 1 (treated by 100 mg/L of $CdCl_2$).**

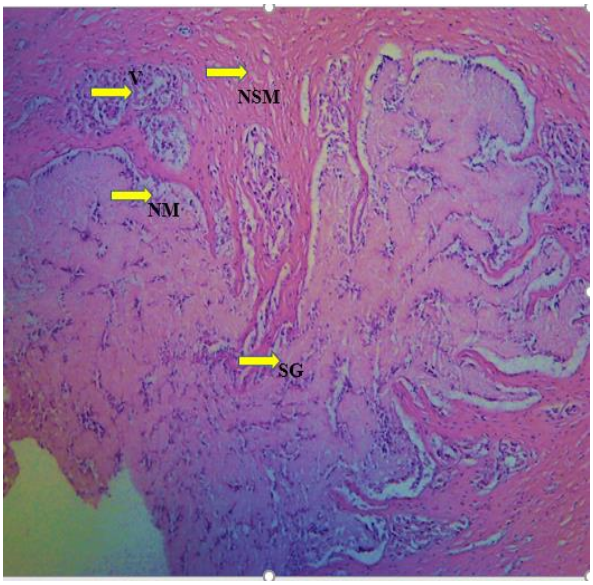


**c. Intestine of treatment 2 (treated by 190.9 mg/L of $CdCl_2$).**

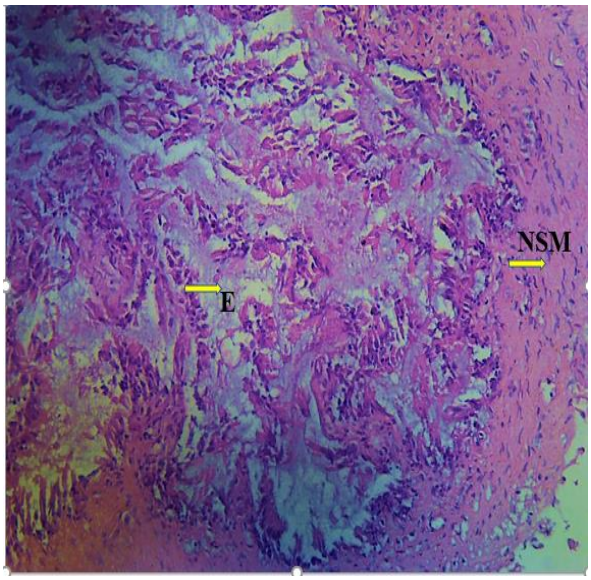


**b. Intestine of treatment 1 (treated by 100 d. The intestine of treatment 3 (treated with 300 mg/L of $CdCl_2$).**

**Fig. 5 (a-d): Pathological changes in intestine tissues. C: columner cells; E: erosion; G: goblet cells; LCT: loose connective tissue; LP: lamina propia; M: mucosa; NM: necrotic mucosal layer; NSM: necrotic submucosal layer; S: serosa; SG: swelling of goblet cell; V: vacuoles; SM: Submucosal Layer.**

In the control group, the photomicrograph of the intestine depicts normal columnar cells, and goblet cells and normal intestinal submucosa with blood capillaries. The photomicrograph of the intestine in the control group shows ordinary columnar and goblet cells, as well as normal intestinal submucosa and blood capillaries, in contrast to the experimental group. Mucosa, intestinal submucosa and lamina propria were well organized (Fig. 5a). The intestine of O. pabda exposed to $CdCl_2$ underwent progressively harmful changes that increased in severity as the concentration of $CdCl_2$ increased. The intactness of serosa, less organized intestinal mucosa, submucosa, and lamina propria was observed in treatment 1 treated with 100 mg/L $CdCl_2$ (Fig. 5b). Photomicrograph of intestine of treatment 2 treated by 190.9 mg/L of $CdCl_2$ shows degenerative changes in tips of villi, loss of structural integrity of mucosal layers, degenerative changes of mucosal epithelium, swelling of goblet cell and necrosis (Fig. 5c). The intestine tissue of treatment 3, treated by 300 mg/L, was eroded. Mucosa, serosa, intestinal submucosa, and lamina propria were totally damaged (Fig. 5d).

## Discussion

Bioassays are the best tool for evaluating the effects and destiny of toxins in the aquatic ecosystem. Heavy metals of anthropogenic origin, such as Cd, are recognized as significant pollutants in the aquatic environment. In this study, we elucidated the effects of the acute toxicity of cadmium on the behavior and histopathology of the freshwater fish *Ompokpabda*. As can be seen from the results of this study, the

water quality parameters were within the optimal range for different treatments. According to APHA (1985), temperature fluctuations should not exceed 4°C and the dissolved oxygen of warm water fish should not be below 4 mg/L. In this experiment, the temperature fluctuations were small (20.35 and 21.15°C), and the dissolved oxygen was in the optimal range of 7.86 and 8.33 mg/L. Evidence available indicates that trace amounts of toxicants can cause abnormal behavioral changes in fish through responsive impairment (Kabir and Begum, 1978).

In aquatic organisms, behavioral changes have been identified as sensitive indicators of chemically induced stress (Sharma and Agarwall, 2005). Stress-related changes in behavior are susceptible indicators of possible toxic effects. Fish treated to various toxicant doses displayed distinct behavioral changes. In the current study, fishes were observed darting around and attempting to escape toxic water. Fishes appeared to trigger mucus secretion over the gills, forcing the opercula to move quickly and exert significant effort. Loss of schooling, vertical orientation, hyperactivity, spiral swimming, gulping, gasping, surfacing activity, and increased mucus secretion were all noted in fish. As the dose was increased, the toxic effects became more pronounced. Our findings are consistent with the findings of the following researchers: According to Woodal et al. (1988), cadmium $LC_{50}$ values on *Salmo gairdneri* and *Xenopus larvae* were between 80 and 100 mg/L; however, Muley et al. (2000) observed that the 96-hour $LC_{50}$ value of cadmium on the fish *Cyprinuscarpio* was 121.8 mg/L and Sehgal and Pandey (1984) determined that the 96 hours $LC_{50}$values of Cadmium for *Heteropneustesfossilis* are 360.50 mg/L (Rai et al., 2008).

Cadmium's $LC_{50}$ value for the goldfish *Carassiusauratus* was found to be 46.8 mg/L (McCarty et al., 1978). The cadmium $LC_{50}$ value for the fish *Labeorohita* was reported to be 89.5 mg/L after 96 hours (Dutta and Kaviraj, 2001). It should be noted that the toxicities of a single toxicant to different types of fish species are hard to compare since they are impacted by parameters such as the test water's temperature, dissolved oxygen content, pH, hardness, and (Schoettger, 1970).The concentration of $CdCl_2$ for acute exposure was calculated based on the results of $LC_{50}$ values from the experiment. The $LC_{50}$ value of $CdCl_2$ for *O.pabda*was found to be 190.9 mg/L, according to the findings of this experiment. Compared to other fishes' 96-hour $LC_{50}$ values, this study shows that *O. pabda*is more resistant to cadmium and might be called the least sensitive fish. Abnormal behavior was observed every 24 hours. $CdCl_2$ in aquariums causes irregular movement, fast operculum movement, jumping out of the experimental media, lateral swimming, and loss of balance. Abnormal reactions in the fish body occur due to the neurotoxic effects. Toxicants are responsible for changing the behavior of jumping out of water. An irritation of the skin is responsible for secretion of mucus from fish body. Damage to the nervous system impaired lateral swimming and caused a loss of equilibrium (Sinha and Kumar, 1992), as found in the current study. In addition to serving as indicators of numerous anthropogenic contaminants, histopathological biomarkers also resemble the general health of the whole population in an ecosystem. Many studies employ alterations in cells and tissues in fish as biomarkers. After 96 hours of exposure, the harmful effect of Cd on fish gills and gut tissues was observed in the present study. On the basis of histological changes from our study, it is speculated that a significant disequilibrium in physiological processes may have resulted in Cd-exposed fishes.

Gills are extremely sensitive organs in the fish body that regulate respiratory, osmoregulatory, and excretory activities. Poisoning of heavy metals is responsible for occurring respiratory distress (Matos et al., 2017). High levels of cadmium taken through gills are very harmful to fish health. In this present study, hyperplasia of primary and secondary lamellae, epithelial edema, lamellar aneurism, and necrosis were the most prominent histopathological abnormalities detected in the gills of *O. pabda* exposed to $CdCl_2$. These toxic effects increased with the dose increased.

## Conclusions

As aquatic organisms, fish are constantly exposed to water contaminated with heavy metals like cadmium. This research provides information on the $LC_{50}$ of $CdCl_2$ for *O. pabda* and the histopathological changes in the gills and intestine of *Ompokpabda*exposed to different $CdCl_2$ concentrations. The present study revealed that the $LC_{50}$ value of $CdCl_2$ for *O. pabda* was 190.9 mg/L. About 53.5% of fish mortality was observed in this dose, and all fish showed behavioral abnormalities. Significant histopathological changes were observed in gill and intestine of fish after exposing this toxicant. From the findings of this experiment, it can be concluded that acute cadmium chloride toxicity has a detrimental effect on the exposed fish's normal behavior and essential organs. The findings clearly show that the usage of a heavy metal such as cadmium must be strictly regulated.

## Author contributions

**Atakiya Galiba:** Sample Collection and preparation, Data interpretation and Visualization and Writing Original Draft. **Md. Mostavi Enan Eshik**: Concept Development, Study Design, Supervision, Data interpretation, reviewing, and Writing. **Mohammad Shamsur Rahman:** Concept Development, Study Design, Data interpretation, Supervision, Writing-Review & Editing.

## Conflict of Interest

The authors declare that they have no known competing financial interests or personal relationships that could have appeared to influence the work reported in this paper.

## References

Ahmed MK, Parvin E, Islam MM, Akter MS, Khan S and Al-Mamun MH. Lead-and cadmium-induced histopathological changes in gill, kidney and liver tissue of freshwater climbing perch *Anabas testudineus* (Bloch, 1792). *Chem. Ecol*. 2014; 30(6): 532-540.

APHA, AWWA and WPCF. Standard methods for the examination of water and wastewater. 15th ed. APHA, Washington: DC, 1985. p.7.

Committee on Methods for Toxicity Tests with Aquatic Organisms. Methods for acute toxicity tests with fish, macroinvertebrates. and amphibians. U.S. Environmental Protection Agency, *Ecol. Res. Serv. EPA*, 1975; 660/3-75-009. 61 pp.

Dutta TK and Kaviraj A. Acute toxicity of cadmium to fish *Labeorohita* and copepod *Diaptomus forbesi* preexposed to CaO and $KMnO_4$. *Chemosphere*, 2001; 42: 955-958.

Ebrahimi M and Taherianfard M. Effects of heavy metals exposure on reproductive systems of cyprinid fish from Kor river. *Iran. J. Fish. Sci.* 2011; 10: 13-24.

Ferro JP, Campos LB, Ossana N, Ferrari L and Eissa BL. Effects of cadmium on the behaviour of *Cnesterodon decemmaculatus*. *Int. J. Environ. Health*, 2019; 4(9): 372-379.

Garcia S, Fontaínhas FA and Wilson JM. Cadmium tolerance in the Nile tilapia (*Oreochromis niloticus*) following acute exposure: assessment of some ion regulatory parameters. *Environ. Toxicol.* 2006; 21: 33-46.

Heath AG. Water Pollution and Fish Physiology. CRC Press:Florida; 1987. p245.

Kabir SMH and Begum R. Toxicity of three organophosphorus insecticides to Singhi fish, *Heteropneustesfossilis* (Bloch). Dhaka University Studies. Part B. 1978; 26: 115-122.

Kumar P, Prasad Y, Sharma R and Patil RD. Histopathological changes in liver and kidney of *Clariasbatrachus* due to cadmium toxicity and its neutralization by Vitamin C, Taurine and Garlic. Proceedings of a national conference held in Chenai, Aquatic Toxicology. 2006; 10: 42.

Matos LA, Cunha ACS, Sousa AA, Maranhão JPR, Santos NRS, de MC Gonçalves M, de M. Dantas SMM, de C. e Sousa JM, Peron AP, da Silva FCC, de Alencar MVOB, Islam MT, de Aguiar

RPS, de C. Melo-Cavalcante AA, Bonecker CC and Junior HFJ. The influence of heavy metals on toxicogenetic damage in a Brazilian tropical river. *Chemosphere*, 2017; 185: 852-859.

McCarty LS, Henry JAC and Houston AH. Toxicity of cadmium to goldfish, *Carassius auratus*, in hard and soft water. *J. Fish. Res. Board Can.* 1978; 35: 35-42.

Muley DV, Kamble GB and Bhilave MP. Effect of heavy metals on nucleic acids in *Cyprinuscarpio*. *J. Environ. Biol.* 2000; 21: 367-370.

Nordberg GF, Fowler BA, Nordberg M and Friberg L. Handbook on the toxicology of metals. Academic press, Amsterdam: 2007. p.1024.

Pandey S, Parvez S, Ansari RA, Ali M, Kaur M, Hayat F and Raisuddin S. Effects of exposure to multiple trace metals on biochemical, histological and ultrastructural features of gills of a freshwater fish, *Channapunctata* Bloch. *Chem. Biol. Interact*. 2008;174(3):183-192.

Pretto A, Loro VL, Baldisserotto B, Pavanato MA, Moraes BS, Menezes C, Cattaneo R, Clasen B, Finamor IA and Dressler V. Effects of water cadmium concentrations on bioaccumulation and various oxidative stress parameters in Rhamdiaquelen. *Arch. Environ. Contam. Toxicol.* 2011; 60: 309-318.

Rai R, Mishra D, Srivastav S and Srivastav AK. Acute toxicity of cadmium against catfish, *Heteropneustes fossilis* (siluriformes heteropneustidae) in static renewal bioassays. *Ethiop. J. Biol. Sci.* 2008; 7(2): 185-191.

Reish DL and Oshida PS. Manual of methods in aquatic environment research. Vol. 10. Food & Agriculture Org., 1975.

Schoettger RA.Toxicology of thiodan in several fish and aquatic invertebrates: Investigations in Fish Control. Series No. 35, U.S. Fish and Wildlife Service, 1970.

Sehgal R and Pandey AK. Effect of cadmium chloride on testicular activities in guppy, *Lebistesreticulatus*. *Comp. Physiol. Ecol.* 1984; 9: 225-230.

Sharma RK and Agrawal M. Biological effects of heavy metals: an overview. *J. Environ. Biol.* 2005; 26(2): 301-313.

Silva AO and Martinez CB. Acute effects of cadmium on Osmoregulation of the freshwater teleost *Prochiloduslineatus*: enzymes activity and plasma ions. *Aquat. Toxicol.* 2014; 156: 16-168.

Sinha TKP and Kumar K. Acute toxicity of mercuric chloride to *Anabas testudineus* (Bloch). *Environ. Ecol.* 1992; 10(3): 720-722.

Soltan HAH, Ata AM and El-Mamlouk EAK. Chemical components and cytotoxic effects of four different types of wastewater. *Egypt. J. Agric. Res.* 2018; 96(2): 547-560.

Sprague JB. Measurement of pollutant toxicity to fish I. Bioassay methods for acute toxicity. *Water Res.* 1969; 3(11): 793-821.

Sprague JB. Measurement of pollutant toxicity to fish. II. Utilizing and applying bioassay results. *Water Res.* 1970; 4(1): 3-32.

Talwar PK and Jhingran AG. Inland fishes of India and adjacent countries. Oxford-IBH Publishing Co. Pvt. Ltd., New Delhi, 1991. p.1158.

USEPA, Short-term methods for estimating the chronic toxicity of effluents and receiving waters to freshwater organisms, 4th edn, U.S. Environmental Protection Agency, Washington, DC, 2002.

Woodal C, Maclean N and Crossley F. Responses of trout fry (*Salmo gairdneri*) and *Xenopuslaevis* tadpoles to cadmium and zinc. *Comp. Biochem. Physiol.* 1988; 89: 93-99.

J. Bangladesh Acad. Sci. 48(2); 231-236: December 2024 DOI:https://doi.org/10.3329/jbas.v48i2.74157

Journal of Bangladesh Academy of Sciences

Journal homepage: http://www.bas.org.bd/publications/jbas.html

**Research Article**

# Analysis of the triga mark-II benchmark ieu-comp-therm-003 with monte carlo code openmc

Saad Islam* and Mohammad Abdul Motalab[1]

*Department of Nuclear Engineering, University of Dhaka, Bangladesh*

**ARTICLE INFO**

**Article History**

Received: 19 June 2024
Revised: 02 September 2024
Accepted: 03 September 2024

**Keywords:** TRIGA, ICSBEP, OpenMC, ENDF, Benchmark, Criticality Experiment.

**ABSTRACT**

Ensuring the reliable use of particle transport computer codes necessitates verification against benchmark experiments. This study aims to verify the Monte Carlo code OpenMC using the criticality benchmark model IEU-COMP-THERM-003 from the International Criticality Safety Benchmark Evaluation Project (ICSBEP) Handbook. The analysis focuses on the TRIGA Mark II reactor cores 132 and 133, employing nuclear cross-section libraries ENDF/B-VIII.0, ENDF/B-VII.1, ENDF/B-VII.0, and ENDF/B-VI.2. Results show that OpenMC provides KEFF values in close agreement with benchmark values, demonstrating its robustness in neutronic simulations. Comparison with MVP code results obtained previously, particularly with JENDL-3.3, shows similar accuracy.

## Introduction

Verifying a particle transport code against a benchmark experiment is essential to ensuring its reliable and effective use. This verification process serves two primary purposes: first, to assess the consistency of the physical models and data utilized in the transport code; second, to identify systematic errors arising from the approximate simulation of the experiment, typically due to simplified model geometry.

In this study, the criticality benchmark model IEU-COMP-THERM-003 in the International Criticality Safety Benchmark Evaluation Project (ICSBEP) Handbook (Jeraj and Ravnik, 1999) was examined using the Monte Carlo code OpenMC (Romano et al., 2015). The model is derived from benchmark experiments conducted in the steady-state operation of the TRIGA Mark II reactor in Ljubljana, Slovenia. These experiments were part of the startup tests following upgrade and reconstruction in 1991 and utilized completely fresh fuel (Mele et al., 1994a; Mele at al., 1994b). This research reactor has a relatively simple and compact geometry, making it an ideal choice for benchmark calculations. Furthermore, the significant effects of diverse material compositions can be thoroughly examined, allowing for the explicit modeling and separate treatment of specific components. The benchmark presents two core configurations identified as Core 132 and Core 133, which differed only in loading pattern. The fuel is the standard commercial TRIGA fuel element with stainless steel cladding. The active region consists of a homogeneous mixture of uranium and zirconium hydride, with a uranium concentration of 12 wt% and an enrichment level of 20 wt%. The analysis was done with the nuclear cross-section libraries based on ENDF/B-VIII.0 (Brown et al., 2018), ENDF/B-VII.1 (Chadwick et al., 2011), ENDF/B-VII.0 (Chadwick et al., 2006), and ENDF/B-VI.2 (Dunford, 1992). This study is intended to provide a verification of the OpenMC code in the neutronics simulation of small research reactors.

The paper is organized as follows: Section 2 describes the neutronic calculation models, Section 3 presents the simulation results, followed by

*Corresponding author:<saadislam@du.ac.bd>

[1]*Bangladesh Atomic Energy Commission (BAEC), Dhaka, Bangladesh*

discussions, and Section 4 summarizes the main conclusions of the study.

**Description of the benchmark model**

There are 91 locations in the core, which are occupied by fuel and control elements. The elements are arranged in six concentric rings about the center position labeled A, B, C, D, E, and F, with 1, 6, 12, 18, 24, and 30 positions, respectively. In Core 132, seven fuel elements are positioned in the E ring on the same side as the transient rod. In contrast, Core 133 places these fuel elements on the opposite side, as illustrated in Fig. 1. The lattice does not have a periodic structure (non-uniform pitch). The core is encircled by a graphite reflector housed within an aluminum casing. An annular groove in the upper part of the reflector body accommodates the carrousel irradiation facility.

The Monte Carlo method is a statistical technique widely used for simulating the behavior of neutrons and photons in complex nuclear systems. It can accurately account for the stochastic nature of particle interactions and capture detailed spatial and energy distributions. Using this method, it is possible to model complex geometries and utilize continuous-energy cross-sections.

Core 132 and 133 were modeled in full three dimensions in OpenMC. OpenMC is an open-source, general-purpose Monte Carlo code designed for continuous-energy, generalized-geometry calculations of stochastic neutron and photon transport. It can perform fixed source, subcritical multiplication, and criticality calculations on three-dimensional models of fuel elements or nuclear reactors using universe-based combinatorial solid geometry (CSG) or computer-aided design (CAD) representations. The code has a versatile and efficient tally system for analyzing various physical quantities. OpenMC is becoming widely regarded for its rich and extensible programming interfaces in Python and C/C++, which allow for a set of features including pre-and post-processing, multigroup cross-section generation, custom source option, material burn-up analysis, multiphysics coupling, geometry, and tally results visualization, as well as workflow automation. OpenMC provides official cross-section data libraries based on several ENDF and JEFF releases in HDF5 format. Multiple temperature evaluations are contained with the same HDF5 file for incident neutron data for each isotope. Additionally, it incorporates a Python-based nuclear data module that allows inspection, modification, and processing of various types of data, including ENDF, ACE, and HDF5 files. Benchmark details were carefully considered in the development of the model to ensure an accurate representation of the geometry and composition. The core, fuel element, control rod, and transient rod modeled in OpenMC are shown in Fig. 2-3.

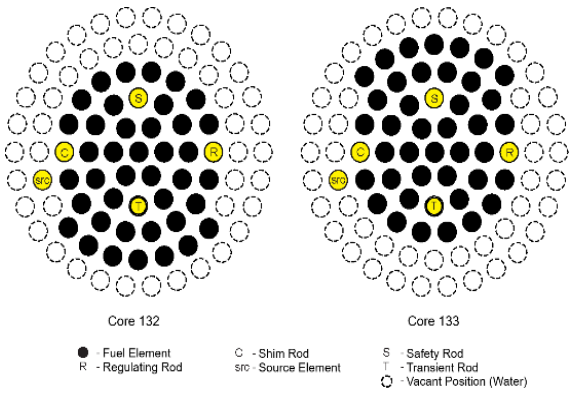


**Fig. 1. Configurations of Core 132 and Core 133 (Jeraj and Ravnik, 1999).**

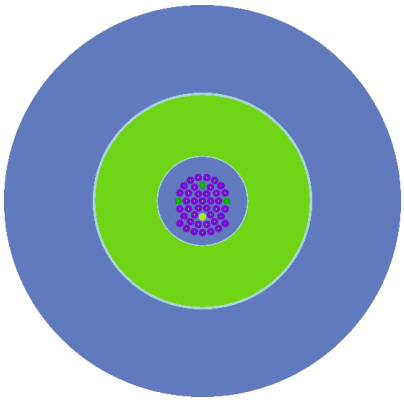

(a)

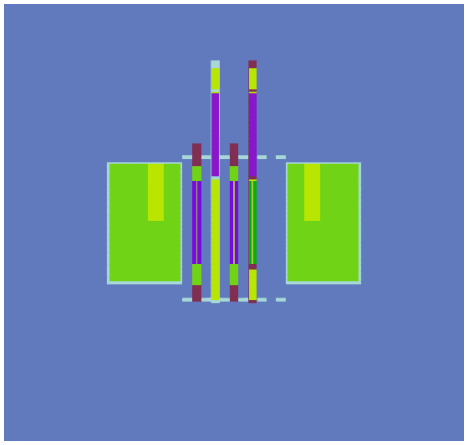

(b)

**Fig. 2. (a) Top view and (b) side view of the benchmark model Core 132 in OpenMC.**

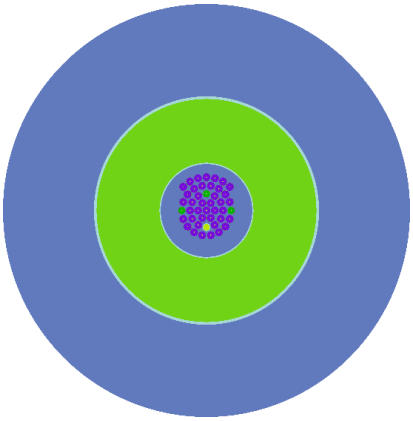

(a)

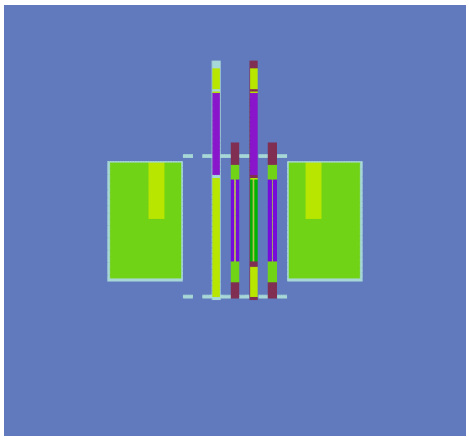

(b)

**Fig. 3. (a) Top view and (b) side view of the benchmark model Core 133 in OpenMC.**

## Results and Discussion

The primary objective of modeling and simulation the critical benchmark core configurations was to assess the reliability and validate the OpenMC code for the neutronic calculation of small reactors like the TRIGA Mark II research reactor. This benchmark, involving enriched uranium in a thermal spectrum, is an important test for evaluating accuracy and reliability in criticality calculations. The code's flexible geometry representation allows precise modeling of complex core configurations, such as those in the IEU-COMP-THERM-003 benchmark, ensuring accurate capture of fuel elements, control rods, transient rods, and structural components. Additionally, the Python interface was utilized to generate custom cross-section libraries. Also, an attempt was made to establish a difference between different cross-section libraries. In each of the OpenMC simulations for the criticality benchmark model, a stable fission source spatial distribution was achieved with the first skipping 50 batches and followed by 200 active batches by tracking histories of 100,000 particles per batch. The initial source distribution was taken from seven isotropic point sources.

As mentioned, continuous-energy neutron data were used from four cross-section libraries, namely ENDF/B-VIII.0, ENDF/B-VII.1, ENDF/B-VII.0, and ENDF/B-VI.2 in the criticality simulations. The calculations also included thermal scattering data for light water, graphite, hydrogen, and zirconium in the U-ZrH fuel. This is to compare and investigate the consistency and differences between different neutron cross-section evaluations. Due to the unavailability of certain data from the ENDF/B-VI evaluation, neutron cross-section data for Cr, Fe, and Ni were sourced from the ENDF/B-V library. The scattering data for hydrogen in ZrH, water molecules, and graphite were obtained from the ENDF/B-IV library. All the cross-section data used was for either 293.6 K or 300 K. It is worth noting that using multiple cross-section libraries provides a more comprehensive analysis and a better understanding of the uncertainties and discrepancies in the results.

The comparison was conducted with previous results (Mahmood et al., 2004) obtained using the MVP code (Mori and Nakagawa, 1994), utilizing cross-section data libraries based on JENDL-3.3 (Shibata et al., 2002), JENDL-3.2 (Nakagawa et al., 1995), and ENDF/B-VI.8 (Dunford, 1992). MVP is a general-purpose continuous-energy Monte Carlo code developed utilizing a vectorized algorithm for neutron and photon transport calculations. The contents of the official MVP library are primarily based on JENDL-3.3. Major features of the code include the treatment of scattering models, time-dependent tallies, reaction rate calculations, and flexible source specifications.

The MVP libraries based on JENDL-3.3 included three types of thermal scattering data for ZrH: the free gas model, ENDF/B-VI, and ENDF/B-III. Similarly, the libraries based on JENDL-3.2 featured thermal scattering data from the free gas model and ENDF/B-III. The libraries derived from ENDF/B-VI.8 used the free gas model and ENDF/B-VI for thermal scattering data. All libraries' data above the thermal energy region were consistent with those from the free gas model. The water temperatures for the models were set at 23.5°C (Core 132) and 22.5°C (Core 133), with a water density of 0.9975 g/cm$^3$, corresponding to the density at 23°C. All the cross-section data were assumed to be at room temperature (27°C). For natural elements, isotopic cross-section data were utilized when available in the libraries. The initial 100 batches were disregarded for the MVP calculations, followed by 2,000 active batches, each tracking 10,000 particle histories.

Several calculations and uncertainty analyses were originally published on this subject (Jeraj et al., 1997); we only compare our model effective multiplication factor, KEFF, with the benchmark values. KEFF is defined as the ratio of the number of neutrons generated by fission in one generation to the number of neutrons lost due to either absorption or leakage in the previous generation. It represents the balance of neutron production and losses in a reactor. The KEFF values for the benchmark core configurations and other calculation results are presented in Table 1-5. The results of the OpenMC presented show the values obtained using the combined collision, track-length, and absorption KEFF estimator. It is to be noted that the source element was not included in either of the two core configurations of the benchmark model, although the source was present in the benchmark experiment.

**Table 1. Criticality benchmark KEFF data.**

| Case | 132 | 133 |
|---|---|---|
| Benchmark | 1.000607 ± 0.00560 | 1.004607 ± 0.00560 |
| MCNP4 (ENDF/B-VI) | 0.9994 ± 0.0002 | 1.0042 ± 0.0002 |

**Table 2. Results of KEFF for OpenMC Core 132.**

| Library | KEFF | Relative Error |
|---|---|---|
| ENDF/B-VIII.0 | 1.00252 ± 0.00020 | 0.19% |
| ENDF/B-VII.1 | 1.00191 ± 0.00020 | 0.13% |
| ENDF/B-VII.0 | 1.00377 ± 0.00020 | 0.32% |
| ENDF/B-VI.2 | 0.99720 ± 0.00019 | 0.34% |

**Table 3. Results of KEFF for OpenMC Core 133.**

| Library | KEFF | Relative Error |
|---|---|---|
| ENDF/B-VIII.0 | 1.00716 ± 0.00021 | 0.65% |
| ENDF/B-VII.1 | 1.00595 ± 0.00020 | 0.53% |
| ENDF/B-VII.0 | 1.00816 ± 0.00019 | 0.75% |
| ENDF/B-VI.2 | 1.00151 ± 0.00020 | 0.09% |

**Table 4. Results of KEFF for MVP Core 132 (Mahmood et al., 2004).**

| Library | KEFF |
|---|---|
| JENDL-3.3 | 0.99910 ± 0.0002 |
| JENDL-3.2 | 1.00333 ± 0.0002 |
| ENDF/B-VI.8 | 0.99831 ± 0.0002 |

**Table 5. Results of KEFF for MVP Core 133 (Mahmood et al., 2004).**

| Library | KEFF |
|---|---|
| JENDL-3.3 | 1.00360 ± 0.0002 |
| JENDL-3.2 | 1.00752 ± 0.0002 |
| ENDF/B-VI.8 | 1.00270 ± 0.0002 |

In both Core 132 and Core 133, the calculated results using OpenMC show reasonable agreement with the benchmark values. The KEFF values for Core 132 were calculated using ENDF/B-VIII.0, ENDF/B-VII.1, and ENDF/B-VII.0 libraries show a slight overestimation compared to the benchmark value, while ENDF/B-VI.2 shows a slight underestimation. The ENDF/B-VIII.0 and ENDF/B-VII.1 libraries provide the closest results to the benchmark, with relative errors within 0.2%.

For Core 133, all libraries overestimate the KEFF value compared to the benchmark value. The ENDF/B-VI.2 library shows results in the smallest relative error at 0.09%, indicating a very close agreement with the benchmark value. The ENDF/B-VIII.0 and ENDF/B-VII.1 libraries also show reasonable agreement, though with slightly higher relative errors.

In both Core 132 and Core 133, the KEFF values obtained using the OpenMC and MVP codes show varying degrees of agreement with the benchmark values. The JENDL-3.3 library for both cores shows good agreement with the benchmark values, while the JENDL-3.2 results tend to overestimate the experimental results by approximately 0.3%. The ENDF/B-VI.8 library results are consistent between OpenMC and MVP, showing no significant differences and suggesting that the choice between these library versions does not significantly impact the KEFF values.

## Conclusion

This study aimed to verify the reliability of the OpenMC code for neutronics simulations by analyzing the criticality benchmark model IEU-COMP- THERM-003, as detailed in the ICSBEP Handbook. The analysis focused on two core configurations of the TRIGA Mark II research reactor, using various nuclear cross-section libraries, including ENDF/B-VIII.0, ENDF/B-VII.1, ENDF/B-VII.0, and ENDF/B-VI.2. The simulation results demonstrate that the OpenMC calculations reasonably agree with the benchmark values for Core 132 and Core 133. Overall, this study confirms the robustness of the OpenMC code in simulating small research reactors like the TRIGA Mark II.

## References

Brown DA, Chadwick MB, Capote R, Kahler AC, Trkov A, Herman MW, Sonzogni AA, Danon Y, Carlson AD, Dunn M, Smith DL, Hale GM, Arbanas G, Arcilla R, Bates CR, Beck B, Becker B, Brown F, Casperson RJ, Conlin J and 50 others. ENDF/B-VIII.0: The 8th major release of the nuclear reaction data library with CIELO-project cross sections, new standards and thermal scattering data. *Nucl Data Sheets*. 2018; 148: 1-142.

Chadwick MB, Herman M, Obložinskỳ P, Dunn ME, Danon Y, Kahler AC, Smith DL, Pritychenko B, Arbanas G, Arcilla R, Brewer R, Brown DA, Capote R, Carlson AD, Cho YS, Derrien H, Guber K, Hale GM, Hoblit S, Holloway S and Young PG. ENDF/B-VII.1 nuclear data for science and technology: cross sections, covariances, fission product yields and decay data. *Nucl Data Sheets*. 2011; 112: 2887-2996.

Chadwick MB, Obložinskỳ P, Herman M, Greene NM, McKnight RD, Smith DL, Young PG, MacFarlane RE, Hale GM, Frankle SC, Kahler AC, Kawano T, Little RC, Madland DG, Moller P, Mosteller RD, Page PR, Talou P, Trellue H, White MC and van der Marck SC. ENDF/B-VII.0: next generation evaluated nuclear data library for nuclear science and technology. *Nucl Data Sheets*. 2006; 107: 2931-3060.

Dunford CL. Evaluated nuclear data file, ENDF/B-VI. *Nuclear Data for Science and Technology: Proceedings of an International Conference, held at the Forschungszentrum Jülich, Fed. Rep. of Germany,* 13-17 May 1991. 1992; 788-792.

Jeraj R, Glumac B and Maučec M. Monte Carlo simulation of the TRIGA Mark II benchmark experiment. *Nucl Technol*. 1997; 120: 179-187.

Jeraj R and Ravnik M. TRIGA Mark II reactor: U [20]-zirconium hydride fuel rods in water with graphite reflector (IEU-COMP-THERM-003). *Int Handb Eval Crit Saf Bench Exp*. 1999; NEA NSCDOC 95.

Mahmood MS, Nagaya Y and Mori T. Analysis of the TRIGA Mark-II benchmark IEU-COMP-THERM-003 with Monte Carlo code MVP. *Tech Rep*, Japan Atomic Energy Research Inst. 2004.

Mele I, Ravnik M and Trkov A. TRIGA Mark II benchmark experiment, Part I: Steady-state operation. *Nucl Technol*. 1994a; 105: 37-51.

Mele I, Ravnik M and Trkov A. TRIGA Mark II benchmark experiment, Part II: pulse operation. *Nucl Technol*. 1994b; 105: 52-58.

Mori T and Nakagawa M. MVP/GMVP: General purpose Monte Carlo codes for neutron and photon transport calculations based on continuous energy and multigroup methods. *Tech Rep*, Japan Atomic Energy Research Inst. 1994.

Nakagawa T, Shibata K, Chiba S, Fukahori T, Nakajima Y, Kikuchi Y, Kawano T, Kanda Y, Ohsawa T, Matsunobu H, Kawai M, Zukeran A, Watanabe T, Igarasi S, Kosako K and Asami T. Japanese evaluated nuclear data library version 3 revision-2: JENDL-3.2. *J Nucl Sci Technol*. 1995; 32: 1259-1271.

Romano PK, Horelik NE, Herman BR, Nelson AG, Forget B and Smith K. Open MC: A state-of-the-art Monte Carlo code for research and development. *Ann Nucl Energy*. 2015; 82: 90-97.

Shibata K, Kawano T, Nakagawa T, Iwamoto O, Katakura J-I, Fukahori T, Chiba S, Hasegawa A, Murata T, Matsunobu H, Ohsawa T, Nakajima Y, Yoshida T, Zukeran A, Kawai M, Baba M, Ishikawa M, Asami T, Watanabe T, Watanabe Y, Igashira M, Yamamuro N, Kitazawa H, Yamano N and Takano H. Japanese evaluated nuclear data library version 3 revision-3: JENDL-3.3. *J Nucl Sci Technol*. 2002; 39: 1125-1136.

J. Bangladesh Acad. Sci. 48(2); 237-250: December 2024 DOI:https://doi.org/10.3329/jbas.v48i2.71659

Journal of Bangladesh Academy of Sciences

Journal homepage: http://www.bas.org.bd/publications/jbas.html

**Research article**

# Avifauna of Noakhali Science and Technology University premises and adjacent areas

Humayra Mahmud*, Sadia Sultana, Nasrin Akter and Rasel Talukder

*Department of Zoology, Noakhali Science and Technology University, Bangladesh*

**ARTICLE INFO**

**Article History**

Received: 27 February 2024
Revised: 04 September 2024
Accepted: 17 September 2024

**Keywords:** Avian diversity, Seasonal variation, Noakhali Science and Technology University.

**ABSTRACT**

A study was carried out from September 2021 to September 2023 to estimate the diversity, seasonal variation, and relative abundance of avifauna of Noakhali Science and Technology University and its adjacent areas. One hundred fourteen bird species were recorded from the study site belonging to 18 different orders. Of these, one species, Grey-headed Fish Eagle *Haliaeetus ichthyaetus*, has been rated globally as Near Threatened (BirdLife International 2021). The distribution of birds among habitat types was significantly different ($f$=7.153, $p<0.05$, $df$=2). The walking trail was inhabited with the highest species diversity (H'= 3.45) with the highest evenness (J= 0.84), while grassland was recorded with the lowest species diversity (H'= 2.69) but had almost similar evenness index (J= 0.84); it could have a relation to the food availability. Considering the richness of bird species, the existing habitats will be restored.

## Introduction

Across all seven continents, birds live and breed in almost all types of habitats ranging from the northern extreme of the North Pole to the southern extreme up to 440 kilometers inland in Antarctica (Welty, 1988; Brooke, 2004; Weir and Schluter, 2007). The highest bird diversity occurs in the tropical rain belt, *i.e.*, the area between $23.5^0$ N latitude and $23.5^0$ S latitude (Welty, 1988; Weir and Schluter, 2007). Previously, people thought that speciation rates had become higher in the tropics due to the high diversity. However, some recent studies revealed that greater extinction rates offset the higher speciation rates in the high latitudes than in the tropics (Schreiber and Joanna, 2001; Weir and Schluter, 2007).

Because of the geographical position of the Tropic of Cancer and the Ganges Delta, Bangladesh is profoundly rich in avian diversity or bird diversity (Khan, 1982, 1988). To assess the quality and condition of the environment, the diversity of birds is one of the most significant benchmarks in terms of ecology (Bilgrami, 1995). But nowadays, the diversity of birds has gone downhill due to the destruction of natural habitats and different types of anthropogenic activities. To meet the massive demand of fast-growing civilization and unplanned urbanization, randomly cutting down many trees for commercial purposes is the main factor responsible for squeezing birds' foraging and nesting sites. As a result, many bird species that are supposed to be adapted to rural environments are now forced to be urban dwellers and have evolved new strategies of survival (Vickery et al., 1995; Shochat et al., 2006).

Under the present circumstances, it can be observed that despite the dignified and regularly updated checklists of the birds of Bangladesh, renovated work on the birds of the Noakhali region was highly demanding. Apart from the random studies on several adjacent areas of Noakhali, no profound work mentions a complete account of the birds of the Noakhali region. The study was designed to

- know the avian diversity and their relative abundance in different habitat types in

*Corresponding author:<humayramahmud@nstu.edu.bd>

Noakhali Science and Technology premises and its adjacent areas;

- find the seasonal variation and then determine their resident status in the study area;

suggest conservation initiatives to compose a sustainable ecosystem. Consequently, the outcome of this study is valuable for area-specific management planners, conservationists, and ecologists. It comes out with baseline information for different scientific communities for further studies of this area and the whole Noakhali district and to create awareness for their conservation.

## Materials and Methods

### *Study area*

Historically, Noakhali is known as Bhulua, a district in southeastern Bangladesh. It is located in the Chittagong Division and bordered by the Cumilla district to the north, the Meghna estuary and the Bay of Bengal to the south, Feni and Chittagong districts to the east and Lakshmipur and Bhola districts to the west. The Noakhali Science and Technology University (NSTU) is located about 8 km southwest of Noakhali Sadar. The total land area of NSTU is 101 acres. The research survey was conducted on the entire campus of NSTU and its adjacent areas, which are positioned between the coordinates of North latitude: 22°47'31" and East longitude: 91°06'07". Being in the tropics, Noakhali, as well as Noakhali Science and Technology University, is used to possess a high rate of humidity varying high rate of humidity from 4% to 92%.

### *Data collection*

Data were collected for twenty-four months (September 2021 - September 2023) by direct observations in the field, mainly in the early mornings and afternoons, the most active periods for avian species. Based on the rainfall distribution of the area, October to March was considered the dry season, while April to September was considered the wet season.

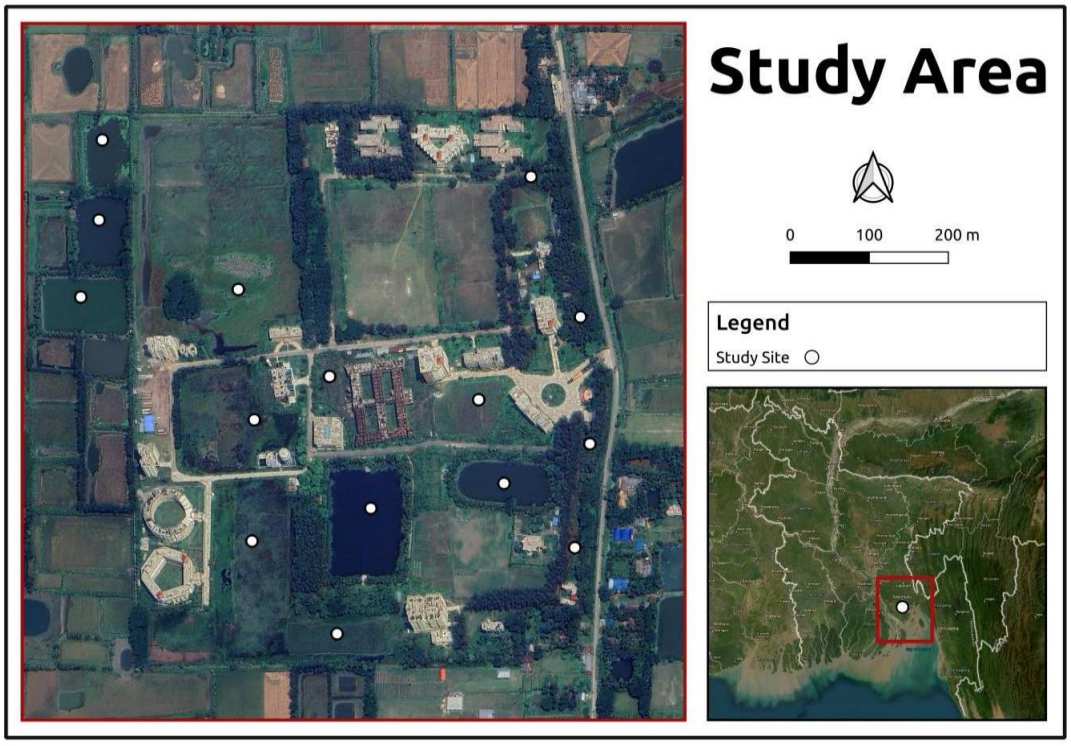


**Fig. 1. Map of study sites.**

Four days in a month and ninety-six days during this whole study period were spent on our field observations. Only the species with confirmed identification have been enlisted. The relative abundance of the birds was assessed as "Common" (seen in almost each visit) and "Uncommon" (seen only in one or two visits). For winter and summer migrants, the abundance was assessed only during the months when they were present in this area.

### *Study design and data collection method*

Based on land cover features, the whole study site was stratified into three habitat types for this study: waterbody (including all water bodies surrounding the area), walking trail (including all walkways in the study site), and grassland (including all grassy areas in the study site). To assess the diversity and abundance of bird species in this area, a stratified random sampling design was used.

Binoculars were used to observe and identify birds. For some species, distinctive calls were recorded, and in many cases, for further identification, observed birds were photographed by using a Canon 60 D camera with Canon EF-S 55- 250 mm f/4.0-5.6 IS II telephoto zoom lens. For the observations of birds, the point transect method was used, and it was done by standing in the middle of the transect and observing gently up to a distance of 30 m radius. At each point, the observation lasted for 15 minutes (Girma et al., 2017).

Bird survey was conducted from 6:00 a.m. to 11:00 a.m. and 3:00 p.m. to 5:30 p.m. in the early evening (Brower et al., 1990; Pomeroy, 1992). A presence-absence approach and replicated point counts were used for bird censuses. All bird species that were observed during the field survey were recorded with a prepared datasheet.

### *Data analysis*

Collected survey data were encapsulated per habitat type in the table during the study period. Shannon diversity index (Magurran, 1988; Jarvis and Robertson, 1999), evenness, relative abundance, and encounter rate (Bibby et al., 1992) were calculated to evaluate the diversity and abundance of birds. By dividing the diversity indices by the natural log of species richness, we have calculated the evenness and relative abundance (RA) of different bird species as the percentage of dividing the total number of contacts of the species by the total number of contacts of all species. One-way ANOVA has been conducted to assess the variation among the habitats.

## Results and Discussion

### *Species richness and abundance of birds*

All the 114 species recorded during the study period belonged to 18 different orders. The highest number (58) comes under the order Passeriformes, and the lowest number (one) comes from six orders: Falconiformes, Podicipediformes, Psittaciformes, Strigiformes, Suliformes, and Bucerotiformes.

Twelve categories of birds were observed in the study area according to feeding habits. Of these, 41.0% were insectivores, considered the highest number and 2.0% were nectarinivores, nectarinivore+insectivores, and insectivore+graminivore, considered the lowest number of the observed species during the study period.

Based on the occurrence rate during the study period, the highest number was considered rare, representing 56.0%, and the lowest number was considered common, representing 7.0% of the total species.

Of those identified species, 78.5% were found to be residents, and 21.5% were migratory species of Bangladesh. Among all those resident species, most were common residents. Of those migrants, the largest part was winter migrants, and very few were summer migrants.

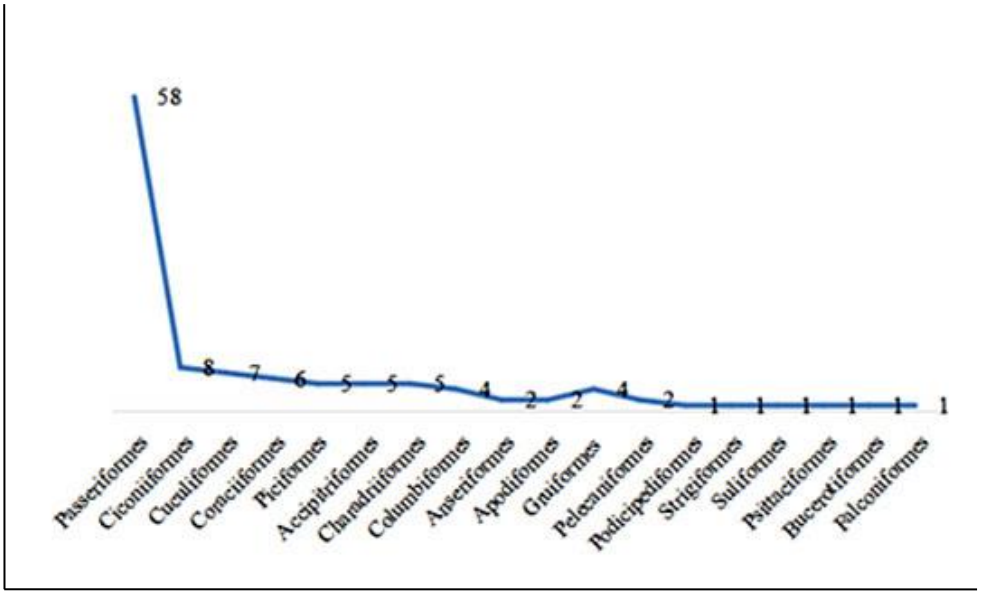


**Fig. 2. Proportion of different orders of birds.**

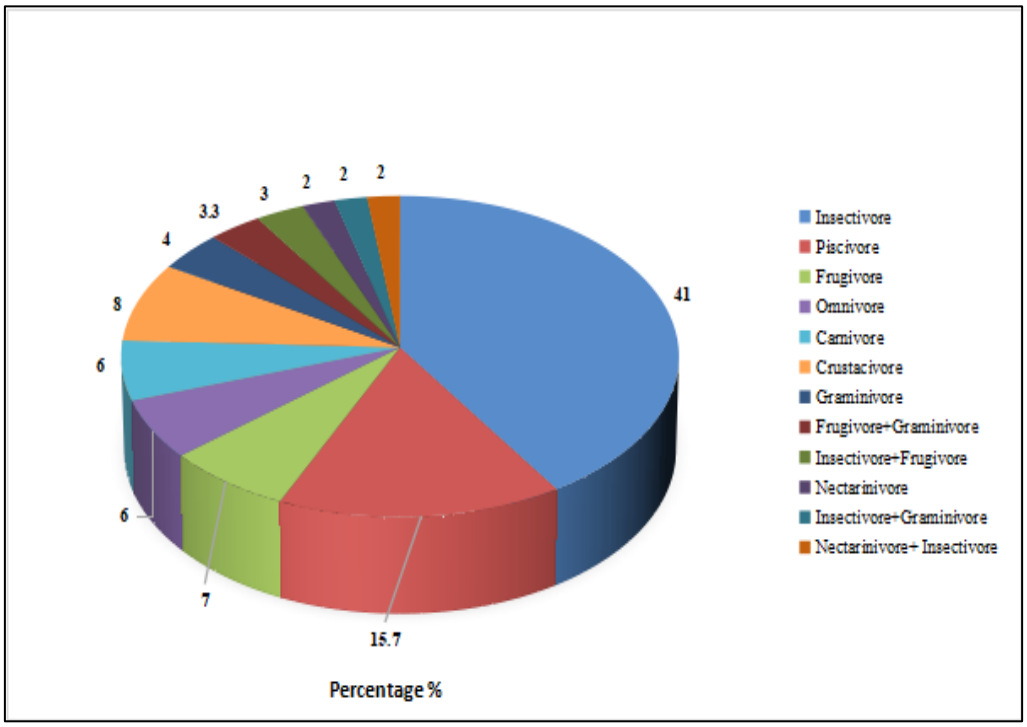


**Fig. 3. The Composition of birds in the study area has different feeding habits.**

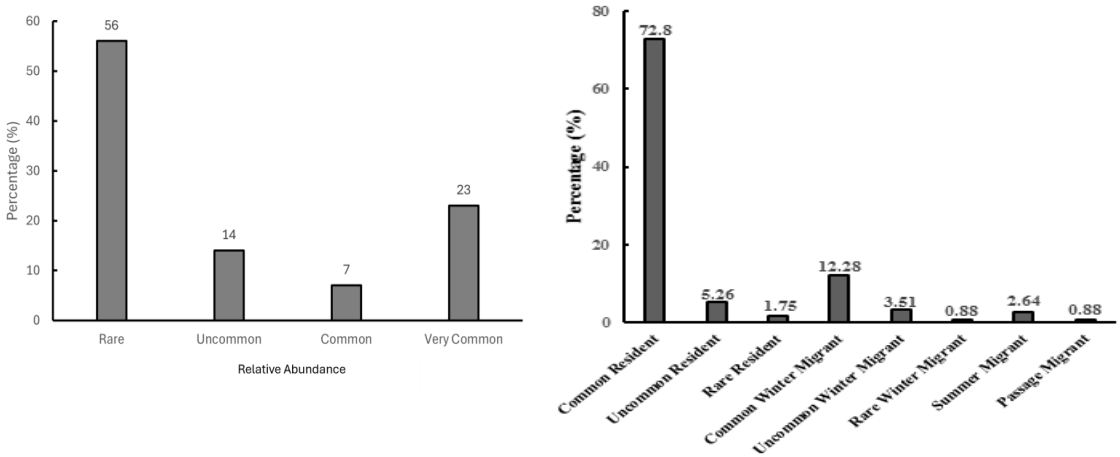


**Fig. 4. Encounter rate (General and Seasonal).**

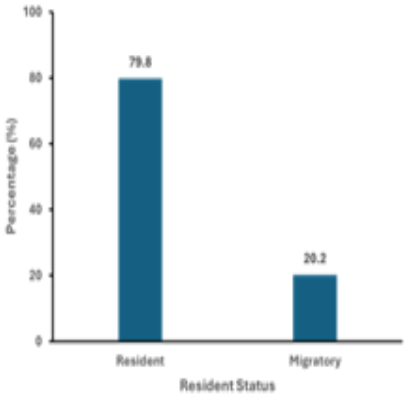


**Fig. 5. Inhabitant status of birds found in the study area.**

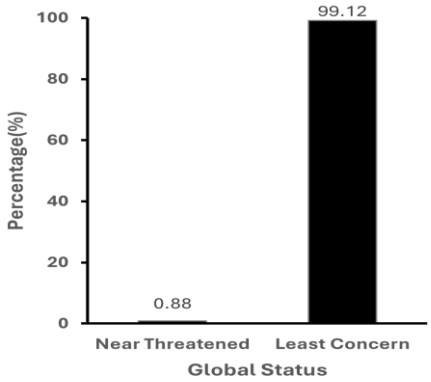


**Fig. 6. Global status of birds found in the study**

On a global scale, one was considered as Near Threatened, Grey-headed Fish Eagle *Haliaeetus ichthyaetus*. The remaining 113 recorded species were categorized as Least Concern (BirdLife International, 2021).

## Diversity and distribution of Bird species

The abundance of bird species was significantly different among all those different habitat types ($f$=7.153, $p$ = 9.06E-04, $df$=2). The highest distribution (30.32±58.31) was recorded on the walking trail. while the lowest distribution (9.53±29.89) was recorded in the grassland. The walking trail was inhabited with the highest species richness, and grassland harbored the lowest species richness in the study area (Table 1).

We have enlisted the highest species diversity of birds (H'= 3.45) with the highest evenness (J= 0.84) in the walking trail, followed by Waterbody (H'= 2.81). In the case of grassland, we have documented the lowest species diversity (H'= 2.69) but an almost similar evenness index (J= 0.84) of the walking trail from the study area.

**Table 1. Distribution of different bird species across habitat types (ANOVA: Single Factor)**.

| **Summary Groups** | **Count** | **Sum** | **Average** | **Variance** | **std.dev** | |
|---|---|---|---|---|---|---|
| Waterbody | 110 | 1532 | 13.927 | 1513.518 | 38.904 | |
| Walking trail | 110 | 3453 | 31.391 | 3491.561 | 59.089 | |
| Grassland | 110 | 1006 | 9.145 | 906.419 | 30.107 | |
| **Anova Source of Variation** | **SS** | **df** | **MS** | **F** | **P-value** | **F crit** |
| Between Groups | 30165.836 | 2 | 15082.918 | 7.654 | 0.000563 | 3.023 |
| Within Groups | 644353.282 | 327 | 1970.499 | | | |
| Total | 674519.118 | 329 | | | | |

**Table 2. Bird species diversity index along habitat types.**

| Habitat types | No. of species | Diversity (H') | Evenness (J) |
|---|---|---|---|
| Walking trail | 60 | 3.451 | 0.842 |
| Waterbody | 30 | 2.809 | 0.826 |
| Grassland | 24 | 2.696 | 0.848 |

We have high bird diversity around the walking trail. It might be due to the abundance of food items besides the trail, the accessibility of these three bird-watching habitats, or the lower number of the other two habitats (water body and grassland). Through this study, we tried to compare three types of habitats and unveil which habitat harbors more bird species. From a conservation perspective, long-term multidisciplinary study is required to understand the ecology of this area's bird community.

## Conclusion

As the university area is crowded, thousands of people visit it daily. They create so much noise, consciously or unconsciously disturbing the avifauna of this area. Besides, some typical anthropological threats were identified as the cause for the declining of the avifaunal diversity. The increase and the ever-spreading situation of these activities are harmonizing the decline of the places suitable for avian feeding, foraging, roosting, and breeding activities.

Though it is a public place with frequent anthropogenic movements, the walking trail still contains a rich diversity of birds.

This could happen due to the availability of food items besides the walking trail, the difference in visibility among those three habitats, or the lower number of the other two habitats (waterbody and grassland). However, this present study found a good number of birds. Some crucial species recorded during the survey are threatened at different levels and rare in Bangladesh. The compelling presence of wintering species justifies that this area is used as a part of the East Asian-Australasian Flyways. It requires more in-depth study studies.

## Acknowledgment

The research cell of Noakhali Science and Technology University provided all the financial support for the research work. The authors expressed their gratitude for the grant.

## Author contributions

**Humayra Mahmud:** Methodology, Data collection, Formal Analysis, Writing - Original Draft, Review & Editing; **Sadia Sultana:** Data collection, Visualization, Review & Editing; **Nasrin Akter:** Data collection, Review & Editing. **Rasel Talukder:** Data collection & Editing.

## Conflict of Interest

The authors declare that they have no known competing financial interests or personal relationships that could have appeared to influence the work reported in this paper.

## References

Bibby CJ, Burgess ND and Hil DH. *Bird Census techniques*. Academic Press, London. 1992

Bilgrami KS. *Concept and Conservation of Biodiversity*. CBS Publishers and Distributors, New Delhi, 1995.

BirdLife International. *Red List of Threatened Birds.* IUCN - International Union for Conservation of Nature, 2021.

Brooke M. *Albatrosses and Petrels across the World*. Oxford University Press, Oxford, UK, 2004.

Brower JE, Zar JH and von Ende C. *Field and laboratory methods for general ecology*. Wm. C. Brown Publishers, Dubuque, 1990.

Girma Z, Mamo Y, Mengesha G, Verma A. and Asfaw T. Seasonal abundance and habitat use of bird species in and around Wondo Genet Forest, south-central Ethiopia. Ecol. Evol. 2017; 7: 3397-3405.

IUCN Bangladesh. *Red Book of Threatened Birds of Bangladesh*. IUCN – International Union for Conservation of Nature, Dhaka, 2000.

Jarvis MA and Robertso A. Predicting population sizes and priority conservation areas for 10 endemic Namibian bird species. *Biol. Conserv*. 1999; 88(1): 121-131.

Khan MAR. The Grassland Avifauna of Bangladesh. In: *Ecology and Conservation of Grassland Birds.*Goriup PD (ed.), Technical Publication No. 7, International Council for Bird Preservation, Cambridge, 1988. pp. 215-219.

Khan MAR. *Wildlife of Bangladesh: A Checklist.* Dhaka University Press, Dhaka, 1982.

Magurran AE. Ecological diversity and its measurement. Croom Helm, London, 1988.

Pomeroy RS. Economic Valuation: Available Methods. In: *Integrative Framework and Methods for Coastal Area Management*. Chua TE and Scura LF (eds), ICLARM Conf. Proc. 37. ICLARM, Manila, Philippines, 1992.

Schreiber EA. and Joanna B. *Biology of Marine Birds*. CRC Press, Florida, 2001.

Shochat E, Warren PS, Faeth SH, Mcintyre NE and Hope D. From patterns to emerging processes in mechanistic urban ecology. *Trends Ecol. Evol.* 2006; 21(4): 186-191.

Vickery PD, Herkert JR, Knopf FL, Ruth J and Keller CE. Grassland birds: An overview of threats and recommended management strategies. In: *Strategies for Bird Conservation: The Partners in Flight Planning Process*. Bonney R, Pashley DN, Cooper R, Niles L (eds); Proceedings of the 3rd . Partners in Flight Workshop; 1995, October 1-5, Cape May, NJ. p.74-77.

Weir JT and Schluter D. The latitudinal gradient in recent speciation and extinction rates of birds and mammals. *Science*, 2007; 315(5818): 1574-1576.

Welty JC. *The life of birds*. Saunders College Publishing Co., Philadelphia. 1988. p.581.

**APPENDIX 1. List of birds found in NSTU & adjacent areas.**

| SI. No. | *Scientific Name* | Common Name | Order | Family | Feeding Habit | Habitat | Passerine/ Non-passerine | No. of Observation | Resident Status | National Status | Global Status | Percentage (%) | Relative abundance |
|---|---|---|---|---|---|---|---|---|---|---|---|---|---|
| 1 | *Dendrocygna bicolor* | Fulvous Whistling Duck | Anseriformes | Anatidae | Piscivore | Waterbody | Non-passerine | 18 | $CM_w$ | NO | LC | 18.75 | R |
| 2 | *Dendrocygna javanica* | Lesser whistling-Duck | Anseriformes | Anatidae | Piscivore | Waterbody | Non-passerine | 168 | $CM_w$ | NO | LC | 100 | VC |
| 3 | *Tachybaptus ruficollis* | Little Grebe | Podicipediformes | Podicipedidae | Piscivore | Waterbody | Non-passerine | 5 | CR | NO | LC | 5.20 | R |
| 4 | *Anastomus oscitans* | Asian Openbill | Ciconiiformes | Ciconiidae | Piscivore | Waterbody | Non-passerine | 178 | CR | NO | LC | 100 | VC |
| 5 | *Butorides striata* | Striated Heron | Ciconiiformes | Ardeidae | Piscivore | Waterbody | Non-passerine | 23 | CR | NO | LC | 24.00 | R |
| 6 | *Ardeola grayii* | Indian Pond Heron | Ciconiiformes | Ardeidae | Piscivore | Waterbody | Non-passerine | 170 | CR | NO | LC | 100 | VC |
| 7 | *Ardea purpurea* | Purple Heron | Ciconiiformes | Ardeidae | Piscivore | Waterbody | Non-passerine | 43 | CR | NO | LC | 48.00 | UC |
| 8 | *Bubulcus ibis* | Cattle Egret | Ciconiiformes | Ardeidae | Piscivore | Waterbody | Non-passerine | 156 | CR | NO | LC | 100 | VC |
| 9 | *Ardea alba* | Great Egret | Ciconiiformes | Ardeidae | Piscivore | Waterbody | Non-passerine | 112 | CR | NO | LC | 100 | VC |
| 10 | *Ardea intermedia* | Intermediate Egret | Ciconiiformes | Ardeidae | Piscivore | Waterbody | Non-passerine | 22 | CR | NO | LC | 23.00 | R |
| 11 | *Egretta garzetta* | Little Egret | Ciconiiformes | Ardeidae | Piscivore | Waterbody | Non-passerine | 145 | CR | NO | LC | 100 | VC |
| 12 | *Anhinga melanogaster* | Oriental Darter | Suliformes | Anhingidae | Piscivore | Waterbody | Non-passerine | 6 | CR | NO | LC | 6.25 | R |
| 13 | *Ixobrychus cinnamomeus* | Cinnamon Bittern | Pelecaniformes | Ardeidae | Piscivore | Waterbody | Non-passerine | 4 | CR | NO | LC | 4.10 | R |
| 14 | *Microcarbo niger* | Little Cormorant | Pelecaniformes | Phalacrocoracidae | Piscivore | Waterbody | Non-passerine | 147 | CR | NO | LC | 100 | VC |
| 15 | *Falco tinnunculus* | Common Kestrel | Falconiformes | Falconidae | Carnivore | Walking trail | Non-passerine | 5 | $CM_w$ | NO | LC | 5.20 | R |
| 16 | *Pandion haliaetus* | Osprey | Accipitriformes | Pandionidae | Carnivore | Waterbody | Non-passerine | 5 | $RM_w$ | NO | LC | 5.20 | R |

| SI. No. | *Scientific Name* | Common Name | Order | Family | Feeding Habit | Habitat | Passerine/ Non-passerine | No. of Observation | Resident Status | National Status | Global Status | % | Relative abundance |
|---|---|---|---|---|---|---|---|---|---|---|---|---|---|
| 17 | *Haliaeetus ichthyaetus* | Grey-headed Fish Eagle | Accipitriformes | Pandionidae | Carnivore | Waterbody | Non-passerine | 3 | UR | NO | NT | 3.10 | R |
| 18 | *Accipiter badius* | Shikra | Accipitriformes | Accipitridae | Carnivore | Walking trail | Non-passerine | 6 | CR | NO | LC | 6.25 | R |
| 19 | *Haliastur indus* | Brahminy Kite | Accipitriformes | Accipitridae | Carnivore | Waterbody | Non-passerine | 31 | CR | NO | LC | 32.20 | UC |
| 20 | *Milvus migrans* | Black Kite | Accipitriformes | Accipitridae | Carnivore | Walking trail | Non-passerine | 43 | CR | NO | LC | 44.80 | UC |
| 21 | *Athene brama* | Spotted Owlet | Strigiformes | Strigidae | Carnivore | Walking trail | Non-passerine | 25 | CR | NO | LC | 26.00 | UC |
| 22 | *Amaurornis phoenicurus* | White-breasted Waterhen | Gruiformes | Rallidae | Crustacivore | Waterbody | Non-passerine | 26 | UR | NO | LC | 27.00 | UC |
| 23 | *Gallinula chloropus* | Common Moorhen | Gruiformes | Rallidae | Crustacivore | Waterbody | Non-passerine | 22 | CR | NO | LC | 23.00 | R |
| 24 | *Fulica atra* | Eurasian Coot | Gruiformes | Rallidae | Crustacivore | Waterbody | Non-passerine | 4 | CR | NO | LC | 4.10 | R |
| 24 | *Porphyrio poliocephalus* | Grey-headed Swaphen | Gruiformes | Rallidae | Crustacivore | Waterbody | Non-passerine | 46 | CR | NO | LC | 48.00 | UC |
| 26 | *Vanellus indicus* | Red-wattled Lapwing | Charadriiformes | Charadridae | Crustacivore | Waterbody | Non-passerine | 16 | CR | NO | LC | 16.70 | R |
| 27 | *Vanellus melabaricus* | Yellow-wattled Lapwing | Charadriiformes | Charadridae | Crustacivore | Waterbody | Non-passerine | 22 | CR | NO | LC | 23.00 | R |
| 28 | *Actitis hypoleucos* | Common Sandpiper | Charadriiformes | Scolopacidae | Crustacivore | Waterbody | Non-passerine | 14 | $CM_w$ | NO | LC | 14.60 | R |
| 29 | *Metopidius indicus* | Bronge-winged Jacana | Charadriiformes | Jacanidae | Crustacivore | Waterbody | Non-passerine | 28 | CR | NO | LC | 29.00 | UC |
| 30 | *Gallinago stenura* | Pin-tailed Snipe | Charadriiformes | Scolopacidae | Crustacivore | Waterbody | Non-passerine | 6 | CR | NO | LC | 6.25 | R |
| 31 | *Columba livia* | Common Rock Pigeon | Columbiformes | Columbidae | Frugivore+Graminivore | Walking trail | Non-passerine | 165 | CR | NO | LC | 100 | VC |
| 32 | *Streptopelia decaocto* | Eurasian Collared Dove | Columbiformes | Columbidae | Frugivore+Graminivore | Walking trail | Non-passerine | 13 | CR | NO | LC | 13.50 | R |

| SI. No. | *Scientific Name* | Common Name | Order | Family | Feeding Habit | Habitat | Passerine/ Non-passerine | No. of Observation | Resident Status | National Status | Global Status | % | Relative abundance |
|---|---|---|---|---|---|---|---|---|---|---|---|---|---|
| 33 | *Spilopelia suratensis* | Western Spotted Dove | Columbiformes | Columbidae | Frugivore+Graminivore | Walking trail | Non-passerine | 14 | CR | NO | LC | 14.60 | R |
| 34 | *Treron phoenicopterus* | Yellow Footed Green Pigeon | Columbiformes | Columbidae | Frugivore+Graminivore | Walking trail | Non-passerine | 7 | CR | NO | LC | 7.30 | R |
| 35 | *Psittacula krameri* | Rose-ringed Parakeet | Psittaciformes | Psittaculidae | Frugivore | Walking trail | Non-passerine | 13 | CR | NO | LC | 13.50 | R |
| 36 | *Centropus sinensis* | Greater Coucal | Cuculiformes | Centropodidae | Omnivore | Walking trail | Non-passerine | 22 | CR | NO | LC | 23.00 | R |
| 37 | *Eudynamys scolopaceus* | Asian koel | Cuculiformes | Cuculidae | Frugivore | Walking trail | Non-passerine | 55 | CR | NO | LC | 57.30 | C |
| 38 | *Cacomantis merulinus* | Plaintive Cuckoo | Cuculiformes | Cuculidae | Frugivore | Walking trail | Non-passerine | 4 | CR | NO | LC | 4.10 | R |
| 39 | *Hierococcyx varius* | Common Hawk-Cuckoo | Cuculiformes | Cuculidae | Frugivore | Walking trail | Non-passerine | 6 | CR | NO | LC | 6.25 | R |
| 40 | *Cuculus micropterus* | Indian Cuckoo | Cuculiformes | Cuculidae | Frugivore | Walking trail | Non-passerine | 2 | $M_s$ | NO | LC | 2.10 | R |
| 41 | *Clamator coromandus* | Chestnut-winged Cuckoo | Cuculiformes | Cuculidae | Frugivore | Walking trail | Non-passerine | 3 | $M_s$ | NO | LC | 3.10 | R |
| 42 | *Clamator jacobinus* | Pied Cuckoo | Cuculiformes | Cuculidae | Frugivore | Walking trail | Non-passerine | 1 | $M_s$ | NO | LC | 1.04 | R |
| 43 | *Cypsiurus balasiensis* | Asian Palm Swift | Apodiformes | Apodidae | Insectivore | Walking trail | Non-passerine | 65 | CR | NO | LC | 67.70 | C |
| 44 | *Apus affinis* | House Swift | Apodiformes | Apodidae | Insectivore | Walking trail | Non-passerine | 77 | CR | NO | LC | 80.20 | VC |
| 45 | *Upupa epops* | Common Hoopoe | Bucerotiformes | Upupidae | Insectivore+ Graminivore | Walking trail | Non-passerine | 24 | UR | NO | LC | 25.00 | UC |
| 46 | *Coracias benghalensis* | Indian Roller | Coraciiformes | Coraciidae | Insectivore+ Graminivore | Walking trail | Non-passerine | 12 | UR | NO | LC | 12.50 | R |
| 47 | *Alcedo atthis* | Common Kingfisher | Coraciiformes | Alcedinidae | Piscivore | Waterbody | Non-passerine | 88 | CR | NO | LC | 91.50 | VC |
| 48 | *Alcedo meninting* | Blue Eared Kingfisher | Coraciiformes | Alcedinidae | Piscivore | Waterbody | Non-passerine | 2 | RR | NO | LC | 2.10 | R |

| SI. No. | *Scientific Name* | Common Name | Order | Family | Feeding Habit | Habitat | Passerine/ Non-passerine | No. of Observation | Resident Status | National Status | Global Status | % | Relative abundance |
|---|---|---|---|---|---|---|---|---|---|---|---|---|---|
| 49 | *Ceryle rudis* | Pied Kingfisher | Coraciiformes | Cerylidae | Piscivore | Waterbody | Non-passerine | 7 | CR | NO | LC | 7.3.00 | R |
| 50 | *Halcyon smyrnensis* | White-throated Kingfisher | Coraciiformes | Halcyonidae | Piscivore | Waterbody | Non-passerine | 37 | CR | NO | LC | 38.50 | UC |
| 51 | *Merops orientalis* | Green Bee-eater | Coraciiformes | Meropidae | Insectivore | Grassland | Non-passerine | 156 | CR | NO | LC | 100 | VC |
| 52 | *Psilopogon haemacephala* | Coppersmith Barbet | Piciformes | Megalaimidae | Frugivore | Walking trail | Non-passerine | 165 | CR | NO | LC | 100 | VC |
| 53 | *Jynx torquilla* | Eurasian Wryneck | Piciformes | Picidae | Insectivore | Walking trail | Non-passerine | 6 | $UM_w$ | NO | LC | 6.25 | R |
| 54 | *Dinopium javanense* | Common Flameback | Piciformes | Picidae | Insectivore | Walking trail | Non-passerine | 178 | CR | NO | LC | 100 | VC |
| 55 | *Micropternus brachyurus* | Rufous Woodpecker | Piciformes | Picidae | Insectivore | Walking trail | Non-passerine | 14 | CR | NO | LC | 14.60 | R |
| 56 | *Dendrocopos macei* | Fulvous-breasted Woodpecker | Piciformes | Picidae | Insectivore | Walking trail | Non-passerine | 56 | CR | NO | LC | 58.30 | C |
| 57 | *Tephrodornis pondicerianus* | Common Woodshrike | Passeriformes | Tephrodomithidae | Insectivore | Walking trail | Passerine | 7 | CR | NO | LC | 7.30 | R |
| 58 | *Coracina melaschistos* | Black-winged Cuckooshrike | Passeriformes | Campephagidae | Insectivore | Walking trail | Passerine | 8 | $UM_w$ | NO | LC | 8.30 | R |
| 59 | *Coracina melanoptera* | Black-headed Cuckooshrike | Passeriformes | Campephagidae | Insectivore | Walking trail | Passerine | 6 | UR | DD | LC | 6.25 | R |
| 60 | *Pericrocotus cantonensis* | Swinhoe's Minivet | Passeriformes | Campephagidae | Insectivore | Walking trail | Passerine | 4 | CR | NO | LC | 4.10 | R |
| 61 | *Pericrocotus cinnamomeus* | Small Minivet | Passeriformes | Campephagidae | Insectivore | Walking trail | Passerine | 43 | CR | NO | LC | 44.80 | UC |
| 62 | *Chloropsis aurifrons* | Golden Fronted Leafbird | Passeriformes | Chloropseidae | Insectivore | Walking trail | Passerine | 6 | CR | NO | LC | 6.25 | R |
| 63 | *Aegithina tiphia* | Common Iora | Passeriformes | Aegithinidae | Insectivore | Walking trail | Passerine | 65 | CR | NO | LC | 67.70 | C |
| 64 | *Lanius cristatus* | Brown Shrike | Passeriformes | Lanidae | Insectivore | Grassland | Passerine | 19 | $CM_w$ | NO | LC | 19.80 | R |

| SI. No. | *Scientific Name* | Common Name | Order | Family | Feeding Habit | Habitat | Passerine/ Non-passerine | No. of Observation | Resident Status | National Status | Global Status | % | Relative abundance |
|---|---|---|---|---|---|---|---|---|---|---|---|---|---|
| 65 | *Lanius schach* | Long-tailed Shrike | Passeriformes | Lanidae | Insectivore | Grassland | Passerine | 48 | CR | NO | LC | 50.0 | C |
| 66 | *Oriolus xanthornus* | Black-hooded Oriole | Passeriformes | Oriolidae | Insectivore | Walking trail | Passerine | 134 | CR | NO | LC | 100 | VC |
| 67 | *Oriolus oriolus* | Eurasian Golden Oriole | Passeriformes | Oriolidae | Insectivore | Walking trail | Passerine | 4 | CR | NO | LC | 4.0 | R |
| 68 | *Dicrurus macrocercus* | Black Drongo | Passeriformes | Dicruridae | Insectivore | Walking trail | Passerine | 187 | CR | NO | LC | 100 | VC |
| 69 | *Dicrurus leucophaeus* | Ashy Drongo | Passeriformes | Dicruridae | Insectivore | Walking trail | Passerine | 7 | $UM_w$ | NO | LC | 7.3.0 | R |
| 70 | *Dicrurus aeneus* | Bronzed Drongo | Passeriformes | Dicruridae | Insectivore | Walking trail | Passerine | 13 | CR | NO | LC | 13.50 | R |
| 71 | *Dendrocitta vagabunda* | Rufous Treepie | Passeriformes | Dicruridae | Omnivore | Walking trail | Passerine | 143 | CR | NO | LC | 100 | VC |
| 72 | *Corvus splendens* | House Crow | Passeriformes | Corvidae | Omnivore | Walking trail | Passerine | 187 | CR | NO | LC | 100 | VC |
| 73 | *Corvus macrorhynchos* | Large-billed Crow | Passeriformes | Corvidae | Omnivore | Walking trail | Passerine | 14 | CR | NO | LC | 14.60 | R |
| 74 | *Artamus fuscus* | Ashy Woodswallow | Passeriformes | Artamidae | Omnivore | Walking trail | Passerine | 56 | CR | NO | LC | 58.30 | C |
| 75 | *Hirundo rustica* | Barn Swallow | Passeriformes | Hirundinidae | Insectivore | Walking trail | Passerine | 66 | $CM_w$ | NO | LC | 68.70 | C |
| 76 | *Prinia inornata* | Plain Prinia | Passeriformes | Cisticolidae | Insectivore | Grassland | Passerine | 41 | CR | NO | LC | 42.70 | UC |
| 77 | *Pycnonotus jocosus* | Red-whiskered Bulbul | Passeriformes | Pycnonotidae | Insectivore +Frugivore | Walking trail | Passerine | 18 | CR | NO | LC | 18.75 | R |
| 78 | *Pycnonotus cafer* | Red-vented Bulbul | Passeriformes | Pycnonotidae | Insectivore +Frugivore | Walking trail | Passerine | 176 | CR | NO | LC | 100 | VC |
| 79 | *Acrocephalus dumetorum* | Blyth's Reed-warbler | Passeriformes | Acrocephalidae | Insectivore | Grassland | Passerine | 7 | $CM_w$ | NO | LC | 7.30 | R |
| 80 | *Phylloscopus fuscatus* | Dusky Warbler | Passeriformes | Phylloscopidae | Insectivore | Grassland | Passerine | 8 | $CM_w$ | NO | LC | 8.30 | R |

| SI. No. | *Scientific Name* | Common Name | Order | Family | Feeding Habit | Habitat | Passerine/ Non-passerine | No. of Observation | Resident Status | National Status | Global Status | % | Relative abundance |
|---|---|---|---|---|---|---|---|---|---|---|---|---|---|
| 81 | *Phylloscopus trochiloides* | Greenish Warbler | Passeriformes | Phylloscopidae | Insectivore | Grasssland | Passerine | 5 | $CM_w$ | NO | LC | 5.20 | R |
| 82 | *Orthotomus sutorius* | Common Tailorbird | Passeriformes | Sylvidae | Insectivore | Grassland | Passerine | 58 | CR | NO | LC | 60.40 | C |
| 83 | *Turdoides striata* | Jungle Babbler | Passeriformes | Sylvidae | Insectivore | Grassland | Passerine | 68 | CR | NO | LC | 70.80 | C |
| 84 | *Malacocincla abbotti* | Abbott's Babbler | Passeriformes | Pellorneidae | Insectivore | Grassland | Passerine | 24 | CR | NO | LC | 25.00 | UC |
| 85 | *Cisticola juncidis* | Zitting Cisticola | Passeriformes | Cisticolidae | Insectivore | Grassland | Passerine | 47 | CR | NO | LC | 49.00 | UC |
| 86 | *Zosterops palpebrosus* | Oriental White-eye | Passeriformes | Zosteropidae | Insectivore | Walking trail | Passerine | 9 | CR | NO | LC | 9.40 | R |
| 87 | *Acridotheres tristis* | Common Myna | Passeriformes | Sturnidae | Omnivore | Walking trail | Passerine | 167 | CR | NO | LC | 100 | VC |
| 88 | *Acridotheres ginginianus* | Bank Myna | Passeriformes | Sturnidae | Insectivore | Walking trail | Passerine | 16 | CR | NO | LC | 16.70 | R |
| 89 | *Acridotheres fuscus* | Jungle Myna | Passeriformes | Sturnidae | Insectivore | Walking trail | Passerine | 145 | CR | NO | LC | 100 | VC |
| 90 | *Sturnus malabaricus* | Chestnut-tailed Starling | Passeriformes | Sturnidae | Insectivore +Frugivore | Walking trail | Passerine | 176 | CR | NO | LC | 100 | VC |
| 91 | *Sturnus contra* | Asian Pied Starling | Passeriformes | Sturnidae | Omnivore | Walking trail | Passerine | 167 | CR | NO | LC | 100 | VC |
| 92 | *Copsychus saularis* | Oriental Magpie-robin | Passeriformes | Muscicapidae | Insectivore | Walking trail | Passerine | 188 | CR | NO | LC | 100 | VC |
| 93 | *Monticola solitaries* | Blue Rock-thrush | Passeriformes | Muscicapidae | Insectivore | Walking trail | Passerine | 2 | $UM_w$ | NO | LC | 2.08 | R |
| 94 | *Ficedula albicilla* | Taiga Flycatcher | Passeriformes | Muscicapidae | Insectivore | Grassland | Passerine | 18 | $CM_w$ | NO | LC | 18.70 | R |
| 95 | *Eumyias thalassina* | Verditer Flycatcher | Passeriformes | Muscicapidae | Insectivore | Walking trail | Passerine | 15 | $CM_w$ | NO | LC | 15.60 | R |
| 96 | *Zoothera citrine* | Orange-headed Thrush | Passeriformes | Turdidae | Insectivore | Grassland | Passerine | 28 | CR | NO | LC | 29.20 | UC |

| SI. No. | *Scientific Name* | Common Name | Order | Family | Feeding Habit | Habitat | Passerine/Non-passerine | No. of Observation | Resident Status | National Status | Global Status | % | Relative abundance |
|---|---|---|---|---|---|---|---|---|---|---|---|---|---|
| 97 | *Hypothymis azurea* | Black-naped Monarch | Passeriformes | Monarchidae | Insectivore | Walking trail | Passerine | 25 | CR | NO | LC | 26.0 | UC |
| 98 | *Rhipidura albicollis* | White-throated Fantail | Passeriformes | Rhipiduridae | Insectivore | Grassland | Passerine | 41 | CR | NO | LC | 42.70 | UC |
| 99 | *Nectarinia zeylonica* | Purple-rumped Sunbird | Passeriformes | Nectariniidae | Nectarinivore | Walking trail | Passerine | 35 | CR | NO | LC | 36.90 | UC |
| 100 | *Nectarinia asiaticus* | Purple Sunbird | Passeriformes | Nectariniidae | Nectarinivore | Walking trail | Passerine | 45 | CR | NO | LC | 46.90 | UC |
| 101 | *Arachnothera longirostra* | Little Spider Hunter | Passeriformes | Nectariniidae | Insectivore | Walking trail | Passerine | 6 | CR | NO | LC | 6.25 | R |
| 102 | *Dicaeum cruentatum* | Scarlet Backed Flowerpecker | Passeriformes | Diciaedae | Nectarinivore + Insectivore | Walking trail | Passerine | 12 | CR | NO | LC | 12.50 | R |
| 103 | *Parus major* | Great Tit | Passeriformes | Paridae | Insectivore | Walking trail | Passerine | 44 | CR | NO | LC | 45.80 | UC |
| 104 | *Passer domesticus* | House Sparrow | Passeriformes | Passeridae | Graminivore | Walking trail | Passerine | 280 | CR | NO | LC | 100 | VC |
| 105 | *Ploceus philippinus* | Baya Weaver | Passeriformes | Ploceidae | Graminivore | Grassland | Passerine | 170 | CR | NO | LC | 100 | VC |
| 106 | *Lonchura malabarica* | Indian Silverbill | Passeriformes | Estrildidae | Graminivore | Grassland | Passerine | 28 | UR | NO | LC | 29.20 | UC |
| 107 | *Lonchura punctulata* | Scaly-breasted Munia | Passeriformes | Estrildidae | Graminivore | Grassland | Passerine | 190 | CR | NO | LC | 100 | VC |
| 108 | *Lonchura atricapilla* | Black-headed Munia | Passeriformes | Estrildidae | Graminivore | Grassland | Passerine | 33 | CR | NO | LC | 34.00 | UC |
| 109 | *Dendronanthus indicus* | Forest Wagtail | Passeriformes | Motacillidae | Insectivore | Grassland | Passerine | 4 | $M_p$ | NO | LC | 4.20 | R |
| 110 | *Motacilla alba* | White Wagtail | Passeriformes | Motacillidae | Insectivore | Grassland | Passerine | 27 | $CM_w$ | NO | LC | 28.10 | UC |
| 111 | *Motacilla madaraspatensis* | Citrine Wagtail | Passeriformes | Motacillidae | Insectivore | Grassland | Passerine | 16 | RR | NO | LC | 16.70 | R |
| 112 | *Motacilla citreola* | Western Yellow Wagtail | Passeriformes | Motacillidae | Insectivore | Grassland | Passerine | 5 | $CM_w$ | NO | LC | 5.20 | R |
| 113 | *Motacilla flava* | White-browed Wagtail | Passeriformes | Motacillidae | Insectivore | Grassland | Passerine | 24 | $CM_w$ | NO | LC | 25.00 | UC |
| 114 | *Anthus rufulus* | Paddyfield Pipit | Passeriformes | Motacillidae | Insectivore | Grassland | Passerine | 21 | CR | NO | LC | 21.09 | R |

Ex= Extinct, CR= Critically Endangered, EN= Endangered, VU= Vulnerable, DD= Data Deficient, NO= Not Threatened, LC= Least Concern, VC= Very Common, C= Common, UC= Uncommon, R=Rare, RR = Rare Resident, $RM_w$ = Rare Winter Migrant, V=vagrant, $M_s$ = Summer Migrant and $M_p$ = Passage Migrant (IUCN Bangladesh, 2000).

J. Bangladesh Acad. Sci. 48(2); 251-264: December 2024 DOI:https://doi.org/10.3329/jbas.v48i2.66072

Journal of Bangladesh Academy of Sciences

Journal homepage: http://www.bas.org.bd/publications/jbas.html

**Research Article**

# The Reve's Puzzle with a single cheat of the Divine rule

Abdullah-Al-Kafi Majumdar*

*Yamanote-cho* 17-2, *Beppu-shi* 874-0828, *Japan*

**ARTICLE INFO**

**Article History**

Received: 05 March 2023
Revised: 12 May 2024
Accepted: 07 October 2024

**Keywords:** The Tower of Hanoi problem, Divine rule, Reve's puzzle, Dynamic programming equation.

**ABSTRACT**

A new variant of the Reve's puzzle, which allows (at most) one violation (or, "cheat") of the "divine rule", has been introduced in an earlier paper. Letting $S(n)$ be the minimum number of moves required to solve the new generalization with $n$ discs, this paper finds an explicit expression of $S(n)$, taking into account all the possible schemes. Some results related to the generalization to the general case of $c$ cheats are derived.

## Introduction

The Tower of Hanoi problem, posed by the French number theorist Lucas (1883), is as follows: Given are three pegs, *S*, *P* and *D* and $n$ ($\geq$1) discs of different radii, $d_1$, $d_2$, …, $d_n$. Initially, the discs rest on the source peg *S* in a tower, with the smallest disc at the top. The problem is to transfer the tower to the destination peg, *D*, in minimum number of "moves", where each "move" transfers only one (topmost) disc from one peg to another peg, under the "divine rule" that, no disc can ever be put directly on top of a smaller disc. It is known that $2^n - 1$ moves are necessary to solve the problem.

The 4-peg generalization, commonly known as the Reve`s puzzle, is due to the English puzzlist Dudeney (1958) and is as follows: There are $n$ discs of varying sizes, and four pegs. Initially, the source peg *S* contains the tower of $n$ discs, as shown in Fig. 1. The objective is to transfer the tower to the destination peg *D* (using the two auxiliary pegs $P_1$ and $P_2$), in minimum number of moves, under the "divine rule" described above.

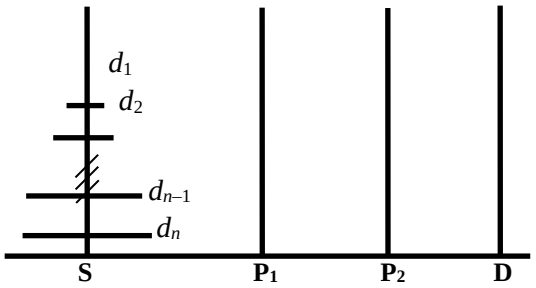


**Fig. 1. The initial configuration of the Reve's puzzle.**

For details on the Reve's puzzle and its various generalizations, the reader is referred to Majumdar (2012, 2013) and Hinz et al. (2018).

A new version of the Tower of Hanoi problem has been proposed and solved by Chen et al. (2007). In the new variant, the objective is to transfer the tower from the source peg *S* to the destination peg *D* in minimum number of moves, such that, for (at most) $c$ moves, the player may put some disc directly on top of a smaller one, thereby violating the "divine rule". Chen et al. (2007) call each such move a "cheat" of the player.

In an earlier paper, Majumdar (2022) proposed a generalization of the problem of Chen et al. (2007) to

*Corresponding author:<aakmajumdar@gmail.com>

the Reve's puzzle, which permits (at most) one relaxation (or, "cheat") of the "divine rule". Thus, during the transfer process, at most once, a larger disc may be placed directly on top of a smaller disc.

Letting $S(n)$ be the minimum number of moves required to solve the Reve's puzzle with $n$ discs and (at most) one relaxation (or, "cheat") of the "divine rule", this paper derives a closed-form expression of $S(n)$, considering in detail all possible schemes. This is done in the third section. The next section gives the necessary background materials, while the following section gives some observations on multiple optimal strategies. The paper concludes with Conclusion in the final section.

## Background materials

Letting $R(n)$ be the minimum number of moves required to solve the Reve's puzzle with $n$ ( $\geq 1$) discs, $R(n)$ satisfies the dynamic programming equation (DPE) below (see, for example, Roth (1974), Wood (1981), Hinz (1989), Chu and Johnsonbaugh (1991), Majumdar (1994, 2012) and Hinz et al. (2018)): For $n \geq 4$,

$$R(n) = \min_{1 \leq \ell \leq n-1} \left\{ 2R(\ell) + 2^{n-\ell} - 1 \right\}, \qquad (1a)$$

with

$$R(n) = 2n - 1 \text{ for all } 1 \leq n \leq 3. \qquad (1b)$$

Obviously, $R(0) = 0$.

Recall that the DPE (1a) is obtained by following the steps below:

1. the tower of the topmost $\ell$ ($\geq 1$) smallest discs is moved from the peg $S$ to the peg $P_1$, using all the four pegs available, in (minimum) $R(\ell)$ moves,
2. next, the tower of the remaining $n-\ell$ discs (on $S$) is moved to the peg $D$, using the three pegs available, in (minimum) $2^{n-\ell} - 1$ moves,
3. finally, the tower of $\ell$ discs is shifted (from $P_1$) to $D$, in (minimum) $R(\ell)$ moves, to complete the tower on $D$.

Now, $\ell$ is chosen so as to minimize the total numbers of moves, which results in the DPE (1a).

Recently, Bousche (2014) presented an analytical proof of optimality of the above scheme, which leads to the DPE (1a).

The solution of the optimality equation (1a) is given below. For proofs, the reader is referred to Majumdar (1994, 2012), Hinz et al. (2018) and Majumdar (2021).

***Lemma* 1:** The expression of $R(n)$ is given as follows:

(1) for $s$ = 1, 2, …, $R\left(\frac{s(s+1)}{2}\right)$ is attained at the unique point $\ell = \frac{s(s-1)}{2}$, with

$$R\left(\frac{s(s+1)}{2}\right) = 2^s(s-1) + 1,$$

(2) for $\frac{s(s+1)}{2} < n < \frac{(s+1)(s+2)}{2}$, $R(n)$ is attained at $\ell = n-s-1, n-s$, with

$$R(n) = 2^s \left\{ n - \frac{s(s-1)}{2} - 1 \right\} + 1.$$

Moreover, for $\frac{s(s+1)}{2} \leq n < \frac{(s+1)(s+2)}{2}$,

$$R(n+1) - R(n) = 2^s.$$

In Lemma 1 above, $\ell$ is the value at which the function $2R(\ell) + 2^{n-\ell} - 1$ in equation (1a) is minimized. The values of $R(n)$ for some small $n$ are tabulated in Table 1.

The result below readily follows from Lemma 1. An alternative proof is given in Majumdar (1994, 2012, 2016).

***Corollary* 1:** For $n \geq 1$,

$$R(n+1) - R(n) \geq R(n) - R(n-1).$$

The following result would be required later.

***Corollary* 2:** For $n \geq 6$, $R(n+1) - R(n) > 4$.

***Proof*:** Since for $n \geq 6$ (see Table 1),

$$R(n+1) - R(n) \geq R(7) - R(6) = 8 > 4 = R(6) - R(5),$$

the result follows (by Corollary 1).

Two other results of importance here are the following ones.

***Corollary* 3:** $R(n+1) - R(n) = 4$ if and only if $n = 3, 4, 5$.

***Proof*:** The proof is evident from the values tabulated in Table 1.

***Corollary* 4:** $R(n+1) - R(n) = 2^n$ if and only if $n = 1$.

***Proof*:** First note that, $R(1)$ and $R(2)$ both are attained at the point $\ell = 0$. To prove the result, it may be assumed, without loss of generality, that $R(n)$ and $R(n+1)$ both are attained at the point $\ell = L$, so that

$R(n) = 2R(L) + 2^{n-L} - 1$,

$R(n+1) = 2R(L) + 2^{n+1-L} - 1$,

and hence,

$R(n+1) - R(n) = 2^{n-L}$.

Then, by the given condition,

$2^{n-L} = 2^n$,

so that $L = 0$, and consequently, $n = 1$.

Letting $S_3(n, c)$ be the minimum number of moves required to solve the problem of Chen et al. (2007) with $n$ ($\geq 1$) discs and (at most) $c$ ($\geq 1$) relaxations (or, "cheats") of the "divine rule", $S_3(n, c)$ is given in the lemma below. The lemma is due to Chen et al. (2007).

***Lemma* 2:** For any $n \geq 1$, $c \geq 1$,

$$S_3(n, c) = \begin{cases} 2n-1, & if\ 1 \leq n \leq r+2 \\ 4n-2c-5, & if\ r+2 \leq n \leq 2r+3 \\ 2^{n-2r} + 6r - 1, & if\ n \geq 2r+3 \end{cases}$$

Recall that, in Lemma 2 above, for $c = 1$, $n \geq 4$, the optimal strategy is as follows:

1. the tower of the topmost $n-3$ smallest discs is transferred (from the peg $S$) to the auxiliary peg $P$, in (minimum) $2^{n-3} - 1$ moves,
2. the disc $d_{n-2}$ is moved (from $S$) to $D$,
3. the disc $d_{n-1}$ is shifted (from $S$) to $P$, violating the "divine rule",
4. the disc $d_{n-2}$ (on $D$) is moved to $P$,
5. the disc $d_n$ is shifted (from $S$) to $D$,
6. the disc $d_{n-2}$ is moved (from $P$) to $S$,
7. the disc $d_{n-1}$ (on $P$) is shifted to $D$,
8. the disc $d_{n-2}$ is moved (from $S$) to $D$,
9. finally, the tower of the $n-3$ smallest discs is transferred (from $P$) to $D$, to complete the tower on the destination peg $D$.

The next section first describes the problem in detail and then finds its solution explicitly.

## The problem and its solution

This section considers the Reve`s puzzle with $n$ discs and (at most) one relaxation (or, "cheat") of the "divine rule". More precisely, the problem may be stated as follows: Given is a tower of $n$ ($\geq 1$) discs (of varying sizes) resting on the source peg $S$, with the smallest disc at the top. The objective is to transfer the tower (from $S$) to the destination peg $D$, using the two auxiliary pegs $P_1$ and $P_2$, in minimum number of moves, where each move shifts only one (topmost) disc from one peg to another, under the condition that (at most) once, some disc may be put directly on top of a smaller one, and in any of the remaining moves, no disc can ever be placed directly on a smaller one.

Let $S(n)$ denote the minimum number of moves necessary to solve the problem described above. In an earlier paper, Majumdar (2022, Theorem 2) gives an expression of $S(n)$ by considering three possible schemes. The following theorem supplements the result of Majumdar (2022), and gives an expression of $S(n)$, taking into consideration all the possible schemes.

***Theorem* 1:** For $1 \leq n \leq 8$, $S(n)$ is given by

$$S(n) = \begin{cases} 2n-1, & if\ 1 \leq n \leq 4 \\ R(n-1) + 2, & if\ n = 5,\ 6,\ 7 \\ R(n-2) + 6, & if\ n = 5,\ 6,\ 7,\ 8 \end{cases}$$

and for $n \geq 6$, $S(n)$ is given as follows: Let

$$\frac{(t+2)(t+3)}{2} \leq n < \frac{(t+3)(t+4)}{2}$$

for some integer $t \in \{1, 2, \ldots\}$; then

$S(n) = R(n-t-2) + 2[R(t) + 2^t + 2]$.

***Proof*:** For $1 \leq n \leq 4$, the proof is immediate.

So, let $n \geq 5$. There are four possible schemes, which are described below.

*Scheme* 1: follows the steps below:

1. the tower $T = \{d_1, d_2, \ldots, d_k\}$ of the topmost $k$ ($\geq 1$) smallest discs is shifted from the source peg $S$ to the auxiliary peg $P_1$ (using all the four available pegs), in (minimum) $R(k)$ moves,
2. the disc $d_{k+1}$ is moved from $S$ to $P_1$, on top of $T$, violating the "divine rule",
3. the tower of remaining $n-k-1$ discs is shifted (from $S$) to $D$ (using the three available pegs), in (minimum) $2^{n-k-1} - 1$ moves,

4. the disc $d_{k+1}$ is moved from $P_1$ to $D$,
5. finally, the tower $T$ (of $k$ discs) on $P_1$ is transferred to $D$, (in (minimum) $R(k)$ moves), thereby completing the tower on the destination peg $D$.

Now, $k$ in Step 1 above is chosen so that the total number of moves is minimized. Thus, Scheme 1 requires minimum

$$\min_{1 \le k \le n-1} 2\{R(k)+1\} + 2^{n-k-1} - 1 = R(n-1) + 2. \quad (2)$$

number of moves, where the expression (2) follows by virtue of the equation (1).

Note that, in equation (2), $R(n-1)$ is attained at a point $k$ with $k \le n-2 < n-1$.

*Scheme* 2: follows the nine steps below:

1. the tower $T$ of the topmost $k$ ($\ge 1$) smallest discs is transferred from the source peg $S$ to the auxiliary peg $P_1$, in (minimum) $R(k)$ moves,
2. the disc $d_{k+1}$ is moved from $S$ to $P_2$,
3. the disc $d_{k+2}$ (on $S$) is put on top of the tower $T$, violating the "divine rule",
4. the disc $d_{k+1}$ is placed on $d_{k+2}$ on $P_1$,
5. the tower of the remaining $n-k-2$ discs (on $S$) is transferred to $D$, in (minimum) $2^{n-k-2}-1$ moves,
6. the disc $d_{k+1}$ on $P_1$ is moved $P_2$,
7. the disc $d_{k+2}$ is shifted from $P_1$ to $D$,
8. the disc $d_{k+1}$ is moved from $P_2$ to $D$,
9. finally, the tower $T$ is transferred from $P_1$ to $D$, to complete the tower on the destination peg $D$.

This scheme requires (minimum)

$$2R(k) + 2^{n-k-2} + 5$$

number of moves, and $k$ is to be chosen so as to minimize the total number of moves. Thus, under this scheme, the minimum number of moves required is

$$\min_{1 \le k \le n-1} \left\{2R(k) + 2^{n-k-2}\right\} + 5 = R(n-2) + 6, \quad (3)$$

where in the last equation (3), equation (1) has been exploited. Recall that, $R(n-2)$ is attained at a point $k$ with $k \le n-3 < n-1$. Thus, the value of $R(n-2)$ is not affected if the range of $k$ is extended (to $n-1$) in equation (3).

Now, for $n \ge 8$ (by Corollary 2),

$$R(n-1) + 2 > R(n-2) + 6.$$

Thus, for $n \ge 8$, Scheme 2 is better than Scheme 1. Again, by Corollary 3,

$$R(n-1) + 2 = R(n-2) + 6.$$

if and only if $n = 5, 6, 7$, so that for these values of $n$, Scheme 2 is as good as Scheme 1.

*Scheme* 3: follows the steps below:

1. first, the tower $T$ of the topmost $k$ ($\ge 1$) smallest discs is transferred from the source peg $S$ to the auxiliary peg $P_1$, in (minimum) $R(k)$ moves,
2. next, the tower of the remaining $n-k$ largest discs on $S$ is moved to $D$, using the three available pegs, in (minimum) $S_3(n-k)$ moves, where $S_3(n)$ is given by Lemma 1,
3. finally, the tower $T$ of $k$ discs (on $P_1$) is shifted to $D$, in (minimum) $R(k)$ moves, to complete the tower on $D$.

The above scheme requires (minimum)

$$2R(k) + S_3(n-k) = 2R(k) + 2^{n-k-2} + 5$$

number of moves, which is the same as that for Scheme 2.

Note that, though Scheme 2 and Scheme 3 both give the same number of moves, the (optimal) strategies employed are different in the two cases.

*Scheme* 4: consists of the steps below:

1. the tower $T_1$ of the topmost $k$ ($\ge 1$) smallest discs is shifted from the source peg $S$ to the auxiliary peg $P_1$, in (minimum) $R(k)$ moves,
2. the tower of the next $t$ consecutive discs, namely, $d_{k+1}, d_{k+2}, \ldots, d_{k+t}$, denoted by $T_2$, is moved (from $S$) to the auxiliary peg $P_2$, using the three pegs available, in (minimum) $2^t - 1$ moves,
3. the disc $d_{k+t+1}$ is shifted (from $S$) to the destination peg $D$,
4. the disc $d_{k+t+2}$ is moved (from $S$) to $P_1$, on top of the tower $T_1$ of $k$ smallest discs, violating the "divine rule",
5. the disc $d_{k+t+1}$ is transferred (from $D$) to $P_1$, on the disc $d_{k+t+2}$,
6. the tower of $t$ discs $T_2$ is shifted (from $P_2$) to $P_1$,

on the disc $d_{k+t+1}$, in (minimum) $R(t)$ moves.

After Step 6, there are two towers on the auxiliary peg $P_1$, namely, the tower of $t+2$ consecutive discs, $d_{k+1}, d_{k+2}, \ldots, d_{k+t}, d_{k+t+1}, d_{k+t+2}$, on top of the tower $T_1$ of the smallest $k$ discs. The peg $S$ contains the tower of $n-k-t-2$ largest discs. The situation is depicted in Fig. 2. Note that, the total number of moves necessary in the above six steps is $R(k)+R(t)+2^t+2$.

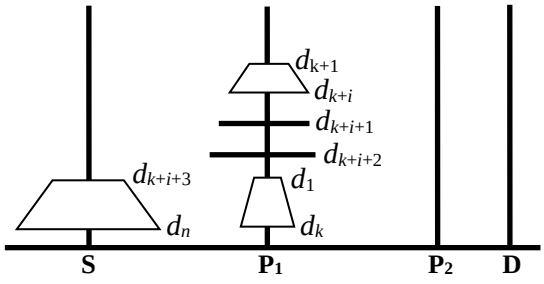


**Fig. 2. The configuration after the first six steps in Scheme 4.**

Next, follow the steps below to complete the transfer process to the peg $D$.

7. the tower of the largest $n-k-t-2$ discs, still lying on the peg $S$, is moved to the peg $D$, using the three pegs available, in (minimum) $2^{n-k-t-2}-1$ moves,
8. the tower of $t$ discs, $T_2$, is transferred (from $P_1$) to $P_2$, in (minimum) $R(t)$ moves,
9. the disc $d_{k+t+1}$ (on $P_1$) is shifted to $S$,
10. the disc $d_{k+t+2}$ (on $P_1$) is moved to $D$,
11. the disc $d_{k+t+1}$ is transferred from $S$ to $D$, on top of the disc $d_{k+t+2}$,
12. the tower $T_2$ (on $P_2$) is shifted to $D$, using the three pegs available, in (minimum) $2^t-1$ moves,
13. finally, the tower of $k$ smallest discs, $T_1$ (on $P_1$), is transferred to $D$, (in (minimum) $R(k)$ moves) so as to complete the tower on the destination peg $D$.

To find the minimum number of moves, $k$ is to be chosen accordingly. Hence, the minimum number of moves involved in this scheme is

$$\min_{1\le k\le n-1} 2\{R(k)+R(t)+2^t+2\}+2^{n-k-t-2}-1$$

$$= R(n-t-2)+2[R(t)+2^t+2], \qquad (4)$$

where $t$ is to be determined such that the expression in (4) is minimized. Note that, in (4), $R(n-t-2)$ is attained at a point $k$ with $k\le n-t-2<n$.

Let

$$S(n,t)\equiv R(n-t-2)+2[R(t)+2^t+2]. \qquad (5)$$

Then, for any $n\ge 1$ fixed,

$$\begin{aligned} S(n,t) &= R(n-t-2)+2[R(t)+2^t+2] \\ &< R(n-t-3)+2[R(t+1)+2^{t+1}+2] \\ &= S(n,t+1) \end{aligned}$$

if and only if

$$\begin{aligned} &R(n-t-2)-R(n-t-3) \\ &< 2^{t+1}+2[R(t+1)-R(t)]. \end{aligned} \qquad (5a)$$

Note that, for any integer $t\ge 1$,

$$2^{t+1}+2[R(t+1)-R(t)]\le 2^{t+2},$$

with the equality sign if and only if $t = 1$ (by Corollary 4).

Let $n$ be such that

$$\frac{(t+1)(t+2)}{2}\le n-t-3<\frac{(t+2)(t+3)}{2} \qquad (6)$$

for some integer $t\ge 1$; then, by virtue of part (2) of Lemma 1,

$$R(n-t-2)-R(n-t-3)=2^{t+1}.$$

Note that, the inequality (6) simplifies to

$$\frac{(t+2)(t+3)}{2}+1\le n<\frac{(t+3)(t+4)}{2}.$$

Now, when $n=\frac{(t+2)(t+3)}{2}$, then

$$R(n-t-2)=R\left(\frac{(t+1)(t+2)}{2}\right)=2^{t+1}t+1,$$

$$\begin{aligned} R(n-t-3) &= R\left(\frac{(t+1)(t+2)}{2}-1\right), \\ &= 2^t(2t-1)+1, \end{aligned}$$

so that

$$R(n-t-2)-R(n-t-3)=2^t.$$

Thus, if $\frac{(t+2)(t+3)}{2}\le n<\frac{(t+3)(t+4)}{2}$, then the inequality (5a) is satisfied.

By Corollary 2,

$$R(n-2)+6>R(n-3)+10, \text{ if } n\ge 9.$$

Hence, when $n \geq 9$, the fourth scheme (with $t = 1$) is better than the second one; moreover, the fourth scheme is the only optimal scheme when $n \geq 9$. To complete the proof, it is necessary to compare the values of $R(n-1)+2$, $R(n-2)+6$ and $R(n-3)+10$ when $5 \leq n \leq 8$. Since,

$$R(4)+2 = 11 = R(3)+6,$$

it follows that, when $n = 5$, the first and the second schemes both are optimal; again, since

$$R(5)+2 = R(4)+6 = R(3)+10 = 15,$$

$$R(6)+2 = R(5)+6 = R(4)+10 = 19,$$

it follows that, all the three schemes are optimal for $n = 6, 7$; and finally, since

$$R(6)+6 = 23 = R(5)+10,$$

it follows that, for $n = 8$, the second and the third schemes are optimal. Thus, so far as the number of moves is concerned, the second scheme as well as the third one may be disregarded.

Now, using the values in Table 1, it can easily be deduced that, for $4 \leq n \leq 7$,

$$R(n-1) = 4n-11.$$

Thus, the minimum number of moves under the first scheme is simply $4n - 9$. Finally, note that, this number remains valid when $n = 8, 9$.

Hence, the theorem is established.

For $t\ (\geq 1)$ fixed, let $k = K(t)$ be the point at which $R(n-t-2)$ is attained, so that

$$R(n-t-2) = 2[R(K) + 2^{n-t-K-3} - 1] + 1.$$

It then follows from equation (4) in Scheme 4 that, $R(K) + R(t) + 2^{n-t-K-3} + 2^t + 1$ is the number of moves required to dismantle the topmost $n-1$ smallest discs on the source peg $S$ and distribute them on the two auxiliary pegs just before transferring the largest disc (from $S$) to the destination peg $D$. Therefore, in describing the optimal strategy, it is sufficient to give such a half-way solution.

Lemma 1 may be exploited to find the properties as well as the closed-form expression of $S(n)$. This is done below.

***Theorem* 2:** Let $n$ be such that

$$\frac{(t+2)(t+3)}{2} \leq n < \frac{(t+3)(t+4)}{2}$$

for some integer $t \in \{1, 2, \ldots\}$; then,

(1) the optimal strategy corresponding to $n = \frac{(t+3)(t+4)}{2} - 1$ is unique with

$$S\left(\frac{(t+3)(t+4)}{2} - 1\right) = (2t+3)2^{t+1} + 2R(t) + 5,$$

(2) the optimal strategy corresponding to $n = \frac{(t+2)(t+3)}{2}$ is unique with

$$S\left(\frac{(t+2)(t+3)}{2}\right) = (t+1)2^{t+1} + 2R(t) + 5,$$

(3) if $\frac{(t+2)(t+3)}{2} < n < \frac{(t+3)(t+4)}{2} - 1$, then there are two optimal strategies for $S(n)$ with

$$S(n) = 2^{t+1}\left[n - \frac{t(t+3)}{2} - 2\right] + 2R(t) + 5.$$

***Proof*:** When $n = \frac{(t+3)(t+4)}{2} - 1$, then by part (1) of Lemma 1,

$$R(n-t-2) = R\left(\frac{(t+2)(t+3)}{2}\right) = (t+1)2^{t+2} + 1,$$

and hence, by Theorem 1,

$$S(n) = [(t+1)2^{t+2} + 1] + 2[R(t) + 2^t + 2],$$

which, after simplification, gives part (1) of the theorem. By part (1) of Lemma 1, the integer $K = \frac{(t+1)(t+2)}{2}$ is unique, where $K$ is the number of discs that are to be stored, in a tower, on the auxiliary peg $P_1$, in Step 1 of Scheme 4, and $t$ is the number of discs to be stored, in a tower, on the peg $P_2$, in Step 2 of Scheme 4.

Next, let $n = \frac{(t+2)(t+3)}{2}$. Since,

$$R(n-t-2) = R\left(\frac{(t+1)(t+2)}{2}\right) = t2^{t+1} + 1,$$

by Theorem 1,

$$S(n) = (t2^{t+1} + 1) + 2[R(t) + 2^t + 2].$$

After some algebraic manipulation, part (2) of the theorem results. By Lemma 1, the integer $K = \frac{t(t+1)}{2}$ is unique.

Finally, consider the case when

$$\frac{(t+2)(t+3)}{2} < n < \frac{(t+3)(t+4)}{2} - 1.$$

Here, since

$$\frac{(t+1)(t+2)}{2} < n-t-2 < \frac{(t+2)(t+3)}{2},$$

it follows, by part (2) of Lemma 1,

$$R(n-t-2) = 2^{t+1}\left[n - \frac{t(t+3)}{2} - 3\right] + 1.$$

Plugging-in this expression for $R(n-t-2)$ in Theorem 1 and simplifying, the desired expression of $S(n)$ is obtained. Note that, $R(n-t-2)$ is attained at two points, namely, at $K = n-2t-4, n-2t-3$.

All these complete the proof.

The above analyses show that, for the new version of the Reve's puzzle with single relaxation (or, "cheat") of the "divine rule", the optimal value function $S(n)$ can be expressed in terms of $R(n)$ only. Note that, of the four schemes, only Scheme 3 makes use of Lemma 2. Also, note that, in Scheme 3, after moving the tower $T$ of $k$ discs (from $S$) to $P_1$ and the tower of next $n-k-3$ largest discs (from $S$) to $P_2$, there are two possibilities: Form the tower of discs $d_{n-1}$ and $d_{n-2}$ either on the peg $P_1$ or on the peg $P_2$ to free the largest disc $d_n$ on $S$. The analyses show further that, for $n \geq 9$, Scheme 4, which depends on $n$, is the only optimal scheme. It then follows that, for "sufficiently large" $n$, the Tower of Hanoi with single relaxation of the "divine rule" does not play any role in the Reve's puzzle variant of the problem, if the concern is in the number of moves only.

**Multiplicity of optimal strategies**

Recall that, if $n-3$ is a triangular number, $R(n-3)$ is attained at a unique point, otherwise, $R(n-3)$ is attained at exactly two points, so that, in this case, there are two optimal solutions of the problem. It is, therefore, an interesting problem to study the multiple optimal solutions. When $n = 4$, there are three optimal strategies, each requiring 7 moves to transfer the tower from the source peg $S$ to the destination peg $D$, of which one is mentioned in the proof of Theorem 1. For the second optimal strategy, the half-way solution is as follows: Move the discs $d_1$ and $d_2$, in this order, from the peg $S$ to the auxiliary peg $P_1$ (violating the "divine rule"), and then shift the disc $d_3$ (from $S$) to the peg $P_2$ to free the largest disc $d_4$ for transfer to $D$. The third optimal strategy is: Move the disc $d_1$ from $S$ to $P_1$, next, shift $d_2$ (from $S$) to $P_2$, finally, place the disc $d_3$ (on $S$) on top of $d_1$ on $P_1$ (violating the "divine rule") to free $d_4$. When $n = 5$, the number of moves required is 11, and the number of optimal strategies jumps to 18. The first optimal half-way strategy is: Move (from $S$) $d_1$ and $d_2$, in this order to $P_1$, violating the "divine rule", next, shift the tower of discs $d_3$ and $d_4$ (from $S$) to $P_2$ to free the largest disc $d_5$ for transfer to the destination peg $D$ in the next move. The second optimal strategy is: Move (from S) $d_1$ to $P_1$ and $d_2$ to $P_2$, next, place $d_3$ on top of $d_1$ on $P_1$, violating the "divine rule", next, move $d_4$ (from $S$) to $P_2$, and finally, move $d_2$ (from $D$) to $P_2$ on top of $d_4$, so that $D$ is free to receive $d_5$ in the next move. The third optimal strategy is: After moving (from $S$) $d_1$ to $P_1$ and $d_2$ to $D$, $d_3$ is put on top of $d_1$ on $P_1$, violating the "divine rule", next, $d_2$ is moved (from $D$) to $P_1$ on top of $d_3$, and finally, $d_4$ is moved (from $S$) to $P_2$ to free $d_5$ on $S$. The fourth optimal strategy is: Move (from $S$) $d_1$ to $P_1$, $d_2$ to $D$ and $d_3$ to $P_2$, next, $d_4$ is placed on top of $d_1$ on $P_1$, violating the "divine rule", and finally, $d_2$ is moved (from $D$) to $P_2$ on top of $d_3$, so that $d_5$ may be shifted to $D$ in the next move. The fifth optimal strategy is: Move (from $S$) $d_1$ to $P_1$, $d_2$ to $D$ and $d_3$ to $P_2$, next, $d_4$ is placed on top of $d_1$ on $P_1$ (violating the "divine rule"), and then $d_2$ (on $D$) is moved to $P_1$ on top of $d_4$. The sixth optimal strategy is: Move (from $S$) $d_1$ to $P_1$, $d_2$ to $P_2$ and $d_3$ to $D$, next, put $d_4$ on top of $d_1$ on $P_1$, violating the "divine rule", and then shift $d_3$ (from $D$) to $P_1$ on top of $d_4$ to free $D$. The seventh optimal strategy is: After moving $d_1$ to $D$, shift the discs $d_2$ and $d_3$, in this order, to $P_1$, violating the "divine rule", next, $d_4$ is shifted (from $S$) to $P_2$, and finally, $d_1$ is moved (from $D$) on top of $d_4$ on $P_2$. The eighth optimal strategy is : After moving $d_1$ to $D$ and $d_2$ and $d_3$, in this order to $P_1$ (thereby violating the "divine rule") and shifting $d_4$ to $P_2$, the disc $d_1$ (on $D$) is put on top of $d_3$ on $P_1$. The ninth optimal strategy is: Move (from $S$) $d_1$ to $D$, $d_2$ to $P_1$ and $d_3$ to $P_2$, next, put $d_4$ on top of $d_2$ on $P_1$, violating the "divine rule", and finally, move $d_1$ (from $D$) to $P_2$ on top of $d_3$ to free $D$ to receive $d_5$ in the next move. The tenth optimal strategy is: After moving $d_1$ to $D$, $d_2$ to $P_1$ and $d_3$ to $P_2$, $d_4$ is placed on top of $d_2$ on $P_1$ (violating the "divine rule"), next, $d_1$ is moved (from $D$) to $P_1$ on top of $d_4$ to free $D$. The eleventh optimal strategy is: Move $d_1$ to $D$, $d_2$ to $P_2$ and $d_3$ to $P_1$, next, put $d_4$ on top of $d_3$ on $P_1$, violating the "divine rule", and finally, shift $d_1$ (from $D$) to $P_1$ on top of $d_4$. The twelfth optimal strategy is: Move (from $S$) the tower of discs $d_1$ and $d_2$, next, put $d_3$ on top of this tower, violating the "divine rule", and

finally, move $d_4$ (from $S$) to $P_2$ to free $d_5$ on $S$. The thirteenth optimal strategy is: After moving (from $S$) the tower of discs $d_1$ and $d_2$ to $P_1$, and $d_3$ to $P_2$, put $d_4$ on $P_1$, on top of the tower of discs $d_1$ and $d_2$, violating the "divine rule", to free $d_5$ on $S$. The fourteenth optimal strategy is: Move the tower of discs $d_1$ and $d_2$ (from $S$) to $P_1$, next, shift the discs $d_3$ and $d_4$, in this order, from $S$ to $P_2$, violating the "divine rule", to free $d_5$. The fifteenth optimal strategy is: First, move (from $S$) $d_1$ to $D$, $d_2$ to $P_2$ and $d_3$ to $P_1$, next, put $d_1$ (on $D$) on top of $d_3$ on $P_1$, and finally, move $d_4$ (from $S$) to $P_1$ on top of the tower of discs $d_1$ and $d_3$, violating the "divine rule". The sixteenth optimal strategy is: Move (from $S$) $d_1$ to $P_1$, $d_2$ to $P_2$ and $d_3$ to $D$, next, put $d_4$ on top of $d_2$ on $P_2$, violating the "divine rule", and finally, move $d_3$ (from $D$) to $P_2$ on top of $d_4$ to free $D$ for $d_5$. The seventeenth optimal strategy is: Move (from $S$) $d_1$ to $P_1$, next, transfer the tower of discs $d_2$ and $d_3$ (from $S$) to $P_2$, and finally, put $d_4$ on top of this tower, violating the "divine rule", to free $d_5$ on $S$. The eighteenth optimal strategy is: Move (from $S$) $d_1$ to $P_1$, $d_2$ to $D$ and $d_3$ to $P_2$, next, place $d_4$ on top of $d_3$ on $P_2$ (violating the "divine rule"), and finally, move $d_2$ (from $D$) to $P_2$ on top of $d_4$ to free the peg $D$. When $n = 6$, there are as many as 40 optimal strategies, each requiring 15 moves. The first optimal half-way solution is: Move the tower of discs $d_1$ and $d_2$ (from $S$) to $P_1$, next, put $d_3$ on top of this tower (violating the "divine rule"), and finally, move the tower of discs $d_4$ and $d_5$ (from $S$) to $P_2$ to free the largest disc $d_6$ for transfer to the peg $D$. The second optimal strategy is: After moving the tower of discs $d_1$ and $d_2$ (from $S$) to $P_1$, place $d_3$ on $D$ and $d_4$ on $P_1$ on top of the tower of two discs, violating the "divine rule", next, move $d_5$ (from $S$) to $P_2$, and finally, shift $d_3$ (from $D$) to $P_2$ on top of $d_5$ so that $d_6$ may be shifted to $D$ in the next move. The third optimal strategy is: After moving (from $S$) the tower of discs $d_1$ and $d_2$ to $P_1$, and the tower of discs $d_3$ and $d_4$ to $P_2$, $d_5$ is placed on top of the tower of discs $d_1$ and $d_2$ on $P_1$ (violating the "divine rule) to free $d_6$ for transfer to $D$. The fourth optimal strategy is: Move the tower of discs $d_1$, $d_2$ and $d_3$ (from $S$) to $P_1$, next, put $d_4$ on top of this tower (violating the "divine rule"), and finally, shift $d_5$ (from $S$) to $P_2$ to free $d_6$ on $S$. If, after moving (from $S$) the tower of discs $d_1$, $d_2$ and $d_3$ to $P_1$, and $d_4$ to $P_2$, $d_5$ is put on top of the tower of three discs on $P_1$ (violating the "divine rule"), the fifth optimal solution is found. Again, if after moving the tower of discs $d_1$, $d_2$ and $d_3$ (from $S$) to $P_1$, the discs $d_4$ and $d_5$ are placed, in this order, on $P_2$ (violating the "divine rule"), the sixth optimal strategy is obtained. The seventh optimal strategy is: Move (from $S$) $d_1$ to $P_1$ and $d_2$ to $D$, next, put $d_3$ on top of $d_1$ on $P_1$, violating the "divine rule", then, shift $d_2$ (from $D$) on top of $d_3$ on $P_1$, and finally, move the tower of discs $d_4$ and $d_5$ (from $S$) to $P_2$, to free $d_6$ on $S$. The eighth optimal strategy is: After moving (from $S$) the tower of discs $d_1$ and $d_2$ to $P_1$ and $d_3$ to $D$, shift $d_4$ to $P_1$ on top of the tower of two discs (violating the "divine rule"), next, move $d_3$ (from $D$) to $P_1$ on top of $d_4$, and finally, put $d_5$ on $P_2$ to free $d_6$. The ninth optimal strategy is: Move (from $S$) $d_1$ to $P_1$, and the tower of discs $d_2$ and $d_3$ to $P_2$, next, move (from $S$) $d_4$ to $D$ and $d_5$ to $P_2$ on top of the tower of two discs (violating the "divine rule"), and finally, move $d_4$ (from $D$) to $P_2$ on top of $d_5$ to free $D$. The tenth optimal strategy is: After moving (from $S$) $d_1$ from $S$ to $P_1$, and the tower of discs $d_2$ and $d_3$ to $P_2$, shift (from $S$) $d_4$ to $D$ and $d_5$ to $P_1$ on top of $d_1$, violating the "divine rule", and finally, move $d_4$ from $D$ to $P_1$ on top of $d_5$ to free $D$. The eleventh optimal strategy is: Move (from $S$) the tower of discs $d_1$ and $d_2$ to $P_1$, $d_3$ to $P_2$ and $d_4$ to $D$, next, put $d_5$ on top of $d_3$ on $P_2$ (violating the "divine rule"), and finally, shift $d_4$ (from $D$) to $P_2$ on top of $d_5$ so that, in the next move, $d_6$ may be shifted to $D$. The twelfth optimal strategy is: Move (from $S$) the tower of discs $d_1$ and $d_2$ to $P_1$, $d_3$ to $P_2$ and $d_4$ to $D$, next, place $d_5$ on $P_1$ (on top of the tower of two discs, violating the "divine rule"), and finally, move $d_4$ (from $D$) to $P_1$ on top of $d_5$ to free $D$ to receive $d_6$ in the next move. The thirteenth optimal strategy is: Move $d_1$ to $P_1$, $d_2$ to $D$ and $d_3$ to $P_2$, next, put $d_4$ on top of $d_1$ on $P_1$ (violating the "divine rule"), then, move $d_3$ (from $P_2$) to $P_1$ on top

of $d_4$, next, move $d_2$ (from $D$) to $P_1$ on top of $d_3$, and finally, place $d_5$ on $P_2$ to free $d_6$. The fourteenth optimal strategy is: After moving (from $S$) $d_1$ to $P_1$, $d_2$ to $D$, $d_3$ to $P_2$, place $d_4$ on top of $d_1$ on $P_1$ (violating the "divine rule"), then, shift $d_3$ (on $P_2$) to $P_1$ on top of $d_4$, next, move $d_5$ (from $S$) to $P_2$, and finally, shift $d_2$ (on $D$) to $P_2$ on top of $d_5$ to free $D$. The fifteenth optimal strategy is: Move (from $S$) $d_1$ to $P_1$, $d_2$ to $P_2$ and $d_3$ to $D$, next, put $d_4$ on top of $d_1$ on $P_1$, violating the "divine rule", then, move $d_2$ (from $P_2$) to $P_1$ on top of $d_4$, next, place $d_5$ on $P_2$, and finally, move $d_3$ (from $D$) to $P_2$ on top of $d_5$ to free $D$. The sixteenth optimal strategy is: Move (from $S$) $d_1$ to $D$, $d_2$ to $P_1$ and $d_3$ to $P_2$, next, put $d_4$ on top of $d_2$ on $P_1$, violating the "divine rule", then, move $d_3$ (from $P_2$) to $P_1$ on top of $d_4$ and $d_1$ (from $D$) to $P_1$ on top of $d_3$, and finally, shift $d_5$ (from $S$) to $P_2$ to free $d_6$. The seventeenth optimal strategy is: After moving (from $S$) $d_1$ to $D$, $d_2$ to $P_1$, $d_3$ to $P_2$, and $d_4$ on top of $d_2$ on $P_1$ (violating the "divine rule"), put $d_3$ (on $P_2$) on top of $d_4$ on $P_1$, next, move $d_5$ (from $S$) to $P_2$, and finally, shift $d_1$ (from $D$) to $P_2$ on top of $d_5$ to free $D$. The eighteenth optimal strategy is: After moving (from $S$) $d_1$ to $P_2$, $d_2$ to $P_1$ and $d_3$ to $D$, put $d_4$ on top of $d_2$ on $P_1$ (violating the "divine rule"), next, put $d_1$ (on $P_2$) on top of $d_4$ on $P_1$, then, move $d_5$ (from $S$) to $P_2$, and finally, shift $d_3$ (from $D$) to $P_2$ on top of $d_5$ to free $D$. The nineteenth optimal strategy is: Move (from $S$) $d_1$ to $D$, $d_2$ to $P_2$ and $d_3$ to $P_1$, next, put $d_4$ on top of $d_3$ on $P_1$, violating the "divine rule", then, move $d_2$ (from $P_2$) to $P_1$ on top of $d_4$ and $d_1$ (from $D$) to $P_1$ on top of $d_2$, and finally, shift $d_5$ (from $S$) to $P_2$ to free $d_6$. The twentieth optimal strategy is: After moving (from $S$) $d_1$ to $D$, $d_2$ to $P_2$, $d_3$ to $P_1$ and $d_4$ on top of $d_3$ on $P_1$, (violating the "divine rule"), put $d_2$ (on $P_2$) on top of $d_4$ on $P_1$, and $d_5$ (on $S$) to $P_2$, and finally, shift $d_1$ (from $D$) to $P_2$ on top of $d_5$ to free $d_6$. The twenty-first optimal strategy is: Move (from $S$) $d_1$ to $P_2$, $d_2$ to $D$ and $d_3$ to $P_1$, next, put $d_4$ on top of $d_3$ on $P_1$, violating the "divine rule", then, move $d_1$ (from $P_2$) to $P_1$ on top of $d_4$, after shifting $d_5$ (from $S$) to $P_2$, place $d_2$ (on $D$) on top of $d_5$ on $P_2$ to free $D$. The twenty-second optimal strategy is: Move (from $S$) the tower of discs $d_1$ and $d_2$ to $P_1$, $d_3$ to $D$ and $d_4$ to $P_2$, next, put $d_5$ on top of the tower of two discs on $P_1$, violating the "divine rule", and then move $d_3$ (from $D$) to $P_1$, on top of $d_5$ to free $D$. The twenty-third optimal strategy is: After moving (from $S$) the tower of discs $d_1$ and $d_2$ to $P_1$, and the tower of discs $d_3$ and $d_4$ to $P_2$, $d_5$ is placed on top of the latter tower, violating the "divine rule", to free $d_6$. The twenty-fourth optimal strategy is: Move (from $S$) the tower of discs $d_1$ and $d_2$ to $P_1$, $d_3$ to $D$ and $d_4$ to $P_2$, next, place $d_5$ on top of $d_4$ on $P_2$, violating the "divine rule", and finally, put $d_3$ (on $D$) on top of $d_5$ on $P_2$ to free $D$. The twenty-fifth optimal strategy is: Move (from $S$) $d_1$ to $P_2$, $d_2$ to $D$ and $d_3$ to $P_1$, next, put $d_1$ on top of $d_3$ on $P_1$, then put $d_4$ on top of $d_1$ on $P_1$, violating the "divine rule", next, move $d_5$ (from $S$) to $P_2$, and finally, put $d_2$ (on $D$) on top of $d_5$ on $P_2$ to free $D$. The twenty-sixth optimal strategy is: After moving (from $S$) $d_1$ to $P_2$, $d_2$ to $D$ and $d_3$ to $P_1$, put $d_1$ (on $P_2$) on top of $d_3$ on $P_1$, next, move $d_4$ to $P_1$ on top of $d_1$ (violating the "divine rule"), then, move $d_2$ (from $D$) to $P_1$ on top of $d_4$, and finally, shift $d_5$ (from $S$) to $P_2$, so that, in the next move, $d_6$ may be transferred from $S$ to $D$. The twenty-seventh optimal strategy is: After moving (from $S$) $d_1$ to $P_2$, $d_2$ to $D$ and $d_3$ to $P_1$, put $d_1$ (on $P_2$) on top of $d_3$ on $P_1$, next, move $d_4$ (from $S$) to $P_2$, and $d_5$ to $P_1$ on top of $d_1$, violating the "divine rule", and finally, put $d_2$ (on $D$) on top of $d_4$ on $P_2$ to free $D$. The twenty-eighth optimal strategy is: After moving (from $S$) $d_1$ to $P_2$, $d_2$ to $D$ and $d_3$ to $P_1$, put $d_1$ (on $P_2$) on top of $d_3$ on $P_1$, next, move (from $S$) $d_4$ to $P_2$ and $d_5$ to $P_1$ on top of $d_1$, violating the "divine rule", and finally, put $d_2$ (on $D$) on top of $d_4$ on $P_2$ to free $D$. The twenty-ninth optimal strategy is: Move (from $S$) $d_1$ to $P_2$, $d_2$ to $D$ and $d_3$ to $P_1$, then put $d_1$ on top of $d_3$ on $P_1$, next, move $d_4$ and $d_5$, in this order, to $P_2$ (violating the "divine rule"), and finally, move $d_2$ (from $D$) to $P_2$ on top of $d_5$ to free $D$. If, after moving (from $S$) $d_1$ to $P_2$, $d_2$ to $D$ and $d_3$ to $P_1$, and putting $d_1$ on top of $d_3$ on $P_1$, $d_4$ is moved to $P_2$, then $d_2$ is shifted (from $D$) to $P_2$ on top of $d_4$, and finally, $d_5$ is put on top of $d_2$ on $P_2$ (violating the "divine rule"), the thirtieth optimal

strategy is obtained. Again, if after moving (from $S$) $d_1$ to $D$, $d_2$ to $P_2$ and $d_3$ to $P_1$, and putting $d_1$ on top of $d_3$ on $P_1$, $d_4$ is first moved to $D$, and after moving $d_5$ to $P_2$ on top of $d_2$ (violating the "divine rule"), $d_4$ is moved (from $D$) to $P_2$ on top of $d_5$, the thirty-first optimal strategy is obtained. The thirty-second optimal strategy is: Move (from $S$) $d_1$ to $D$ and the tower of discs $d_2$ and $d_3$ to $P_1$, next, move (from $S$) $d_4$ to $P_1$ on top of this tower (violating the "divine rule") and $d_5$ to $P_2$, and finally, move $d_1$ (from $D$) to $P_2$ on top of $d_5$ to free $D$. If, after moving (from $S$) $d_1$ to $D$ and the tower of discs $d_2$ and $d_3$ to $P_1$, $d_4$ is put on this tower (violating the "divine rule"), and $d_5$ is shifted to $P_2$, and finally, $d_1$ is moved (from $D$) to $P_1$ on top of $d_4$, the thirty-third optimal strategy is obtained. The thirty-fourth optimal strategy is: Move (from $S$) $d_1$ to $D$ and the tower of discs $d_2$ and $d_3$ to $P_1$, next, move (from $S$) $d_4$ to $P_2$ and $d_5$ to $P_1$ on top of the tower (violating the "divine rule"), and finally, move $d_1$ (from $D$) to $P_2$ on top of $d_4$ to free $D$. If, after moving (from $S$) $d_1$ to $D$ and the tower of discs $d_2$ and $d_3$ to $P_1$, $d_4$ is moved to $P_2$ and $d_5$ is shifted to $P_1$ on top of the tower (violating the "divine rule"), and finally, $d_1$ is moved (from $D$) to $P_1$ on top of $d_5$, the thirty-fifth optimal strategy is obtained. The thirty-sixth optimal strategy is: Move (from $S$) $d_1$ to $D$ and the tower of discs $d_2$ and $d_3$ to $P_1$, next, move (from $S$) $d_4$ and $d_5$, in this order, to $P_2$ (violating the "divine rule"), and finally, move $d_1$ (from $D$) to $P_2$ on top of $d_5$ to free $D$ to receive $d_6$ in the next move. The thirty-seventh optimal strategy is: After moving (from $S$) $d_1$ to $D$ and the tower of discs $d_2$ and $d_3$ to $P_1$, $d_4$ is put on $P_2$, and after placing $d_1$ (on $D$) on top of $d_4$ on $P_2$, $d_5$ is placed on top of $d_1$ on $P_2$, violating the "divine rule". The thirty-eighth optimal strategy is: Move (from $S$) $d_1$ to $D$, $d_2$ to $P_1$ and $d_3$ to $P_2$, next, shift $d_1$ (from $D$) to $P_2$ on top of $d_3$, then move (from $S$) $d_4$ to $D$ and $d_5$ to $P_2$ on top of $d_1$ (violating the "divine rule"), and finally, move $d_4$ (from $D$) to $P_2$ on top of $d_5$ to free $D$. The thirty-ninth optimal strategy is: Move (from $S$) $d_1$ to $P_2$ and the tower of discs $d_2$ and $d_3$ to $P_1$, next, put $d_4$ on $D$, and after placing $d_5$ on top of $d_1$ on $P_2$ (violating the "divine rule"), put $d_4$ (on $D$) on top of $d_5$ on $P_2$. The fortieth optimal strategy is: Move (from $S$) $d_1$ to $D$, and $d_2$ and $d_3$, in this order, to $P_1$, violating the "divine rule", next, shift (from $D$) $d_1$ on top of $d_3$ on $P_1$, and finally, move the tower of discs $d_4$ and $d_5$ (from $S$) to $P_2$ to free $d_6$ on $S$. When $n = 7$, there are as many as 30 optimal strategies, each requiring 19 moves. The first optimal half-way strategy is: Transfer the tower of discs $d_1$, $d_2$ and $d_3$ (from $S$) to $P_1$, next, put $d_4$ on top of this tower (violating the "divine rule"), and finally, move the tower of discs $d_5$ and $d_6$ (from $S$) to $P_2$ to free the largest disc $d_7$. The second optimal strategy is: After transferring the tower of discs $d_1$, $d_2$ and $d_3$ (from $S$) to $P_1$, move $d_4$ to $D$ and $d_5$ to $P_1$ on top of the tower of three discs (violating the "divine rule"), next, move $d_6$ (from $S$) to $P_2$ and then shift $d_4$ (from $D$) to $P_2$ on top of $d_6$, so that, in the next move, the largest disc $d_7$ may be shifted to $D$. If, after shifting the tower of discs $d_1$, $d_2$ and $d_3$ (from $S$) to $P_1$, the tower of discs $d_4$ and $d_5$ is formed on $P_2$, and finally, $d_6$ is put on $P_1$ on top of the tower (violating the "divine rule"), the third optimal strategy is found. Again, if after forming the tower of discs $d_1$, $d_2$ and $d_3$ on $P_1$, and the tower of discs $d_4$ and $d_5$ on $P_2$, the discs $d_6$ is put on $P_2$ on top of the tower of two discs, the fourth optimal strategy is obtained. The fifth optimal strategy is: Move (from $S$) the tower of discs $d_1$, $d_2$ and $d_3$ to $P_1$, $d_4$ to $D$ and $d_5$ to $P_2$, next, put $d_6$ on top of $d_5$ on $P_2$, violating the "divine rule", and finally, shift $d_4$ (from $D$) to $P_2$ on top of $d_6$ to free $d_7$. The sixth optimal strategy is: Move (from $S$) the tower of discs $d_1$ and $d_2$ to $P_1$ and $d_3$ to $P_2$, next, put $d_4$ on top of the tower of two discs on $P_1$, violating the "divine rule", then, move $d_3$ (from $P_2$) on top of $d_4$ on $P_1$, and finally, shift the tower of discs $d_5$ and $d_6$ (from $S$) to $P_2$ to free $d_7$. The seventh optimal strategy is: Transfer (from $S$) the tower of discs $d_1$, $d_2$ and $d_3$ to $P_1$ and $d_4$ to $P_2$, then, after placing $d_5$ on $P_1$ on top of the tower of three discs (violating the "divine rule"), $d_4$ is put on $d_5$, and finally, $d_6$ is moved (from $S$) to $P_2$ to free $d_7$. The eighth optimal strategy is: Move (from $S$) the tower of discs $d_1$ and $d_2$ to $P_1$, and the tower of discs $d_3$ and $d_4$ to $P_2$, next,

move (from *S*) $d_5$ to *D* and $d_6$ to $P_2$ (on top of the tower of two discs, violating the "divine rule"), and finally, put $d_5$ (on *D*) on top of $d_6$ on $P_2$. If, after moving (from *S*) the tower of discs $d_1$ and $d_2$ to $P_1$, and the tower of discs $d_3$ and $d_4$ to $P_2$, the tower of discs $d_5$ and $d_6$ is formed on $P_1$ (violating the "divine rule"), the ninth optimal strategy is found. The tenth optimal strategy is as follows: Move (from *S*) the tower of discs $d_1$, $d_2$ and $d_3$ to $P_1$, $d_4$ to $P_2$ and $d_5$ to *D*, then, after placing $d_6$ on top of $d_4$ on $P_2$ (violating the "divine rule"), put $d_5$ on top of $d_6$, so that *D* is ready to accept $d_7$ in the next move. If, after moving (from *S*) the tower of discs $d_1$, $d_2$ and $d_3$ to $P_1$, $d_4$ to $P_2$ and $d_5$ to *D*, the disc $d_6$ (on *S*) is placed on $P_1$ on top of the tower (violating the "divine rule"), and then, $d_5$ is put on $d_6$ on $P_1$, the eleventh optimal strategy is found. The twelfth optimal strategy is: Move (from *S*) $d_1$ to $P_1$, $d_2$ to *D* and $d_3$ to $P_2$, next, shift $d_4$ (from *S*) to $P_1$ on top of $d_1$ (violating the "divine rule"), then put $d_3$ (on $P_2$) on top of $d_4$ on $P_1$ and $d_2$ (on *D*) on top of $d_3$ on $P_1$, and finally, move the tower of discs $d_5$ and $d_6$ to $P_2$ to free $d_7$. The thirteenth optimal strategy is: Move (from *S*) the tower of discs $d_1$ and $d_2$ to $P_1$, $d_3$ to *D* and $d_4$ to $P_2$, next, place $d_5$ (on *S*) on $P_1$ on top of the tower of two discs, violating the "divine rule", then, move $d_4$ (from $P_2$) on top of $d_5$ on $P_1$ and $d_3$ (on *D*) on top of $d_4$ on $P_1$, finally, move $d_6$ (from *S*) to $P_2$ to free $d_7$ on *S*. The fourteenth optimal strategy is: Move (from *S*) the tower of discs $d_1$, $d_2$ and $d_3$ to $P_1$, $d_4$ to *D* and $d_5$ to $P_2$, next, put $d_6$ on top of the tower on $P_1$, violating the "divine rule", then, move $d_4$ (on *D*) on top of $d_6$ on $P_1$ to free *D* to receive $d_7$ in the next move. The fifteenth optimal strategy is: Move (from *S*) the tower of discs $d_1$ and $d_2$ to $P_1$, $d_3$ to $P_2$ and $d_4$ to *D*, next, place $d_5$ (on *S*) on $P_1$ on top of the tower, violating the "divine rule", then, move $d_3$ (on $P_2$) on top of $d_5$ on $P_1$, now, shift $d_6$ (on *S*) to $P_2$, and finally, move $d_4$ (from *D*) to $P_2$ on top of $d_6$ to free *D*. The sixteenth optimal strategy is: After moving (from *S*) the tower of discs $d_1$ and $d_2$ to $P_1$, $d_3$ to *D* and $d_4$ to $P_2$, place $d_5$ (on *S*) on $P_1$ on top of the tower, violating the "divine rule", then, move $d_4$ (from $P_2$) on top of $d_5$ on $P_1$, next, shift $d_6$ (on *S*) on $P_2$, and finally, move $d_3$ (from *D*) to $P_2$ on top of $d_6$ to free *D*. The seventeenth optimal strategy is: Move (from *S*) $d_1$ to *D*, $d_2$ to $P_2$ and $d_3$ to $P_1$, next, place $d_1$ (on *D*) on top of $d_3$ on $P_1$, then put $d_4$ on top of $d_1$ on $P_1$, violating the "divine rule", now, place $d_2$ (on $P_2$) on top of $d_4$ on $P_1$, and finally, move the tower of discs $d_5$ and $d_6$ (from *S*) to $P_2$ to free $d_7$. The eighteenth optimal strategy is: After moving (from *S*) $d_1$ to *D*, $d_2$ to $P_2$ and $d_3$ to $P_1$, put $d_1$ (on *D*) on top of $d_3$ on $P_1$, next, put $d_4$ on *D* and $d_5$ on top of $d_1$ on $P_1$, violating the "divine rule", now, place $d_2$ (on $P_2$) on top of $d_5$ on $P_1$, and $d_6$ (on *S*) on $P_2$, and finally, move $d_4$ (on *D*) to $P_2$ on top of $d_6$ to free *D*. The nineteenth optimal strategy is: Move (from *S*) $d_1$ to $P_2$, $d_2$ to *D* and $d_3$ to $P_1$, next, put $d_1$ on top of $d_3$ on $P_1$, then shift (from *S*) $d_4$ to $P_2$, and $d_5$ on top of $d_1$ on $P_1$, violating the "divine rule", now, place $d_4$ (on $P_2$) on top of $d_5$ on $P_1$, next, shift $d_6$ to $P_2$, and finally, move $d_2$ (on *D*) to $P_2$ on top of $d_6$ to free *D*. The twentieth optimal strategy is: After moving (from *S*) $d_1$ to $P_2$, $d_2$ to *D* and $d_3$ to $P_1$, put $d_1$ on top of $d_3$ on $P_1$, and then shift (from *S*) $d_4$ to $P_2$, and $d_5$ on top of $d_1$ on $P_1$, violating the "divine rule", now, place $d_4$ (on $P_2$) on top of $d_5$ on $P_1$, and $d_2$ on top of $d_4$ on $P_1$, and finally, move $d_6$ (on *S*) to $P_2$ to free $d_7$. The twenty-first optimal strategy is: After moving (from *S*) $d_1$ to $P_2$, $d_2$ to *D* and $d_3$ to $P_1$, put $d_1$ on top of $d_3$ on $P_1$, and $d_4$ on $P_2$, next, put $d_2$ (on *D*) on top of $d_4$ on $P_2$, and $d_5$ (on *S*) on *D*, now, place $d_6$ (on *S*) on top of $d_1$ on $P_1$, violating the "divine rule", and finally, move $d_5$ (from *D*) to $P_1$ on top of $d_6$ to free *D*. The twenty-second optimal strategy is: After moving (from *S*) $d_1$ to $P_2$, $d_2$ to *D* and $d_3$ to $P_1$, put $d_1$ on top of $d_3$ on $P_1$, and $d_4$ on $P_2$, next, put $d_2$ (on *D*) on top of $d_4$ on $P_2$, now, shift (from *S*) $d_5$ to *D* and $d_6$ to $P_2$ on top of $d_2$, violating the "divine rule", and finally, move $d_5$ (on *D*) to $P_2$ on top of $d_6$ to free *D*. The twenty-third optimal strategy is: Move (from *S*) $d_1$ to $P_2$, $d_2$ to *D* and $d_3$ to $P_1$, next, place $d_2$ (on *D*) on top of $d_3$ on $P_1$, then put $d_4$ on top of $d_2$ on $P_1$, violating the "divine rule", now, place $d_1$ (on $P_2$) on top of $d_4$ on $P_1$, and finally, move the tower of discs $d_5$ and $d_6$ (from *S*) to

$P_2$ to free $d_7$. The twenty- fourth optimal strategy is: After moving (from $S$) $d_1$ to $P_2$, $d_2$ to $D$ and $d_3$ to $P_1$, put $d_2$ (on $D$) on top of $d_3$ on $P_1$, then shift (from $S$) $d_4$ to $D$ and $d_5$ on top of $d_2$ on $P_1$, violating the "divine rule", now, place $d_1$ (on $P_2$) on top of $d_5$ on $P_1$, next, put $d_6$ on $P_2$, and finally, move $d_4$ (on $D$) on top of $d_6$ on $P_2$ to free $D$. The twenty-fifth optimal strategy is: After moving (from $S$) $d_1$ to $D$, $d_2$ to $P_2$ and $d_3$ to $P_1$, put $d_2$ (on $P_2$) on top of $d_3$ on $P_1$, next, shift (from $S$) $d_4$ to $P_2$ and $d_5$ on top of $d_2$ on $P_1$, violating the "divine rule", now, place $d_4$ (on $P_2$) on top of $d_5$ on $P_1$, then put $d_6$ on $P_2$, and finally, move $d_1$ (on $D$) on top of $d_6$ on $P_2$ to free $D$. The twenty-sixth optimal strategy is: After moving (from $S$) $d_1$ to $D$, $d_2$ to $P_2$ and $d_3$ to $P_1$, put $d_2$ (on $P_2$) on top of $d_3$ on $P_1$, then, shift (from $S$) $d_4$ to $P_2$ and $d_5$ on top of $d_2$ on $P_1$, violating the "divine rule", next, place $d_4$ (on $P_2$) on top of $d_5$ on $P_1$, and $d_1$ (on $D$) on top of $d_4$ on $P_1$, and finally, move $d_6$ (from $S$) to $P_2$ to free $d_7$. The twenty- seventh optimal strategy is: After moving (from $S$) $d_1$ to $D$, $d_2$ to $P_2$ and $d_3$ to $P_1$, put $d_2$ (on $P_2$) on top of $d_3$ on $P_1$, next, shift $d_4$ to $P_2$ and place $d_1$ (on $D$) on top of $d_4$ on $P_2$, now, shift (from $S$) $d_5$ to $D$ and $d_6$ on top of $d_2$ on $P_1$, violating the "divine rule", now, place $d_1$ (on $P_2$) on top of $d_5$ on $P_1$, and finally, move $d_5$ (on $D$) on top of $d_6$ on $P_1$ to free $D$. The twenty-eighth optimal strategy is: After moving (from $S$) $d_1$ to $D$, $d_2$ to $P_2$ and $d_3$ to $P_1$, put $d_2$ (on $P_2$) on top of $d_3$ on $P_1$, next, shift $d_4$ to $P_2$ and on $d_4$ put $d_1$ (from $D$), now, shift (from $S$) $d_5$ to $D$ and $d_6$ on top of $d_1$ on $P_2$, violating the "divine rule", and finally, move $d_5$ (on $D$) on top of $d_6$ on $P_2$ to free $D$. The twenty-ninth optimal strategy is: Move (from $S$) $d_1$ to $D$, $d_2$ to $P_1$, $d_3$ to $P_2$ and $d_4$ on top of $d_2$ on $P_1$, violating the "divine rule", next, put $d_3$ (on $P_2$) on top of $d_4$ on $P_1$, and $d_1$ (on $D$) on top of $d_3$ on $P_1$, and finally, shift (from $S$) the tower of discs $d_5$ and $d_6$ on $P_2$ to free $d_7$. The thirtieth optimal strategy is: Move (from $S$) $d_1$ to $D$, $d_2$ to $P_2$, $d_3$ to $P_1$, and $d_4$ on top of $d_3$ on $P_1$, violating the "divine rule", next, shift $d_2$ (on $P_2$) on top of $d_4$ on $P_1$, and $d_1$ (on $D$) on top of $d_2$ on $P_1$, now, shift (from $S$) the tower of discs $d_5$ and $d_6$ to $P_2$ to free $d_7$. When $n$ = 8, there are nine optimal strategies, each requiring 23 moves. The first optimal half-way solution is: Move (from $S$) the tower of discs $d_1$, $d_2$ and $d_3$ to $P_1$, and $d_4$ to $D$, next, shift $d_5$ (on $S$) to $P_1$ on top of the tower of three discs, violating the "divine rule", then, shift $d_4$ (on $D$) to $P_1$ on top of $d_5$, and finally, move the tower of discs $d_6$ and $d_7$ from $S$ to $P_2$ to free the largest disc $d_8$ on $S$. The second optimal strategy is: Move (from $S$) the tower of discs $d_1$, $d_2$ and $d_3$ to $P_1$, and the tower of discs $d_4$ and $d_5$ to $P_2$, next, shift (from $S$) $d_6$ to $D$ and $d_7$ on top of the tower of discs $d_4$ and $d_5$ on $P_2$, violating the "divine rule", and finally, move $d_6$ (on $D$) on top of $d_7$ on $P_2$, so that $d_8$ may now be shifted to $D$. The third optimal strategy is: Move (from $S$) the tower of discs $d_1$, $d_2$ and $d_3$ to $P_1$, and the tower of discs $d_4$ and $d_5$ to $P_2$, next, shift (from $S$) $d_6$ to $D$ and $d_7$ to $P_1$, on top of the tower of three discs, violating the "divine rule", and finally, put $d_6$ (on $D$) on top of $d_7$ on $P_1$ to free $D$. The fourth optimal strategy is: Move (from $S$) the tower of discs $d_1$ and $d_2$ to $P_1$, $d_3$ to $D$ and $d_4$ to $P_2$, next, put $d_5$ (on $S$) on top of the tower of three discs on $P_1$, violating the "divine rule", then, move $d_4$ (on $P_2$) and $d_3$ (on $D$), in this order, to $P_1$ to form the tower of discs $d_3$, $d_4$ and $d_5$, and finally, move the tower of discs $d_6$ and $d_7$ to $P_2$ to free $d_8$. The fifth optimal strategy is: Transfer (from $S$) the tower of discs $d_1$, $d_2$ and $d_3$ to $P_1$, $d_4$ to $D$ and $d_5$ to $P_2$, next, put $d_6$ (on $S$) on top of the tower of three discs on $P_1$, violating the "divine rule", then, move $d_5$ (on $P_2$) and $d_4$ (on $D$), in this order, to $P_1$ to form the tower of discs $d_4$, $d_5$ and $d_6$, and finally, move $d_7$ (from $S$) to $P_2$ to free $d_8$. The sixth optimal strategy is: Move (from $S$) the tower of discs $d_1$, $d_2$ and $d_3$ to $P_1$, $d_4$ to $D$ and $d_5$ to $P_2$, next, put $d_6$ (on $S$) on top of the tower of three discs on $P_1$, violating the "divine rule", now, place $d_5$ (on $P_2$) on top of $d_6$ on $P_1$, then, shift (from $S$) $d_7$ to $P_2$, and finally, move $d_4$ (on $D$) on top of $d_7$ on $P_2$ to free $D$. The seventh optimal strategy is: Move (from $S$) the tower of discs $d_1$, $d_2$ and $d_3$ to $P_1$, $d_4$ to $P_2$ and $d_5$ to $D$, next place $d_6$ (on $S$) on top of the tower of three discs on $P_1$, violating the "divine rule", then, move $d_4$ (from $P_2$) to $P_1$ on top of $d_6$, now, shift (from $S$) $d_7$ to $P_2$, and

finally, move $d_5$ (from $D$) to $P_2$ on top of $d_7$ to free $D$. The eighth optimal strategy is: Move (from $S$) $d_1$ to $D$, $d_2$ to $P_2$, $d_3$ to $P_1$, and then put $d_2$ (on $P_2$) on top of $d_3$ on $P_1$, next, shift (from $S$) $d_4$ to $P_2$ and $d_5$ to $P_1$ on top of $d_2$, violating the "divine rule", now, move $d_4$ (on $P_2$) and $d_1$ (on $D$), in this order, to $P_1$ on top of $d_5$, and finally, move (from $S$) the tower of discs $d_6$ and $d_7$ to $P_2$ to free $d_8$ on $S$. The ninth optimal strategy is: Move (from $S$) $d_1$ to $P_2$, $d_2$ to $D$, $d_3$ to $P_1$, and then put $d_1$ (on $P_2$) on top of $d_3$ on $P_1$, next, shift (from $S$) $d_4$ to $P_2$ and $d_5$ to $P_1$ on top of $d_1$, violating the "divine rule", now, move $d_4$ (on $P_2$) and $d_2$ (on $D$), in this order, to $P_1$ on top of $d_5$, and finally, shift (from $S$) the tower of discs $d_6$ and $d_7$ to $P_2$ to free $d_8$ on $S$ to move next. There is a unique optimal strategy, namely, Scheme 4 (with $k = 3$), when $n = 9$.

So far, the focus has been on the multiple optimal strategies when $4 \le n \le 8$. In this connection, the following result may be established.

***Lemma* 3:** $S(n, t) = S(n, t+1)$ if and only if $t = 1$, $10 \le n \le 13$.

***Proof*:** First note that

$$S(n, t) = S(n, t+1)$$

if and only if

$$R(n-t-2) - R(n-t-3) = 2^{t+1} + 2[R(t+1) - R(t)].$$

Now, $R(n-t-2) - R(n-t-3) = 2^{t+2}$ if and only if $t = 1$ (by Corollary 4). In this case, by part (2) of Lemma 1,

$$\frac{(t+2)(t+3)}{2} < n - t - 3 < \frac{(t+3)(t+4)}{2}$$

so that

$$\frac{(t+3)(t+4)}{2} \le n < \frac{(t+3)(t+6)}{2}.$$

Putting $t = 1$, the desired result is obtained.

Applying Lemma 3, three optimal solutions are obtained when $n = 10$, when $n = 11$, there are four optimal solutions, when $n = 12$, there are four optimal solutions, while three optimal solutions are obtained when $n = 13$.

**Table 1. $R(n)$ and $S(n)$ for $4 \le n \le 8$.**

| $n$ | 4 | 5 | 6 | 7 | 8 |
|---|---|---|---|---|---|
| $R(n)$ | 9(3) | 13(18) | 17(40) | 25(30) | 33(9) |
| $S(n)$ | 7 | 11 | 15 | 19 | 23 |

In Table 1 above, the number within parentheses gives the number of optimal strategies. Thus, for example, when $n = 4$, the number of moves required is $R(4) = 9$, and there are three optimal strategies each requiring 9 moves. Table 2 gives the values of $R(n)$ and $S(n)$ for $9 \le n \le 19$.

**Table 2. $R(n)$ and $S(n)$ for $9 \le n \le 19$.**

| $n$ | $R(n)$ | $S(n)$ |
|---|---|---|
| 9 | 41 | 27 |
| 10 | 49 | 35 |
| 11 | 65 | 43 |
| 12 | 81 | 51 |
| 13 | 97 | 59 |
| 14 | 113 | 75 |
| 15 | 129 | 79 |
| 16 | 161 | 95 |
| 17 | 193 | 111 |
| 18 | 225 | 127 |
| 19 | 257 | 143 |

## Generalizations

An immediate generalization of the present problem is the Reve's puzzle with (at most) $c$ ($\ge 2$) relaxations (or, "cheat") of the "divine rule". Let $S(n, c)$ be the minimum number of moves required to solve the Reve's puzzle with $n$ ($\ge 1$) discs when (at most) $c$ relaxations of the "divine rule" are allowed. Then, we can prove the following result.

***Lemma* 4:** For $1 \le n \le c + 3$, $S(n, c) = 2n - 1$.

***Proof*:** It is sufficient to consider the case when $n = c + 3$. In this case, the half-way optimal strategy is to form the inverted tower with the smallest $c + 1$ discs on the peg $P_1$ (violating the "divine rule" $c$ times), in $c + 1$ moves, followed by the transfer of the disc $d_{c+2}$ to the peg $P_2$, to free the largest disc $d_{c+3}$ on the peg $S$. The total number of moves required is

$$2(c+2) + 1 = 2c + 5 = 2n - 1.$$

Another problem of interest is to extend the concept of the relaxation of the "divine rule" to the $p$-peg Tower of Hanoi problem with $p \geq 5$.

## Conclusion

The primary objective of the paper is to initiate the study on a new generalization of the Reve's puzzle, which permits relaxation of the "divine rule". This paper considers in complete detail the variant with $n$ discs, allowing the possibility of a single relaxation (or, "cheat") of the "divine rule". It is found analytically that the optimal value function, $S(n)$, can be expressed in terms of $R(n)$. It is also found that, for $n \geq 9$, Scheme 4 is the only optimal strategy. When $4 \leq n \leq 8$, there are multiple optimal strategies which have been found. Lemma 4 shows that there are multiple optimal solutions when $10 \leq n \leq 13$.

## Conflict of interest

The author declares that there is no conflict of interest regarding the publication of this article.

## References


Bouche T. La quartrieme tour de Hanoi. *Bulletin Belgian Math. Soc.* 2014; 21: 895-912.

Chen X, Tian B and Wang L. Santa Claus' Towers of Hanoi. *Graphs & Comb.* 2007; 23 (Supplement): 153-167.

Chu I-Ping and Johnsonbaugh R. The four-peg Tower of Hanoi puzzle. *SIGCSE Bull.* 1991; 23(3): 2- 4.

Claus N. (= Lucas, E.) La tour d` Hanoi. *Jeu de Calcul. Sci. Nat.* 1883; 1(8) : 127 -128.

Dudeney HE. *The Canterbury puzzles*. 4th Ed. Dover, U.S.A.; 1958.

Hinz AM. An iterative algorithm for the Tower of Hanoi with four pegs. *Computing*, 1989; 42: 133-140.

Hinz AM, Klavzar S and Petr C. *The Tower of Hanoi – Maths & Myths.* 2nd Ed. Springer; 2018.

Majumdar AAK. The generalized four-peg Tower of Hanoi problem. *Optimization*, 1994; 29: 349 -360.

Majumdar AAK. *The classical tower of Hanoi problem and its generalizations, Vol.* 1: *Multi-peg generalizations.* Lambert Academic Publishing, U.S.A., 2012.

Majumdar AAK. *The classical tower of Hanoi problem and its generalizations, Vol.* 2: *Other generalizations.* Lambert Academic Publishing, U.S.A., 2013.

Majumdar AAK. Some local-value relationships for the recurrence relation related to the Tower of Hanoi problem. *Proceedings Pakistan Acad. Sci.* 2016; 53(2): 187 - 201.

Majumdar AAK. The Reve's puzzle revisited. *Proceedings Pakistan Acad. Sci.* 2021; 58(2): 11- 18.

Majumdar AAK. The Reve's puzzle with single relaxation of the divine rule. *J. Bangladesh Acad. Sci.* 2022; 46(2): 213 -217.

Roth T. The tower of Brahma revisited. *J. Recreational Math.* 1974; 7(2): 116-119.

Wood D. The towers of Brahma and Hanoi revisited. *J. Recreational Math.* 1981; 14: 17- 24.

J. Bangladesh Acad. Sci. 48(2); 265-271: December 2024 DOI:https://doi.org/10.3329/jbas.v48i2.73899

Journal of Bangladesh Academy of Sciences

Journal homepage: http://www.bas.org.bd/publications/jbas.html

**Research Article**

# Geographic range extension of zebra mantis shrimp *Lysiosquilla maculata* (Fabricius 1793) (Stomatopoda: Lysiosquillidae) through DNA barcoding from the Bay of Bengal, Bangladesh

Md. Sagir Ahmed*, Tonmoy Saha[1], Saikt Rahman[2], Durjoy Raha Antu[1] and Sujan Kumar Datta

*Department of Zoology, Faculty of Biological Sciences, University of Dhaka, Bangladesh*

**ARTICLE INFO**

**Article History**

Received: 06 June 2024
Revised: 19 October 2024
Accepted: 20 October 2024

**Keywords:** *Lysiosquilla maculata*, New record, Phylogeny, Zebra mantis,16S rRNA.

**ABSTRACT**

A new record of zebra mantis shrimp *Lysiosquilla maculata* (Fabricius 1793) was confirmed for the first time from the Bay of Bengal, Bangladesh. Morphological and molecular investigations were used to validate this new record. It possesses ten teeth on the dactylus of raptorial claw that can be differentiated easily from its congener species. A partial large subunit ribosomal RNA (16S rRNA) gene sequence was generated and revealed 100% similarity with pre-existing sequences that validated the morphological identification of the species. Including present species, the number of mantis shrimp has increased to nine in Bangladesh. Further extensive study on its biology, ecology, and conservation is highly recommended.

## Introduction

Bangladesh is situated on the Ganges Delta and the Bay of Bengal stands in the southern portion of the country. The total marine area of Bangladesh is about 207,000 sq. km with a 711 km coastline rich with aquatic faunal diversity (Minar et al., 2013).

Stomatopods are marine crustaceans usually known as 'mantis shrimp' because of their large and powerful raptorial appendages. Worldwide, there are over 500 species of stomatopods that are reported to belong to over 120 genera, 18 families, and seven superfamilies (Ahyong, 2012). Since 2022, Lysiosquillidae has consisted of three genera *viz. Lysiosquilla* (Dana, 1852), *Lysiosquillina* (Manning, 1995), and *Lysiosquilloides* (Manning, 1977). Recently, Ahyong & Lin (2022) reassessed the status and composition of the lysiosquillid genera by cladistic analysis using all known species in the family. They found species transitional between *Lysiosquilla* and *Lysiosquillina*, which challenges the validity of the present generic system and recommends *Lysiosquillina* be synonymized with *Lysiosquilla*. *Lysiosquilla glabriuscula* (Lamarck, 1818), *L. lisa* (Ahyong and Randall, 2001), *L. maculata* (Fabricius, 1793), and *L. sulcata* (Manning, 1978) are the valid documented species from the family Lysiosquillidae. *L. maculata* is the largest mantis shrimp in the world with a length reaching up to 38.5 cm (Manning, 1978; Ahyong, 2001). It is distributed across the Indo-Pacific, ranging from East Africa to the Galápagos, Japan, Australia, and the Hawaiian Islands (Ahyong, 2001).

Stomatopods are economically utilized in various regions globally, with significant fisheries activity focused on *Squilla mantis* (Linnaeus, 1758) in the Mediterranean and *Oratosquilla oratoria* (de Haan, 1844) in Japan (Ahyong, 2001). Recently, these creatures have gained recognition as valuable bioindicators for assessing the impact of marine pollution stress on coral reefs (Erdmann and Caldwell, 1997). This newfound role impetus to understand the taxonomy and systematics of stomatopods.

*Corresponding author:<sagir@du.ac.bd>

[1]*Department of Zoology, Faculty of Life and Earth Science, Jagannath University, Bangladesh*

[2]*Department of Genetic Engineering and Biotechnology, Faculty of Biological Sciences,University of Dhaka, Bangladesh*

According to Ahmed et al. (2008) 185 crustacean species were documented from Bangladesh and the threat status of 141 species of crustaceans was assessed (IUCN Bangladesh, 2015). Eight species of mantis shrimps so far reported from Bangladesh water including *Acanthosquilla multifasciata* (Wood-Mason, 1895), *Bigelowina phalangium* (Fabricius, 1798), *Clorida decorata* (Wood-Mason, 1875), *C. latreillei* (Eydoux and Souleyet, 1842), *Harpiosquilla harpax* (de Haan, 1844), *H. raphidea* (Fabricius, 1798), *Oratosquillina interrupta* (Kemp, 1911) and *O. perpensa* Kemp, 1911) (Tabassum and Akash, 2022). *Oratosquillina perpensa* (Kemp, 1911) is the only species that is enlisted in these two recent vast documentations of crustaceans' diversity Bangladesh (Ahmed et al., 2008; IUCN Bangladesh, 2015).

*Lysiosquilla maculata* as *Squilla maculate* was first described from the Indian Subcontinent (Fabricius, 1793) and the species was reported as *Lysiosquilla maculate* Kemp (1913) from several location of Indian water. Apart from this, Lyla et al. (1997), Roy and Gokul (2012), and Babu et al. (2023) reported the species from Indian waters. This paper represents the first documentation of *Lysiosquilla maculata* from the Bangladesh based on morphological and molecular characteristics.

## Materials and Methods

### Sampling and Morphological Analysis

Two specimens of *Lysiosquilla maculata were* collected on December 10, 2022 from Dublar Char, Sundarban area, (21.758693 N 89.616616 E) Bagerhat and one from Cox's Bazar (21.238105 N 91.756600 E) on September 4, 2022. Specimens were caught as a bycatch during pelagic fishing.Following collection, the Samples were quickly preserved in ice and transported to the Advanced Fisheries and DNA Barcoding Laboratory at the Department of Zoology, University of Dhaka. Photograph in fresh condition was taken, and kept in the refrigerator (-18℃) for further analysis. Taxonomic identification of the specimen was conducted following Manning (1978) and Ahyong (2001). A portion of tissue (20mg) was transfer to a vial for genetic analysis, tagged the specimen as DUZM_CR_084B, DUZM_CR_084B.2, DUZM_CR_084B.3, and deposited at Dhaka University Zoology Museum.

### Extraction and PCR amplification of genomic DNA

DNA was extracted using a Monarch® Genomic DNA Purification Kit (USA) following the manufacturer's instructions. A NanoDrop spectrophotometer was utilized to evaluate the quality and quantity of the extracted DNA. The contigs were amplified using polymerase chain reaction (PCR) with the primers 16Sar 5′-CGCCTGTTTATCAAAAACAT-3′ and 16Sbr 5′-CCGGTCTGAACTCAGATCATGT-3′ (Palumbi et al., 1991). The amplification protocol included an initial denaturation at 95°C for 5 minutes, followed by 35 cycles of 94°C for 45 seconds, 48°C for 30 seconds, 72°C for 45 seconds, and a final extension at 72°C for 7 minutes.Amplified gene bands were visualized on a 1% agarose gel. PCR purification and sequencing were performed by an outsourcing company (Celemics Inc., Korea).

### Bioinformatics analysis

The quality of the generated sequences was viewed using CHROMAS software. The sequence was confirmed by BLASTn search against the best-matching sequences in the nucleotide database and deposited in NCBI GenBank. Phylogenetic tree was constructed based on the neighbor-joining (NJ) statistical method with gamma distribution rates by bootstrap analysis with 1000 replicates in MEGA 11 (Tamura et al., 2021) and iTOL v5 (Letunic and Bork, 2021). Sequences of this species and some other species that were found in Bangladesh (not barcoded yet) were downloaded from GenBank to compare with the present species.

## Results and Discussion

### Systematic account

Order: Stomatopoda
Suborder: Unipeltata
Family: Lysiosquillidae
Genus: *Lysiosquilla*

***Lysiosquilla maculata* (Fabricius, 1793)**

**Material examined**: Bangladesh: Cox's Bazar, BFDC fish landing centre, 21.238105 N 91.756600 E, 4-September-2022, 1 female (TL: 92.0 mm); and Dublar char, Sundarban area, 21.758693 N 89.616616 E, 10-December-2022, 2 females (TL: 100.1 and 96.0 mm); DUZM_CR_084B & DUZM_CR_084B.2, DUZM_CR_084B.3

**Diagnostic Character**: The outer scale of *Lysiosquilla maculata* (Fabricius, 1793) is triangular, and erect and the anterior portion of the outer scale is inclined (Fig. 1). The rostrum shape is cordiform but sometimes sub-triangular in shape, and the length is smaller than the width.

Usually, 10 teeth are present in the dactylus of raptorial claw, but this number may be varied from 10 to 11 in larger females. TS8 sternal keel round shape. Mandibular palp present and three segment presents on mandibular palp. 7–9 movable spines present on the outer margin of the uropodal exopod proximal segment and triangular lobes with ventro laterally anterior to each uropod's articulation make up the uropodal protopod. Distal ¾ of the uropodal endopod is black in color.


**Fig. 1. Dorsal view of *Lysiosquilla maculata* (TL: 92 mm) voucher ID DUZM_CR_084B, collection date: 4-September-2022, place: Cox's Bazar, Bangladesh.**

**Description**

Large eye with bilobed cornea, set slightly obliquely on stalk. The carapace is convex and broad in size. Antennular peduncle short, about ½ of the carapace. The antennal scale is broad and curved with a large dark spot on the surface. The rostrum shape is cordiform but sometimes sub-triangular in shape, and the length is smaller than the width. The representation of blunt longitudinal carina on the anterior third plate. Dactylus of raptorial claw with 8-11 teeth (usually 10-11). The number and size of teeth reduced in large females. Propodus and carpus are comparatively more inflated in large females and males. The ventral keel of the eighth thoracic somite rounded. Abdomen smooth, unarmed. Sixth somite smooth medially, with low, broad lateral boss flanked mesially by a shallow longitudinal groove. Telson is much broader than long, smooth or slightly wrinkled. About 3-4 pairs of fixed projections in the posterior margin of the telson. Basal segment of uropod with slender dorsal spine. The proximal segment of the exopod is shorter than the distal, with 8 movable spines, distalmost not exceeding midlength of distal segment. Endopod broad, length about or less than twice greatest width.

**Coloration**

During collection, Pale yellow dorsum base with black transverse bands was noted. A carapace with three dark transverse bands intervened by pale bands of about the same width. Distal ½ of the proximal segment and proximal 2/3 of the distal segments are black in uropodal exopod. About ¾ of the distal uropodal endopod is black in color.

**Measurement**

Three female specimens (TL 92-100.1 mm) were collected and morphometric measurements were taken. Morphometric data of the specimens are given in Table 1.

**Table 1. Morphometric data of the specimens of *Lysiosquilla maculata* (DUZM_CR_084B, DUZM_CR_084B.2 and DUZM_CR_084B.2) and comparisons with other species.**

| Characteristic | Mean Length (mm) n=3 | % to TL | *L. lisa* (Ahyong and Randall, 2001) | *L. maculata* (Ahyong, 2001) | *L. sulcata* (Manning, 1978) |
|---|---|---|---|---|---|
| Total Length | 96.03 | | 192-308 | 81-335 | 41-150 |
| Carapace Length | 18.95 | 19.73 | | | |
| Eye Diameter | 05.33 | 05.55 | | | |
| Dactylus length | 21.87 | 22.78 | | | |
| Telson Length | 12.90 | 13.44 | | | |
| Telson Wide | 19.29 | 20.09 | | | |
| Abdomen Length | 51.51 | 53.64 | | | |
| Thorax Length | 18.37 | 19.13 | | | |
| Teeth on Raptorial claw dactylus | 10 | | 9-10 | 7-11 (usually 10-11) | 7-8 |
| Color of uropodal endopod | Dark | | Dark Brown | Dark | Light/Pale |
| Color ratio of endopod | ¾ dark | | | ¾ dark | |

## Remarks

This species is widespread in the Indo-Pacific, ranging from East Africa to the Hawaiian Islands and the Galápagos (Ahyong, 2001). Recently Babu et. al. (2023) reported this species from the Chennai coast, Tamil Nadu, India. *L. maculata* is very close to *L. sulcirostris* and *L. sulcata.* The two species can be differentiated easily through the teeth on raptorial claw dactylus and colouration of the uropodal endopod. *L. maculata* has 10 teeth on the raptorial claw dactylus whereas *L. sulcirostris* has 7-8 teeth. On the other hand, the distal half of the uropodal endopod is dark in *L. maculata* but not in *L. sulcata*.

## Molecular Analysis

One partial large subunit ribosomal RNA gene sequence of 473 bp was generated and submitted to the NCBI GenBank database with an accession number PP065678. The BLAST search results have shown 100% query coverage with the pre-existing sequences of *L. maculata* (MT490885) that was submitted from Japan which validated the morpho-taxonomic identification of the species. The nucleotide base frequencies were found as T (31.71%), C (12.68%), A (34.88%) and G (20.72%). The percentage of GC was found lower than AT and was 33.41% and 66.59%, respectively. To compare with other species of squilla found in Bangladesh (not barcoded yet, collected from NCBI) were used in this study from GenBank. *Lysiosquilla sulcirostris* was found as the nearest species of *L. maculata* with a distance of 8.01% and the divergence with the other species was more than 13% (Table 2).

A Neighbor-Joining (NJ) phylogenetic tree was constructed using a total of 10 sequences belonging to 9 species of mantis shrimp. One sequence obtained from this study was designated as DUZM, and the remaining nine sequences were retrieved from the NCBI database (Fig. 2). In the phylogenetic tree, *L. maculata* forms a distinct clade with the same species from Japan with a 100% bootstrap value (Fig. 2).

**Table 2. Genetic divergence (% K2P distance) of *L. maculate* with other species.**

| Species | | Interspecies Distance % |
|---|---|---|
| *Lysiosquilla maculata* | *Lysiosquilla sulcirostris* | 8.01 |
| | *Oratosquilla perpensa* | 13.42 |
| | *Oratosquilla oratoria* | 13.82 |
| | *Clorida decorata* | 13.84 |
| | *Harpiosquilla harpax* | 15.33 |
| | *Acanthosquilla multifasciata* | 18.09 |
| | *Bigelowina phalangium* | 18.81 |

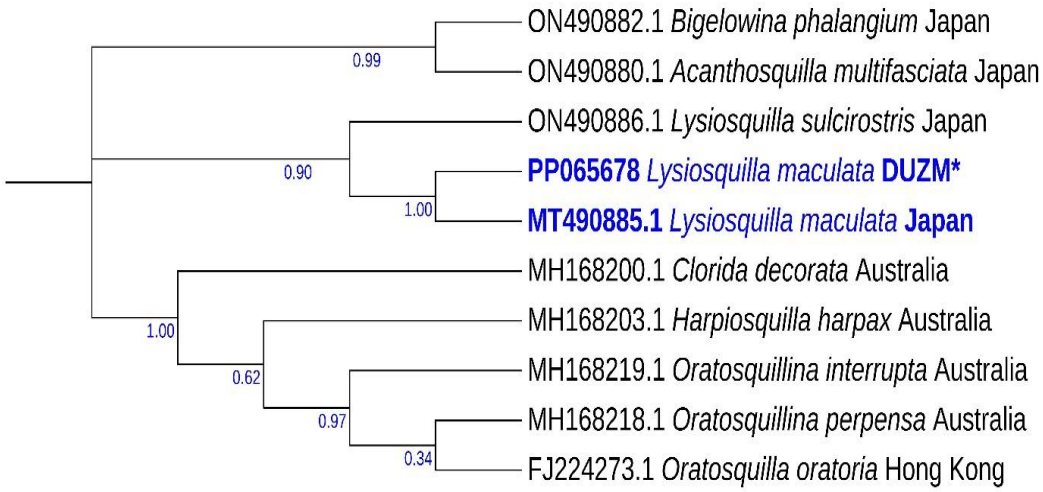


**Fig. 2. Phylogenetic analysis of *Lysiosquilla maculata* with closely related species by the Neighbor-joining method in MEGA 11 and iTOL v5. DUZM* represents the generated sequence of the present study.**

## Conclusions

Classical taxonomy based on morphometric and meristic characters, along with DNA barcoding based on 16S rRNA marker confirms the taxonomic identity and the first occurrence of *L. maculata* from the Bangladesh coast. It is suspected that this species could be distributed throughout the entire coastal belt of the country. More extensive research is needed to know about its biology, local distribution and population status.

## Acknowledgments

We sincerely acknowledge the financial support of Bangladesh Academy of Science.

## Author contributions

**Md. Sagir Ahmed:** Conceptualization, Supervision, Methodology, Data curation, Writing - original draft, Writing - review & editing. **Tonmoy Saha, Saikt Rahman and Durjoy Raha Antu:** Field collection, Data curation, Formal analysis, Writing - original draft, Writing - review & editing. **Sujan Kumar Datta:** Conceptualization, Methodology, Field collection, Laboratory analysis, Data curation & analysis, Writing - original draft, Writing - review & editing.

## Declaration of competing interest

The authors declare that they have no known competing financial interests or personal relationships that could have appeared to influence the work reported in this paper.

## Ethical Approval

No ethical approval was required as the studied animals were not listed in CITES appendices I or II or in the threatened categories of the IUCN Red List Species.

## Funding

The study was financially supported by Bangladesh Academy of Science under the BAS-USDA Endowment Program for Applied Research in Natural Sciences Focused on Food Security, (Grants No. FI 18).

## References

Ahmed ATA, Kabir SMH, Ahmad M, Rahman AKA, Haque EU, Ahmed ZU, Begum ZNT, Hassan MA and Khondker M. (eds.). Encyclopedia of flora and fauna of Bangladesh, (Vol. 18. Arthropoda) Dhaka: Asiatic Society of Bangladesh. 2008. p. 226.

Ahyong ST and Lin CW. Phylogenetic appraisal of Lysiosquillidae Giesbrecht, 1910, and a new species of *Lysiosquilloides* Manning, 1977, from Taiwan (Crustacea: Stomatopoda: Lysiosquilloidea). Zool Stud. 2022; 61: 12.

Ahyong ST and Randall JE. *Lysiosquillina lisa*, a new species of mantis shrimp from the Indo-West Pacific (Stomatopoda: Lysiosquillidae). J. South Asian Nat. Hist. 2001; 5(2): 167-172.

Ahyong ST. Revision of the Australian stomatopod Crustacea. Rec Aus Mus, Suppl. 2001; 26: 1-326.

Ahyong ST. The Marine Fauna of New Zealand: Mantis Shrimps (Crustacea: Stomatopoda). NIWA Biodiv Memo. 2012; 125: 1-112

Babu C, Silambarasan K, Anrose AP and Tiburtius AP. First DNA barcoding-based record of *Lysiosquilla maculata* (Crustacea: Stomatopoda) from Chennai coast, Tamil Nadu, India. *Mar. Fish Sci.* (MAFIS); 2023; 37(2).

Dana JD. Crustacea, Part I. In: United States Exploring Expedition. During the Years 1838, 1839, 1840, 1841, 1842. Under the Command of Charles Wilkes, U.S.N. C. Sherman: Phildelphia; 1852; 13: i-viii + 1-685.

De Haan W. Crustacea. In: von Siebold, P.F., Fauna Japonica sive Descriptio Animalium, quae in Itinere per Japoniam, Jussu et Auspiciis Superiorum, qui Summum in India Batava Imperium Tenent, Suspecto, Annis 1823-1830 Collegit, Notis, Observationibus et Adumbrationibus Illustravit*;* 1833-1850; i–xxxi, ix–xvi, 1–243, pls. A–J, L–Q, 1–55.

Erdmann MV and Caldwell RL. Stomatopod crustaceans as bioindicators of marine pollution stress on coral reefs. Proc 8th Int Coral Reef Symp. 1997; 2: 1521-1526.

Eydoux F, Souleyet LFA. Voyage Autour du Monde, Exécuté Pendant les Années 1836 et 1837 sur la

Corvette La Bonite, Commandée par M. Vaillant. Zoologie. Tome Premier, Seconde Partie. Arthus Bertrand, Paris; 1842; 133-334.

Fabricius JC. Entomologia Systematica Emendata et Aucta. Secundum Classes, Ordines, Genera, Species. Adjectis Synonimis, Locis, Observationibus, Descriptionibus. 1793. p.519.

Fabricius JC. Supplementum Entomologiae Systematicae. Hafniae: Proft et Storck; 1798; 1-572.

IUCN Bangladesh. Red List of Bangladesh. Volume 6: Crustaceans. IUCN International Union for Conservation of Nature, Bangladesh Country Office, Dhaka, Bangladesh; 2015; pp. xvi+256

Kemp S. An account of the Crustacea Stomatopoda of the Indo-Pacific region, based on the collection in the Indian Museum. Mem Ind Mus. 1913; 4: 1-217.

Kemp S. Preliminary descriptions of new species and varieties of Crustacea Stomatopoda in the Indian Museum. Rec. Zool. Smb. Indian, 1911; 6 (2): 93-100.

Lamarck JB. [volume 5 of] Histoire naturelle des Animaux sans Vertèbres, préséntant les caractères généraux et particuliers de ces animaux, leur distribution, leurs classes, leurs familles, leurs genres, et la citation des principales espèces qui s'y rapportent; precedes d'une Introduction offrant la determination des caracteres essentiels de l'Animal, sa distinction du vegetal et desautres corps naturels, enfin, l'Exposition des Principes fondamentaux de la Zoologie. Paris, Deterville; 1818; 5: p. 612.

Letunic I and Bork P. Interactive Tree of Life (iTOL) v5: an online tool for phylogenetic tree display and annotation. Nucleic Acids Research; 2021; 49(W1): W293-W296.

Linnaeus C. Systema Naturae per regna tria naturae, secundum classes, ordines, genera, species, cum characteribus, differentiis, synonymis, locis. Vol. 1 (10th revised ed.) Laurentius Salvius: Holmiae; 1758; p.824.

Lyla PS, Chandrasekaran VS and Khan S. Stomatopoda of Parangipettai coast. Centre of Advanced Study in Marine Biology. Annamalai University, Parangipettai; 1997. p. 47.

Manning RB. A monograph of the West African Stomatopod Crustacea. Atlantide Report. 1977. 12: 1-181.

Manning RB. New and rare stomatopod crustacea from the Indo-West Pacific region. Smith Contr Zool. 1978. 264:1-44

Manning RB. Stomatopod Crustacea of Vietnam: The Legacy of Raoul Serène. Crustacean Research; 1995; Special Number 4. viii + 339.

Minar MH, Hossain MB and Shamsuddin MD. Climate change and coastal zone of Bangladesh: vulnerability, resilience and adaptability. Middle East J. Sci. Res. 2013; 13(1): 114-20.

Palumbi SR, Martin A, Romano S, McMillan WO, Stice L, Grabowski G. *The simple fool's guide to PCR*. Dept. of Zoology and Kewalo Marine Laboratory, University of Hawaii: Honolulu; 1991.

Roy MKD and Gokul A. A checklist of Indian Stomatopods (crustacea: stomatopoda). J Environ Socio Biol. 2012; 9(1):87-92.

Tabassum A and Akash M. First record of *Clorida latreillei* (Stomatopoda: Squillidae) from Bangladesh, with an annotated checklist of the Bangladeshi stomatopods. J. Asia-Pac. Biodivers. 2022; 15(2): 280-284.

Tamura K, Stecher G and Kumar S. MEGA 11: Molecular Evolutionary Genetics Analysis Version 11. Mol. Biol. Evol. 2021; 38(7): 3022-3027.

Wood-Mason J. Figures and descriptions of nine species of Squillidae from the collection in the Indian Museum. 1895; p. 1-11.

Wood-Mason J. On new or little-known crustaceans. Pro. Asiat. Soc. Bengal. 1875; 1875: 230-232.

J. Bangladesh Acad. Sci. 48(2); 273-276: December 2024 DOI:https://doi.org/10.3329/jbas.v48i2.75208

Journal of Bangladesh Academy of Sciences

Journal homepage: http://www.bas.org.bd/publications/jbas.html

## Short Communication

# Physical and chemical properties of soils collected from surrounding areas of Payra thermal power plant

Md Fazlul Hoque, Abrar Mahir Nitol and Mohammad Asadul Haque*

*Department of Soil Science, Patuakhali Science and Technology University, Bangladesh*

**ARTICLE INFO**

**Article History**

Received: 30 July 2024
Revised: 08 September 2024
Accepted: 10 September 2024

**Keywords:** Acid sulfate soil, Electrical conductivity, Phosphorus, Saline soil, Sodium.

**ABSTRACT**

The study was conducted to observe the physical and chemical properties of the soils of the Payra thermal power plant's surrounding areas. The textural class of 55 collected soil samples was mostly Silt loam, with few Silty clay loam soils. Soil pH ranges from 3.72 to 7.82, with more than 80 % being acidic and only 4% slightly alkaline. The 23 % of samples were highly acidic (pH<4.5). The electrical conductivity ranged from 0.91 to 23.95 dS/m, with 47% of the samples having EC values greater than 8 dS/m; those sample sites were unsuitable for crop cultivation. There was a significant difference between Olsen P and Bray P in soil, having 0.73 to 13.87 and 9.29 to 42.60 ppm, respectively. All the samples had very high sulfur contents (34.3 to 601.4 ppm). Most soil samples (78%) contained very high sodium content.

## Introduction

Suspended particulate matter produced from construction activities of the Payra thermal power plant at KalaparaUpazila of Patuakhali district may accumulate in the nearby areas and impact the changing properties of agricultural lands. The duration and extent of tidal water flooding may also greatly influence the deposition of sediments and plant nutrients in the coastal ecosystem (Haque et al., 2023a). The tidal waterborne fine soil particles contain a high quantity of nutrients in available form (Haque et al., 2014). Little attention has been given to characterizing the coastal soils for their suitability for growing various crops (Jodder et al., 2016). The study aimed to assess soil's physical and chemical properties at the Payra thermal power plant's surrounding areas and their impact on crop production.

Fifty-five soil samples were collected from farmers' fields within a 1-5 km radius of the power plant. Soils collected from 0 to 15 cm soil depth from 15 to 20 March were dried, crushed, sieved using a 2-mm sieve, and then analyzed following standard procedures.

Sand, silt, and clay percentages varied from 1.7 to 29.7, 62 to 86.5, and 5.8 to 23.8 with an average of 9.9, 76.6, and 13.5, respectively (Table 1). Textural classes of the soils were Silt loam (69%), Silty clay loam (27%), and Clay loam (4%). The silt and clay fractions were dominant over sand fractions in all the collected samples. The silt and clay-dominated textures in the coastal ecosystem were also reported by Kumar et al. (2018), Haque and Hoque (2023), Sume et al. (2023), and Haque et al. (2023b; 2024a).

**Table 1. Textural classes of the soils.**

| Soil particles | Range of particles (%) | Textural classes | Sample size | % of the total 55 samples |
|---|---|---|---|---|
| Sand (%) | 1.7 - 29.7 (9.9) | Silt loam | 38 | 69 |
| Silt (%) | 62 - 86.5 (76.6) | Silty clay loam | 15 | 27 |
| Clay (%) | 5.8 - 23.8 (13.5) | Clay loam | 2 | 4 |

Values in the parenthesis indicate the average value

*Corresponding author:<masadulh@yahoo.com, masadulh@pstu.ac.bd>

In reaction, most of the top soils were strongly acidic to slightly alkaline (pH 3.72 to 7.82) (Table 2). More than 80 % of the soil samples were acidic, 15% neutral, and only 4 % were slightly alkaline in reaction. Extreme acidity (pH <4.5) was found in 23 samples out of 55, indicating that the soil was probably an actual acid-sulfate soil (Haque et al., 2008; Haque et al., 2023c; 2024b). Electrical conductivity (EC) varied from 0.91 to 23.95 dS/m (Table 2). Most of the agronomical crops can tolerate EC values up to 4 dS/m. Among the samples, 38% had EC values lower than 4 dS/m, and those soils are suitable for growing all crops. The salt-tolerant rice varieties can tolerate EC values up to 8 dS/m; in the present study, only 15% of samples were within this range. The 47% of samples had EC values greater than eight dS/m; those sample sites were unsuitable for crop cultivation. Similar electric conductivity was also described by Haque (2018).

**Table 2. pH and EC data of soils at Pa.**

| Interpretation class | Sample size | % of total samples |
|---|---|---|
| **Soil acidity (pH)** | | |
| Very strongly acid (<4.5) | 23 | 42 |
| Strongly acid (4.5 - 5.5) | 10 | 18 |
| Slightly acid (5.6 - 6.5) | 12 | 22 |
| Neutral (6.6 - 7.3) | 08 | 15 |
| Slightly alkaline (7.4 - 8.4) | 02 | 4 |
| Strongly alkaline (8.5 - 9.0) | - | - |
| pH Range | 3.72 - 7.82 | |
| pH Mean | 5.29 | |
| **Soil salinity class based on EC (dS/m)** | | |
| Nonsaline (0 - 2) | 06 | 11 |
| Slightly saline (2 - 4) | 15 | 27 |
| Moderately saline (4 - 8) | 08 | 15 |
| Saline (8 - 12) | 15 | 27 |
| Highly saline (>12) | 11 | 20 |
| EC Range | 0.91 - 23.95 | |
| EC Mean | 7.75 | |

There was a big difference between Olsen P and Bray P contents of the same soil sample. The Olsen P varied from 0.73 to 13.87 ppm (Table 3). 96% of samples were very low, and 4% of samples were low in available P content, which indicates that all the tested soils were deficient in P content. However, the opposite result was recorded when the soils were analyzed using the Bray method. Based on the Bray method, none of the samples were very low. Only 2% soils were low, 7% samples were medium and 15% samples were optimum in P content (Table 3). Interestingly, 76% of samples were high and very high in P content. However, phosphorus fixation due to low soil pH in the dry season is also reported in the ecosystem (Hoque et al., 2010).

**Table 3. P contents (ppm) of soils.**

| Interpretation class | Sample size | % of total samples |
|---|---|---|
| **Olsen P** | | |
| Very Low (≤ 7.5) | 53 | 96 |
| Low (7.51 - 15.0) | 02 | 4 |
| Medium (15.1 - 22.5) | - | - |
| Optimum (22.51 - 30.0) | - | - |
| High (30.1 - 37.5) | - | - |
| Very high (> 37.5) | - | - |
| P range | 0.73 - 13.87 | |
| P means | 2.47 | |
| **Bray P** | | |
| Very Low (≤ 5.25) | - | - |
| Low (5.25 - 10.5) | 01 | 2 |
| Medium (10.51 - 15.75) | 04 | 7 |
| Optimum (15.76 - 21.0) | 08 | 15 |
| High (21.1 - 26.25) | 10 | 18 |
| Very high (> 26.25) | 32 | 58 |
| Bray P range | 9.29 - 59.97 | |
| Bray P mean | 27.29 | |

Available sulfur was observed to be very high in all (100%) soil samples, and it ranged from 34.3 to 601.4 ppm (Table 4), which has a chance of being toxic through the formation of acid sulfate soils (Hoque et al., 2011). The exchangeable potassium content ranged from 0.11 to 0.51 meq/100g soil (Table 4). Of 55 soil samples, 62 % contained low K, and 20 % had medium K concentration. Only 8% of samples had high and very high K content. The lowland rice in delta soils would rarely respond to the application of potassium, although only some upland rabi crops, including maize, responded to K application, especially in saline soils (Haque, 2020).

**Table 4. S, K, and Na contents of soils.**

| Interpretation class | Sample size | % of total samples |
|---|---|---|
| **Available S (ppm)** | | |
| Very Low (≤ 7.5) | - | - |
| Low (7.51 - 15.0) | - | - |
| Medium (15.1 - 22.5) | - | - |
| Optimum (22.51 - 30.0) | - | - |
| High (30.1 - 37.5) | - | - |
| Very high (> 37.5) | 5 | 100 |
| Range | 34.3 - 601.4 | |
| Mean | 272.9 | |
| **Exchangeable potassium (meq/100 g soil)** | | |
| Very Low (≤ 0.09) | 01 | 02 |
| Low (0.91- 0.18) | 34 | 62 |
| Medium (0.181 - 0.27) | 11 | 20 |
| Optimum (0.271 - 0.36) | 05 | 09 |
| High (0.361 - 0.45) | 02 | 04 |
| Very high (> 0.45) | 02 | 04 |
| Range | 0.06 - 0.51 | |
| Mean | 0.20 | |
| **Exchangeable sodium (meq/100 g soil)** | | |
| Very Low (≤ 0.09) | - | - |
| Low (0.91- 0.18) | 03 | 06 |
| Medium (0.181 - 0.27) | - | - |
| Optimum (0.271 - 0.36) | 09 | 16 |
| High (0.361 - 0.45) | - | - |
| Very high (> 0.45) | 43 | 78 |
| Range | 0.17 - 2.70 | |
| Mean | 1.01 | |

Exchangeable sodium was found to be very high compared to the potassium content of the collected soil samples (Table 4) and varied from 0.17 to 2.53 meq/100g soil. Among the tested soil samples, only 6 % had low, and 16 % had optimum P levels. Unfortunately, 78 % of samples had very high Na content. Although sodium is not an essential plant nutrient element, in lower concentrations, it enhances plant growth; similarly, in higher concentrations, it is excessively toxic to plants (Shila et al., 2016; Sikder et al., 2016; Akter et al., 2021; Sultana et al., 2021). There was a very strong and significant relation ($R^2$=0.948) of the soil's sodium content with the soil's electrical conductivity. It was found that increasing sodium content in soil linearly increases the electrical conductivity of soil (Fig. 1).

It might be concluded that in the surrounding areas of the Payra thermal power plant, fine textured silt and clay particles were dominant, the soils were generally acidic in reaction with a very low percentage of slightly alkaline reaction, and widespread deficiency of Olsen P with low to medium availability of K. The sodium toxicity was very consistent over the study area.

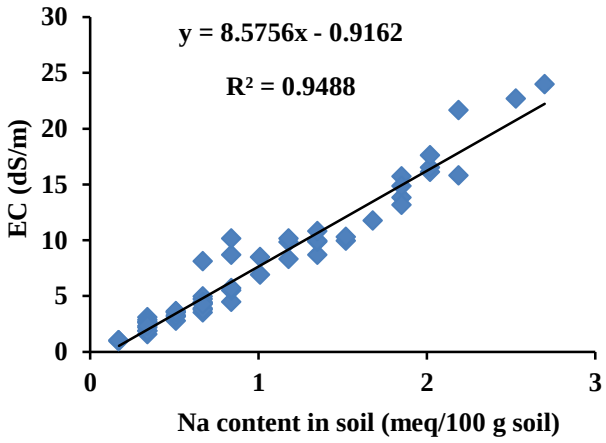


**Fig. 1. Regression relation of Na content with EC of soil (n=55).**

## References


Akter N, Haque MA and Hoque MF. Improvement of maize growth by application of silicon through its suppressing effect on sodium uptake under salt stress conditions. *J. Bangladesh Acad. Sci.* 2021; 45(2): 251-253.

Haque MA and Hoque MF. Nitrogen fertilizer requirement and use efficiency in sunflower at Ganges delta coastal salt-affected soils. *Commun. Soil Sci. Plant Anal.* 2023; 54(16): 2248-2262.

Haque MA, Hoque MF, Jahiruddin M, Hossain MB, Satter MA, Haque ME and Bell RW. Performance evaluation of different sources and rates of silicon in rice at eastern Gangetic coastal plains. *J. Soil Sci. Plant Nutr*. 2023b; 23: 5084-5096.

Haque MA, Jahiruddin M, Hoque MA, Rahman MZ and Clarke D. Temporal variability of soil and water salinity and its effect on the crop at Kalapara upazila. *J. Environ. Sci. Nat. Resourc.* 2014; 7(2): 111-114.

Haque MA, Jahiruddin M, Hoque MF, Islam MS, Hossain MB, Satter MA, Haque ME and Bell RW. Increasing the use efficiency of fertilizer phosphorus for maize in low-P Ganges delta soils. *J. Plant Nutr*. 2023c; 46(10): 2257-2275.

Haque MA, Jharna DE, Hoque MF, Uddin MN and Saleque MA. Soil solution electrical conductivity and basic cations composition in the rhizosphere of lowland rice in coastal soils. *Bangladesh J. Agril. Res*. 2008; 33(2): 243-250.

Haque MA, Kabir ME, Akhter S, Hoque MF, Sarker BC, Anik MFA, Ahmed A, Pranto S, Sima AS, Lima F, Jahiruddin M, Hossain MB, Haque ME, Satter MA and Bell RW. Crop nutrient limitations in intensified cropping sequences on the Ganges delta coastal flood plains. *J. Soil Sci. Plant Nutr*. 2023a; 23: 1996-2006.

Haque MA, Mobaswera A, Sume MA, Pranto S, Jahiruddin M, Hoque MF and Bell RW. Silicon supplementation improves yield and silicon uptake in maize at eastern Ganges delta coastal soils. *J. Plant Nutr*. 2024a, 47(2): 190-204.

Haque MA, Sima AS, Jahiruddin M and Bell RW. Minimizing phosphorus mining through optimum phosphorus fertilization in maize. *J. Soil Sci. Plant Nutr*. 2024b; 24(1): 1-13

Haque MA. Increasing yield of maize through potash fertilizer management in saline soil. *J. Bangladesh Agric. Univ*. 2020; 18(2): 362-366.

Haque MA. Variation in salinity through the soil profile in south coastal region of Bangladesh. *J. Bangladesh Acad. Sci*. 2018; 42(1): 11-23.

Hoque MF, Haque MA, Hossain MK, Haque MZ and Hussain ASMI. Characterization of some coastal delta soils of Bangladesh. *J. Bangladesh Soc. Agric. Sci. Technol*. 2011; 8(1 & 2): 77-82.

Hoque MF, Saleque MA, Rashid MH, Haque MA and Islam MR. Phosphorus sorption as influenced by soil characteristics on four Ganges Tidal Floodplain soils of Bangladesh. *J. Patuakhali Sci. Tech. Univ.* 2010; 2(1):1-11.

Jodder R, Haque MA, Kumar T, Jahiruddin M, Rahman MZ and Clarke D. Climate change effects and adaptation measures for crop production in South-West coast of Bangladesh. *Res. Agric. Livest. Fish.* 2016; 3(3): 369-378.

Kumar T, Haque MA, Islam MS, Hoque MF and Jodder R. Effect of polythene mulch on growth and yield of sunflower (*Helianthus annuus*). *Arch. Crop Sci*. 2018; 2(1): 38-46.

Shila A, Haque MA, Ahmed R and Howlader MHK. Effect of different levels of salinity on germination and early seedling growth of sunflower. *World Res. J. Agric. Sci.* 2016; 3(1): 048-053.

Sikder MU, Haque MA, Jodder R, Kumar T and Mondal D. Polythene mulch and irrigation for mitigation of salinity effects on maize (*Zea mays* L.). *The Agriculturists*, 2016; 14(2): 01-13.

Sultana N, Haque MA, Hoque MF, Hossain MB, Satter MA and Jahiruddin M. Effect of silicon application on growth and biomass yield of rice under salinity stress. *J. Bangladesh Agric. Univ*. 2021; 19(4): 429-436.

Sume MA, Haque MA, Mobaswera A, Hoque MF, Jahiruddin M and Bell RW. Identifying varietal differences for silicon mediated improvement of leaf architecture and plant growth in rice. *Silicon*, 2023; 15: 6299-6311.

# INSTRUCTION FOR AUTHORS

**The Journal of Bangladesh Academy of Sciences** is published four times a year in March, June, September and December. Original research articles, review articles, and short communications of high standards of all branches of Science and Technology are considered for publication in this journal. Review articles are generally by invited authors; however, the Editor welcomes suggestions of potential topics and potential authors.

The following instructions must be followed while preparing the manuscript intended for publication in this journal:

1. **Research Article:** Manuscripts should be concise and consistent with the style of the journal. The manuscript must be typed using Times New Roman font, size 12 on A4 size page, and wide (1 inch) margins on all four sides. The main text must be typed in a two-column format with 1.5 spacing, and for full papers, it should not exceed 10-20 typed pages, including figures, tables, and references. In general, an article may contain the following sub-titles in sequence: **Title, Abstract, Keywords, Introduction, Materials and Methods, Results and Discussion, Acknowledgement (**if any), and **References.**

**A. Title:** The first page of the paper, the title page, should have the title and the names of the authors. The title should be brief and specific. Abbreviations and formulae should be avoided where possible. The next line in italics should be the authors' affiliation addresses (where the actual work was done) below the names. Indicate all affiliations with a lowercase superscript letter immediately after the author's name and in front of the appropriate address. The corresponding author, along with email address, should be indicated at the footnote with a proper asterisk.

**B.** The second page should carry the Title of the paper, Abstract, and Keywords. Author(s) name must not be typed on this page.

**(i) Abstract:** It should not exceed 150 words and should briefly state the purpose of the research, the significant results, and meaningful conclusions. Nonstandard or uncommon abbreviations should be avoided, but if essential, they must be defined at their first mention in the abstract itself.

**(ii) Keywords:** Immediately after the abstract, provide a maximum of 6 keywords.

**C.** The next pages (a maximum of 15 printed pages), will contain the main text of the paper.

**(i) Introduction:** It should be concise and relevant to the objectives of the study. The importance of the research work described should be pointed out. An appropriate review of the current literature should be made to identify the frontier of existing knowledge and point out the need for further work. The knowledge contributed to the study should be mentioned.

**(ii) Materials and Methods:** Materials used should be mentioned precisely along with their sources and any pre-treatment undertaken.

The description of methods must be brief but clear enough to enable a reader to reproduce the results. References must be considered sufficient for methods described in earlier publications: only relevant modifications should be described.

It is recommended that authors use the nomenclature and symbols adopted by IUPAC document UIFII (S.U.N. 65-3) 1965, symbols, units, and nomenclature in Physics or by IUPAC Manual of Physiochemical symbols,

Terminology and similarly for other disciplines.

**(iii) Results and Discussion:** This section should include descriptions of results obtained with the help of figures, tables, graphs, and photographs as may be necessary. Tables should have a descriptive title. Large and cumbersome tables should be avoided. Figures and graphs should be prepared and should be properly labelled with bold solid lines such that no further size reduction will be necessary. The paper should contain a minimum number of **Tables, Graphs,** and **Figures.** The same data should not be depicted using both tables and figures. The photographs are to be submitted in JPEG format.

The discussion should include thorough analysis and interpretation of results, and comparison with existing relevant published results, if any, and self-evaluation of the new knowledge contributed, avoiding extensive citations and discussion of published literature.

**(iv) Conclusions**

The study's main conclusions may be presented in a short Conclusions section, which may stand alone or form a part of the Results and Discussion section.

**(v) Acknowledgment:** The following support for the research work should be acknowledged:

- Funding by any agency;
- The use of instruments in a laboratory other than those of the authors;
- Individual's help during the research (e.g., providing an interpretation of results, language help, writing assistance, or proofreading, etc.).

**(vi) Author contributions**

For transparency, we encourage authors to submit an author contribution statement outlining each author's contributions to the paper. The authors should have participated sufficiently in the work to take public responsibility for appropriate portions of the content.

**(vii) References and Text Citations:**

In the text, references should be cited within brackets quoting the first author's surname followed by et al. if necessary and the year of publication in the appropriate place, e.g. (Bhuiyan, 2020), Khan et al. (2021) or (Khan et al., 2021). In the case of only two authors, surnames of both need to be mentioned, e.g., (Khan and Rahman, 2021). A semi colon should separate two or more references when putting within the same bracket. At the end of the manuscript, references should be listed and arranged alphabetically according to the first author's surname according to the style described below:

**(a) Journal article:**

In each reference, names of all authors' will have to be given in the same style, e.g., surname followed by initials, lumped together without using a full stop. The names will be followed by the full title of the article and the journal's abbreviated title (in italics). The year of publication will be given next, followed by volume number (issue number) and page ranges. For abbreviations of the names of journals, authors are advised to follow the *World List of Scientific Periodicals.* For online publications, the URL address must be given. Note: Please list ALL authors' names in the list of references, do not use (et al.). **Examples:**

Islam S. The Induced Morphological and Root Anatomical Changes in Lentil. *J. Bangladesh Acad. Sci.* 2019; 43(2):107-112.

James BD and Bennett DA. Causes and Patterns of Dementia: An Update in the Era of Redefining

Alzheimer's Disease. *Annu. Rev. Public Health;* 2019; 40: 65-84.

Moniruzzaman M, Khatoon R and Qamruzzaman AKM. Influence of Plant growth Regulators on Vegetative Growth, Sex Expression and Yield of Summer Bottle Gourd. *Bangladesh J. Agril. Res*. 2019; 44(4): 577-590.

**(b) Book or Chapter in a Book:**

The place and name of the publisher, year of publication, will have to be given in addition to the name of the author(s), the title of the book (in italics), edition number (if not first), and the number of pages. In the case of an article or chapter in a book or proceedings of a conference, author(s) name and the title of the article or chapter will be followed by the title of the book (in italics), the names of the editors of the book, edition number (if not first), the place and name of the publisher, year of publication and page or page numbers of chapter. **Examples:**

**Book:**

Carlson BM. *Human Embryology and Developmental Biology*. 4th ed. St. Louis: Mosby; 2009. p. 541.

Cassese A, Acquaviva G, Fan M and Whiting A. *International Criminal Law: Cases and Commentary*. Oxford University Press; 2011, p. 600.

**Chapter in an edited book:**

Muhammad HFL and Dickinson KM. Nutrients, energy values and health impact of conventional beverages, Chapter 3. In: *The Science of Beverages*, *Volume 12: Nutrients in Beverages*. Grumezescu AM, Holban AM, eds., Elsevier Science; 2019; pp. 77-109.

Balsam KF, Martell CR, Jones KP, Safren SA. Affirmative cognitive behavior therapy with sexual and gender minority people. In: *Culturally Responsible Cognitive Behavior Therapy: Practice and Supervision*. Iwamasa GY, Hays PA, eds., 2nd edition, American Psychological Association. 2019; p. 287-314.

**(c) Proceedings of a Conference:**

Luca J and Tarricone P. Does emotional intelligence affect successful teamwork? In: *Meeting at the Crossroads*. Kennedy G, Keppell M, McNaught C (eds.), Proceedings of the 18th Annual Conference of the Australasian Society for Computers in Learning in Tertiary Education, 2001 Dec 9-12; Melbourne: Biomedical Multimedia Unit, The University of Melbourne; 2001. pp. 367-376.

**(d) Reports:**

*Bangladesh Bureau of Statistics (BBS). Population census - 2011*. Preliminary report. Bangladesh Bureau of Statistics, Ministry of Planning, Government of the People's Republic of Bangladesh, Dhaka, 2011.

Rowe IL and Carson NE. *Medical manpower in Victoria. East Bentleigh (AU)*: Monash University, Department of Community Practice; 1981. p. 35. Report No.: 4.

2. **Short communication:** Important research findings that may initiate further research in the relevant field may be published in the form of a short communication. This should not exceed three printed pages (900 words), including Graphs, Tables, and Figures. The presentation should be continuous and paragraphed, i.e., without headings like Introduction, Materials, and Methods, etc. A short communication paper should have an **Abstract** containing the gist of the article and should not exceed 60 words, followed by **Keywords.**

3. **Declarations:** While submitting, the corresponding **a**uthor will have to make a declaration mentioning the laboratory/laboratories in which the work was carried out and certifying that the contents of the paper were not published before or submitted for publication in any other journal and that all the co-authors have given their consent for the article to be considered by the Editorial Board for publication in the Journal of Bangladesh Academy of Sciences.

**Declaration of conflicting interests**

The corresponding author must provide a formal conflict of interest statement for all authors disclosing any financial and personal relationships with other people or organizations that could inappropriately influence (bias) their work. If no conflict exists, please state that 'The author(s) declare(s) that they have no conflicts of interest regarding the publication of this article.'

4. The manuscript should be submitted in pdf or MS Word or LaTex files through online at www.bas.org.bd/publications/jbas.html. Equations generated by using Math Type or Math ML should be incorporated in the text.

   Soft copies of manuscripts with tables, graphs, illustrations, and photographs placed correctly in a printable format are to be submitted. Authors wishing to publish coloured schemes/diagrams/ sketches/photographs in their papers need to pay for the printing charges of one format. This will be charged only after the acceptance of the manuscripts for publication in the JBAS.

   The manuscript submitted should also contain a separate list of tables, figures, illustrations, photographs, and sketches with appropriate captions.

5. Electronic versions of final galley proofs will be sent to authors. No alteration in the title or additions in the text is desirable at this stage.

6. All correspondence for publication should be made on www.bas.org.bd/publications/jbas.html to the **Editor, Journal of Bangladesh Academy of Sciences, National Science and Technology Complex, Agargaon, Dhaka 1207.**

**N.B.: No paper will be accepted for publication if it does not conform to the style specified for the journal and approved by the Editorial Board, which has the authority to accept or reject the manuscript of a paper submitted without showing any reason.**